Functional characterization of the centrosomal protein PCMD-1 in bridging the centrioles and the pericentriolar material in *C. elegans*

Dissertation der Fakultät für Biologie
der Ludwig-Maximilians-Universität München

Lisa Kristin Stenzel

München, 2021

Diese Dissertation wurde angefertigt
unter der Leitung von Dr. Tamara Mikeladze-Dvali
im Bereich der Zell- und Entwicklungsbiologie
an der Ludwig-Maximilians-Universität München

Erstgutachterin:	Prof. Dr. Barbara Conradt
Zweitgutachter:	Prof. Dr. Michael Boshart
Tag der Abgabe:	08. Juli 2021
Tag der mündlichen Prüfung:	27. Januar 2022

Eidesstattliche Erklärung

Ich versichere hiermit an Eides statt, dass die vorgelegte Dissertation von mir selbständig und ohne unerlaubte Hilfe angefertigt ist.

München, den 08. Juli 2021

_____

Lisa Stenzel

Erklärung

Hiermit erkläre ich, dass die Dissertation nicht ganz oder in wesentlichen Teilen einer anderen Prüfungskommission vorgelegt worden ist und dass ich mich nicht anderweitig einer Doktorprüfung ohne Erfolg unterzogen habe.

München, den 08. Juli 2021

_____

Lisa Stenzel

Publications originating from this thesis

In this thesis, I present my doctoral research results, which I conducted from November 2017 until October 2020. Parts of the conducted results have been published in Current Biology and as a preprint on bioRxiv. Published results are referenced in the corresponding figure legends. Parts of the results have been submitted to Development (as of July 4th, 2021).

Erpf, A. C., **Stenzel, L.**, Memar, N., Antoniolli, M., Osepashvili, M., Schnabel, R., Conradt, B., and Mikeladze-Dvali, T. (2019). PCMD-1 Organizes Centrosome Matrix Assembly in *C. elegans*. Current Biology *29*, 1324-1336.

Stenzel, L., Mehler, J., Schreiner, A., Üstüner, S., Zuccoli, E., Zanin, E., and Mikeladze-Dvali, T. (2020). PCMD-1 bridges the centrioles and the PCM scaffold in *C. elegans*. bioRxiv, doi: 10.1101/2020.11.09.375865.

Stenzel, L., Schreiner, A., Zuccoli, E., Mehler, J., Üstüner, S., Zanin, E., Mikeladze-Dvali T: PCMD-1 bridges the centrioles and the PCM scaffold in *C. elegans.* (Manuscript submitted to Development, as of July 4th, 2021)

Contributions

Dr. Anna Christina Erpf, Dr. Tamara Mikeladze-Dvali, Judith Mehler, Alina Schreiner, Elisa Zuccoli, Sim Üstüner, Dr. Nadine Memar, Martina Antoniolli, Nupur Sharma, Dr. Heinrich Flaswinkel, Dr. Elisabeth Kremmer, Mari Museridze, Marie Zimmer, and Marta Plotnikova, have contributed to this work. Their contributions are indicated in the text, figure legends, or tables.

CONTENTS

Table of Contents

List of Figures

List of Tables

List of abbreviations

All units are abbreviated according to the International System of Units.

Abbreviation	Description
aa	amino acid(s)
a.u.	arbitrary unit
bp	base pair(s)
CA	centrosome amplification
Cat. No.	catalog number
cDNA	complementary DNA
CDK	cyclin-dependent kinase
C-terminal/-terminus	carboxy-terminal/-terminus
DIC	differential interference contrast
DOB	drop-out base
dsRNA	double-stranded RNA
EDTA	ethylenediaminetetraacetic acid
GFP	green fluorescent protein
IB	immunoblot
IF	immunofluorescence
IDRs	intrinsically disordered regions
IPTG	isopropyl-β-D-thiogalactoside
kDa	kilodalton
LB	lysogeny broth
LLPS	liquid-liquid phase separation
MAPK	mitogen-activated protein kinase
MCPH	autosomal recessive primary microcephaly
MTOC	microtubule-organizing center
MT(s)	microtubule(s)
MW	molecular weight
NA	not available
NGM	nematode growth medium
N-terminal/-terminus	amino-terminal/-terminus
OD_{600}	optical density at 600 nanometers
PAGE	polyacrylamide gel electrophoresis
PCM	pericentriolar material
PCR	polymerase chain reaction
PNEB	pronuclear envelope breakdown
PEG	polyethylene glycol
PBS	phosphate-buffered saline
PNM	pronuclear meeting
PNMi	pronuclear migration
rcf	relative centrifugal force
RFP	red fluorescent protein
RNAi	ribonucleic acid interference
rpm	revolutions per minute
RT	room temperature
SDS	sodium-dodecyl-sulfate
SEM	standard error of the mean
SIM	structured illumination microscopy
T	temperature
t	time
TBS	tris-buffered saline
w/o	without
w/v	weight per volume
Y2H	yeast two-hybrid

SUMMARY

Centrosomes establish the microtubule-based mitotic spindle that ensures faithful cell division in animal cells. The centrosome consists of a centriole pair embedded in pericentriolar material (PCM), which nucleates microtubules. The PCM assembles as a thin organized layer around centrioles during interphase, referred to as PCM core. In order to gain microtubule nucleating activity, the PCM expands upon mitosis by assembling a less-organized outer layer in a process termed centrosome maturation. Towards the mitotic exit, the PCM dissolves, and centrioles separate to enable centrosome duplication for the next cell cycle. The *C. elegans* PCM core proteins SPD-5, SPD-2, and PLK-1 form an evolutionarily conserved module required for centrosome maturation. It has been described that the recently identified protein PCMD-1 is essential for the initiation of PCM core assembly and organization of the mitotic PCM. However, the precise mechanism of PCMD-1 function and PCMD-1 interactions with other centrosomal proteins have not been addressed yet.

With this thesis, I contribute to the characterization of the biological function of PCMD-1. Analysis of the *pcmd-1(t3421)* and *pcmd-1(syb975)* mutant alleles and RNAi experiments confirm the critical role of PCMD-1 in PCM assembly and embryonic viability. Furthermore, we describe that endogenous PCMD-1 localizes to centrioles, where it strongly colocalizes with SAS-7, and it is weakly associated with the PCM and, unexpectedly, with microtubules. While this indicates that PCMD-1 might be associated with centrioles and the PCM, the question remains which parts of the protein and upstream regulators are required for its centrosomal localization. I show that PCMD-1 localization to the centrosome is facilitated through more than one domain of the PCMD-1 protein. A region in the C-terminal part of PCMD-1 is sufficient to target the protein to the centrosome. The coiled-coil domain of PCMD-1 additionally promotes centrosomal localization, which is probably conferred through its self-interaction, which I have been proven using the yeast two-hybrid system. The data presented in this thesis demonstrate that PCMD-1 is placed downstream of the centriole proteins SAS-7 and SAS-4 in the centrosome assembly pathway. I provide evidence that SAS-7 regulates PCMD-1 localization independently of SPD-2 and SPD-5 *in vivo*. Performing a yeast two-hybrid screen, I determine that PCMD-1 and SAS-7 physically bind to the centriole protein SAS-4, which potentially mediates PCMD-1 regulation by SAS-7. I also identify physical binding between PCMD-1 and the PCM proteins SPD-5 and PLK-1. Applying a novel translocation assay, I demonstrate that PCMD-1 can force the PCM proteins SPD-5 and PLK-1 to an ectopic locus within the cell. Further, my data suggest that PLK-1 potentially regulates centrosomal PCMD-1 accumulation or initiates its removal from the centrosome as it has been shown for its functional homolog PCNT in humans.

Collectively, this work shows that PCMD-1 acts as a functional bridge between centriole and PCM proteins and thereby initiates PCM assembly and organizes the PCM.

1 INTRODUCTION

1.1 The mitotic spindle

Accurate cell division is essential for the generation and continuation of every living organism. In eukaryotes, error-free chromosome segregation into two daughter cells, and thus genomic integrity, relies on the assembly of a mitotic spindle (reviewed in Walczak and Heald, 2008).

The formation of the mitotic spindle is based on microtubule nucleation. The major microtubule-organizing centers (MTOCs) in animal cells are centrosomes (reviewed in Lüders and Stearns, 2007). The centrosomes actively nucleate three different types of microtubules (MTs) involved in the mitotic spindle assembly (**Figure 1**). Kinetochore and interpolar MTs are critical for chromosome segregation and point towards the center of the spindle (**Figure 1**). Kinetochore MTs, also called K-fibers, attach to the kinetochores of chromosomes to pull them apart during cell division (reviewed in Meunier and Vernos, 2012; Prosser and Pelletier, 2017; Tolić, 2018). Interpolar MTs interact with MTs nucleated from the opposite centrosome. As cell division progresses, interpolar MTs elongate and drive centrosomes apart (reviewed in Meunier and Vernos, 2012; Prosser and Pelletier, 2017). Astral MTs, which are not essential for chromosome segregation but correct positioning of the spindle, are nucleated towards the cell cortex (**Figure 1**) (reviewed in Meunier and Vernos, 2012; Prosser and Pelletier, 2017).

Although the centrosome is the predominant MTOC, other acentrosomal drivers can nucleate, stabilize, and organize MTs, even in systems where centrosomes are present (reviewed in Lüders and Stearns, 2007; Wu and Akhmanova, 2017). Some eukaryotes that do not have centrosomes, such as higher plants and fungi, have evolved alternative mechanisms to undergo cell division (reviewed in Dumont and Desai, 2012; Masoud et al., 2013; Meunier and Vernos, 2016). For instance, yeast possesses spindle pole bodies with MTOC functions equivalent to centrosomes (reviewed in Cavanaugh and Jaspersen, 2017; Kilmartin, 2014).

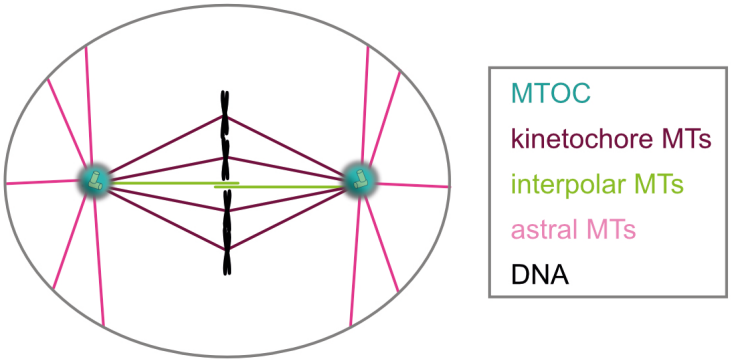

Figure 1. The mitotic spindle during metaphase. Microtubules (MTs) are nucleated from the MTOC, which is the centrosome in most of the animal cells. Kinetochore MTs and interpolar MTs grow towards the center of the spindle. Kinetochore MTs attach to kinetochores of chromosomes, and interpolar MTs connect the two poles by interacting with interpolar MTs from the opposite pole. Astral MTs point towards the cortex of a cell. Schematic modified based on Meunier and Vernos (2012).

1.2 The centrosome

1.2.1 Discovery of the centrosome

Almost a century and a half ago, centrosomes were illustrated for the first time by Walther Flemming (1875). One year later, Édouard van Beneden (1876) published a study with drawings of centrosomes of the parasite *Dicyemidae*, and he recognized the organelles and called them polar corpuscules. In his subsequent study about the fertilization and the cellular division of the parasitic nematode *Ascaris megalocephala,* now termed *Parascaris equorum*, he drew the organelles in more detail (van Beneden, 1883). Only in 1887, when Édouard van Benenden with Adolphe Neyt and Theodor Boveri independently published studies on cell divisions of *Ascaris megalocephala*, special attention was given to the centrosomes. Édouard van Benenden showed that the central polar corpuscules are associated with the mitotic spindle, and he even pointed out that they can undergo cycles of duplication and separation (van Beneden and Neyt, 1887). Theodor Boveri gave the organelles the modern scientific name centrosomes because of their central position in the cell. He described centrosomes as the dynamic centers of a cell, which mediate the nuclear and cellular division (Boveri, 1887). Furthermore, he observed a denser structure in the center of the centrosome, which he named centriole (Boveri, 1888). Later he published the cyclical behavior of centrioles and a collection of more than a hundred extraordinary drawings of stained sea urchin and *Ascaris megalocephala* eggs (Boveri, 1900). He proposed that an abnormal number of centrosomes, which leads to unequal distribution of the chromosomes, might be correlated with tumor formation (Boveri, 1902, 1914). Remarkably, most of Boveri's stained samples are still preserved without damage. Joseph Gall (1996, 2004) and Ulrich Scheer (2014) took images of Boveri's slides and compared them to his original drawings, which were incredibly detailed.

In Boveri's and van Beneden's studies, vital observations about the centrosome, mitotic spindle formation, and cell division were made more than a hundred years ago. However, centrosome research remained untouched for decades. Only towards the end of the 20th-century, centrosome research was resumed when new technologies emerged that allowed investigations on a molecular level (reviewed in Bornens and Gönczy, 2014). Although substantial progress in understanding the centrosomal structure, its role, and its regulation has been made in the last two decades through modern technologies, the fascinating organelles are still not completely understood, and therefore still widely studied.

1.2.2 General structure and function of the centrosome

In a large number of animal cells, centrosomes fulfill the role of the major MTOC. The capacity to nucleate MTs makes the centrosome an indispensable driver in several cellular processes, such as organelle positioning, cell polarity establishment, bipolar spindle formation, and chromosome segregation (reviewed in Conduit et al., 2015; Doxsey, 2001;

Meraldi, 2016). Centrosomes are non-membrane-bound organelles composed of a centriole pair and the surrounding electron-dense PCM (**Figure 2**). The centriole pair duplicates each cell cycle in S-Phase by assembling a new procentriole, the daughter centriole, in the orthogonal direction to the existing mother centriole (reviewed in Fırat-Karalar and Stearns, 2014; Nigg and Holland, 2018). Both centrioles are barrel-shaped with an evolutionary conserved nine-fold radial symmetry (reviewed in Azimzadeh and Marshall, 2010; Gönczy, 2012; Nigg and Holland, 2018). During interphase, the PCM core assembles around the mother centriole as a thin organized layer (Lawo et al., 2012; Mennella et al., 2012). Upon mitotic entry, the PCM massively increases several-fold in size by accumulating a less-organized layer in a kinase-regulated process, termed centrosome maturation (Conduit et al., 2014; Lane and Nigg, 1996; Lee and Rhee, 2011; Woodruff et al., 2015; Wueseke et al., 2016). Downstream effectors, such as the γ-tubulin ring complex (γTuRC) proteins, are recruited for MT nucleation (**Figure 2**) (Moritz et al., 1995; Moritz et al., 1998; Murphy et al., 2001; Oegema et al., 1999; Schnackenberg et al., 1998; Zheng et al., 1995). Furthermore, centrosomes have been implicated in the organization of actin filaments (Farina et al., 2016). Regardless of their MTOC function, centrosomes act as signaling centers and regulators in many cellular processes, such as cell cycle progression and DNA damage response (reviewed in Arquint et al., 2014; Mullee and Morrison, 2016; Rieder et al., 2001).

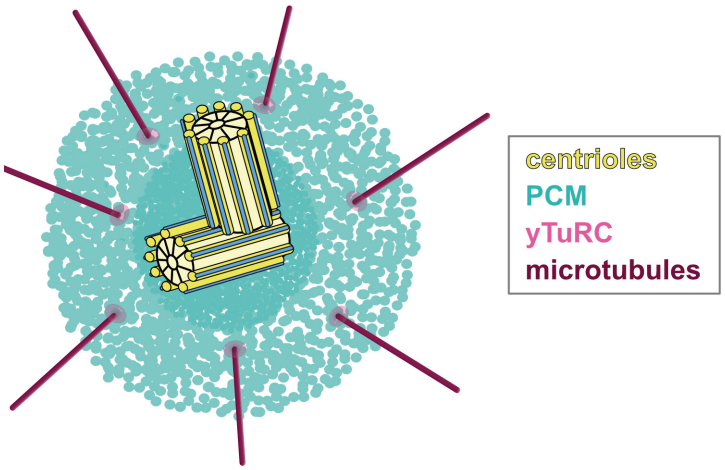

Figure 2. The structure of the centrosome. The centrosome is built of a centriole pair consisting of a mother and a daughter centriole, and the PCM that is assembled around centrioles. In addition to other proteins, γ-tubulin rings (γTuRC) are recruited for microtubule nucleation. Schematic modified based on Ohta et al. (2017), Pintard and Bowerman (2019), and Teixidó-Travesa et al. (2012).

Besides their centrosomal functions, centrioles have another distinct function as basal bodies in cilia formation. Distant eukaryotic lineages possess centrioles, which are required for cilia formation but not for cell division. This indicates that centrioles evolved primarily for their function in ciliogenesis and only secondarily acquired their function in cell division (reviewed in Carvalho-Santos et al., 2011). During ciliogenesis, mature

centrioles can exit the cell cycle and anchor at the cell membrane to initiate the assembly of the axoneme, which forms the base of cilia (reviewed in Carvalho-Santos et al., 2011; Ishikawa and Marshall, 2011). Motile cilia play a role in motility and fluid flow, whereas immotile cilia are crucial in sensing signals from its environment (reviewed in Bettencourt-Dias et al., 2011; Ishikawa and Marshall, 2011; Nigg and Raff, 2009).

1.2.3 Role of the centrosome in human disease

The association of centrosomal abnormalities with severe diseases, such as cancer and developmental disorders accentuates the importance of centrosomes in cell cycle progression.

Boveri has already proposed more than a century ago that chromosome segregation defects caused by multipolar mitosis might give rise to malignant tumors (Boveri, 1914). Indeed, various studies have demonstrated that centrosome amplification (CA) is a hallmark of cancer, and it is correlated with aneuploidy, multipolar mitosis, and chromosomal instability in tumor cells (Basto et al., 2008; Castellanos et al., 2008; Levine et al., 2017; Lingle et al., 2002; Lingle et al., 1998; Pihan et al., 1998). Besides its contribution to tumor formation, it has been suggested that CA promotes tumor progression and invasive behavior of cancer cells (Godinho et al., 2014). Indeed, CA is a promising candidate for therapeutics and prognostics; for instance, in indicating higher risks or poor clinical outcomes in different cancer types through scoring expression levels of genes inducing CA (de Almeida et al., 2019; Ogden et al., 2017). Experiments to reverse CA and its oncogenic effects are in progress and will potentially help cure cancer in the future (reviewed in Sabat-Pośpiech et al., 2019).

Furthermore, centrosome alterations are implicated in developmental disorders (reviewed in Kuijpers and Hoogenraad, 2011). A disease correlated with mutations in genes encoding centrosomal proteins is microcephalic primordial dwarfism (reviewed in Chavali et al., 2014; Klingseisen and Jackson, 2011). The growth of primordial dwarfism patients is restricted, starting already *in utero* and continuing postnatally, which results in overall small body stature but normal proportions (reviewed in Chavali et al., 2014; Klingseisen and Jackson, 2011). Mutations in these patients have been mapped to genes encoding pericentrin (PCNT), centrosomal protein 152 (CEP152), centrosomal protein 63 (CEP63), centrosomal p4.1-associated protein (CPAP), and polo-like kinase 4 (PLK4) (reviewed in Chavali et al., 2014; Jaiswal and Singh, 2021). Another disorder correlated with mutations in genes encoding centrosomal proteins is autosomal recessive primary microcephaly (MCPH), characterized by a reduced brain size but average body size (Barbelanne and Tsang, 2014; Chavali et al., 2014; Thornton and Woods, 2009). Mutations have been found in CDK5 regulatory subunit associated protein 2 (CDK5RAP2), CEP152, CPAP, centrosomal protein 135 (CEP135), and SCL-interrupting locus protein (STIL) (reviewed in Barbelanne and Tsang, 2014; Chavali et al., 2014; Faheem

et al., 2015; Nigg and Holland, 2018). It is known that global growth failures in humans are correlated with reduced cell numbers (reviewed in Klingseisen and Jackson, 2011). However, how the mutations in centrosomal proteins are linked to this phenotype is not entirely understood, and different hypotheses have been suggested. One possible explanation is that the mutations lead to defective PCM expansion, which leads to a failure in mitotic progression and, in turn, an increased rate of apoptosis (reviewed in Fry et al., 2017; Nigg and Holland, 2018). Another presumption is that disturbed PCM activates cell cycle regulators that terminate cell cycle progression (reviewed in Arquint et al., 2014; Fry et al., 2017). The brain-specific growth reduction in MCPH patients is proposed to be caused by cell division or proliferation defects in neuronal progenitor cells (reviewed in Fry et al., 2017; Jaiswal and Singh, 2021).

1.3 *Caenorhabditis elegans* – a model to study cell division

1.3.1 The model organism *C. elegans*

Since Sydney Brenner introduced the nematode *Caenorhabditis elegans (C. elegans)* as a model for neuronal development and genetic studies (Brenner, 1974), the organism has been intensively studied worldwide.

C. elegans can easily be cultured in a laboratory environment due to several advantages. For instance, it is small in size (~1 mm) and grows on agar plates with *Escherichia coli (E.coli)* as a food source. Its life span is only around fourteen days at 20°C, and the growth rate can be temperature-controlled with temperatures ranging from 12°C to 25°C (Corsi et al., 2015). Furthermore, the development of young larval-stage animals can be arrested by food deprivation, and the arrested larvae survive several months, which allows keeping them in stocks. For long-term storage, strains can be frozen at -80°C.

The entirely mapped invariable cell lineage (Sulston and Horvitz, 1977; Sulston et al., 1983) and the transparency are compelling advantages for monitoring the development of *C. elegans* using differential interference contrast (DIC) microscopy. *C. elegans* has two natural forms of sexes: self-fertilizing hermaphrodites with two X chromosomes and males with only one X chromosome. The ability of hermaphrodites to self-fertilize leads to fast reproduction and genetically identical animals. Males only occur at low frequencies of 0.1%-0.2% through spontaneous X chromosome nondisjunction (Hodgkin and Doniach, 1997; Hodgkin et al., 1979). Fertilization of hermaphrodites by males enhances genetic diversity (Brenner 1974). In addition to the sex chromosome, the genome contains five autosomal chromosomes and the mitochondrial genome. The *C. elegans* genome was the first genome to be sequenced among eukaryotes (*C. elegans* Sequencing Consortium, 1998). Compared to the human genome, which comprises approximately 3.2 billion base pairs (bp), the *C. elegans* genome is relatively small, with about 103 million bp (WBcel235 *WormBase*). However, the number of protein-coding genes is

similar in humans and *C. elegans* (~20000). Around 38% of the protein-coding genes in *C. elegans* are predicted to have orthologs in humans (Shaye and Greenwald, 2011). Important cellular pathways were first described in the worm, making it an important model organism. For instance, genes involved in centriole duplication have been first discovered through genetic screens in *C. elegans* (Kamath and Ahringer, 2003; Maeda et al., 2001; O'Connell et al., 1998; Piano et al., 2000; Sönnichsen et al., 2005; Zipperlen et al., 2001). Based on this work, the pathway was then dissected in humans.

C. elegans worms are amenable to genetic manipulations using both traditional and state-of-the-art editing techniques. As mentioned above, many genes in *C. elegans*, such as centrosomal genes, have been identified and investigated using forward genetic screens. Forward genetics is used to identify mutant phenotypes with defects in a biological process of interest (reviewed in Kutscher and Shaham, 2014; Sin et al., 2014). Loss-of-function phenotypes can be generated by specific messenger RNA degradation through RNA interference (RNAi) (Fire et al., 1998; Tabara et al., 1998; Timmons et al., 2001). Nevertheless, some genes are not sensitive to RNAi, or the generated phenotype is not consistent (Kamath and Ahringer, 2003). Another standard method used in forward genetic screens, which mostly provides more consistent phenotypes, is the generation of non-directed genome-wide mutations introduced by chemicals, radiation, or transposon insertions (reviewed in Kutscher and Shaham, 2014). Among other chemicals, ethyl methanesulfonate (EMS) is most widely and efficiently used for mutagenesis (Brenner, 1974; Flibotte et al., 2010). Once an interesting defective mutant is found, the mutations can be mapped, and the gene can be further characterized. Applying reverse genetics, a target gene is edited without altering the whole genome to investigate its function (reviewed in Kutscher and Shaham, 2014). In *C. elegans*, this can be facilitated by enzyme-based techniques, such as CRISPR/Cas9 (reviewed in Dickinson and Goldstein, 2016), and transposon-based techniques, such as *Mos1*-based gene conversion or deletion (Frøkjaer-Jensen et al., 2010; Robert and Bessereau, 2007). The *Mos1*-mediated Single-Copy Insertion (MosSCI) technique is not mutagenic, but it allows the integration of single copies in the genome (Frøkjaer-Jensen et al., 2008; Frøkjær-Jensen et al., 2014).

All these available tools and the simplicity in handling and investigating the organism make *C. elegans* an indispensable model for discovering evolutionarily conserved genes.

1.3.2 The first cell division in *C. elegans*

During the early embryonic development of *C. elegans,* cell cycles only consist of the DNA synthesis phase (S phase) and the mitotic phase (M phase) due to the lack of gap phases until the 28-cell stage (Edgar and McGhee, 1988). The first mitotic division of *C. elegans* has been a widely studied model to elucidate cell division and cell polarity mechanisms. The division process only takes around fourteen minutes from DNA condensation until full

ingression of the cytokinetic furrow (reviewed in Oegema and Hyman, 2006). Due to the fast division, the large size (50x30x30 µm), and the transparency of the embryo, it is easy to follow cell cycle progression in great detail by live-cell imaging. Remarkably, the cell cycle even progresses in the absence of essential proteins for cell division, albeit more slowly. This is due to silenced checkpoint response to DNA damage and weak checkpoint response to spindle disruption in early *C. elegans* embryos (Encalada et al., 2005; Holway et al., 2006). The silenced or weak response systems in the early embryo allow studying the role of these essential proteins.

In *C. elegans,* oocytes are arrested in the prophase of meiosis I (Ward and Carrel, 1979). At fertilization, the sperm enters the oocyte on the opposite side of its pronucleus and specifies the posterior side of the embryo (Goldstein and Hird, 1996). Thereby, the sperm introduces a centriole pair, which is associated with the paternal pronucleus, to the oocyte that has lost its centrioles through centriole elimination during oogenesis (Mikeladze-Dvali et al., 2012). Sperm entry also initiates the resumption of meiosis of the oocyte nucleus (Hill et al., 1989). In two rounds of meiotic divisions facilitated by an acentriolar meiotic spindle, the redundant chromosomes are extruded into two polar bodies (**Figure 3A**) (Albertson and Thomson, 1993; Clark-Maguire and Mains, 1994; Yang et al., 2003). Upon completing the maternal meiosis, DNA decondensation starts in both pronuclei, and their size increases (Nigon, 1949). Meanwhile, an impermeable eggshell has formed around the zygote (Chitwood and Chitwood, 1974). Intense cytoplasmic and cortical flows, ruffling of the anterior membrane, and a central constriction with accumulating P-granules, called pseudocleavage, can be observed (reviewed in Goldstein et al., 1993). In parallel, the paternally contributed centrioles duplicate, and PCM proteins are assembled around the centrioles that nucleate MTs (Pelletier et al., 2004). The two centrosomes are associated with the paternal pronucleus. The maternal pronucleus is captured by the MTs emanating from the centrosomes (**Figure 3B**). The pronuclei migrate towards each other and meet in the posterior half of the embryo in a process termed pronuclear migration (PNMi). At the pronuclear meeting (PNM), both centrosomes are localized at the two contact sites of the pronuclei (**Figure 3C**). When cytoplasmic streams decrease, and the pseudocleavage furrow recedes, the pronuclei move together with the associated centrosomes to the center of the cell and rotate until the complex is positioned along the anterior-posterior axis (Albertson, 1984; Hyman and White, 1987). After the pronuclear envelope break down (PNEB) the bipolar spindle is formed driven by the centrosomes (**Figure 3D**). The chromosomes align in the metaphase plate (**Figure 3E**). Subsequently, the mitotic spindle is shifted to the posterior side by higher pulling forces on the posterior cortex during metaphase (Labbé et al., 2004; Oegema et al., 2001). It is even further displaced to the posterior during anaphase through asymmetric elongation. While chromosomes start to segregate, the cleavage furrow starts to ingress (**Figure 3F**) (Albertson, 1984; Grill et al., 2001). Meanwhile, the centrioles of each centrosome disengage (reviewed in Pintard and Bowerman, 2019). The

chromosomes are pulled towards the opposite spindle poles during telophase (**Figure 3G**). The last step of cell division is cytokinesis, where the cleavage furrow separates the zygote (P_0) asymmetrically, halfway of the shifted mitotic spindle (**Figure 3H**). Thus, two unequally sized daughter cells are produced, a bigger anterior blastomere (AB) and a smaller posterior blastomere (P_1), and the embryo can progress into S-Phase II (Sulston et al., 1983).

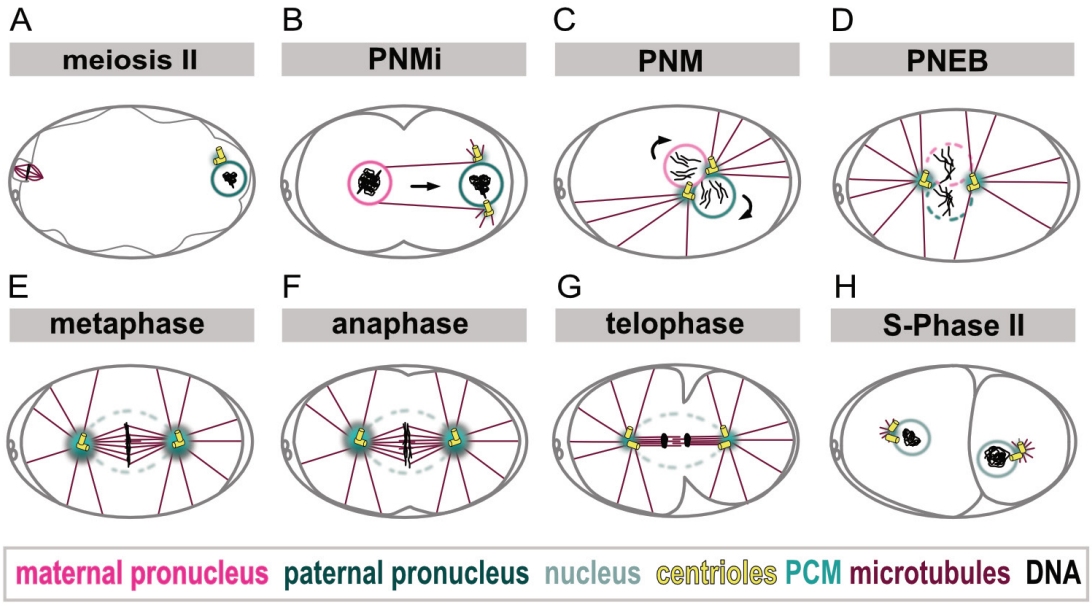

Figure 3. The first cell cycle of the *C. elegans* embryo. Schematic illustrates embryos in different stages following fertilization. **A)** Upon fertilization, the sperm enters the oocyte at the posterior side and introduces the paternal nucleus and centrioles. Maternal meiosis II is completed, and the polar bodies are extruded. **B)** PCM is assembled around the duplicated centrioles, the maternal pronucleus is captured by the nucleated MTs, and the pronuclei migrate towards each other at the stage of pronuclear migration (PNMi). Simultaneously, a pseudocleavage furrow forms. **C)** Pronuclear meeting (PNM) occurs, and the pronuclei rotate. **D)** The complex of centrosomes and pronuclei is positioned along the anterior-posterior axis, and the pronuclear envelope breaks down (PNEB). **E)** At metaphase, chromosomes align in the metaphase plate, and the spindle is pushed towards the posterior side. **F)** During anaphase, the spindle is further pushed towards the posterior side, and chromosomes segregate. **G)** During telophase the centrioles disengage, the chromosomes are pulled towards the opposite parts of the embryo, and the cleavage furrow ingresses. **H)** Two unequally sized daughter cells are produced, and the embryo progresses in S-Phase II. Schematic modified based on Oegema and Hyman (2006).

1.4 Centrosome assembly and disassembly in *C. elegans*, *D. melanogaster*, and humans

As already described in chapter **1.2.2**, in dividing cells, centrioles duplicate once per cell cycle by assembling a daughter centriole adjacent to the mother centriole (reviewed in Fırat-Karalar and Stearns, 2014; Nigg and Holland, 2018). Centrioles are essential for PCM assembly and mitotic PCM expansion (Basto et al., 2006; Cabral et al., 2019). During mitosis, the PCM promotes centriole engagement and prevents premature centriole

disengagement (Barrera et al., 2010; Cabral et al., 2013; Pagan et al., 2015). Disassembly of the PCM at the end of mitosis is a prerequisite for centriole separation, which licenses a subsequent round of centrosome duplication (reviewed in Fırat-Karalar and Stearns, 2014; Nigg and Holland, 2018). In the following chapters, centriole architecture and assembly, PCM structure and assembly, as well as PCM disassembly and centriole separation will be explained in detail.

1.4.1 Centrioles

1.4.1.1 Centriole architecture

Centrioles are barrel-shaped structures arranged in a nine-fold symmetry of stabilized microtubule arrays (reviewed in Azimzadeh and Marshall, 2010; Gönczy, 2012; Nigg and Holland, 2018). Dependent on the species, centriole length ranges from 150 to 500 nm, and the diameter ranges from 100 nm to 250 nm (reviewed in Gönczy, 2012; Nigg and Holland, 2018; Winey and O'Toole, 2014). Particularly in *C. elegans,* centrioles are relatively small, with a length of 150 nm and a width of 100 nm (reviewed in Pintard and Bowerman, 2019). The centriole center is formed by a cartwheel structure consisting of a central hub and nine emanating spokes in humans and flies (reviewed in Azimzadeh and Marshall, 2010; Gönczy, 2012; Nigg and Holland, 2018). A similar structure was only recently discovered in *C. elegans* (Sugioka et al., 2017). The centriole wall is formed by microtubule arrays, which can consist of singlets, doublets, and triplets depending on cell types and species; for instance, singlets in most of the *C. elegans* cells*,* doublets in the fruit fly *Drosophila melanogaster (D. melanogaster)* somatic cells*,* and triplets in vertebrates, such as *Homo sapiens (H. sapiens)* (reviewed in Azimzadeh and Marshall, 2010; Carvalho-Santos et al., 2011; Gönczy, 2012). In *C. elegans,* doublet MTs have been observed only in a few sensory neurons (Serwas et al., 2017); those doublets might be necessary for cilia formation. In humans, mother centrioles are decorated with appendages. Distal appendages mediate membrane attachment during ciliogenesis, and subdistal appendages are required for anchoring MTs (reviewed in Azimzadeh and Marshall, 2010; Uzbekov and Alieva, 2018; Winey and O'Toole, 2014). However, these appendages are not necessarily required for cell division (Ishikawa et al., 2005) and are not present in *C. elegans* and *D. melanogaster*.

1.4.1.2 Centriole assembly

During centriole duplication, a daughter centriole grows perpendicularly to the mother centriole. The initial step of the daughter centriole assembly is the cartwheel formation. In *C. elegans,* this step is driven by the coiled-coil protein spindle-defective protein 2 (SPD-2), which recruits the kinase zygote-defective 1 (ZYG-1) (**Figure 4**) (Delattre et al., 2006; Kemp et al., 2004; O'Connell et al., 2001; Pelletier et al., 2006; Pelletier et al., 2004). Subsequently, ZYG-1 directly interacts with spindle assembly abnormal protein 6

(SAS-6), and thereby brings the complex of the coiled-coil proteins SAS-6 and spindle assembly abnormal protein 5 (SAS-5) to the centriole (**Figure 4**) (Dammermann et al., 2004; Delattre et al., 2006; Kitagawa et al., 2011; Leidel et al., 2005; Lettman et al., 2013). It has been shown that the ZYG-1 kinase activity itself is not necessary for the recruitment of the complex but the oligomerization and stable incorporation of SAS-6 (Lettman et al., 2013). The assembly of MTs depends on the coiled-coil protein spindle assembly abnormal protein 4 (SAS-4), which binds with its TCP domain to SAS-5 (**Figure 4**) (Cottee et al., 2013). The stable incorporation of SAS-4 inversely requires γ-tubulin (TBG-1) and MT assembly (α-tubulin and β-tubulin) (Dammermann et al., 2008). SAS-4 was shown to play an essential role in controlling centriole size, centriole duplication, and PCM accumulation (Dammermann et al., 2008; Kirkham et al., 2003; Leidel and Gönczy, 2003). After the centriole wall is assembled, spindle assembly abnormal protein 7 (SAS-7) is needed for the so-called paddlewheel formation. The paddlewheels are arranged in a nine-fold manner at the periphery of the centrioles (**Figure 4**) (Sugioka et al., 2017). After centrioles have separated, SAS-7 initiates a new round of daughter centriole assembly by recruiting centriolar SPD-2 (Sugioka et al., 2017).

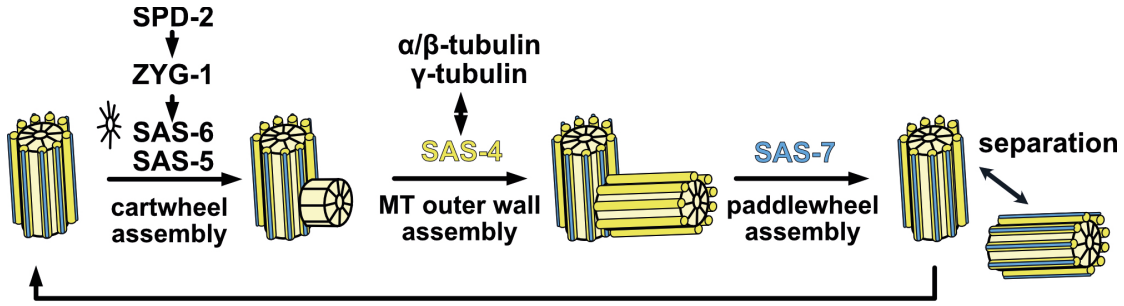

Figure 4. Model of the centriole assembly pathway in *C. elegans*. Daughter centriole assembly starts with the formation of a cartwheel structure through SPD-2, which recruits ZYG-1, which in turn recruits SAS-6 and SAS-5. These proteins recruit SAS-4, which assembles the outer microtubule wall. SAS-4 is stabilized by γ-tubulin an MT assembly (α/β-tubulin). In the last step, but at the same time first step, paddlewheel structures are assembled through SAS-7, which make the mother centriole competent for duplication and lead to SPD-2 recruitment. Schematic modified based on Pintard and Bowerman (2019) and Ohta et al. (2017).

The centriole assembly pathway is conserved across species with only little divergences. Respective functional homologs of *C. elegans* proteins in *H. sapiens* and *D. melanogaster* are listed in **Table 1**. Alterations in almost all of the human homologs cause severe developmental disorders (see chapter **1.2.3**).

In humans, cartwheel formation is initiated by CEP192 together with CEP152 and in flies by asterless (Asl). The proteins recruit PLK4 in humans and Plk4 in flies, which are functional homologs of ZYG-1 (Bettencourt-Dias et al., 2005; Cizmecioglu et al., 2010; Dzhindzhev et al., 2010; Habedanck et al., 2005; Hatch et al., 2010; Kim et al., 2013; Sonnen et al., 2012). While PLK-4 in humans regulates SAS6 and STIL recruitment, Plk4

in flies regulates Sas-6 and anastral spindle 2 (Ana2) recruitment (Dzhindzhev et al., 2014; Kratz et al., 2015; Ohta et al., 2014). In contrast to their functional homolog SAS-5 in *C. elegans*, STIL in humans and Ana2 in flies require phosphorylation by PLK4/Plk4 to recruit SAS-6/Sas-6 (Arquint et al., 2015; Dzhindzhev et al., 2014; Kratz et al., 2015; McLamarrah et al., 2018; Moyer et al., 2015; Moyer and Holland, 2019; Ohta et al., 2014). For the MT outer wall assembly, CPAP in humans and SAS-4 in flies, recruited by SAS6/Sas-6, are required to assemble the outer MT wall and control centriole length (Kohlmaier et al., 2009; Schmidt et al., 2009; Sharma et al., 2016; Tang et al., 2009; Zheng et al., 2016). CEP135 in humans links SAS-6 with CPAP, and Cep135 in flies also stabilizes centrioles, but a functional homolog is unknown in *C. elegans* (Hiraki et al., 2007; Lin et al., 2013). In addition, CEP135/Cep135 recruit Centrosomal protein 295 (CEP295) in humans and Ana1 in flies, which are required for centrosome elongation and initiation of daughter centriole assembly by localizing CEP152 and CEP192 in humans and AsI to the site of daughter centriole assembly (Chang et al., 2016; Fu et al., 2016; Saurya et al., 2016; Tsuchiya et al., 2016).

Table 1. Centriole proteins, which are involved in the evolutionarily conserved daughter centriole assembly pathway. *C. elegans*, *H. sapiens* and *D. melanogaster proteins*. *: functional homolog, -: not identified

C. elegans	***H. sapiens***	***D. melanogaster***	**Function in centriole biogenesis**
SPD-2	CEP192	-	Cartwheel assembly
-	CEP152	Asl	Cartwheel assembly
ZYG-1 *	PLK4	Plk4	Cartwheel assembly
SAS-6	SAS6	Sas-6	Cartwheel assembly
SAS-5 *	STIL	Ana2	Cartwheel assembly
SAS-4	CPAP	Sas-4	Centriole outer wall assembly
-	CEP135	Cep135	Centriole outer wall assembly
SAS-7	-	-	Paddlewheel assembly
-	CEP295	Ana1	Centriole elongation

It has been proposed that PCM proteins also play an essential role in daughter centriole assembly by targeting duplication factors into proximity to the site of daughter centriole assembly (Loncarek et al., 2008). For instance, TBG-1, which also stabilizes SAS-4 incorporation, as described above, and spindle-defective protein 5 (SPD-5) are implicated in daughter centriole assembly in *C. elegans* (Dammermann et al., 2004). The human PCM protein PCNT was also described to recruit SAS6 to daughter centrioles (Ito et al., 2019).

1.4.2 Pericentriolar material

1.4.2.1 Pericentriolar material structure

Investigating PCM architecture has been complicated for a long time because the PCM consists of many different proteins and has a high electron density. However, several

high-resolution imaging studies have led to a better understanding of the PCM architecture in humans and flies (Fu and Glover, 2012; Lawo et al., 2012; Mennella et al., 2012; Sonnen et al., 2012). It has been shown that the components of the thin interphase layer of PCM are organized in concentric rings. These concentric rings are stabilized by fibrils of PCNT in humans or its fly homolog pericentrin-like protein (PLP), respectively. The fibrils extend outwards from the mother centriole. Upon mitotic entry, the PCM expands. The mitotically recruited PCM proteins are not organized in concentric rings as described for the inner PCM layer. Instead, PCNT and PLP extend to the outer layer, and CEP192 and CDK5RAP2 in humans and Spd-2 and centrosomin (Cnn) in flies form scaffold-like structures. The structure of the *C. elegans* PCM has not been studied in detail yet. It is generally assumed that the *C. elegans* PCM is comparable in its structure. An analysis, which was restricted by diffraction-limited imaging, also suggests a layered organization of the PCM (Magescas et al., 2019).

1.4.2.2 Pericentriolar material assembly

The core set of PCM assembly proteins is conserved and functionally similar between *C. elegans*, humans, and flies. However, there are also divergences regarding the PCM assembly between species, and the PCM in humans and flies contains additional proteins, which do not have known homologs in worms. This chapter focuses on proteins that are involved in PCM assembly in *C. elegans* and their homologs or functional homologs in humans and flies (**Table 2**). The function of human and fly proteins, which are not included here, are reviewed in Fry et al. (2017) and Woodruff et al. (2014). However, some human homologs of the *C. elegans* proteins mentioned in this chapter lead to severe developmental disorders in an altered form (see **1.2.3**).

Table 2. Conserved PCM core proteins. * indicates functional conservation only

C. elegans	***H. sapiens***	***D. melanogaster***
SPD-5	Cdk5Rap2 *	Cnn *
SPD-2	CEP192	Spd-2
PLK-1	PLK1	Polo

During interphase, a thin and highly organized PCM layer, referred to as PCM core, assembles around the centrioles consisting of a functionally conserved protein module (**Table 2**, **Figure 5**). The major component of the functionally conserved PCM protein module is the coiled-coil protein SPD-5 in *C. elegans*, or functionally similar CDK5RAP2 in humans and Cnn in flies (Fong et al., 2008; Hamill et al., 2002; Megraw et al., 1999; Woodruff et al., 2015). The two other factors of the module are the pericentriolar pool of SPD-2, CEP192 in humans or Spd-2 in flies, and the mitotic kinase Polo-like-kinase 1 (PLK-1), PLK1 in humans, or Polo in flies (Conduit et al., 2014; Decker et al., 2011; Dix and Raff, 2007; Giansanti et al., 2008; Gomez-Ferreria et al., 2007; Kemp et al., 2004; Lane and Nigg, 1996; Pelletier et al., 2004; Wueseke et al., 2016;

Zhu et al., 2008). How the PCM core initially is recruited to the interphase centrosome in *C. elegans* was not uncovered for a long time. It has been shown that SAS-7, besides its role in daughter centriole assembly, is required for proper PCM formation by promoting pericentriolar SPD-2 recruitment to the centrioles (Sugioka et al., 2017). SPD-2, in turn, recruits PLK-1 (Decker et al., 2011; Ohta et al., 2021). In humans and flies, a major component of the PCM is PCNT and its homolog PLP, respectively. These proteins mediate the recruitment of the PCM core module to the centrioles and organize the PCM structure, as mentioned in the previous chapter (Lawo et al., 2012; Martinez-Campos et al., 2004; Mennella et al., 2012). A potential functional homolog of these proteins in *C. elegans* has recently been identified in our group (Erpf et al., 2019). The potential candidate PCMD-1 will be introduced in detail in chapter **1.4.2.3**.

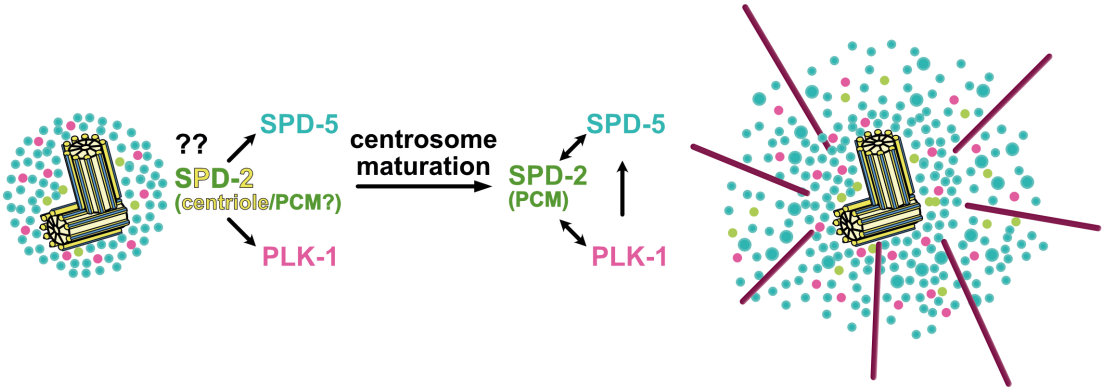

Figure 5. Proposed model of PCM assembly in *C. elegans* missing an important regulator. The PCM core module is assembled in a thin organized layer, in which centriolar and/or pericentriolar SPD-2 were thought to regulate PLK-1 and SPD-5. Upon mitotic entry, the PCM expands in a PLK-1 dependent manner by accumulating an outer more disorganized layer, in which SPD-5 and SPD-2 are co-dependent. The expanded PCM nucleates MTs. Schematic modified based on Erpf et al. (2019) and based on data from Cabral et al. (2019), Decker et al. (2011), Kemp et al. (2014), Pelletier et al. (2004), Woodruff et al. (2015), Wueseke et al. (2014), Wueseke et al. (2016).

When cells prepare for mitosis, PLK-1, PLK1, or Polo activity facilitates PCM expansion, termed centrosome maturation (reviewed in Petronczki et al., 2008). In *C. elegans*, SPD-2 and PLK-1 phosphorylating SPD-5 are required for the mitotic expansion of the PCM (**Figure 5**) (Cabral et al., 2019; Decker et al., 2011; Hamill et al., 2002; Pelletier et al., 2004; Woodruff et al., 2015; Wueseke et al., 2016). More SPD-5 can be incorporated via a feedback loop (Wueseke et al., 2016), and SPD-5 acts co-dependently with SPD-2 (Kemp et al., 2004; Pelletier et al., 2004; Wueseke et al., 2014). Similarly, in flies, PCM growth is driven by phosphorylation of Cnn through Polo (Conduit et al., 2014). Cnn and PLP form a scaffold to recruit downstream proteins (Lerit et al., 2015). In humans, PLK1 is known to phosphorylate PCNT to initiate centrosome maturation (Lee and Rhee, 2011). PCNT forms a scaffold together with CDK5RAP2, the functional homolog of SPD-5 and Cnn (Watanabe et al., 2020). Interestingly, the self-assembly capacity of recombinant SPD-5 accelerated by PLK-1 and SPD-2 and its competence to concentrate tubulin has been reconstructed *in vitro* (Woodruff et al., 2017; Woodruff et al., 2015).

Another regulator of PCM expansion *in C. elegans* is the Aurora-A kinase (AIR-1), which activates PLK-1 (Cabral et al., 2019; Hamill et al., 2002; Hannak et al., 2001). In humans and flies, Aurora-A kinase is also known to regulate centrosome maturation by phosphorylating its substrates PLK-1 and Polo (Berdnik and Knoblich, 2002; Joukov et al., 2014; Macůrek et al., 2008; Seki et al., 2008).

The PCM anchors γ-tubulin ring complexes (γTURC) that facilitate MT nucleation (Moritz et al., 1995; Moritz et al., 1998; Murphy et al., 2001; Oegema et al., 1999; Schnackenberg et al., 1998; Zheng et al., 1995). In parallel to the PCM expansion, the microtubule nucleation activity dramatically increases during centrosome maturation. It has only recently been shown in *C. elegans* that the increased nucleation of MTs is not a passive consequence of PCM expansion (Ohta et al., 2021). PLK-1 regulates the assembly of the γ-tubulin docking sites by phosphorylating SPD-5 and thus promotes the interaction between SPD-5 and TBG-1 (γ-tubulin) (Ohta et al., 2021).

1.4.2.3 PCMD-1 – the missing factor of PCM assembly in *C. elegans*

The novel protein pericentriolar matrix deficient 1 (PCMD-1) has been recently identified and characterized by our group. This work builds on the characterization of PCMD-1 and continues further characterization, published in Erpf et al. (2019). Therefore, this section summarizes the prominent phenotype and the mapping of the *pcmd-1(t3421)* mutant allele described in Erpf et al. (2019). The *pcmd-1(t3421)* mutant allele was identified in an EMS mutagenesis forward genetic screen for temperature-sensitive embryonic lethal phenotypes (unpublished, N. Memar and R. Schnabel). Interestingly, the gene encoding the PCMD-1 protein has not been found in earlier screens. At the restrictive temperature of 25°C, *pcmd-1(t3421)* embryos are not viable. In the *pcmd-1(t3421)* embryos, a monopolar spindle is formed in the first cell cycle and a tripolar spindle in the second cell cycle instead of bipolar spindles as in wild-type embryos (**Figure 6A**). Nevertheless, *pcmd-1(t3421)* is partially conditional, and a fraction of the embryos can survive at 15°C, and the strain is homozygous viable. The affected gene was mapped to the right arm of the first chromosome by whole-genome sequencing combined with single-nucleotide polymorphism mapping. A point mutation, which introduces a premature nonsense mutation at amino acid (aa) Q54, causing the embryonic lethality in *pcmd-1(t3421)* was identified in the *pcmd-1* gene. The gene codes for a 630 aa protein with one predicted coiled-coil domain in the N-terminal part of the protein and four predicted low complexity regions (**Figure 6B**). Furthermore, PCMD-1 is predicted to be enriched in intrinsically disordered regions, which partially overlap with low-complexity regions (UniProtKB O62071; UniProtConsortium, 2019). Interestingly, a computational analysis revealed that centrosomal proteins are enriched in IDRs and coiled-coil domains in all organisms considered and that the enrichment of both together occurs in more complex organisms (Nido et al., 2012).

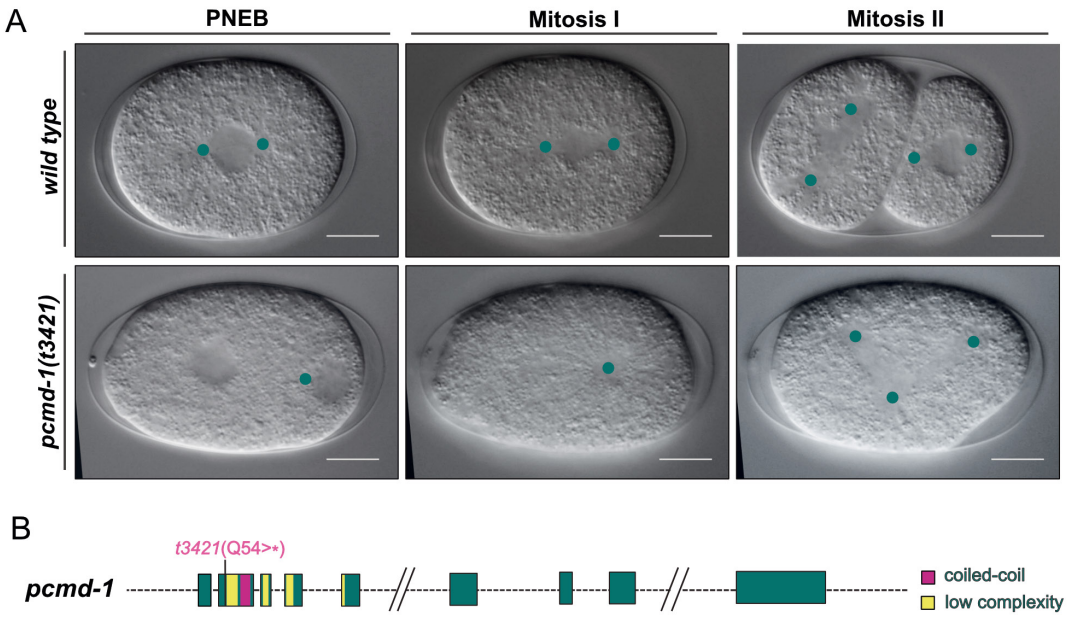

Figure 6. PCMD-1 is required for bipolar spindle formation. A) Representative stills of time-lapse DIC movies of wild-type and *pcmd-1(t3421)* embryos in the first and second cell-cycle at PNEB, mitosis I, and mitosis II. While wild-type embryos form a bipolar spindle in the first and the second cell cycle, *pcmd-1(t3421)* embryos form a monopolar spindle in the first cell cycle and a tripolar spindle in the second cell cycle. Spindles are highlighted with green dots. Scale bar indicates 10 µm. **B)** Schematic illustration of the *pcmd-1* gene locus showing the exon structure with the segments coding for the coiled-coil domain in magenta and low complexity regions in yellow. The *pcmd-1(t3421)* allele carries a point mutation at aa Q54, which introduces a premature stop codon. Introns are not to scale. Figure adapted from Erpf et al. (2019).

It has been demonstrated in rescue experiments that a single-copy insertion of *pcmd-1* rescues the *pcmd-1(t3421)* mutant phenotype, unlike a single-copy insertion of *pcmd-1(t3421)*. The single-copy of *pcmd-1* fused to a *gfp* (green fluorescent protein) reporter at the 5' end under *mai-2* regulatory elements localizes to centrosomes in embryos (**Figure 7A**) and all tissues, including germline and sperm as well as sensory cilia. While PCMD-1 colocalizes with the centriole pair during interphase, it can be detected

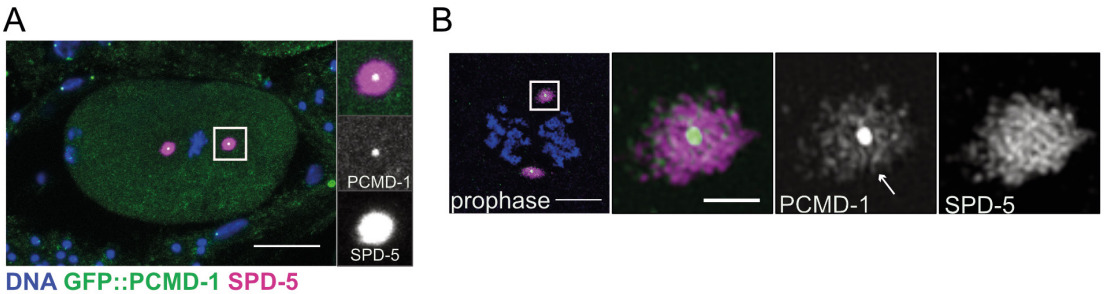

Figure 7. Transgenic GFP::PCMD-1 localizes to centrosomes. A) Confocal image of a $P_{mai\text{-}2}$*gfp::pcmd-1* embryo in metaphase stained against GFP and SPD-5 to mark centrosomes. The box with the centrosomal area is enlarged as single channels and merge. Scale bar indicates 10 µm **B)** A $P_{mai\text{-}2}$*gfp::pcmd-1* two-cell stage embryo in pro-metaphase stained against GFP and SPD-5 to mark the expanding PCM. Arrow indicates filamentous structures formed by PCMD-1. The box with the centrosomal area is enlarged as single channels and merge. Scale bars indicate 5 µm or 1 µm (magnified section). Figure adapted from Erpf et al. (2019).

at both the centrioles and the surrounding PCM during mitosis (**Figure 7B**). Hence, PCMD-1 is considered as both a centriole and a PCM protein.

It was shown that PCMD-1 recruits SPD-5 to the interphase centrosome and facilitates the PCM core formation (**Figure 8**) (Erpf et al., 2019). Additionally, PCMD-1 plays a role in the recruitment of the PCM proteins SPD-2 and PLK-1. SPD-2 and PLK-1 promote the recruitment of SPD-5 (**Figure 8**). Thus, PCMD-1 is considered one of the significant factors of the PCM core, which is the basis of organized centrosome maturation, already explained in chapter **1.4.2.2**. Furthermore, it is known that in the absence of PCMD-1, the integrity of the mitotic PCM is destroyed, but it is not clear whether this is the consequence of the defective PCM core or whether PCMD-1 plays a direct role in the organization of the mitotic PCM (Erpf et al., 2019).

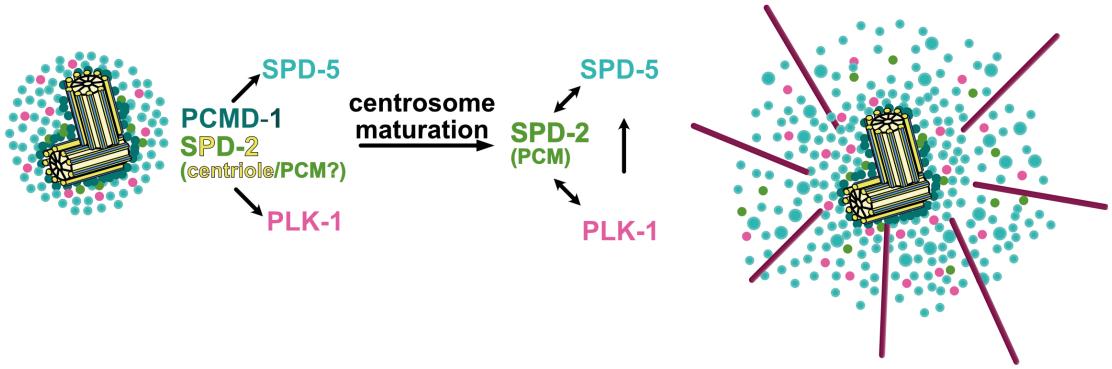

Figure 8. Proposed role of PCMD-1 in PCM core assembly and PCM organization. The assembly of the PCM core consisting of SPD-5, SPD-2, and PLK-1 is facilitated through PCMD-1. PCMD-1 recruits SPD-5 to the centrosome, and it is also involved in SPD-2 and PLK-1 recruitment. Upon mitotic entry, the PCM expands in a process termed centrosome maturation in a PLK-1 dependent manner to a more disorganized scaffold, and MTs are nucleated. Schematic modified based on Erpf et al. (2019) and based on data from Cabral et al. (2019), Decker et al. (2011), Kemp et al. (2014), Pelletier et al. (2004), Woodruff et al. (2015), Wueseke et al. (2014), Wueseke et al. (2016).

A more recent study has demonstrated that PCMD-1 plays a role in PCM formation at the cilia, similar to its role at centrosomes in one-cell embryos. It is necessary to recruit and maintain the PCM protein SPD-5 during interphase (Garbrecht et al., 2021).

1.4.3 Pericentriolar material disassembly and centriole separation

During mitosis, engagement of the two centrioles is supported by PCM proteins, such as CDK5RAP2 and PCNT in humans (Barrera et al., 2010; Pagan et al., 2015) or SPD-5 in early *C. elegans* embryos (Cabral et al., 2013). Towards the end of mitosis, PCM disassembly allows centriole separation, which, in turn, licenses centriole duplication for the next cell cycle (reviewed in Fırat-Karalar and Stearns, 2014; Nigg and Holland, 2018). While PCM assembly has been studied extensively in various organisms, only little is known about the mechanisms of PCM disassembly and its impact on centriole separation.

Flow perturbation experiments in *C. elegans* have revealed that the PCM material properties change dynamically during the cell cycle, and the PCM loses strength and ductility as the one-cell embryo exits mitosis (Mittasch et al., 2020). Furthermore, it was uncovered that the PCM is disassembled in a two-step mechanism. First, the PCM is disassembled in a phosphatase-dependent process. In a second step, the PCM is ruptured through cortical pulling forces acting on the PCM. The dephosphorylation process is driven by the catalytic subunit of the protein phosphatase 2A (PP2A, encoded by let-92 in *C. elegans*) targeting SPD-5 and acting as an antagonist to PLK-1 kinase (Enos et al., 2018; Magescas et al., 2019). While PLK-1 and SPD-2 inhibit the PCM disassembly process, PP2A promotes PCM disassembly (Mittasch et al., 2020). Similarly, the activity of PP2A is required for centriole separation at the transition from meiosis II to mitosis (Boudreau et al., 2019). In humans, another crucial factor of centriole disengagement during mitotic exit in humans is the proteolytic cleavage of intercentriolar linkers, such as the cohesin complex and the PCM protein PCNT, by the cysteine protease separase (reviewed in Sluder, 2013). In *C. elegans*, separase (SEP-1) activity and cleavage of cohesin through SEP-1 seem critical for centriole disengagement during meiosis and the first mitosis but not in later mitotic cell divisions (Cabral et al., 2013; Schvarzstein et al., 2013). PCNT, the putative human homolog of PCMD-1, also functions as an intercentriolar linker, which is cleaved by separase (Lee and Rhee, 2012). Phosphorylation of PCNT by PLK-1 is required for both PCM maturation and proteolytic cleavage through separase (Kim et al., 2015; Lee and Rhee, 2011). The cleavage of PCNT leads to centriole disengagement and induces daughter centrioles to mother centriole conversion in human cells (Kim et al., 2019). In *C. elegans* and *D. melanogaster,* a similar mechanism has not been described yet.

1.5 Coiled-coil domains

1.5.1 Structure and functions of coiled-coil domains

Coiled-coil domains, which occur globally in every living organism, are typically formed through two or more α-helices twisted around each other (Crick, 1952, 1953; Pauling and Corey, 1953). The coiled-coil sequences are mostly repeated periodically after the seventh residue (Landschulz et al., 1988; Lupas, 1996a). Nonetheless, there are many possible alterations and high variabilities of coiled coils in lengths and structures (Hernandez Alvarez et al., 2019; Lupas and Bassler, 2017). Characteristic functions of coiled-coil domains are conferring stability or mediating protein-protein interactions and oligomerization (reviewed in Lupas and Bassler, 2017; Truebestein and Leonard, 2016). However, coiled-coil domains are also involved in more complex functions and processes, such as catalytic activity, communicating conformational changes, and molecular spacing to separate functional domains or to scaffold large complexes (reviewed in Truebestein and Leonard, 2016).

1.5.2 Functions of coiled-coil domains in centrosomal proteins

Many centrosomal proteins contain coiled-coil domains, and it is supposed that the coiled-coil domains play a distinct role in centrosome assembly (reviewed in Kuhn et al., 2014; Nigg and Holland, 2018; Salisbury, 2003). However, structural evidence is scarce. One exception is the centriole protein SAS-6 in *C. elegans.* There is evidence that the coiled-coil domains of SAS-6 act as a molecular spacer by mediating protein-protein interactions and oligomerization, which both play a regulatory role in centriole formation (Hilbert et al., 2013; Kitagawa et al., 2011; Lettman et al., 2013; Qiao et al., 2012; Rogala et al., 2015). Many centrosomal coiled-coil proteins are involved in organizing the PCM. Computational analysis revealed that human centrosomal proteins with coiled-coil domains form more likely scaffolds than proteins without coiled-coil domains (Kuhn et al., 2014). The scaffold proteins, such as SPD-5 in *C. elegans* and its functional homolog Cnn in flies, direct other proteins to the centrosome (Feng et al., 2017; Hamill et al., 2002; Lucas and Raff, 2007; Megraw et al., 1999; Woodruff et al., 2015). For Cnn, the crystal structure of two of its coiled-coil domains interacting with each other has been solved (Feng et al., 2017). This interaction leads to the entwining of the two dimeric regions and thereby a conformational change, which allows oligomerization with other Cnn dimers. These data lead to the assumption that oligomerization and potentially scaffold formation is promoted through coiled-coil domains.

Moreover, it has been proposed that domains that promote self-interaction and aggregate formation, such as coiled-coil domains, low-complexity regions, and IDRs, promote liquid-liquid phase separation (LLPS) (Alberti et al., 2018; Banani et al., 2017). The non-membrane-bound centrosomes are described to be formed through the LLPS process, in which macromolecules from a homogenous mixture rearrange and separate into distinct phases in a concentration-dependent manner. Thereby, biomolecules often assemble liquid-like or gel-like droplets, called biomolecular condensates (reviewed in Alberti et al., 2019; Banani et al., 2017; Hyman et al., 2014; Raff, 2019; Shin and Brangwynne, 2017). However, the material properties of the condensates are highly debated (Woodruff, 2021). Indeed, theoretical modeling and *in vitro* reconstitution experiments with the C*. elegans* centrosomal coiled-coil protein SPD-5 and its homolog Cnn in flies have demonstrated that the PCM proteins can undergo LLPS (Jiang et al., 2020; Woodruff et al., 2017; Zwicker et al., 2014). For the human centrosomal protein PCNT, a potential functional homolog of PCMD-1, it has been shown *in vivo* that it undergoes LLPS with a higher probability in regions enriched with coiled-coil domains and low-complexity regions (Jiang et al., 2020). Since PCMD-1 contains a single coiled-coil domain and IDRs partially overlapping with low complexity regions (Erpf et al., 2019, Uniprot-KB O62071; UniProtConsortium, 2019), it would also have the appropriate architectural features for LLPS.

1.6 Aim of this work

Understanding centrosome assembly and disassembly is essential for understanding cell division and severe diseases associated with centrosomal abnormalities. Many studies have uncovered molecular mechanisms of centrosome assembly and dynamics. However, the *C. elegans* protein PCMD-1 has not been considered in these studies until it was characterized in our study (Erpf et al., 2019).

The aim of this work is to characterize further the centrosomal protein PCMD-1, focusing on its molecular function and regulation in centrosome assembly.

First, I aim to characterize the PCMD-1 phenotype in-depth. Therefore, I analyze the localization and expression pattern of transgenic and endogenously GFP-tagged PCMD-1. Another aim of this thesis is to confirm the mutant phenotype of *pcmd-1(t3421)* and the role of PCMD-1 in centrosome assembly by analyzing the *pcmd-1(syb975)* deletion allele and embryos silenced with RNAi against *pcmd-1*.

The major aim of this thesis is to obtain insight into how PCMD-1 is anchored and incorporated at the centrosome. The focus is on mapping different functional sites of PCMD-1 and unraveling genetic regulators of PCMD-1 *in vivo.* Identifying physical binding partners of PCMD-1 in a candidate-based yeast two-hybrid screen dissects the role of PCMD-1 in centrosome assembly. Furthermore, a novel translocation assay is used to investigate whether PCMD-1 localizing ectopically at the plasma membrane can serve as a loading platform for different centrosomal proteins.

Another aspect of this work is to investigate the role of potential PLK phospho-binding sites in PCMD-1.

The insights of this work will help to understand the role of PCMD-1 in PCM assembly and how PCMD-1 itself is regulated.

2 MATERIAL AND METHODS

2.1 Plasmids and oligonucleotides

2.1.1 Plasmids and oligonucleotides used in this work

In this work, plasmids (**Table 3**) were generated and used for double-stranded RNA (dsRNA) amplification for RNAi by microinjection, generating bacterial clones for RNAi by feeding, generating *C. elegans* strains, generating *Saccharomyces cerevisiae* strains, and raising antibodies. Cloning strategies for plasmids are described in chapter **2.1.2**. Oligos, which were used for the cloning, were ordered from Eurofins Genomics or Thermo Fisher Scientific (**Table 4**).

Table 3. Plasmids used in this work. Plasmid names, descriptions, and origins of the plasmids are listed. *=with J. Mehler, **=with N. Sharma, ***=with S. Üstüner.

Plasmid name	Description	Origin
pBluescript II KS+	empty cloning plasmid (referred to as pBKS)	Stratagene
pEG202	empty bait plasmid	MobiTec
pEG202-Gal4	autoactivation control plasmid	MobiTec
pEG202-p53	pEG202-*p53* (positive control bait)	MobiTec
pJG45	empty prey plasmid	MobiTec
pJG45-LTA	pJG45-*LTA* (positive control prey)	MobiTec
pTMD49	pCFJ350-*gfp-pcmd-1(cDNA)*	Erpf et al., 2019
pTMD54	pBKS-*pcmd-1(cDNA)*	this work
pTMD66	pET19-*6x-HIS-pcmd-1(aa2-314_ cDNA)*	M. Antoniolli
pTMD71	pBKS-*spd-5(cDNA)*	this work
pTMD72	pEG202-*pcmd-1(cDNA)*	M. Zimmer
pTMD73	pJG45-*pcmd-1(cDNA)*	this work (*)
pTMD74	pBKS-*sas-4(cDNA)*	S. Üstüner
pTMD75	pBKS-*spd-2(cDNA)*	M. Museridze
pTMD78	pCFJ350-*gfp-pcmd-1(T228A_cDNA)*	this work (**)
pTMD79	pCFJ350-*gfp-pcmd-1(T228A, T298A_cDNA)*	this work (**)
pTMD80	pCFJ350-*gfp-pcmd-1(S56A, T228A, T298A_cDNA)*	this work (**)
pTMD81	pCFJ350-*gfp-pcmd-1(S56A, T228A, T298A, S359A_cDNA)*	this work (**)
pTMD84	pJG45-*spd-5(cDNA)*	this work
pTMD85	pBKS-*pcmd-1(bp40-780_cDNA)*	this work (**)
pTMD87	pBKS-*gfp(cDNA)*	this work
pTMD89	pJG45-*sas-7(cDNA)*	this work (**)
pTMD90	pJG45-*spd-2(cDNA)*	this work (**)
pTMD92	pJG45-*sas-4(cDNA)*	this work
pTMD93	pCFJ350-*gfp-pcmd-1(aa2-117_cDNA)*	this work (***)
pTMD94	pJG45-*plk-1(cDNA)*	this work (***)
pTMD95	pCFJ350-*gfp-pcmd-1(aa118-630_cDNA)*	this work (***)
pTMD97	pEG202-*sas-7(cDNA)*	S. Üstüner
pTMD98	pEG202-*pcmd-1_Cterm(aa118-630_cDNA)*	S. Ünüster
pTMD99	pEG202-*pcmd-1_Nterm(aa2-117_cDNA)*	S. Ünüster
pTMD100	pEG202-*pcmd-1(T228A, T298A, S56A, S359A_cDNA)*	this work
pTMD111	pJG45-*pcmd-1(ΔCC_cDNA)*	this work
pTMD115	pJG45-*pcmd-1_C2(aa343-630_cDNA)*	A. Schreiner
pTMD120	pL4440-*sas-4(bp4-1363_cDNA)*	T. Mikeladze-Dvali

Table 4. Oligonucleotides used in this work as primers. The primers were used for cloning, site-directed mutagenesis, sequencing, and genotyping. * gift from B. Conradt laboratory.

Oligo number	Sequence (5' -> 3')
TM_235	cgattcgagtagagctccacgagctgtgatt
TM_242	cacaaacgagcccgcacgga
TM_400	actgttgctgagagcggc
TM_401	gaagaataatcccgcctccc
TM_562	cgtcagcagagcttcacc
TM_557	ctttttaaagactaatttgcagtacaagaacgcg
TM_558	actgcaaattagtctttaaaaagtgcattatgaat
TM_570	gacatttgagaatggcattga
TM_571	tttacaaggacttggataaattgg
TM_585	gagctcatcggcaccgcgcaaagaacgacgaa
TM_586	ttgcgcggtgccgatgagctcagaggcttcggaat
TM_587	atgtcagattgcgccgaaaaagagcgaaaaaaagtc
TM_588	gctctttttcggcgcaatctgacataaatccagtc
TM_589	ggagaaggaagctccgattatgagaaattcg
TM_590	ataatcggagcttccttctccaaactcctgtg
TM_591	accgtacaaatggccccaaccaaaaaaaaattcg
TM_592	tttggttggggccatttgtacggtggatatcg
TM_625	caaaaagtgagaattcggccgactcgagaag
TM_626	ggccgaattctcacttttgcgaatttccttcac
TM_627	tgcctctcccgaggataattctgtgctcaacga
TM_628	gaattatcctcgggagaggcataatctggca
TM_629	tgcctctcccgaagatgatgctccaatgaatctct
TM_630	gcatcatcttcgggagaggcataatctggca
TM_631	tagaaagtaagaattcggccgactcgagaag
TM_632	cggccgaattcttactttctattcgaaaatcttgtattgg
TM_644	ggccgaattctcatttttttccactggaacaaagt
TM_645	ggaaaaaatgagaattcggccgactcgagaag
TM_656	cggccgaattctcaatgattggatagggttc
TM_657	caatcattgagaattcggccgactcgagaag
TM_660	ggccgaattcctatcgacgtgggtgaatattg
TM_661	cacgtcgataggaattcggccgactcgagaagc
TM_669	tgcctctcccgcttccgatgaaaatatcggtg
TM_670	catcggaagcgggagaggcataatctggca
TM_671	tgcctctcccggagaaattccaccgacagac
TM_672	ggaatttctccgggagaggcataatctggca
TM_687	cgaaaattaagctaattccgggcgaatttcttatga
TM_703	cggccgaattcttagtctttaaaaagtgcattatgaataat
TM_704	tgcctctcccgaggtggaatacgacgagg
TM_709	ggaaactgcttcaacgcatcgaggataattctgtgctcaacgag
TM_710	gagcacagaattatcctcgatgcgttgaagcagtttccctgaattaaa
TM_711	gaaattcgcaaaaagatgcaagatcctttcaagcattcccttcttc
TM_712	gcttgaaaggatcttgcatctttttgcgaatttccttcacagc
TM_713	ctcttgctgagtggagatgcc
TM_714	gtattccacctcgggagaggcataatctggca
TM_715	ttaaagactaagaattcggccgactcgagaag
TM_716	catcgattcaactcgtttgc
TM_717	cggagctgctgaatgtgatc
TM_718	gcgctccgttgagaatctcgta
TM_719	atgagtaaaggagaagaactt
TM_722	tttgtatagttcatccatg
TM_723	gcatcatcttcgggagaggcataatctggcacat
TM_729	aatcagacatttgtcaacgacgttacaattgt
TM_730	gtcgttgacaaatgtctgattacggaaagct
TM_731	tgcctctcccaatcgacttcccaacattg

TM_732	gggaagtcgattgggagaggcataatctggcaca
TM_737	aggtggaggtactttcagtaaaaatgccgctc
TM_738	atttttactgaaagtacctccacctcctttg
TM_739	aggtggaggtactgaggtggaatacgacgag
TM_740	gtactgcaaattaattttcgagtaattctttaaaattcttc
TM_741	gtattccacctcagtacctccacctcctttg
TM_742	ttactcgaaaattaatttgcagtacaagaacgc
TM_743	acaaccttgattggagact
TM_749	atgccgactagacttccag
TM_750	ctcataataggtcccacg
TM_751	cgctcacgatcggcattg
TM_753	gctggaattcgaggtggaatacgacgag
TM_754	cggaattagcttagtctttaaaaagtgcattatg
TM_756	attccacctcgaattccagccagtcgcc
TM_761	cataagaaattcgcccgg
TM_771	gtcaatattaagcagtaaaaatgccgct
TM_772	ggcatttttactgcttaatattgacaatttag
CMo24 *	ttgtaaaacgacggccag
CMo25 *	catgattacgccaagcgc

2.1.2 Plasmid generation

DNA was amplified by polymerase chain reaction (PCR) using the Phusion High Fidelity Polymerase kit (New England Biolabs, Cat. No. E0553). The NucleoSpin™ Gel and PCR Clean-up kit (Marchery-Nagel, Cat. No. 740609) was used for gel purification of PCR products. Gibson assembly was performed using the Gibson Assembly® Master Mix (New England Biolabs, Cat. No. E2611) or the NEBuilder® HiFi DNA Assembly Master Mix (New England Biolabs, Cat. No. E2621).

2.1.2.1 Cloning strategy for RNAi plasmids

For the generation of dsRNA against *gfp* and *pcmd-1,* plasmids containing cDNA fragments of *gfp* (pTMD87) and *pcmd-1* (pTMD85) were generated. The *gfp* fragment was amplified from cDNA of the EU3000 (*sas-7(or1940[gfp::sas-7]); itIs37[pie-1p::mCherry::H2B, unc-119(+)])* worm strain by PCR using the primers TM_719 and TM_722 (annealing temperature (T): 52°C, elongation time (t): 30 s). The *pcmd-1* fragment was amplified from plasmid DNA (pTMD49) using the primers TM_235 and TM_401 (annealing T: 66°C, elongation t: 30 s). After gel extraction, the fragments were cloned into the linearized pBluescript II KS(+) vector, which contains the *lacZ* gene, using T4 DNA ligase (New England Biolabs, Cat. No. M0202). After transformation, white colonies were selected through blue-white screening (see chapter **2.1.3**).

2.1.2.2 Cloning strategy for single-copy insertion plasmids

All plasmids used for single-copy insertion of transgenes (see chapter **2.2.4**) were generated based on the original plasmid pCFJ350-*gfp-pcmd-1* (pTMD49) containing the *pcmd-1* full-length cDNA fused to *gfp* at its 5' end flanked by *mai-2* regulatory elements. The plasmid encoding GFP::PCMD-1 with four substituted predicted PLK phospho-binding

sites (see **2.6.2.2**, pTMD81) was cloned in several steps by site-directed mutagenesis. The different mutations were generated by two-step PCRs with an annealing/elongation temperature of 72°C for 10.5 min (16 PCR cycles). Subsequently, the PCR product was treated with the DpnI enzyme (New England Biolabs, Cat. No. R0176) and transformed into bacteria. After the plasmid pTMD49 was used as an initial template to introduce the first mutation, the three other mutations were introduced step-by-step using the previously generated plasmid as a template (**Table 5**).

Table 5. Site-directed mutagenesis of the pCJF350-*gfp-pcmd-1* plasmid used for MosSCI. Plasmid number, plasmid name, substitutions, template, and the primer pairs are listed.

Plasmid number	Plasmid name	Substitution	Plasmid template	Primer pair
pTMD78	pCJF350-*gfp-pcmd-1(T228A_cDNA)*	T228A	pTMD49	TM_585, TM_586
pTMD79	pCJF350-*gfp-pcmd-1(T228A, T298A_cDNA)*	T298A	pTMD78	TM_587, TM_588
pTMD80	pCJF350-*gfp-pcmd-1(S56A, T228A, T298A_cDNA)*	S56A	pTMD79	TM_589, TM_590
pTMD81	pCJF350-*gfp-pcmd-1(S56A, T228A, T298A, S359A_cDNA)*	S259A	pTMD80	TM_591, TM_592

The plasmids encoding the truncations of *gfp-pcmd-1*, both the N-terminal part (pTMD93) and the C-terminal part (pTMD95), were cloned by pursuing a similar strategy. Two PCR fragments were amplified with overhangs by PCR, increasing the annealing T after five cycles (**Table 6**). Both the backbone and the insert were amplified from the pTMD49 plasmid. After the PCR products were gel purified, the fragments were joined by Gibson assembly.

Table 6. Gibson assembly of the truncated versions of *gfp-pcmd-1* used for MosSCI. Plasmid number, plasmid name, and primer pairs used for cloning, including annealing temperatures and elongation times, are listed.

Plasmid number	Plasmid name	Primer pair insert (annealing T, elongation t)	Primer pair backbone (annealing T, elongation t)
pTMD93	pCJF350-*gfp-pcmd-1 (aa2-117_cDNA)*	TM_739, TM_740 (57°C (5x)/ 72°C (30), 50 s)	TM_741, TM_742 (59°C (5x)/ 72°C (30x), 10 min)
pTMD95	pCJF350-*gfp-pcmd-1 (aa118-630_cDNA)*	TM_737, TM_558 (56°C (5x)/66°C (30x), 1.5 min)	TM_557, TM_738 (58°C (5x)/72°C (30x), 10 min)

2.1.2.3 Cloning strategy for yeast two-hybrid plasmids

The bait plasmid pTMD100 (pEG202-*pcmd-1(T228A, T298A, S56A, S359A)*) was cloned by amplifying two fragments with overhangs. The insert was amplified without the start codon from the pTMD81 plasmid using the primers TM_753 and TM_754 (annealing T: 60°C (5x) / 66°C (25x), elongation t: 2 min). The backbone fragment was amplified from the pTMD92 plasmid (pEG202-*pcmd-1*) using the primers TM_687 and TM_756 (annealing

T: 64°C (5x)/ 68°C (25x), elongation t: 10 min). After the PCR products were gel purified, the fragments were joined by Gibson assembly. The other bait plasmids (pTMD72, pTMD81, pTMD98, pTMD99) were cloned by other laboratory members (**Table 3**). Inserts of all bait plasmids were sequenced with the primers TM_562 and TM_761.

The prey plasmids were cloned by pursuing a similar strategy. The backbone fragments and the full-length cDNA fragments without a start codon were amplified with overhangs by PCR and different primer pairs (**Table 7**). The empty pJG45 vector was used as a template for the backbones, while different cDNA templates were used for the inserts (**Table 7**). After the PCR products were gel purified, the fragments were joined together by Gibson assembly. Before the plasmids pTMD73, pTMD84, pTMD90, and pTMD92 were generated, the inserts were cloned into the linearized pBluescript II KS (+) vector using the same primers for the inserts as for the final cloning (**Table 7**). The generated plasmids (pTMD54, pTMD71, pTMD74, pTMD75) were used as templates. The template pTMD75 contained a point mutation, which was transferred to the plasmid pTMD90 via PCR. The mutation was removed by site-directed mutagenesis using the primer pair TM_729 and TM_730 (annealing T: 72°C, elongation t: 8 min, PCR cycles: 16) and subsequent DpnI enzyme (New England Biolabs, Cat. No. R0176) treatment. The plasmid pTMD111 with a deletion encoding the coiled-coil domain was amplified from pTMD72 (**Table 7**).

All plasmids were transformed into yeast cells (see chapter **2.3.2**).

Table 7. Gibson assembly of prey plasmids used in the Y2H assay. Plasmid numbers, plasmid names, templates, primer pairs (including annealing temperatures and elongation times) are listed.

Plasmid number	Plasmid name	Template used for insert	Primer pair insert (annealing T, elongation t)	Primer pair backbone (annealing T, elongation t)
pTMD73	pJG45-*pcmd-1(cDNA)*	pTMD54	TM_703, TM_704 (62°C (5x)/ 72°C (25x), 2.25 min)	TM_714, TM_715 (69°C (5x)/ 72°C (25x), 6 min
pTMD84	pJG45-*spd-5(cDNA)*	pTMD71	TM_626, TM_627 (69°C (5x)/ 72°C (25x), 3.5 min)	TM_628, TM_625 (69°C (5x)/ 72°X (25x), 6.5 min)
pTMD89	pJG45-*sas-7(cDNA)*	cDNA	TM_656, TM671 (61°C (5x)/ 72°C (30x), 3min)	TM_657, TM_672 (66°C (5x)/ 72°C(30x), 5 min)
pTMD90	pJG45-*spd-2(cDNA)*	pTMD75	TM_629, TM_632 (68°C (5x)/ 72°C (25x), 2 min)	TM_630, TM_723 (66°C (5x)/ 72°C(30x), 5 min)
pTMD92	pJG45-*sas-4(cDNA)*	pTMD74	TM_644, TM_669 (67°C (5x)/ 72°C (30x), 2.5 min)	TM_645, TM_670 (68°C (5x)/ 72°C (30x), 6 min)
pTMD94	pJG45-*plk-1(cDNA)*	cDNA	TM_660, TM_731 (59°C (5x)/ 71°C (25x), 2 min)	TM_661, TM_732 (69°C (5x)/ 72°C (25x), 6 min)
pTMD111	pJG45-*pcmd-1(ΔCC_cDNA)*	pTMD72	TM_771, TM_772 (54°C (5x)/66°C(30x), 9 min)	

2.1.3 Bacterial transformation

E. coli DH5α cells (Thermo Fisher Scientific) were transformed with the Gibson assembly reaction (5µl) or plasmid DNA (1 µl). The bacterial cells were incubated on ice for 20 min and heat-shocked at 42°C for 45 sec. After 2 min incubation on ice, 1 ml LB (lysogeny broth) medium (10% Bacto™ Tryptone, 5% yeast extract, 10% NaCl, pH 7.5) was added, and the cells were incubated at 37°C and 200 rpm for 30 min. After the cell suspension was centrifuged at 6000 rcf for 1 min, the pellet was resuspended in 200 µl sterile $_{dd}H_2O$ and spread on LB agar plates (10% Bacto™ Tryptone, 5% yeast extract, 10% NaCl, 15% agar, pH 7.5) containing carbenicillin (100 µg/ml). For blue-white screening, 50 µl of 0.1 M Isopropyl-β-D-thiogalactopyranoside (IPTG, Carl-Roth, Cat. No. CN08.2) and 50 µl of 20 mg/ml 5-Brom-4-chlor-3-indoxyl-β-D-galactoside (X-β-gal, Carl-Roth, Cat. No. 2315.3) were freshly spread on the carbenicillin selection plates. The plates were incubated at 37°C overnight.

2.1.4 Plasmid isolation

For the isolation of low quantities of plasmid DNA, the standard alkaline lysis method was performed. Transformed colonies were picked from antibiotic selection plates, and 2 ml LB medium was inoculated and incubated at 37°C and 220 rpm overnight. The overnight culture was centrifuged at 10000 rcf for 5 min, and the pellets were resuspended in 100 µl Solution I (25 mM Tris-HCl pH 8.0, 10 mM ethylenedinitrilotetraacetic acid (EDTA), 50 mM glucose). Subsequently, 200 µl of Solution II (0.2 M NaOH, 1% sodium dodecyl sulfate-polyacrylamide (SDS)) was added, and tubes were inverted, followed by 5 min incubation on ice. After the addition of 150 µl Solution III (5 M KO acetate, pH 4.8), cells were centrifuged at 10000 rpm and 4°C for 5min. Next, the supernatant was transferred to a new tube, and 70% ethanol was added for DNA precipitation, followed by centrifugation at 12000 rpm and 4°C for 10 min. After washing the pellet with 96% ethanol, it was air-dried for 30 min and resuspended in 50 µl $_{dd}H_2O$. Alternatively, for clean plasmid preps and high quantities of plasmid DNA, the plasmid preparation was performed with the Qiaprep Spin Miniprep kit (Qiagen, Cat. No. 27104) or the Plasmid Midi Kit (Qiagen, Cat. No. 12143). For sequencing, 50-100 ng plasmid DNA was sequenced (Genomic Service Unit, LMU Biozentrum).

2.2 *C. elegans* strains and methods

2.2.1 *C. elegans* strains, general maintenance, and experimental use

C. elegans strains were maintained on nematode growth medium (NGM) agar plates seeded with *E. coli* OP50 (Caenorhabditis Genetics Center) as a nutrition source at 15°C or 25°C, as previously described (Brenner, 1974). The OP50 *E. coli* were grown in B. Broth

(10 g/l Bacto™ Tryptone, 5 g/l NaCl, pH to 7.0). The Bristol N2 isolate was used as the wild-type reference. The alleles and transgenes generated and used in this study are listed in **Table 8**.

For experimental use, parental worms were shifted to 25°C in the L4 larval stage for 16 to 20 hours. Experiments with the strain TMD123 were conducted differently. Young adults of the TMD123 strain (*pcmd-1(syb486[gfp::pcmd-1]);unc-32(e189) sas-7(or452)/qC1[dpy-19(e1259) glp-1(q339)])* were allowed to lay eggs at 25°C for 3 hours. The eggs from the layoff developed into adults at 25°C within 68 hours. The progeny of *pcmd-1(syb486[gfp::pcmd-1]);unc-32(e189) sas-7(or452)* worms without the *qC1* balancer were used for further analysis.

For harvesting, washing, and keeping worms in liquid for microscopy experiments, M9 buffer (3 g/l KH_2PO_4, 5.8 g/l Na_2HPO_4, 0.5 g/l NaCl, 1 g/l NH_4Cl) or MPEG (M9 buffer with 0.1% polyethylene glycol (PEG) 8000 (Carl Roth, Cat. No. 0263)) were used. For long-term storage, worms were harvested with M9 and frozen with an equal volume of 2x freezing solution (0.1 M NaCl, 0.05 M KH2PO4, 30% glycerol, pH 6; freshly added 30 µl 1M $MgSO_4$ in 100 ml solution).

Table 8. *C. elegans* strains used in this work. Strain names, genotypes, and origin of the strains are listed.

Strain name	Genotype	Origin
N2	*wild-type; Bristol isolate*	Caenorhabditis Genetics Center
EG6699	*ttTi5605 II; unc-119(ed3) III; oxEx1578*	Caenorhabditis Genetics Center
EU2836	*unc-32(e189) sas-7(or452) / qC1[dpy-19(e1259) glp-1(q339)] III*	Caenorhabditis Genetics Center
EU3000	*sas-7(or1940[gfp::sas-7]) III; itIs37[P_{pie-1}mCherry::H2B, unc-119(+)] IV*	Caenorhabditis Genetics Center, Sugioka et al., 2017
GZ1522	*sas-7(is1[rfp::sas-7+loxP]) III; glo-1(zu931) X*	Klinkert et al., 2019
PHX486	*pcmd-1(syb486[gfp::pcmd-1]) I*	Sunnybiotech
PHX980	*pcmd-1(syb975)/hT2 I*	Sunnybiotech
PHX1285	*pcmd-1(syb1285 (syb486[gfp::pcmd-1]) I*	Sunnybiotech
TMD44	*pcmd-1(t3421) I (7x outcrossed)*	Erpf et al., 2019
TMD92	*mikSi6[P_{mai-2} gfp:: pcmd-1::mai-2] II*	Erpf et al., 2019
TMD94	*mikSi7[P_{mai-2} gfp::pcmd-1(t3421)::mai-2] II*	Erpf et al., 2019
TMD95	*mikSi8[P_{mai-2} pcmd-1(t3421)::gfp::mai-2] II*	Erpf et al., 2019
TMD101	*pcmd-1(t3421) I; mikSi6[P_{mai-2} gfp::pcmd-1::mai-2] II*	Erpf et al., 2019
TMD102	*pcmd-1(t3421) I; mikSi7[P_{mai-2} gfp::pcmd-1(t3421) ::mai-2] II*	Erpf et al., 2019
TMD103	*mikSi9[P_{mai-2} pcmd-1::gfp::mai-2] II*	Erpf et al., 2019
TMD107	*pcmd-1(t3421) I; sas-7(or1940[gfp::sas-7]) III; ltIs37 [(pAA64) P_{pie-1}mCherry::his-58 +unc-119(+)] IV*	this work

TMD117	*pcmd-1(t3421) I;* *mikSi9[P_{mai-2} pcmd-1::gfp::mai-2] II*	this work, Erpf et al., 2019
TMD118	*pcmd-1(t3421) I;* *mikSi8[P_{mai-2} pcmd-1(t3421)::gfp::mai-2] II*	this work, Erpf et al.,2019
TMD119	*pcmd-1(syb486[gfp::pcmd-1]) I* *(1x outcrossed)*	Erpf et al., 2019
TMD120	*spd-2(or293) I;* *pcmd-1(syb486[gfp::pcmd-1]) I*	Erpf et al., 2019
TMD121	*spd-5(or213) I;* *pcmd-1(syb486[gfp::pcmd-1]) I*	Erpf et al., 2019
TMD123	*pcmd-1(syb486[gfp::pcmd-1]) I;* *unc-32(e189) sas-7(or452) / qC1[dpy-19(e1259) glp-1(q339)] III*	this work
TMD141	*pcmd-1(syb486[gfp::pcmd-1]) I;* *sas-7(is1[rfp::sas-7+loxP]) III;* *glo-1 (zu931) X*	this work
TMD145	*pcmd-1(syb975) I*	T. Mikeladze-Dvali
TMD151	*pcmd-1(t3421) I; ltSi202[pVV103/pOD1021; P_{spd-2}gfp::spd-5_RNAi-resistant;* *cb-unc-119(+)] II;* *mikSi11[$P_{hs16.41}$PH::mKate2::pcmd-1::tbb-2] IV*	S. Üstüner
TMD152	*pcmd-1(t3421) I;* *mikSi14[P_{mai-2} gfp::pcmd-1_ N(1-117)::mai-2] II*	S. Üstüner
TMD153	*pcmd-1(t3421) I;* *mikSi15[P_{mai-2} gfp::pcmd-1_C(118-630)::mai-2] II*	S. Üstüner
TMD154	*pcmd-1(t3421) I;* *mikSi13[P_{mai-2}* *pcmd-1((S56A,T228A,T298A,S359A)::mai-2] II*	this work, E. Zuccoli
TMD157	*ltSi202[pVV103/pOD1021;* *P_{spd-2}gfp::spd-5_RNAi-resistant; cb-unc-119(+)] II*; *mikSi11[$P_{hs16.41}$ph::mkate2::pcmd-1::tbb-2] IV*	S. Üstüner, T. Mikeladze-Dvali
TMD158	*plk-1(lt18[plk-1::sGFP]::loxp) III;* *mikSi11[$P_{hs16.41}$ph::mkate2::pcmd-1::tbb-2] IV*	this work
TMD159	*pcmd-1(t3421) I; sas-7(or1940[gfp::sas-7]) III;* *mikSi11[$P_{hs16.41}$ph::mkate2::pcmd-1::tbb-2] IV*	S. Üstüner
TMD164	*pcmd-1(t3421);mikSi6[P_{mai-2} gfp::pcmd-1::mai-2] II; mikSi11[$P_{hs16.41}$ph::mkate2::pcmd-1::tbb-2] IV*	M. Plotnikova, T. Mikeladze-Dvali
TMD165	*pcmd-1(t3421) I; mikSi6[P_{mai-2} gfp::pcmd-1::mai-2] II; ltIs37 [(pAA64)* *P_{pie-1}mCherry::his-58+unc-119(+)] IV*	M. Plotnikova, T. Mikeladze-Dvali
TMD166	*pcmd-1(t3421) I;* *mikSi15[P_{mai-2}gfp::pcmd-1_C(118-630)::mai-2] II;* *ltIs37 [(pAA64) P_{pie-1}mCherry::his-58 + unc-119(+)] IV*	M. Plotnikova, T. Mikeladze-Dvali
TMD167	*pcmd-1(t3421) I;* *svieSi[pAD154;P_{sas-4}gfp:sas-4_reencoded;* *cb-unc-119(+)] II;* *mikSi11[$P_{hs16.41}$ph::mkate2::pcmd-1::tbb-2] IV*	E. Zuccoli, T. Mikeladze-Dvali
TMD168	*pcmd-1(t3421) I;* *plk-1(lt18[plk-1::sgfp]::loxp) III;* *mikSi11[$P_{hs16.41}$ph::mkate2::pcmd-1::tbb-2] IV*	this work
TMD175	*pcmd-1(t3421) I;* *mikSi15[P_{mai-2}gfp::pcmd-1_C1(118-342)::mai-2] II;* *itIs37[P_{pie-1}mCherry::h2b, unc-119(+)] IV*	A. Schreiner, T. Mikeladze-Dvali
TMD177	*pcmd-1(t3421) I;* *mikSi15[P_{mai-2}gfp::pcmd-1_C2(343-630)::mai-2] II;* *itIs37[P_{pie-1}mCherry::h2b, unc-119(+)] IV*	A. Schreiner, T. Mikeladze-Dvali

2.2.2 Preparing genomic DNA for genotyping

For genotyping single worm lysis was performed in 20 µl worm lysis buffer (50 mM KCl, 10 mM Tris pH 8.2, 2.5 mM $MgCl_2$, 0.45% Nonidet P-40, 0.45% Tween20, 0.01% gelatine) with freshly added 0.2 µl Proteinase K (20 mg/ml, AppliChem, Cat. No. A3830). Lysates were incubated for 10 min at -80°C. Subsequently, the samples were incubated at 65°C for 1 hour and heat-inactivated at 95°C for 20 min.

2.2.3 Genotyping of CRISPR/Cas9 edited *C. elegans* strains

The *pcmd-1(syb975)/hT2* allele (PHX980), which was supposed to contain a 1201 bp deletion from the start codon, was verified by performing PCR with two different primer pairs. As a negative control, the primer pair TM_242 and TM_400, which binds inside the deletion, was used for amplification (annealing T: 56°C, elongation t: 1 min). The fragment of interest was amplified with the primers TM_718 and TM_242 (annealing T: 56°C, elongation t: 1 min), which annealed outside the deletion. Subsequently, the amplified product was sequenced (Genomic Service Unit, LMU Munich).

The *pcmd-1(syb1285 syb486[gfp::pcmd-1(ΔCC)])* allele (PHX1285), which was supposed to contain a 99 bp deletion encoding 33 amino acids from E86 including F118 spanning the coiled-coil domain (E86-N117, see chapter **2.6.2.2**), was verified by performing PCR and subsequent sequencing (Genomic Service Unit, LMU Munich). The amplification of the fragment of interest was performed using the primer pair TM_402 and TM_522 (annealing T: 55°C, elongation t: 1 min).

2.2.4 Mos1-mediated Single-Copy Insertion (MosSCI)

Single copies of the plasmids pTMD93, pTMD95, and pTMD81 were inserted into the *C. elegans* genome. Therefore, the plasmid DNA was micro-injected into the gonad of young adults of the EG6699 strain (*ttTi5605; unc-119(ed3); oxEx1578*) for targeted MosSCI insertion into chromosome II to generate new alleles according to the standard protocol (performed by T. Mikeladze-Dvali) (Frøkjær-Jensen et al., 2014). The generated strains were screened according to the standard protocol. Screening for potential insertions at chromosome II was performed by PCR using the primers TM_570 and TM_571 (annealing T: 56°C, elongation t: 2 min).

2.2.5 RNA interference in *C. elegans*

2.2.5.1 RNAi by feeding

For RNAi against *sas-4*, the plasmid pTMD120 was transformed into *E. coli* HT115(DE3) cells (see chapter **2.1.3**) (Timmons et al., 2001). The clone was selected on LB agar plates (10% Bacto™ Tryptone, 5% yeast extract, 10% NaCl, 15% agar, pH 7.5)

containing carbenicillin (100 µg/ml) and tetracycline (12.5 µg/ml). The *mock* clone (pL4440 in *E.coli* HT115(DE3)) served as a negative control (Kamath and Ahringer, 2003). After restreaking the *mock* and the *sas-4* RNAi clones, LB medium containing carbenicillin (100 µg/ml) was inoculated with a single colony, respectively. RNAi clones were grown at 37°C and 200 rpm overnight. The starter culture was diluted and grown to a final OD600 ranging between 0.6 and 0.9. The *sas-4(RNAi)* plasmid expression was induced by 0.1 M IPTG (Carl-Roth, Cat. No. CN08.2). The cultures were kept for 30 min at RT before seeding them to the standard NGM plates (Brenner, 1974) supplemented with 6 mM IPTG (Carl-Roth, Cat. No. CN08.2) and carbenicillin (100 µg/ml). L4 larval stage worms were transferred to new IPTG plates seeded with *E. coli* HT115 containing the RNAi plasmids. L4 larval stage worms were placed onto the IPTG plates three days after seeding the bacterial cells. The worms were allowed to feed for 28-33 hours at 25°C to generate a hypomorphic phenotype. The progeny was used for analysis by microscopy (see chapter **2.5.3**).

2.2.5.2 RNAi by microinjection

For dsRNA generation, *gfp* and *pcmd-1* targeting regions were amplified from plasmid DNA. The plasmid pTMD87 was used as a template for *gfp,* and the plasmid pTMD85 was used as a template for *pcmd-1*. For both amplifications, the T3/T7 primer pair CMo24 and CMo25 (annealing T: 50°C, elongation t: 1 min) and the Standard Taq polymerase (New England Biolabs, Cat. No. M0273) were used. The PCR products were gel purified using the QIAEX II Gel Extraction kit (Qiagen, Cat. No. 20021). According to the manufacturer's protocol, dsRNA was transcribed *in vitro* from the PCR products using the MEGAscript T3 and T7 kits (Thermo Fisher Scientific, Ambion, Cat. No. AM1338 and AM1333). After incubating the reaction at 37°C for 15 hours, 0.5 µl of the reaction was run on an 0.8% agarose gel containing GelRed® Nucleic Acid Gel Stain (Biotium, Cat. No. 41003) to estimate the amount of ssRNA. The dsRNA was synthesized by mixing T7 ssRNA with T3 ssRNA in a 1:3 ratio, heating the mixtures at 75°C for 5 min, and cooling them down at RT. The samples were run on an 0.8% agarose gel containing GelRed® Nucleic Acid Gel Stain to visualize the dsRNA, and the concentrations were measured with a Nanophotometer (Implen P330). The dsRNAs were frozen at -80°C for further use in microinjection in the worms. Young adults of the strain TMD119 (*pcmd-1(syb486[gfp::pcmd-1])*) were injected with dsRNA against *pcmd-1* and *gfp* (concentration: ~ 0.4 µg/ml; with the help of Nadine Memar). Injected worms were placed on NGM plates at 25°C for 46 hours and transferred to new plates after 18, 24, 39 hours. Embryonic lethality was monitored after three days.

2.2.6 Embryonic survival assay

L4 stage worms were maintained at either 25°C or 15°C. When the embryonic survival assay was performed at 25°C, the worms were singled on NGM plates with freshly seeded OP50 bacteria the next day after approximately 16 hours. After the worms laid eggs for 4 hours, the worms were transferred to a second plate, and the laid eggs were counted. Then the worms were allowed a second time to lay eggs for 4 hours, the mother worms were removed from the second plate, and the laid eggs were counted. Finally, the hatched worms were counted 24 hours later. When the embryonic survival assay was performed at 15°C, the worms laid eggs for 24 hours, and the eggs were counted.

2.2.7 Translocation assay

L4 larval stage worms, which carry the Mos1-mediated Single-Copy inserted PH::mkate2::PCMD-1 under a heat-shock promoter (TMD151, TMD157, TMD158, TMD159, TMD164, TMD167, TMD168), were shifted to 25°C and incubated for 15 to 16 hours until they developed into adults. The adult worms laid eggs for 2 hours at 25°C. The embryos were directly picked from the seeded bacteria and mounted in a 5 µl M9 buffer onto a 2% agarose square. Subsequently, embryos were covered with an 18 mm^2 coverslip, and the edges were sealed with vaseline. Slides were incubated at 30°C for 1 hour (Bio-Rad thermocycler, incubation T: 30°C; lid T: 40°C). The heat-shock treatment was followed by 2 hours recovery at 20°C in an incubator. No heat shock was performed for control embryos, which were instead directly incubated at 20°C for 2 hours. Images from embryos were taken at the SP5 Leica confocal microscope (see chapter **2.5.1**). Embryos were defined as GFP positive when a GFP signal was visible as a defined line at the plasma membrane of at least two cells.

2.2.8 Immunofluorescence staining of *C. elegans* embryos

Immunofluorescence (IF) stainings were performed according to a previously published freeze-cracking protocol (Delattre et al. 2004). 15-20 adult worms grown overnight at 25°C were dissected in 5 µl M9 buffer on a microscope slide, which was beforehand coated with poly-D-lysine (1 mg/ml) and put onto a heating plate for polymerization. The worms were dissected, covered with a coverslip, and placed on a pre-cooled metal block for 10 to 20 min. The coverslip was removed with a razor blade to crack the eggshells of the embryos. Subsequently, slides were fixed in -20°C cold methanol for 2 to 20 min. After two wash steps in a chamber with PBS (0.137 M NaCl, 2.7 mM KCl, 0.01 M Na2HPO4, 1,8 mM KH2PO4, pH 7.4) for 5 min, cells were blocked with 2% bovine serum albumin (BSA) dissolved in phosphate-buffered saline (PBS) for 20 min. Slides were washed twice for 5 min, first in a chamber with PBST (PBS, 0.05% Tween20) and second in a chamber with PBS. Excess PBS was removed, and a square of ~18 mm^2 PBS with the fixed embryos and parts of the worms was left. Embryos were incubated in 50 µl of the primary

antibodies (**Table 9**) diluted in PBS overnight at 4°C in a humid chamber. After another two 5 min wash steps in chambers with PBS-T and PBS, PBS was wiped off, as described above. Embryos were incubated in a drop of 50 µl of the secondary antibodies (**Table 10**) together with Hoechst diluted in PBS (1:1000 of 1 mg/ml, Hoechst, Sigma-Aldrich, Cat. No. B2883) for 1 hour at RT. The slides were washed for 10 min in a PBS chamber. Access PBS was removed, as described above. The slide was placed inversely onto an 18 mm^2 coverslip with 6 µl mounting medium (4% n-Propyl-Gallate, 90% glycerol, 1x PBS), and the edges were sealed with transparent nail polish. The slides were stored at 4°C until imaging. Slides were imaged using a confocal microscope (see chapter **2.5.1**), and images were processed using Fiji software 2.0.0 (Schindelin et al., 2012).

Table 9. Primary antibodies used for immunofluorescence staining. Animal sources, working dilutions, and manufacturers/origins are listed.

Primary antibody	Species	Dilution	Manufacturer/Origin
anti-IFA (human GFAP)	mouse	1:50	a generous gift from P. Gönczy (Leung et al., 1999; Pruss et al., 1981)
anti-GFP	mouse	1:200	Sigma-Aldrich, Cat. No. 11814460001 (initially generated by Roche)
anti-SAS-4	rabbit	1:500	Santa Cruz Biotechnology, Cat. No. sc-98949
anti-SPD-5 (MEDNSVLNEDSNL)	rabbit	1:500	a generous gift from B. Bowerman (Hamill et al., 2002)

Table 10. Secondary antibodies used for immunofluorescence staining. Animal sources, working dilutions, and manufacturers are listed.

Secondary antibody	Species	Dilution	Manufacturer
Goat anti-mouse Alexa488	goat	1:500	Invitrogen Molecular Probes/ThermoFisher, Cat. No. A11001
Goat anti-rabbit Alexa568	goat	1:500	Invitrogen Molecular Probes/ThermoFisher, Cat. No. A11011

2.2.9 Harvesting *C. elegans* for biochemical experiments

For probing *C. elegans* proteins in Western blot, worms were maintained on NGM plates (Ø 10 cm) until seeded bacteria were almost devoured, and most of the worms reached the adult or embryonic stage. Plates were shifted for 3 to 5 hours to 25°C. Mixed-stage worms were rinsed off the NGM plates with MPEG and were allowed to sediment through gravity on ice for at least 30 min. The worm pellet was washed three times with M9, and after each step, the worms were allowed to sediment through gravity on ice. The equal volume of 2x Laemmli buffer (100 mMTris-HCl, pH 6.8, 4% SDS, 20% glycerol, 0.014% β-mercaptoethanol, 0.01% saturated bromphenol blue) was added to the worm pellet. The samples were denatured at 95°C for 5 min and sonicated for 20 min at 60°C (Bandelin

Sonorex Digitec). The samples were centrifuged at 13.000 rpm for 30 s. The supernatant was loaded onto SDS-gels (see chapter **2.4.1**).

2.3 *Saccharomyces cerevisiae* methods

2.3.1 Culturing and handling of *S. cerevisiae*

Saccharomyces cerevisiae (*S. cerevisiae*) EGY48 cells (MATα, trp1, his3, ura3, leu2::6 LExAop-LEU2) were handled in sterile conditions. The strain is distinguished by the genome integrated LEU2 reporter gene, which contains six copies of the LexA operator. The cells were grown in liquid YPD (1% yeast extract, 2% Bacto™ Peptone, 2% D-glucose, pH 5.5) medium at 30°C while shaking at 160 rpm or on YPD agar plates at 30°C. The transformed S. cerevisiae EGY48 cells were grown in liquid Drop-out Base (DOB) medium or on DOB agar plates for plasmid selection. Depending on the selection, the DOB medium was prepared with two different DOB mixes (**Table 11**) with either glucose (6.7 g/l yeast nitrogen base, 2% D-glucose, pH 5.5) or galactose and raffinose (6.7 g/l yeast nitrogen base, 2% galactose, 1% raffinose, pH 5.5) as a sugar source. The DOB media were supplemented with the desired amino acids as auxotrophic markers (**Table 12**) to select transformed plasmids. Therefore, stock solutions were prepared and sterile filtered. When agar was prepared, 2% agar was added.

Plates with grown cells were stored at 4°C. For long-term storage, cells were grown on an agar plate to a high density. The cells were transferred and resuspended in 500 µl of sterile 15% glycerol (diluted in $_{dd}H_2O$). The vial was vortexed and stored at -80°C.

Table 11. Drop-out mixes used for DOB media/agar. Final concentrations and the manufacturers are listed.

Drop-out Mix	Final concentration	Manufacturer
Drop-out Mix Synthetic w/o Adenine, Histidine, Leucine, Tryptophan, Uracil	1.37 g/l	US Biological Life Sciences, Cat. No. 9540-05
Drop-out Mix Synthetic w/o Arginine, Histidine, Leucine, Uracil	1.4 g/l	US Biological Life Sciences, Cat. No. 9539-09

Table 12. Amino acids used as auxotrophic markers. Final and stock concentrations are indicated.

Amino acid	Stock concentration	Final concentration
Adenine	2 mg/ml	20 mg/l
Arginine	10 mg/ml	20 mg/l
Leucine	10 mg/ml	60 mg/l
Tryptophan	10 mg/ml	20 mg/l
Uracil	2 mg/ml	20 mg/l

2.3.2 Transformation of *S. cerevisiae*

For the transformation of *S. cerevisiae,* 5 ml of YPD or DOB medium was inoculated with a single colony and grown overnight. The starter culture was diluted to OD_{600} 0.25 in an appropriate medium and grown until an OD_{600} between 0.8 and 1 was reached. The yeast cells were harvested by centrifugation at 5000 rpm for 3 min (5 ml per transformation). Next, the pellet was resuspended using 1 ml 100 mM lithium acetate. After another centrifugation, a master mix of the following reagents was prepared and then added to the pellet: 240 µl 50% (w/v) PEG3500, 34 µl $_{dd}H_2O$, 10 µl carrier DNA, and 36 µl 1 M lithium acetate. Salmon sperm DNA (10 mg/ml dissolved in 10 mM Tris HCl pH 8.5 and 1 mM EDTA pH 8.0; AppliChem, Cat. No. APA2159.0001) was used as a carrier DNA and boiled at 95°C for 5 min before use. The pellet was resuspended by vortexing, and 200 ng of plasmid DNA was added. After vortexing, the cell suspension was incubated at 30°C while slowly agitating at 400 rpm for 30 min. Next, the cell suspension was heat-shocked at 42°C for 15 min. Subsequently, cells were centrifuged at 5000 rpm for 3 min, and the pellet was resuspended in 100 µl $_{dd}H_2O$. The cell suspension was plated on appropriate agar plates. The different plasmids were selected with DOB media lacking histidine, uracil, tryptophan, and leucine.

2.3.3 Yeast two-hybrid assay

According to the manufacturer's protocol, the Y2H assay was performed using the Grow'N'Glow GFP Yeast two Hybrid System (Mobitech, Cat. No. GNGK01).

2.3.3.1 Leu2 autoactivation assay

To exclude that the bait protein autoactivates the reporter gene, a Leucine2 autoactivation assay was performed after transforming the different bait plasmids (pTMD72, pTMD92, pTMD97, pTMD98, pTMD100) and the pEG202-*Gal4* plasmid, which was used as a positive control due to its autoactivation activity. First, single colonies of bait strains were resuspended in 500 µl $_{dd}H_2O$ and vortexed. The concentration was reduced by serial dilution in $_{dd}H_2O$ (1:10 and 1:100). Next, the diluted cell suspensions were vortexed, and 100 µl of the cell suspension was plated on galactose/raffinose DOB agar plates lacking histidine or lacking histidine and leucine. After two days, the plates were checked for growth, and images were acquired with the ChemiDoc XRS+ Documentation System (Bio-Rad). If cells were growing only on the plates lacking histidine, the *gfp* reporter plasmid pGNG1 was transformed in the next step.

2.3.3.2 GFP autoactivation assay

After strains containing the bait plasmid were transformed with the *gfp* reporter plasmid pGNG1, it was tested whether the expression of the bait plasmids and the *gfp* reporter led to autoactivation. The pGNG1 plasmid was selected through the URA3 selection

marker on galactose/raffinose DOB media lacking histidine, uracil, and leucine. Single colonies were restreaked, and green light emission was checked using a Stereomicroscope (see chapter **2.5.4**). If no GFP signal, and thus no autoactivation, was detectable, prey plasmids were transformed.

2.3.3.3 Protein-protein interaction screening

Prey plasmids (pTMD73, pTMD84, pTMD89, pTMD90, pTMD92, pTMD94, pTMD111, pTMD115) were transformed into the strains expressing bait plasmids together with the *gfp* reporter plasmid. The plasmids pEG202-*p53* with pJG45-*LTA* were positive controls, whereas the empty pJG45 plasmid was used as a negative control. The prey plasmids were selected with a tryptophan marker on glucose DOB agar lacking histidine, uracil, and tryptophan. For the protein-protein interaction assay, a glucose DOB medium lacking histidine, uracil, and tryptophan was inoculated with a single colony and grown overnight. The OD_{600} of the starter cultures were measured, and the cultures were diluted to an OD_{600} of 0.3 in a 5 ml medium. The diluted cultures were grown until OD_{600} 0.7-1.0, and 1 ml of the cultures were centrifuged at 5000 rpm for 3 min. The pellets were washed with $_{dd}H_2O$ and centrifuged for 3 min at 5000 rpm three times. The OD_{600} of the pellet was set to 1, and 1.3 µl of the cell suspensions were pipetted on three different plates. The glucose agar plates lacking histidine, uracil, and tryptophan served as growth control. *S. cerevisiae* colonies growing on galactose/raffinose agar plates lacking histidine, uracil, tryptophan, and leucine are putative positives. To exclude false negatives, growth was also checked on glucose agar plates lacking histidine, uracil, tryptophan, and leucine, where colonies grew when autoactivation occurred. Growth and GFP fluorescence were monitored after three and five days under a Stereomicroscope (see chapter **2.5.4**).

2.3.4 Verification of the *S. cerevisiae* plasmids

To verify that the *S. cerevisiae* strains contain the transformed plasmids, 5 ml glucose DOB medium lacking histidine, uracil, and tryptophan was inoculated with the yeast strain of interest and grown to saturation overnight. The yeast overnight culture was centrifuged at 600 rcf for 4 min. Plasmid extraction was adapted from a standard bacterial plasmid alkaline lysis protocol using the GeneJET™ Plasmid Miniprep Kit (Thermofisher, Cat. No. K0503). The pellet resuspension step was adapted by adding 0.35 g acid-washed glass beads (Sigma-Aldrich, Cat. No. G8772) in addition to 250 µl resuspension buffer to the pellet. After resuspension, the suspension containing the glass beads was mixed at 600 rpm for 5 min. All subsequent steps were performed according to the GeneJET™ Plasmid Miniprep Kit protocol, and the pellet was diluted in 25 µl $_{dd}H_2O$. After plasmid purification, fragments of the bait plasmids were amplified with the primers TM_562 and TM_761 (annealing T: 47°C, elongation t: 1 min/1 kb), and prey plasmids were amplified with the primers TM_713 and TM_743 (annealing T: 47°C, elongation t: 1 min/1 kb) using Taq DNA polymerase with standard Taq buffer (New England Biolabs, Cat. No. M0273).

Enzymatic purification of the PCR products was performed by adding 0.5 µl ExoSap (Affymetrix, Cat. No. 15513687) to 5.5 µl of the PCR product and incubating the reaction at 37℃ for 30 min and 80℃ for 15 min in a thermocycler (Bio-Rad). After adding the primer of interest (1 µl), the sample was sequenced (Genomic Service Unit, LMU Munich).

2.3.5 Preparation of *S. cerevisiae* for biochemical experiments

To analyze the expression levels of the preys, the cells were grown overnight in a galactose/raffinose medium lacking histidine, uracil, and tryptophane. The starter cultures were diluted to OD_{600} 0.25 and grown until an OD_{600} of 2.5. After cells were centrifuged at 5.000 rpm for 5 min, the pellets were washed with $_{dd}H_2O$ and resuspended in 100 µl $_{dd}H_2O$. Subsequently, 100 µl 0.2 M NaOH was added. After vortexing, the samples were incubated at RT for 5 min. The samples were centrifuged, and the supernatant was discarded. The pellet was resuspended in 25 µl 2x Laemmli buffer (100 mMTris-HCl, pH 6.8, 4% SDS, 20% glycerol, 0.014% β-mercaptoethanol, 0.01% saturated bromphenol blue) and incubated at 95°C for 3 min. The samples were centrifuged at 13.000 rpm for 30 s. 5 µl of the supernatant was loaded onto SDS-gels (see chapter **2.4.1**).

2.4 Biochemical methods

2.4.1 SDS PAGE

C. elegans lysates (see chapter **2.2.9**), *S. cerevisiae* lysates (see chapter **2.3.5**), and purified peptide samples (see chapter **2.4.5**) were separated by sodium dodecyl sulfate-polyacrylamide gel electrophoresis (SDS-PAGE) using the Mini-PROTEAN Tetra Cell system (Bio-Rad). The molecular weight (MW) of proteins and peptides was estimated by the Precision Plus Protein™ Dual Color Standard (Bio-Rad, Cat. No.1610374). Proteins were allowed to migrate through the SDS gels (80 V stacking gel, 150 V resolving gel (7.5%, 10% or 12%) in electrophoresis running buffer (25 mM Tris, 190 mM glycine, 0.1% SDS). After protein separation, Coomassie staining or Western blotting were performed.

2.4.2 Coomassie staining

Unspecific staining of proteins separated by SDS-PAGE was performed using Coomassie staining solution (20% ethanol, 10% glacial acetic acid, 10 mg/ml Brilliant Blue R (Sigma-Aldrich, Cat. No. B0149). Gels were incubated in the staining solution for at least 1 hour. This was followed by the destaining of the gels was performed for 2 hours with the destaining solution (50% ethanol, 10% glacial acetic acid), which was exchanged several times. Gels were further destained in $_{dd}H_2O$ overnight at 4°C. Images of the stained SDS gels were acquired using the ChemiDoc XRS+ Documentation System (Bio-Rad).

2.4.3 Western blotting

Separated proteins were transferred to either PVDF membrane (Sigma-Aldrich, Cat. No. IPVH00010), which was activated before in 96% ethanol, or nitrocellulose membrane (Sigma-Aldrich, Cat. No. GE10600001) by wet Western blotting with transfer buffer (20% ethanol, 25 mM Tris, 190 mM Glycine) using the Mini-PROTEAN Tetra Cell system (Bio-Rad). All blotting components were soaked in transfer buffer and were assembled as follows: sponge, Whatman™ Cellulose paper (Hartenstein Laborbedarf, Cat. No. GB3M), membrane, gel, Whatman® Cellulose paper, and sponge. The transfer was performed at 200 mA for 2 hours in a Mini-PROTEAN Tetra Cell system (BioRad) at RT or 4°C. After the protein transfer, the membrane was washed in tris-buffered saline (25 mM Tris, 1.4 M NaCl) with 0.1% Tween20 (TBS-T) for 10 min. Next, the membrane was blocked with 5% non-fat dried milk (Sigma-Aldrich, Cat. No. M7409) in TBS-T at RT for 1 hour. The membrane was incubated with the primary antibody (**Table 13**) diluted in blocking solution at 4°C overnight. Unspecifically bound antibodies were removed by wash the membrane with TBS-T three times for 10 min. Following the incubation with the secondary antibody (**Table 14**) diluted in blocking solution at RT for one hour, the membrane was washed three times for 10 min, twice with TBS-T and once with TBS. The membrane was developed using developing reagents with different sensitivity (**Table 15**). For the detection of the protein bands, the ChemiDoc XRS+ Documentation System (Bio-Rad) was used.

Table 13. Primary antibodies used in Western blotting. Animal sources (species), working dilutions, and manufacturers/origins are listed.

Primary antibody	Species	Dilution	Manufacturer/Origin
anti-GFP	mouse	1:600	Sigma-Aldrich, Cat. No. 11814460001 (initially generated by Roche)
anti-HA tag	rabbit	1:2500	Abcam, Cat. No. ab9110
anti-Histone-H3	mouse	1:2000	ActiveMotif, Cat. No.61475
anti-PCMD-1(16C11)	mouse	1:100	this work
anti-PCMD-1 (18G8)	mouse	1:100	this work
anti-SPD-2 (CNEQFEEIEDSPIDDN DNESFY)	rabbit	1:3000	a generous gift from M. Glotzer (Delattre et al., 2006)
anti-α-tubulin DM1a	mouse	1:7500	Sigma-Aldrich, Cat. No. T6199
His-probe (H-3)	mouse	1:500	Santa Cruz, Cat. No. sc8036

Table 14. Secondary antibodies used in Western blotting. Animal sources (species), working dilutions, and manufacturers are listed.

Secondary antibody	Species	Dilution	Manufacturer
Peroxidase AffiniPure Goat Anti-Mouse IgG, Fcγ fragment specific	goat	1:10000	Jackson ImmunoResearch Europe Ltd., Cat. No. 115035071
Goat Anti-Mouse IgG (H+L)-HRP Conjugate	goat	1:7500	Bio-Rad Laboratories, Cat. No. 1706516
Goat Anti-Rabbit IgG (H+L)-HRP Conjugate	goat	1:7500	Bio-Rad Laboratories, Cat. No. 1721019

Table 15. Western blotting developing reagents. Developing reagents, their sensitivity, and manufacturers are listed.

Developing reagent	Sensitivity	Manufacturer
Amersham ™ECL™ Western Blotting Detection Reagent	up to 10 pg	Sigma-Aldrich, Cat. No. GERPN2236 (originated from Cytiva)
Amersham ™ ECL™ Prime Western Blotting Detection Reagent	up to 1 pg	Sigma-Aldrich Cat. No. GERPN2106 (originated from Cytiva)
SuperSignal™ West Femto Maximum Sensitivity Substrate	up to low fg	Thermo Fisher Scientific, Cat. No. 34095

2.4.4 Bradford assay

The protein concentration was determined by performing a dye-binding assay based on Bradford's protocol (Bradford, 1976). The Quick Start™ Bradford 1x Dye Reagent (Bio-Rad, Cat. No. 5000205) changes in response to different protein concentrations. Samples were diluted in 1 ml of the Bradford reagent and incubated at RT for 5 min. The absorption was measured at 595 nm, and the protein concentration was calculated using a calibration curve with BSA.

2.4.5 PCMD-1 peptide purification for antibody generation

2.4.5.1 Transformation via electroporation

SoluBL21 competent *E. coli* cells were transformed with the pTMD66 plasmid. Therefore, 1 µl plasmid DNA was added to 50 µl of the competent cells and transferred to a sterile cuvette. The cell suspension was electroporated with 2.5 V using the Gene Pulser machine (Bio-Rad). Transformed bacterial cells were immediately transferred to a tube containing 500 µl SOC medium (10 mM NaCl, 0.5% yeast extract, 2% Bacto™ Tryptone, 2.5 mM KCl, 10mM KCl, 10 mM $MgCl_2$, 10mM glucose, pH 7.0) and were incubated at 37°C for 45 min while shaking at 220 rpm. The bacterial cells were centrifuged at 3500 rpm for 1 min. The cell pellet was resuspended in the remaining SOC medium, and the suspension was plated on antibiotic selection agar plates (10% NaCl, 5% yeast extract, 10% Bacto™

Tryptone, 20% agar) containing carbenicillin (100 µg/mL). The plates were incubated overnight at 37°C.

2.4.5.2 Recombinant protein expression

A single colony was resuspended in a 5 ml liquid culture with carbenicillin (100 µg/mL) and incubated at 37°C and 220 rpm overnight. The overnight culture was diluted to an OD_{600} of 0.15 into SOB media (20% Bacto™ Tryptone, 5% yeast extract, 0.5% NaCl, 2.5 mM KCl, pH 7.0) containing carbenicillin, and incubated for 2 hours at 37°C and 220 rpm until an OD_{600} between 0.5 and 0.7 was reached. Expression was induced with 0.5 mM IPTG (Carl-Roth, Cat. No. CN08.2), and the protein was expressed at 16°C and 180 rpm for 22 hours. Small portions of each fraction were kept for SDS-PAGE with subsequent Coomassie staining or Western blotting (see chapters **2.4.1**-**2.4.3**).

2.4.5.3 Protein extraction from inclusion bodies

E. coli cells expressing the PCMD-1 peptide were harvested by centrifugation at 4000 rpm and 4°C for 20 min. The cell pellet was resuspended in lysis buffer (20 mM Tris/Cl pH 8.0, 10% glycerol, 0.5 M NaCl, 1mM PMSF, 1x cOmplete™ EDTA-free Protease Inhibitor Cocktail (Sigma-Aldrich, Cat. No. 4693132001), 0.1 mg/ml DNAse (PanReac/AppliChem, Cat. No. A3778) and disrupted with high pressure (1.35 kbar) in a Constant Cell Disruptor. After disruption, the cells were incubated on ice for 10 min. Following centrifugation at 4°C for 10 min, the pellet was resuspended in 4°C cold wash buffer (20 mM Tris/Cl pH 8.0, 0.5 M NaCl, 6 M Guanidine hydrochloride (Sigma-Aldrich, Cat. No. G4505), 1 mM ß-mercaptoethanol). The centrifugation step and the wash step were repeated once after another centrifugation step. The pellet was resuspended in 10 ml extraction buffer (20 mM Tris/Cl pH 8.0, 0.5 M NaCl, 6 M Guanidine hydrochloride, 1 mM ß-mercaptoethanol) and mixed with the Rotator "Digi Mixer" (SunLab) for 45 min at RT. The suspension was centrifuged at 10000 rcf and 4°C for 10 min. The supernatant was kept for Ni-NTA purification. Small portions of each fraction were kept for SDS-PAGE with subsequent Coomassie staining or Western blotting (see chapters **2.4.1**-**2.4.3**).

2.4.5.4 Ni-NTA purification

Four columns (Pierce™ Disposable Columns, 10 mL, Cat. No. 29924) were packed with 2 ml Ni-NTA Agarose (Qiagen, Cat. No. 30210) according to the manufacturer's protocols. Each column was equilibrated with 3 ml $_{dd}H_20$ and 10 ml extraction buffer (20 mM Tris/Cl, pH 8.0; 0.5 M NaCl, 6 M guanidine HCl, 1 mM ß-mercaptoethanol). All subsequent purification steps were performed through gravity flow at 4°C. The lysate was applied to the columns and incubated for 90 min at RT. After the samples passed the columns, the flow-throughs were collected and applied another time onto the column. After 30 min incubation, the samples passed the columns, and the flow-throughs were kept for SDS-PAGE analysis. The buffer was exchanged by washing with a two-fold column volume

of exchange buffer (20 mM Tris/HCl, pH 8.0; 0.5 M NaCl, 6 M urea, 1 mM ß-mercaptoethanol). Next, a wash step with a two-fold column volume wash buffer (20 mM Tris/Cl, pH 8.0; 0.5 M NaCl, 6 M urea, 1 mM ß-mercaptoethanol, 20 mM imidazole) was performed. The peptide was eluted in four steps, each with 2 ml elution buffer (20 mM Tris/Cl, pH 8.0; 0.5 M NaCl, 6 M urea, 1 mM ß-mercaptoethanol, 250 mM imidazole) and collected in four tubes. Small portions of each fraction were kept for SDS-PAGE analysis. Guanidine-containing samples were diluted at 1:30 and loaded while hot. Binding efficiency, purity, and yield were checked by performing SDS-PAGE with subsequent Coomassie staining (see chapter**s 2.4.1**, **2.4.2**). Eluates were pooled, and the protein concentration was determined using the Bradford assay (see chapter **2.4.4**).

2.4.5.5 Protein concentration

To concentrate the protein and exchange the buffer, 3.5 ml of the pooled eluates and 1.5-ml elution buffer (see above) were applied to a 10K MWCO Pierce™ Protein Concentrator Spin Column (Thermo Fisher Scientific Scientific, Cat. No. 88527). All steps were performed at 4°C with 4°C pre-cooled buffers. The eluates were centrifuged at 8000 rcf for 25 min until the volume decreased to 0.5 ml. The column was refilled with 5 ml of the final buffer (20 mM Tris-HCl, pH 8.0, 2M Urea), suitable for injection into mice, and centrifuged for 25 min 3 times until the elution buffer was removed with a factor of 1000. The last centrifugation step was performed at 8000 rcf for 22 min until the final volume reached 1 ml. Small portions of each fraction were kept for SDS-PAGE analysis and subsequent Coomassie staining (see chapter **2.4.1**, **2.4.2**) and the Bradford assay (see chapter **2.4.4**). The peptide was injected into mice by E. Kremer and H. Flaswinkel to raise antibodies.

2.5 Microscopy

2.5.1 Confocal microscopy

Embryos from the translocation assay experiment or immunofluorescence stained embryos as well as adult worms were imaged on a laser confocal TCS SP5 microscope (Leica) controlled by the Leica Application Suite (LAS) Software 2.7.2 and equipped with a resolution of 1024x1024 pixels with HCX PL APO Lambda Blue 63x 1.4 oil objective. Dual or trial Z-series with the laser lines of 405 nm, 88 nm, and 561 nm were taken with a step size of 0.7 µm.

2.5.2 4D time-lapse microscopy

For live-cell imaging, young adult worms were dissected in 6 µl M9 buffer on a coverslip and reversely mounted onto a 2% agar pad on a microscope slide. Time-lapse movies were taken using a Zeiss Axio Imager.M2 equipped with an epifluorescence controlled by

the Time to Live software from Caenotec. Z-series with a step size of DIC were taken every 35 sec at 25°C. Fluorescence scans were acquired only at the required time points by manual operation.

2.5.3 Spinning disk confocal microscopy

For live-cell imaging of embryos, young adult worms were either dissected in 6 µl Polybeads® Microspheres 20.00 µm (diluted 1:10 in M9 buffer) on a microscope slide and covered with a coverslip or dissected in 6 µl M9 buffer on a coverslip and reversely mounted onto a 2% agar pad on a microscope slide. Imaging was performed at 25°C using an inverted Eclipse Ti spinning disc confocal microscope that was controlled by the NIS Elements 5.02 software (Nikon) and equipped with an Andor DU-888 X-11056 camera (1024 x 1024 pixels), a 100× 1.45-NA Plan-Apochromat oil immersion lens, and a 488 nm and 561 nm laser lines. Dual or trial z-series of DIC, 488 nm (2x2 binning) laser line, and optionally the 561 nm laser line were acquired every 30 s with a step size of 0.7 µm.

2.5.4 Stereo microscopy

Brightfield and 488 nm fluorescence images of grown *S. cerevisiae* spots generated in the Y2H protein-protein interaction assay were acquired using a Leica Stereomicroscope M205 FA. The microscope was controlled by the Leica Application Suite software (3.2.0.9652) and equipped with a 1x 2.11 NA Plan Apo lens and a Leica DigitalDFC340x FX camera.

2.6 Computational methods

2.6.1 Image Analysis

2.6.1.1 Fluorescence intensity measurements

Centrosome fluorescence intensities were quantified using the open-source Fiji Plugin Trackmate on raw images by analyzing Z-stacks with ManualTrackMate in Fiji (Schindelin et al., 2012; Tinevez et al., 2017). This plugin provides automated, semi-automated, and manual tracking of single particles. Due to the small centrosome structures and low centrosomal fluorescence intensities in the experiments performed in this work, automated tracking was not possible; hence, mostly manual tracking was applied.

Time points of measurements were either defined through the stage of DNA condensation visualized by the mCherry::H2B marker or corresponding DIC recordings. When there was no GFP signal recognizable, the centrosomal position was determined by DIC. A fixed radius (GFP::PCMD-1: 0.788 µm, GFP::SAS-7 0.828 µm) was applied to measure the total intensities of the centrosomal signal (C), background signal (B), and cytoplasmic background signal (CBS) in three dimensions. The centrosome fluorescence intensity was

calculated for each centrosome with the following formula: **Centrosome fluorescence intensity = (C-B) – (CBS-B)**. The cytoplasmic signal was calculated for each embryo with the following formula **Cytoplasmic fluorescence intensity = (CBS) - (B)**. For direct comparison of fluorescence intensities between different strains, the mean fluorescence intensity of the control strains was arbitrarily defined as 1. To compare fluorescence intensities between different time points within a group, the mean fluorescence intensity of the earliest time point was arbitrarily defined as 1.

2.6.1.2 Circularity and aspect ratio measurements

Centrosomal circularities and aspect ratios were evaluated in one-cell embryos and two-cell embryos immunostained with antibodies against the PCM protein SPD-5, the centriole marker intermediate filament protein A1 (IFA), or GFP. The cell stage was determined based on the stage of DNA condensation, which was visualized by Hoechst staining. Image analysis was performed using the Fiji Software 2.0.0 (Schindelin et al., 2012). Maximum Z-projections were created, and the PCM shapes were converted into black/white outlines using the 'Huang' threshold for one-cell embryos (TMD119, PHX1285, TMD101, TMD153, TMD54) or the "Default" threshold for two-cell embryos (N2 and TMD145). The circularity was measured and calculated by Fiji using the formula: **circularity = 4 x π (area/perimeter^2)**. A perfect circle would have a value of 1.00. As more elongated the object is, the value approaches 0.00. The aspect ratio was measured and calculated by Fiji using the formula: **aspect ratio = major axis/minor axis**. A value of 1.00 would represent an object with two equal axes.

2.6.2 Protein predictions and illustration

2.6.2.1 Protein domain prediction and domain illustration

Intrinsically disordered regions in the PCMD-1 protein were annotated premised on UniProt's predictions (Uniprot-KB O62071; UniProtConsortium, 2019). The coiled-coil domain of the PCMD-1 protein was predicted from amino acid E86 to N117 using the COILS program with a 28-residue window comparing weighted and unweighted MTK and weighted and unweighted MTIDK matrices (Lupas, 1996b; Lupas et al., 1991).

The PCMD-1 protein domain structures were visualized using the DOG 2.0 software (Ren et al., 2009).

2.6.2.2 Phospho-binding and phosphorylation site prediction

The PLK phospho-binding sites and phosphorylation sites were predicted using the GPS-Polo 1.0 software (Liu et al., 2012). Consensus kinase phosphorylation sites superimposing with PLK phospho-binding sites in PCMD-1 were predicted using the GPS 5.0 software (Xue et al., 2008).

2.6.3 Multiple sequence alignment

Sequence conservation of the PLK phospho-binding sites predicted in PCMD-1 was checked by aligning the *C. elegans* PCMD-1 protein sequence with homologous protein sequences in other *Caenorhabditis* species. The protein sequences of *Caenorhabditis japonica* (CJA08956), *Caenorhabditis brenneri* (CBN02262), *Caenorhabditis briggsae* (CBG15805), and *Caenorhabditis remanei* (CRE04201) were downloaded from *WormBase* (WS269). A multiple sequence alignment was performed using MUSCLE (Edgar, 2004) under default parameters in JalView Version 2 (Waterhouse et al., 2009).

2.6.4 Statistical analysis

Statistical analysis was performed using the software R Studio version 1.3.1073 (R Core Team, 2019), the car package (Fox and Weisberg, 2019), and the FSA package (Ogle et al., 2019). Datasets were tested for equal distribution using the Shapiro-Wilk normality test and equal variances with Levene's test.

Two equally distributed independent groups with equal variances were compared applying an unpaired two-sample (two-tailed) t-test. Two equally distributed independent groups with unequal variances were compared by applying an unpaired two-sample (two-tailed) t-test with Welch's correction. If two independent groups were unequally distributed, the Mann-Whitney-U test was applied for comparison.

To compare two dependent samples (time-points) with equal distributions and equal variances, the paired two-sample (two-tailed) t-test was performed. When two dependent samples (time-points) from one group were compared, which were unequally distributed, the Wilcoxon signed-rank test was performed.

More than two groups with unequal distribution were analyzed using the Kruskal-Wallis test with a post-hoc Dunn's multiple comparison test and Holm's p-value adjustment.

Data were illustrated using GraphPad Prism v6.

3 RESULTS

3.1 Characterization of PCMD-1

3.1.1 Transgenic PCMD-1 and PCMD-1*(t3421)* function, localization, and expression

As described in chapter **1.4.2.3**, the *pcmd-1(t3421*) mutant carries a mutation in the *pcmd-1* gene introducing a premature stop codon at amino acid position Q54. At the restrictive temperature of 25°C, *pcmd-1(t3421)* mutant embryos are 100% lethal, and the lethality was determined to depend on the mutation in the *pcmd-1* coding sequence (Erpf et al., 2019). However, the *pcmd-1(t3421)* phenotype shows some degree of variability, and at 15°C, a fraction of the embryos can survive (Erpf et al., 2019). In our previous publication (Erpf et al., 2019), we were able to show that at restrictive temperature, the *pcmd-1(t3421)* mutant phenotype can be rescued by a single-copy insertion of *pcmd-1* cDNA fused to *gfp* at the 5' end encoding PCMD-1 tagged with GFP at the N-terminus. Further, the GFP::PCMD-1 protein was detected at centrosomes. In contrast, a transgene carrying the mutation present in the *pcmd-1(t3421)* allele did not rescue embryonic lethality at 25°C, and GFP::PCMD-1*(t3421)* was not detectable at centrosomes. However, as mentioned above, the *pcmd-1(t3421)* mutant shows some degree of variability at 15°C. Since several potential alternative start codons are present downstream of the point mutation in the *pcmd-1(t3421)* allele (Erpf, 2020), these codons might initiate transcription, and transcripts lacking an N-terminal part of the protein could be generated.

To examine whether the function of transgenic PCMD-1 and PCMD-1*(t3421)* is comparable when the GFP is fused to the C-terminus, I repeated the above-described rescue experiments with both *pcmd-1* and *pcmd-1(t3421)* cDNA single-copy insertion transgenes fused to a *gfp* reporter at the 3' end under *mai-2* regulatory elements (**Figure 9A**), which I crossed into *pcmd-1(t3421)* mutant background. To examine whether the constructs might rescue the embryonic lethality of *pcmd-1(t3421)*, I performed an embryonic survival assay at 25°C. While 97.41% of wild-type embryos were viable, 100% of the *pcmd-1(t3421)* embryos were lethal (**Figure 9B**). In wild-type background, 95.30% of the $P_{mai\text{-}2}$*pcmd-1::gfp* embryos and 95.19% of the $P_{mai\text{-}2}$*pcmd-1(t3421)::gfp* embryos were viable (**Figure 9B**). In *pcmd-1(t3421)* mutant background, $P_{mai\text{-}2}$*pcmd-1::gfp* was sufficient to rescue the embryonic lethality of the *pcmd-1(t3421)* allele with a survival rate of 98.09% (**Figure 9B**). In contrast, $P_{mai\text{-}2}$*pcmd-1(t3421)::gfp*, which contains the point mutation of the *pcmd-1(t3421)* allele, did not rescue the embryonic lethality of *pcmd-1(t3421)*. Thus, single-copy insertions with *gfp* in the 5' end and the 3' end of *pcmd-1* and *pcmd-1(t3421)* show similar degrees of rescue.

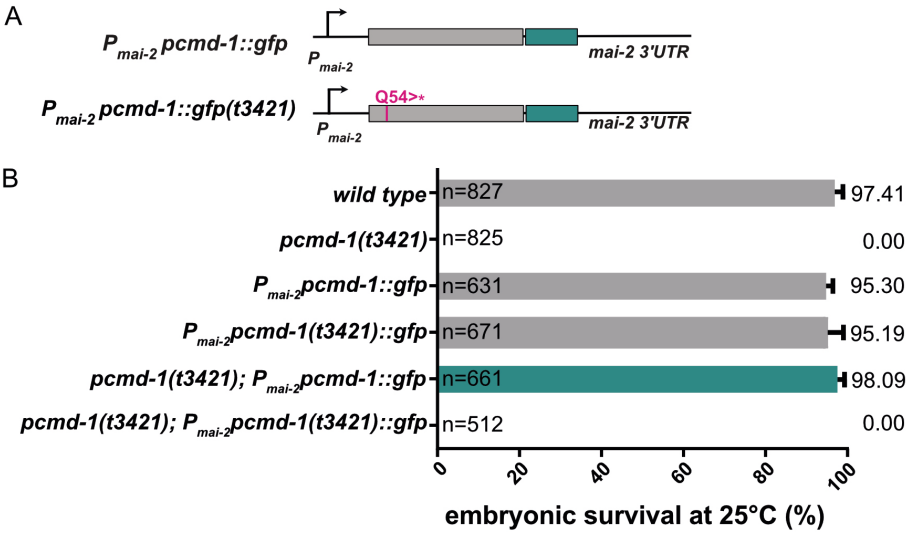

Figure 9. The *pcmd-1(t3421)* lethal phenotype is rescued by transgenic PCMD-1::GFP but not by transgenic PCMD-1*(t3421)*::GFP. A) Schematic illustration of single-copy integrations of *pcmd-1::gfp* and *pcmd-1(t3421)::gfp* under *mai-2* regulatory elements**. B)** Embryonic survival assay performed at 25°C. Both $P_{mai\text{-}2}$*pcmd-1::gfp* (95.30±0.95%, n=631) and $P_{mai\text{-}2}$*pcmd-1(t3421)::gfp* (95.19±2.22%, n=671) did not affect the survival in wild-type background compared to wild-type embryonic viability (97.41±0.63%, n=827). The embryonic viability of *pcmd-1(t3421)* (0.00±0.00%, n=825) was restored by $P_{mai\text{-}2}$*pcmd-1::gfp* (98.09±1.00%, n=661), but not by $P_{mai\text{-}2}$*pcmd-1(t3421)::gfp* (0.00±0.00%, n=512). Data are represented as mean and SEM, n=total number of counted embryos. Data of wild-type and *pcmd-1(t3421)* embryos were acquired by A.C. Erpf. Figures are adpated from Erpf et al. (2019).

To determine whether PCMD-1::GFP and PCMD-1(*t3421)*::GFP can localize to centrosomes, centrosomal fluorescence intensities were monitored by live-cell imaging in $P_{mai\text{-}2}$*pcmd-1::gfp* and $P_{mai\text{-}2}$*pcmd-1(t3421)::gfp* one-cell embryos in *pcmd-1(t3421)* background at 25°. PCMD-1::GFP was detected at centrosomes throughout the first cell cycle in all analyzed embryos (**Figure 10**). 83.33% of the PCMD-1::GFP expressing embryos were dividing like wild-type embryos. In contrast, in $P_{mai\text{-}2}$*pcmd-1(t3421)::gfp* embryos, no PCMD-1*(t3421)*::GFP signal was visible at the centrosomes at any cell cycle stage (**Figure 10**), which indicates that no truncated PCMD-1 is transcribed, or that a potentially transcribed protein cannot be detected at centrosomes. Further, it could be observed that in 83.33% of the $P_{mai\text{-}2}$*pcmd-1(t3421)::gfp* embryos, the paternal pronuclei did not meet and bipolar spindle formation, and in turn, cell division failed (**Figure 10**).

Dynamic changes of the centrosomal signals over the cell cycle have been previously observed for GFP::PCMD-1 (Erpf, 2020). GFP::PCMD-1 levels slightly increased at the beginning of mitosis and decreased towards the end of mitosis compared to centrosomal GFP::SAS-4 control levels, which remained similar throughout the cell cycle. I wondered whether similar dynamic changes at centrosomes, as described for GFP::PCMD-1, could be observed for PCMD-1::GFP during mitosis.

To examine whether the dynamic levels of PCMD-1 tagged with GFP in the C-terminus are comparable to PCMD-1 tagged with GFP in the N-terminus, I assayed centrosomal

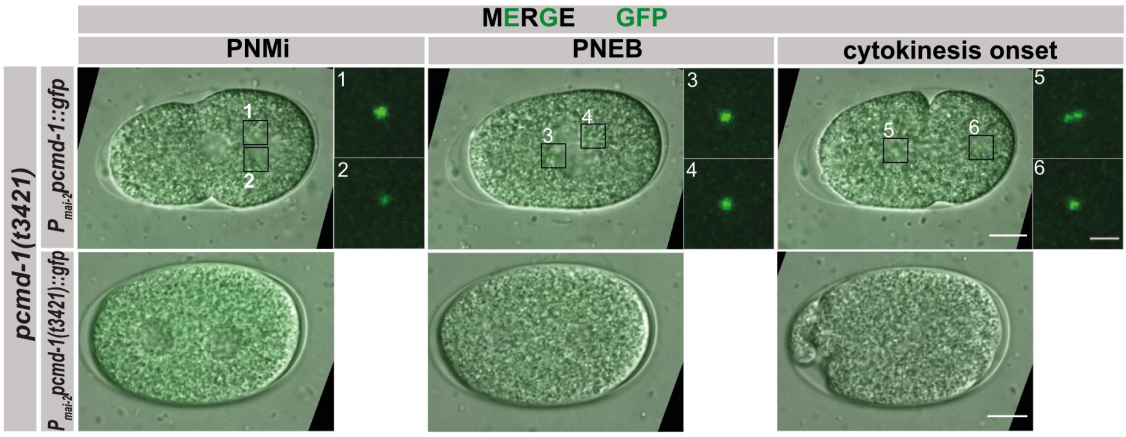

Figure 10. Transgenic PCMD-1::GFP localizes to centrosomes, whereas transgenic PCMD-1*(t3421)*::GFP does not localize to centrosomes. Representative stills of time-lapse sequences at the time point of PNMi, PNEB, and cytokinesis onset of *P*$_{mai-2}$*pcmd-1::gfp* (n=6) or *P*$_{mai-2}$*pcmd-1(t3421)::gfp* (n=6) one-cell embryos in *pcmd-1(t3421)* background recorded with a spinning disc confocal microscope. In 83.3% of the *P*$_{mai-2}$*pcmd-1::gfp* embryos a bipolar spindle was formed, and the embryos divided normally and in all embryos PCMD-1::GFP was detected at the centrosome. Images are displayed as z-projected GFP images merged with a single DIC z-plane. Insets show enlarged centrosomal areas labeled with corresponding numbers (1-6). 83.3% of the *P*$_{mai-2}$*pcmd-1(t3421)::gfp* embryos failed to form a bipolar spindle and did not divide and in none of the embryos a centrosomal GFP signal was detected. Scale bars indicate 10 µm or 2 µm (insets).

PCMD-1::GFP and GFP::PCMD-1 intensities throughout the first cell cycle in *P*$_{mai-2}$*pcmd-1::gfp* and *P*$_{mai-2}$*gfp::pcmd-1* embryos in *pcmd-1(t3421)* background by live-cell imaging (**Figure 11A**). I observed that the GFP::PCMD-1 and PCMD-1::GFP signal was decreasing towards the end of mitosis. Therefore, the mean centrosomal fluorescence intensities of PCMD-1::GFP and GFP::PCMD-1 were quantified at the beginning of mitosis (PNEB) and the end of mitosis (cytokinesis onset). The mean centrosomal intensity of GFP::PCMD-1 significantly dropped from 1.00 arbitrary units (a.u.) at PNEB to 0.60 a.u. at cytokinesis onset (**Figure 11B**). Similarly, the mean centrosomal intensity of PCMD-1::GFP embryos significantly decreased from 1.00 a.u. at PNEB to 0.51 a.u. at cytokinesis onset (**Figure 11B**). In contrast, no significant difference was calculated for the mean centrosomal fluorescence intensities between GFP::PCMD-1 (1.00 a.u.) and PCMD-1::GFP (1.06 a.u.) at PNEB and GFP::PCMD-1 (1.00 a.u.) and PCMD-1::GFP (0.90 a.u.) at cytokinesis onset (**Figure 11C**). The number of analyzed centrosomes is relatively low in this experiment, but I could confirm that the observed drop of the GFP::PCMD-1 signal is also detectable for PCMD-1::GFP. Even if it was shown in Erpf et al. (2020) that the GFP::SAS-4 control is not decreasing during the cell cycle, it could not be completely excluded that photobleaching contributed to the decreasing PCMD-1 centrosomal fluorescence intensities. However, I will show in chapter **3.6.1** that centrosomal GFP::PCMD-1(4A) intensities were not decreasing significantly in contrast to GFP::PCMD-1 centrosomal intensities, which indicates that photobleaching plays a minor role.

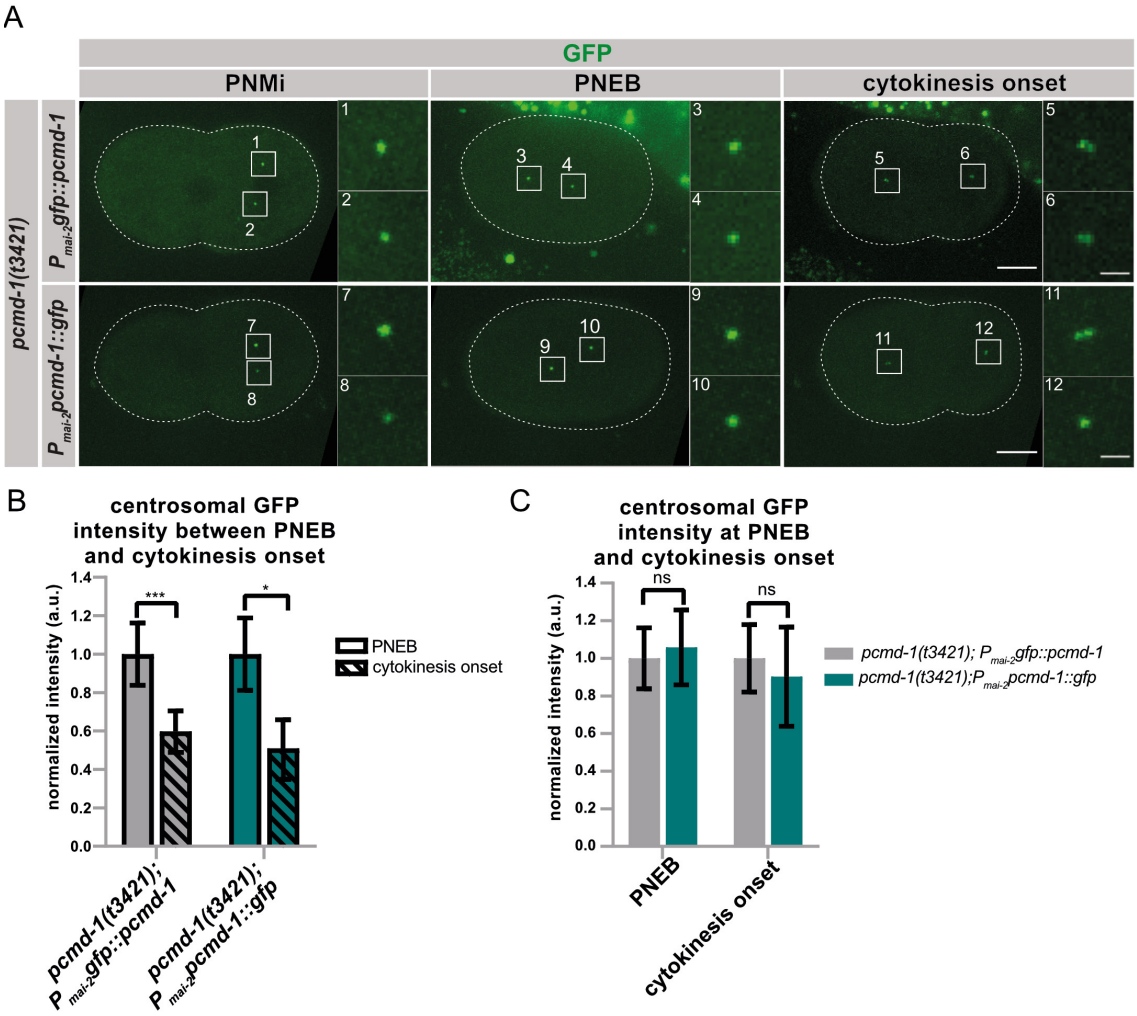

Figure 11. Transgenic PCMD-1 centrosomal levels decrease towards the mitotic exit. Representative stills of time-lapse sequences at PNMi, PNEB and cytokinesis onset of *P*$_{mai-2}$*gfp::pcmd-1* (n=5) and *P*$_{mai-2}$*pcmd-1::gfp* (n=3) one-cell embryos in *pcmd-1(t3421)* background recorded with a spinning disc confocal microscope. In all analyzed embryos, GFP::PCMD-1 and PCMD-1::GFP were detected throughout the cell cycle but the signal decreased over time. Images are displayed as z-projections. Insets show enlarged centrosomal areas labeled with corresponding numbers (1-8). Scale bars indicate 10 µm or 2 µm (insets). **B)** Quantification of centrosomal signal intensities in *P*$_{mai-2}$*gfp::pcmd-1* embryos between PNEB (1.00±0.16 a.u., n=10 centrosomes) and cytokinesis onset (0.59±0.10 a.u., n=10 centrosomes), and *P*$_{mai-2}$*pcmd-1::gfp* embryos between PNEB (1.00±0.19 a.u., n=6 centrosomes) and cytokinesis onset (0.51±0.15 a.u., n=6 centrosomes). Values were normalized to the mean intensity at PNEB. Paired two-sample t-test for both strains (*** p<0.001,* p<0.05). **C)** Quantification of centrosomal signal intensities in *P*$_{mai-2}$*gfp::pcmd-1* (1.00±0.16 a.u., n=10) and *P*$_{mai-2}$*pcmd-1::gfp* (1.06±0.20 a.u., n=6) embryos at PNEB, and *P*$_{mai-2}$*gfp::pcmd-1* (1.00±0.18 a.u., n=10,) and *P*$_{mai-2}$*pcmd-1::gfp* (0.90±0.27 a.u., n=6) embryos at cytokinesis onset. Values were normalized to the mean intensity of GFP::PCMD-1. Two-sample t-test for both time points (ns: not significant). Data in **B)** and **C)** are represented as mean±SEM. Note that quantifications of *P*$_{mai-2}$*gfp::pcmd-1* control embryos were pooled with control embryos in chapter 3.6.1/Figure 36 (same experimental setting).

To test whether the point mutation in *pcmd-1(t3421)* leads to a loss of the PCMD-1 protein, the single-copy insertion transgenes encoding the N-terminally and C-terminally GFP-tagged PCMD-1 and PCMD-1*(t3421)* fusion proteins were probed against GFP by Western blot analysis. Therefore, mixed-stage worms were cultured at the permissive

temperature of 15°C before lysates were prepared. The expression was first checked in the wild-type background. Wild-type lysate was used as a negative control (**Figure 12A**). GFP::PCMD-1 and PCMD-1::GFP bands were detected at the expected molecular weight (MW) of 98 kDa in the wild-type background (**Figure 12A**). Note that the bands with the MW of around 30 kDa might be GFP, which was cleaved (**Figure 12A**). In contrast, in the wild-type background, no band was detectable for GFP::PCMD-1*(t3421)* and PCMD-1*(t3421)*::GFP (**Figure 12A**). Second, the expression was analyzed in the *pcmd-1(t3421)* background to exclude that PCMD-1 is preferentially expressed in the wild-type background. Wild-type lysate was used as a negative control (**Figure 12B**). However, similarly, as in wild-type background, GFP::PCMD-1 and PCMD-1::GFP bands were detected at the expected molecular weight (MW) of 98 kDa, but no band was detectable for GFP::PCMD-1*(t3421)* and PCMD-1*(t3421)*::GFP (**Figure 12B**). Taken together, the Western blot analysis demonstrates that the mutation in *pcmd-1(t3421)* causes a strong reduction of the PCMD-1 protein level. Nevertheless, the residual protein of the conceivably truncated proteins containing an alternative start codon might be under the detection level.

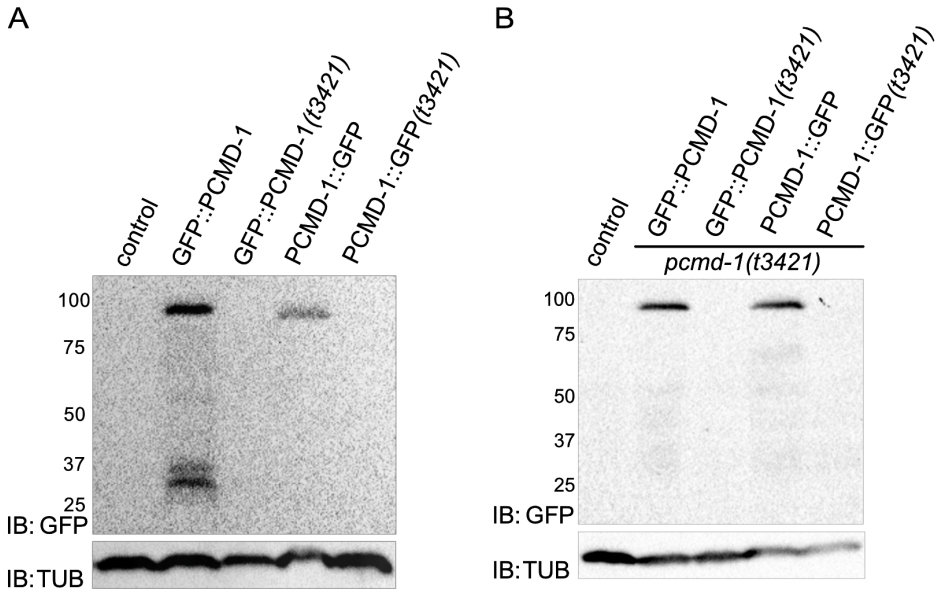

Figure 12. Expression levels of transgenic GFP-tagged PCMD-1 and PCMD-1*(t3421)*. Mixed-stage worm lysates of GFP::PCMD-1 (98 kDa), PCMD-1::GFP (98 kDa), GFP::PCMD-1*(t3421)* (no band) and PCMD-1*(t3421)*::GFP (no band) expressing worms were immunoblotted (IB) with an antibody against GFP and an α-tubulin antibody as loading control. N2 wild-type lysates were used as negative controls. **A)** In wild-type background, GFP::PCMD-1 and PCMD-1::GFP showed bands at the expected MW. The additional bands at ~30 kDa in GFP::PCMD-1 might be cleaved GFP. **B)** In *pcmd-1(t3421)* background, bands at the expected MW were expected only for GFP::PCMD-1 and PCMD-1::GFP. Figure **B)** adapted from Erpf et al. (2019).

In summary, GFP::PCMD-1 and PCMD-1::GFP rescued the embryonic lethality of *pcmd-1(t3421).* As GFP::PCMD-1(t3421), PCMD-1(t3421)::GFP is also not able to rescue the embryonic lethality of *pcmd-1(t3421)*. Furthermore, both proteins behave similarly

regarding their localization and dynamics. As described for GFP::PCMD-1*(t3421)*, PCMD-1*(t3421)*::GFP is not detectable by confocal microscopy and Western blot analysis. This suggests that a functional PCMD-1 protein is not transcribed in the *pcmd-1(t3421)* mutant. However, there is still the possibility that a truncated PCMD-1 is transcribed but not targeted to the centrosome. I will demonstrate in chapter **3.1.2** that the endogenous levels of PCMD-1 are very low and almost undetectable in Western blots. Thus, it cannot be excluded that a truncated PCMD-1 protein is transcribed, which might cause the partial survival of *pcmd-1(t3421)* embryos at 15°C.

3.1.2 Endogenous PCMD-1 localization and expression

To investigate expression patterns of endogenous PCMD-1, an allele with a *gfp* reporter integrated at the 5' end of the *pcmd-1* genomic locus *(syb370[gfp::pcmd-1])* was generated and analyzed (Erpf, 2020). Endogenously GFP-tagged PCMD-1 was localizing to the centrosomes in embryos and other tissues of the worms and cilia in adult worms. Compared to the transgenic GFP::PCMD-1 signal under *mai-2* regulatory elements, the endogenous GFP::PCMD-1 signal appeared much weaker (Erpf, 2020). In the *gfp::pcmd-1* transgene under *mai-2* regulatory elements, a sequence encoding a small flexible glycine linker was inserted between *gfp* and *pcmd-1* to prevent misfolding of the protein. However, the sequence encoding the linker was omitted in the *syb370[gfp::pcmd-1]* allele.

To determine whether the lower expression levels were due to weaker expression under the endogenous promoter or were attributed to the missing linker between GFP and PCMD-1, and potential misfolding, another allele with a *gfp* reporter and the sequence encoding the glycine linker integrated at the 5' end of the *pcmd-1* genomic locus (*pcmd-1* (*syb486[gfp::pcmd-1]*)) was generated. The endogenous GFP::PCMD-1 fusion protein with the flexible linker localized to centrosomes in embryos and other tissues of the worms as well as cilia of sensory neurons in the head and tail of adult worms (**Figure 13A**, **C**). In *pcmd-1* (*syb486[gfp::pcmd-1])* one-cell embryos, GFP::PCMD-1 was detected at the centrosomes throughout the whole cell cycle with decreasing signals towards the end of mitosis (**Figure 13A**). To examine whether endogenous GFP::PCMD-1 intensities at the centrosomes are decreasing towards the end of mitosis, I quantified the mean centrosomal fluorescence intensities of endogenous GFP::PCMD-1 at the beginning of mitosis (PNEB) and at the end of mitosis (cytokinesis onset). The mean centrosomal intensity of endogenous GFP::PCMD-1 significantly dropped from 1.00 a.u. at PNEB to 0.61 a.u. at cytokinesis onset (**Figure 13B**). Thus, endogenous GFP::PCMD-1 resembles the spatiotemporal localization and dynamics at centrosomes of the transgenic GFP::PCMD-1 expressed under the *mai-2* promoter. However, in comparison to the transgenic GFP::PCMD-1 expressed under the *mai-2* promoter, the signal intensities of endogenous GFP::PCMD-1 at centrosomes but also cilia appeared much weaker in

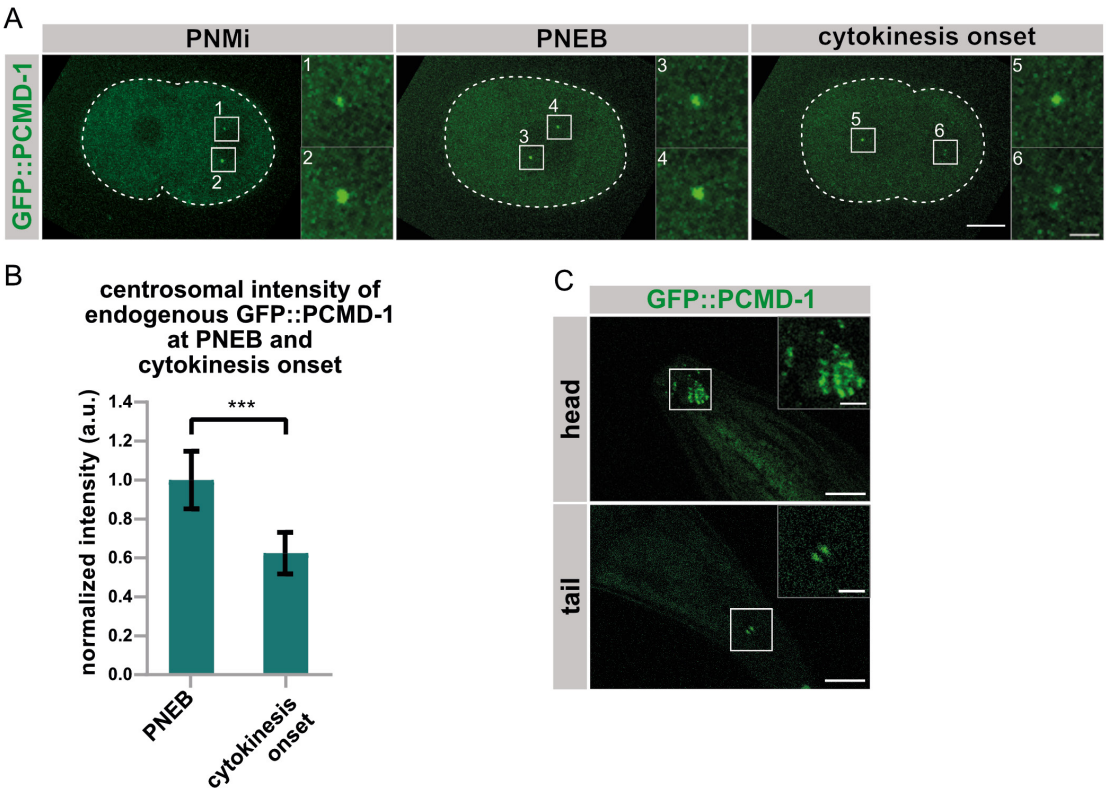

Figure 13. Endogenous PCMD-1 localizes to centrosomes, cilia, and centrosomal levels decrease towards the mitotic exit. A) Representative stills of time-lapse sequences at PNMi, PNEB, and cytokinesis onset of a *gfp::pcmd-1* (n=6) one-cell embryo recorded with a spinning disc confocal microscope. In all embryos, GFP::PCMD-1 was visible throughout the cell cycle. Images are displayed as z-projections. Insets show enlarged centrosomal areas labeled with corresponding numbers (1-6). Scale bars indicate 10 µm or 2 µm (insets). **B)** Quantification of centrosomal endogenous GFP::PCMD-1 intensities in *gfp::pcmd-1* embryos between PNEB (1.00±0.15 a.u., n=12 centrosomes) and cytokinesis onset (0.61±0.12 a.u., n=12 centrosomes). Values were normalized to the mean intensity at PNEB. Paired two-sample t-test (*** $p<0.001$). **C)** Representative fluorescent images of cilia of sensory neurons in the head and the tail of adult *gfp::pcmd-1* worms (n=4) recorded with a confocal microscope. GFP::PCMD-1 was detected at the cilia. Images are displayed as z-projections. Insets show enlarged areas with cilia. Scale bars indicate 10 µm or 4 µm (insets).

pcmd-1(*syb486[gfp::pcmd-1])* worms, similarly as observed in the *pcmd-1(syb370[gfp::pcmd-1]* worms. Therefore, I examined whether less PCMD-1 is expressed on the cellular level. To this end, a Western blot analysis was performed on mixed-stage worm lysates against the GFP-tag. In addition, staining against α-tubulin was performed as a loading control. Lysates of wild-type worms served as negative controls. The Western blot analysis revealed that in both lysates of *pcmd-1(t3421); $P_{mai\text{-}2}$gfp::pcmd-1* transgene embryos and in-locus tagged *gfp::pcmd-1* embryos, bands were detectable at the expected MW of 98 kDa. However, the expression level of endogenous GFP::PCMD-1 was much lower than the single-copy transgenic GFP::PCMD-1 expressed under the *mai-2* promoter in *pcmd-1(t3421)* background (**Figure 14A**). Note that the additional bands detected in the *pcmd-1(t3421); $P_{mai\text{-}2}$gfp::pcmd-1* lysate might be degradation product as this was not seen in other Western blots (**Figure 12A, B**). For

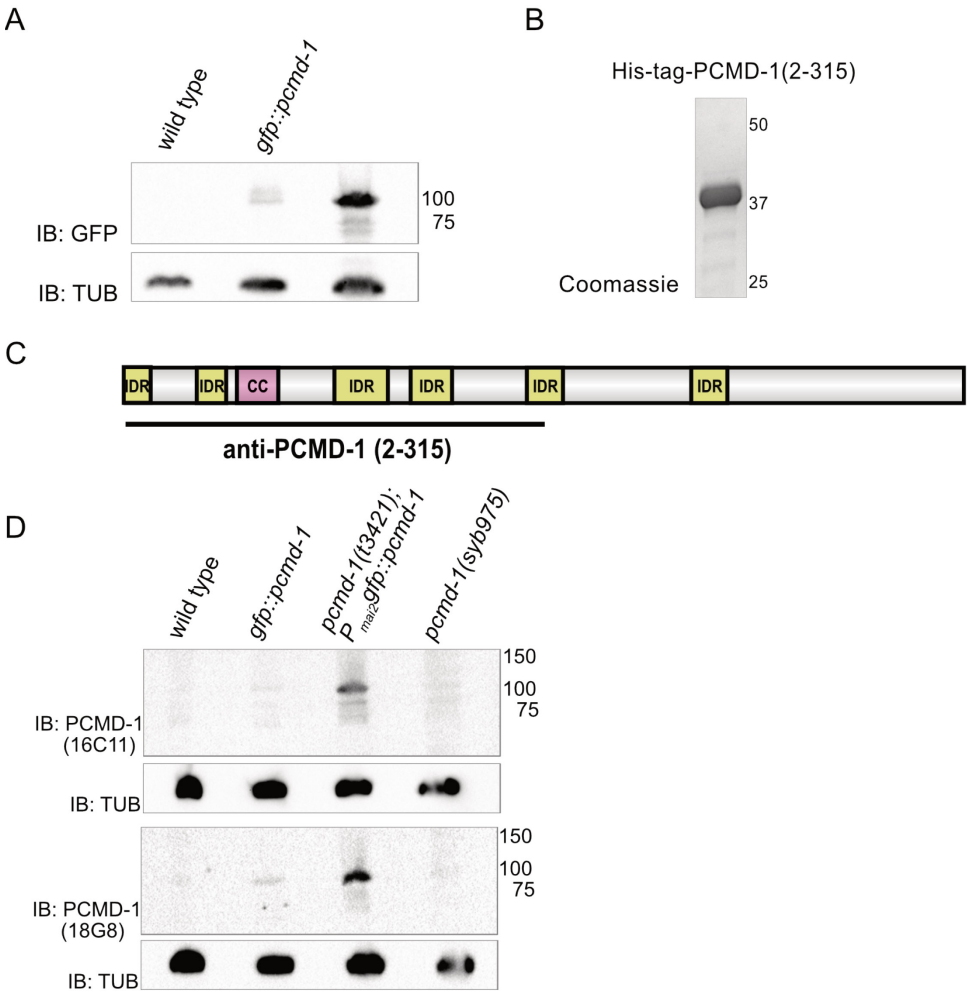

Figure 14. Endogenous PCMD-1 is expressed at lower levels than transgenic PCMD-1. A) Western blot analysis of worm lysates of mixed-stage wild-type, *gfp::pcmd-1, pcmd-1(t3421); P_{mai-2}gfp::pcmd-1* worms stained with a GFP antibody against the GFP-tags and an α-tubulin (TUB) antibody as a loading control. Both endogenous GFP::PCMD-1 and transgenic GFP::PCMD-1 under *the mai-2* promoter showed a band at the expected MW of 98 kDa. **B)** Coomassie staining after purification and concentration of the 38-kDa His-tagged PCMD-1(aa E2-E315) peptide. **C)** Schematic illustration of the domain structure of full-length PCMD-1, with an indication of the purified region of PCMD-1 (aa E2-E315) used for antibody generation. The predicted coiled-coil domain (CC) is highlighted in magenta, and the IDRs are highlighted in yellow. **D)** Western blot analysis of worm lysates of mixed-stage wild-type, *gfp::pcmd-1, pcmd-1(t3421); P_{mai-2}gfp::pcmd-1*, and *pcmd-1(syb975)* worms. *pcmd-1(syb975)* was used as a negative control. Worm lysates were immunoblotted (IB) with antibodies against PCMD-1 (18G8 and 16C11), and with an α-tubulin (TUB) antibody as a loading control. Both PCMD-1 antibodies, 16C11 and 18G8, stained the band at the expected MW of 98kDa in the *pcmd-1(t3421); P_{mai-2}gfp::pcmd-1* worm lysates. Very weak bands were detected at the same MW of 98kDa in *gfp::pcmd-1* worm lysates. However, in wild-type, no band was detectable at the expected MW of 71 kDa.

detection of endogenous PCMD-1, a rabbit polyclonal peptide antibody against PCMD-1 was previously raised by Davids Biotechnology, which worked reasonably in immunofluorescence stainings, but did not work in Western blots (Erpf et al., 2019). Therefore, I aimed to raise a monoclonal mouse antibody to detect endogenous PCMD-1 in Western blotting. To this end, I purified a 38-kDa recombinant hexahistidine-tagged peptide comprising the N-terminal part of PCMD-1 (aa E2-E315) (**Figure 14B, C**). The purified and concentrated peptide was injected into mice by Dr. H. Flaswinkel and

Dr. E. Kremmer to raise monoclonal antibodies. We screened many candidates in immunofluorescence stainings and Western blots, and four of them were recloned by Dr. H. Flaswinkel and Dr. E. Kremmer. In immunofluorescence stainings, all four anti-PCMD-1 antibodies (11C6, 16C11, 17E11, 18G8) did stain centrosomal signals in wild-type embryos but not in *pcmd-1(t3421)* embryos, which proves the specificity of the antibodies (Data not shown, acquired by T. Mikeladze-Dvali). Moreover, the applicability of the antibodies in Western blots was examined. Two antibodies (16C11 and 18G8) specifically stained bands in Western blot analysis (**Figure 14C**). While the PCMD-1(16C11) and PCMD-1(18G8) antibodies did not stain endogenous PCMD-1 at the expected MW of 71 kDa in wild-type lysates, both antibodies extremely weakly stained endogenous GFP::PCMD-1 at 98 kDa in *gfp::pcmd-1* worm lysates. Possibly, GFP might act to stabilize the low-expressed PCMD-1 protein. Transgenic GFP::PCMD-1 expressed under the *mai-2* promoter in the *pcmd-1(t3421*) background was visible as a clear band at the expected 98 kDa with both antibodies. Lysates of *pcmd-1(syb975)* worms were used as a negative control. The *pcmd-1(syb975)* allele is a deletion mutant of *pcmd-1*, which will be further characterized in the next chapter **3.1.3**. In the *pcmd-1(syb975)* lysate probed with the PCMD-1(16C11) antibody, a faint smear is visible, which is unlikely an unspecific signal as this is not visible in the wild-type lysate.

In summary, the subcellular localization and dynamic changes of endogenous GFP::PCMD-1 are comparable to the subcellular localization and dynamics of transgenic GFP::PCMD-1 expressed under the *mai-2* promoter. However, endogenous GFP::PCMD-1 expression is much lower than the transgenic GFP::PCMD-1 under the *mai-2* promoter.

3.1.3 Characterization of the *pcmd-1(syb975)* allele

As already mentioned before, the *pcmd-1(t3421)* allele leads to a premature stop codon at amino acid 54 (**Figure 15A**) and could represent a partial loss-of-function allele. It has been shown that the *pcmd-1(t3421)* embryos are not viable at 25°C, and at 15°C, 38% of the *pcmd-1(t3421)* embryos survive (Erpf et al., 2019). Furthermore, PCM formation is severely compromised in *pcmd-1(t3421)* embryos (Erpf et al., 2019). Immunofluorescence stainings revealed that compared to wild-type one-cell embryos with 100% colocalization of the major PCM protein SPD-5 and centrioles, in *pcmd-1(t3421)* embryos, only 13% of SPD-5 were colocalizing with centrioles before PNM in interphase, and 53% between PNM and pro-metaphase at the beginning of mitosis (Erpf et al., 2019).

Another *pcmd-1(syb975)* mutant allele was generated and characterized to verify the previous findings. In the *pcmd-1(syb975)* allele, the first 1201 bp, including the coding regions for the coiled-coil domain and low-complexity regions, are deleted (**Figure 15A**). Embryonic survival assays revealed that *pcmd-1(syb975)* embryos are not viable at 25°C, and 23% of the embryos survive at 15°C, which is lower than the survival rate of *pcmd-1(t3421)* embryos at 15°C (Erpf et al., 2019).

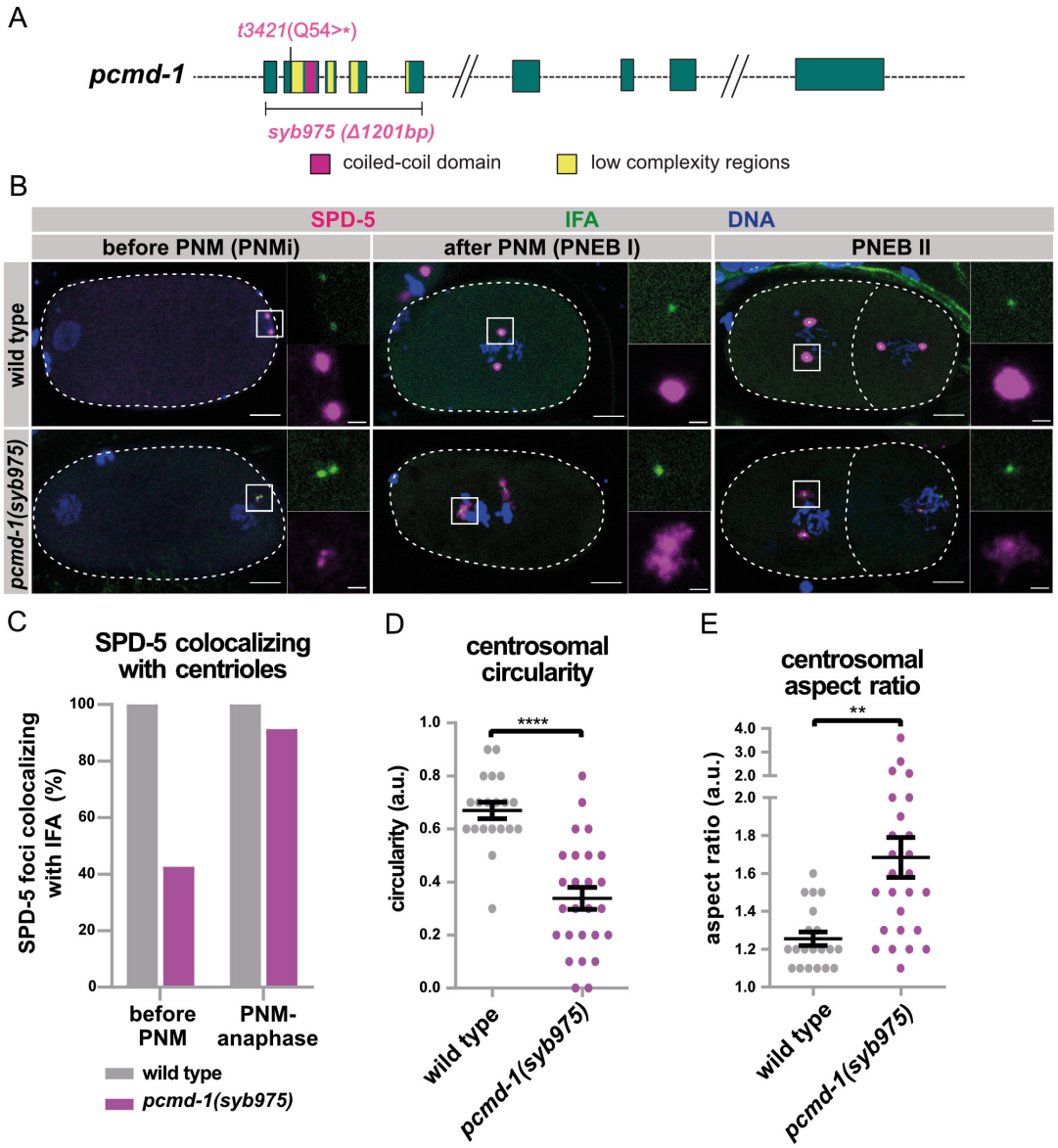

Figure 15. SPD-5 localization to the interphase centrosome is compromised, and PCM integrity of the mitotic PCM is disrupted in *pcmd-1(syb975)* mutant embryos. A) Schematic illustration of the *pcmd-1* gene locus, including the *pcmd-1(t3421)* mutation and the *pcmd-1(syb975)* deletion. The exon structure is shown with the regions coding for the coiled-coil domain in magenta and low complexity regions in yellow. The *pcmd-1(syb975)* allele has a 1201 bp deletion from the beginning, including the coiled-coil domain and low complexity regions, which causes a frameshift. Introns are not to scale. **B)** Representative z-projected fluorescent images of fixed wild-type embryos at PNMi (n=4), PNEB I (n=6), and PNEB II (n=5), and *pcmd-1(syb975)* embryos at PNMi (n=8), PNEB I (n=12), and PNEB II (n=5), respectively stained with antibodies against SPD-5 and IFA. The DNA was stained using Hoechst. Insets show enlarged centrosomal areas as single channels. Scale bars indicate 5 µm and 1 µm (insets). **C)** Quantification of percentage of SPD-5 colocalizing with IFA in wild-type (100.00%, n=7 centrosomes) and *pcmd-1(syb975)* (95.00%, n=20) embryos before PNM and in wild-type (100.00%, n=16 centrosomes) and *pcmd-1(syb975)* (41.67%, n=12 centrosomes) embryos from PNM to anaphase. **D)** Quantification of centrosomal SPD-5 circularity in wild-type (0.67±0.03, n=20 centrosomes) and *pcmd-1(syb975)* (0.34±0.04, n=26 centrosomes) embryos from two-cell stage between PNM and anaphase. Welch two-sample t-test (****p<0.0001). **E)** Quantification of centrosomal SPD-5 aspect ratio in wild-type (1.26±0.04, n=20 centrosomes) and *pcmd-1(syb975)* embryos (1.69±0.11, n=26 centrosomes). Mann-Whitney-U test (**p<0.01). Data in **C)-E)** are represented as mean±SEM. Figure **A)** adapted from Erpf et al. (2019).

To examine whether the PCM assembly around the centrioles is also affected in *pcmd-1(syb975)* embryos, we performed immunofluorescence stainings of wild-type and *pcmd-1(syb975)* embryos as previously for *pcmd-1(t3421)* embryos (Erpf et al., 2019). Centrioles were visualized by staining with antibodies against the intermediate filament protein A1 (IFA-1), which labels centrioles in *C. elegans,* and the PCM protein SPD-5. In addition, DNA was visualized by Hoechst staining. First, I analyzed wild-type and *pcmd-1(syb975)* embryos during interphase (before PNM). SPD-5 was localizing to all analyzed centrioles (100%) in wild-type embryos (**Figure 15B, C**). In contrast, in *pcmd-1(syb975)* embryos, SPD-5 was localizing to 41.67% of the centrioles, and it was missing from 58.33% of the centrioles (**Figure 15B, C**). Second, I analyzed dividing embryos from PNM to anaphase. In wild-type embryos, SPD-5 was localizing to all analyzed centrioles (100%). Interestingly, the detachment of the PCM from centrioles is not as prevalent in dividing *pcmd-1(syb975)* embryos. In *pcmd-1(syb975)* embryos between PNM and anaphase, SPD-5 protein localized with centrioles in 95.00% of the analyzed centrioles (**Figure 15B**, **C**). SPD-5 was missing at only 5.00% of the centrioles. These observations are different from the SPD-5 colocalization observed in *pcmd-1(t3421)* embryos, where the proportion of SPD-5 colocalizing with centrioles (53%) was lower than in *pcmd-1(syb975)* embryos (Erpf et al., 2019). Additionally, the PCM shapes of SPD-5 in *pcmd-1(syb975)* were not spherical but disorganized and fragmented in one-cell embryos (**Figure 15B**). This phenotype was even more prominent in later stages, for instance, in two-cell embryos during mitosis (**Figure 15B**). To characterize the SPD-5 PCM shapes, the mean circularity and aspect ratio of dividing wild-type and *pcmd-1(syb975)* two-cell embryos was determined between PNM and anaphase. A perfect circular centrosome would have a circularity value of and an aspect ratio of 1.00. As more elongated the centrosome is, the circularity value approaches 0.00. The aspect ratio is calculated by dividing the major axis of the centrosome by the minor axis of the centrosome. The more unequal the aspect ratio of a centrosome is, the more the value will differ from 1. In *pcmd-1(sy975)* embryos, the mean circularity of 0.34 was significantly lower than the mean circularity of 0.67 in wild-type embryos (**Figure 15D**). Similarly, the mean aspect ratio of 1.69 in *pcmd-1(sy975)* was significantly higher than the mean aspect ratio of 1.26 in wild-type (**Figure 15E**).

To summarize, *pcmd-1(syb975)* is a strong loss-of-function allele and has a similar phenotype to *pcmd-1(t3421*). Like *pcmd-1(t3421)* embryos, *pcmd-1(syb975)* embryos are lethal at 25°C, and a fraction of the embryos fails to divide in the first cell cycle. In addition, the PCM appears disorganized in both *pcmd-1(syb975)* and *pcmd-1(t3421)* embryos. It cannot be excluded that the variability, which is also observed in this mutant, might be due to an alternative start codon downstream of the 1201 bp deletion in *pcmd-1(syb975)* (Erpf, 2020). In this work, the *pcmd-1(t3421)* allele was used in further experiments as a putative null background under the consideration of its temperature dependency.

3.1.4 RNAi-mediated depletion of *pcmd-1*

In addition to analyzing the strong loss-of-function alleles *pcmd-1(syb975)* and *pcmd-1(t3421),* I aimed to validate the lethal *pcmd-1* mutant phenotype by post-transcriptional silencing applying RNAi treatment. RNAi against *pcmd-1* by feeding performed in our laboratory did not elicit the same phenotype as the mutant alleles.

To post-transcriptionally silence *pcmd-1* by RNAi, dsRNA against *pcmd-1* or *gfp* was injected into the in locus tagged GFP::PCMD-1 (*pcmd-1(syb486[gfp::pcmd-1]*) expressing worms (microinjection was performed together with the Dr. Nadin Memar). A preliminary experiment revealed that RNAi by injection was slightly more efficient when embryonic survival was monitored at 25°C compared to 20°C (Data not shown). Therefore, the embryonic survival of the progeny (F1) was monitored between 24 and 46 hours post-injection at 25°C. In previous RNAi screens, embryonic survival was monitored at 20°C for 24 hours (Sönnichsen et al., 2005). Monitoring the survival rates 39 hours after injection revealed that the survival of *gfp::pcmd-1* embryos was strongly reduced after *pcmd-1(RNAi)* (17.03%, n=54) and *gfp(RNAi)* (18.34%, n=82) treatment compared to the embryonic survival of the control embryos (99.76%, n=335). Note that the number of total eggs laid by the *pcmd-1* depleted worms was much smaller than the number of eggs laid by the control worms. The differences in temperature between the experimental setups and time of monitoring might be the reason why *pcmd-1* was not identified in previous whole-genome RNAi screens (Sönnichsen et al., 2005)

These data validate the *pcmd-1* mutant phenotype regarding embryonic lethality. Thus, even if the RNAi against *pcmd-1* was only partially efficient, it could be demonstrated that PCMD-1 plays an essential role in embryonic development.

3.2 Functional analysis of the PCMD-1 domains and regions

Domain predictions revealed that PCMD-1 contains a single coiled-coil domain and six IDRs (**Figure 16A**) (Erpf et al., 2019; Uniprot-KB O62071; UniProtConsortium, 2019). To map the functional parts of PCMD-1 and investigate different domains and regions of the protein, worm strains with different truncations of PCMD-1 were generated.

3.2.1 The coiled-coil domain of PCMD-1 promotes its centrosomal localization

In centrosomal proteins, coiled-coil domains play regulatory roles and mediate protein-protein interactions, including oligomerization (Kitagawa et al., 2011; Leidel et al., 2005; Lettman et al., 2013; Qiao et al., 2012; Rogala et al., 2015). Here, the focus was on determining the role of the predicted coiled-coil domain in PCMD-1. By performing a prediction using the COILS program (Lupas, 1996b; Lupas et al., 1991), I refined the boundaries of the previously predicted coiled-coil domain in PCMD-1 to the region

between E86 and N117 (Erpf et al., Uniprot-KB O62071; UniProtConsortium, 2019). The region encoding E86 to F118 was deleted in the context of the endogenously tagged *gfp::pcmd-1* using the CRISPR/Cas9 system and is further referred to as *gfp::pcmd-1(ΔCC)* (**Figure 16A**).

An embryonic survival assay performed at 25°C revealed that the viability of the *gfp::pcmd-1* and *gfp::pcmd-1(ΔCC)* embryos significantly differs. While 97.45% of the *gfp::pcmd-1* embryos survived, only 87.63% of the *gfp::pcmd-1(ΔCC)* embryos were viable (**Figure 16B**).

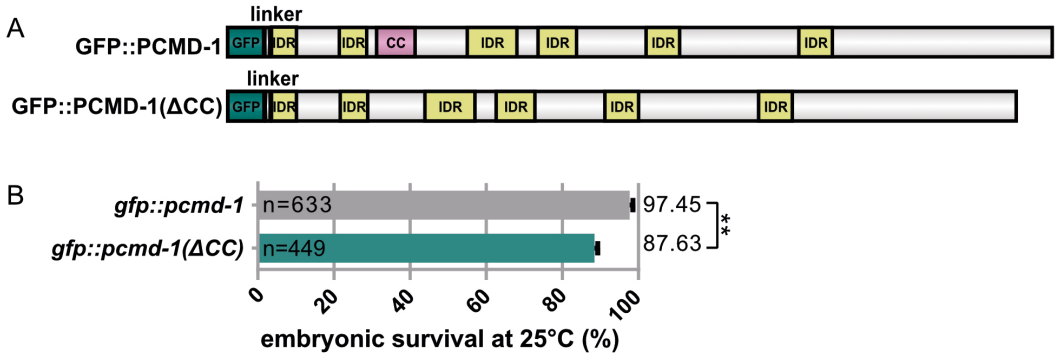

Figure 16. The absence of the coiled-coil domain in PCMD-1 only mildly affects embryonic viability. A) Schematic illustration of the domain structure of the endogenously GFP-tagged full-length PCMD-1 protein (aa E2-D630) and the endogenously GFP-tagged truncated PCMD-1 version with the deleted coiled-coil domain (ΔE86-N118). The predicted coiled-coil domain (CC) is highlighted in magenta and the IDRs (aa 1-20, 56-78, 159-199, 216-247, 303-330, 426-453) are highlighted in yellow. Note that all domains except GFP are represented to the correct ratio; GFP is scaled down in a ratio of ~1:10. **B)** Embryonic survival assay performed at 25°C. The embryonic survival of *gfp::pcmd-1(ΔCC)* embryos (87.63±0.03%, n=633) was significantly reduced compared to *gfp::pcmd-1* embryos (97.45±0.06%, n=449). Mann-Whitney-U test (** p<0.01). Data are represented as mean and SEM, n=total number of embryos. Figure adapted from Stenzel et al. (2020).

Next, I examined whether cell division is impaired in *gfp::pcmd-1(ΔCC)* one-cell embryos and whether GFP::PCMD-1(ΔCC) is localizing to the centrosome like GFP::PCMD-1 performing live-cell imaging. All GFP::PCMD-1(ΔCC) expressing embryos were normally dividing as the GFP::PCMD-1 expressing embryos. However, the centrosomal localization of GFP::PCMD-1 and GFP::PCMD-1(ΔCC) was different. Compared to GFP::PCMD-1, which was visible at centrosomes in all analyzed embryos, the GFP::PCMD-1(ΔCC) centrosomal signal was much weaker in all analyzed embryos, even not detectable at 3 out of 18 spindle poles, which were defined by the DIC channel (**Figure 17A**). When the centrosomal fluorescence intensities were quantified at the stage of PNEB, the mean centrosomal GFP::PCMD-1(ΔCC) intensity of 0.34 a.u. was significantly decreased compared to the mean centrosomal GFP::PCMD-1 intensity of 1.00 a.u. (**Figure 17B**). Cytoplasmic GFP signals were quantified to exclude that the centrosomal GFP::PCMD-1(ΔCC) intensities are lower due to lower expression on the cellular level. The

cytoplasmic GFP::PCMD-1(ΔCC) intensity of 1.09 a.u. was not lower but slightly higher than the GFP::PCMD-1 cytoplasmic signals (1.0 a.u.) (**Figure 17C**). This finding provides evidence that PCMD-1 expression is not reduced in the absence of the coiled-coil domain.

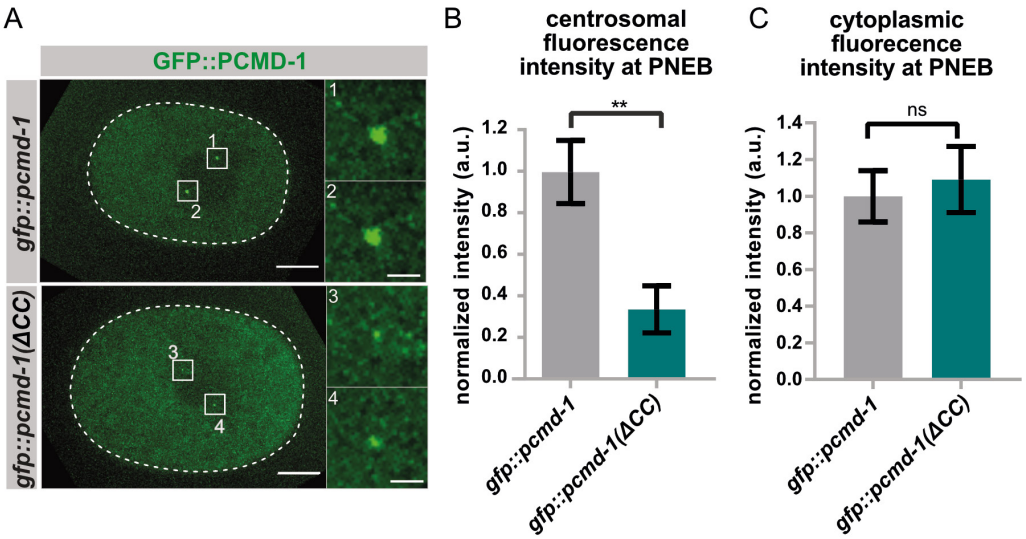

Figure 17. The coiled-coil domain in PCMD-1 promotes its centrosomal localization. **A)** Representative stills of time-lapse sequences at the time point of PNEB of *gfp::pcmd-1* (n=7) or *gfp::pcmd-1(ΔCC)* (n=9) one-cell embryos recorded with a spinning disc confocal microscope. In all *gfp::pcmd-1* embryos, GFP::PCMD-1 was detected at centrosomes (n=14). In *gfp::pcmd-1(ΔCC)* embryos, GFP::PCMD-1(ΔCC) was detected at 15 out of 18 centrosomes. Images are displayed as z-projections. Centrosomal areas were defined by DIC imaging. Insets show enlarged centrosomal areas labeled with corresponding numbers (1-4). Scale bars indicate 10 µm or 2 µm (insets). **B)** Quantification of centrosomal signal intensities in *gfp::pcmd-1* (1.00±0.15 a.u., n=14 centrosomes) and *gfp::pcmd-1(ΔCC)* embryos (0.34±0.11 a.u., n=18 centrosomes) at PNEB. Values were normalized to the mean intensity of GFP::PCMD-1. Mann-Whitney-U test (**p<0.01). **C)** Quantification of cytoplasmic intensities in *gfp::pcmd-1* (1.00±0.14 a.u, n=7) and *gfp::pcmd-1(ΔCC)* (1.09±0.18 a.u., n=9) embryos at PNEB. Values were normalized to the mean intensity of GFP::PCMD-1. Two-sample t-test (ns: not significant). Data in **B)** and **C)** Data are represented as mean±SEM. Figure adapted from Stenzel et al. (2020).

In summary, these findings suggest that the coiled-coil domain of PCMD-1 promotes its accumulation at the centrosome. However, the absence of the coiled-coil domain only mildly impairs the viability of the embryos.

3.2.2 The coiled-coil domain of PCMD-1 is required for PCM scaffold organization

Even though the embryonic survival rate of the *gfp::pcmd-1(ΔCC)* embryos with reduced PCMD-1 levels at the centrosome was decreased, most of the embryos were still able to divide. Therefore, the question was raised whether the PCM scaffold might be normally assembled in embryos lacking the coiled-coil domain of PCMD-1.

To analyze the appearance of the PCM scaffolds, immunofluorescence stainings of *gfp::pcmd-1* and *gfp::pcmd-1(ΔCC)* one-cell embryos during mitosis with antibodies against GFP and the PCM protein SPD-5 were performed. The DNA was visualized by Hoechst staining. As observed in the time-lapse movies, the centrosomal GFP::PCMD-1(ΔCC) signal was much lower than the centrosomal GFP::PCMD-1 signal in immunofluorescence stainings (**Figure 18A**). SPD-5 was detected at centrosomes in all analyzed *gfp::pcmd-1* and *gfp::pcmd-1(ΔCC)* embryos (**Figure 18A**). However, in *gfp::pcmd-1(ΔCC)* embryos, the SPD-5 signal appeared much more disorganized compared to the SPD-5 scaffold in *gfp::pcmd-1* embryos (**Figure 18A**). Therefore, the circularity and the aspect ratio of the SPD-5 shapes were quantified in *gfp::pcmd-1* and *gfp::pcmd-1(ΔCC)* one-cell embryos. As explained in chapter **3.1.3**, a perfect circle would have a circularity and an aspect ratio of 1.0. The mean centrosomal circularity of 0.49 in *gfp::pcmd-1(ΔCC)* embryos was significantly lower than the mean centrosomal circularity of 0.74 in *gfp::pcmd-1* embryos (**Figure 18B**). Similarly, quantification of the aspect ratio in the one-cell embryos revealed a significant difference between the mean aspect ratio of 1.44 in *gfp::pcmd-1(ΔCC)* and 1.21 in *gfp::pcmd-1* embryos (**Figure 18C**).

Together, these data show that the SPD-5 scaffold is less circular and less coherent when the coiled-coil domain is depleted. Therefore, I propose that the coiled-coil domain promotes the integrity of the SPD-5 PCM scaffold.

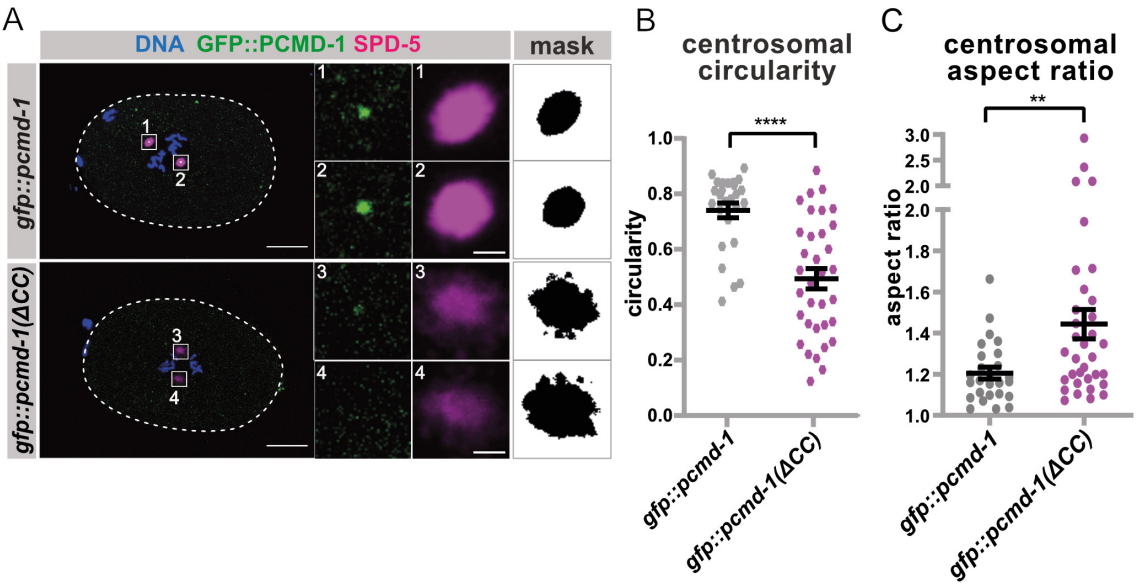

Figure 18. The coiled-coil domain in PCMD-1 promotes PCM scaffold integrity. A) Representative z-projected fluorescent images of fixed *gfp::pcmd-1* (n=13) and *gfp::pcmd-1(ΔCC)* (n=17) one-cell embryos during mitosis stained with antibodies against GFP and SPD-5. DNA was stained with Hoechst. Insets show enlarged centrosomal areas as single channels labeled with corresponding numbers, including the SPD-5 masks used for the shape measurements. Scale bars indicate 10 µm and 1 µm (insets)**. B)** Quantification of centrosomal SPD-5 circularity in *gfp::pcmd-1* (0.74±0.03, n=26 centrosomes) and *gfp::pcmd-1(ΔCC)* (0.49±0.04, n=34 centrosomes) embryos. Mann-Whitney-U test (**** p<0.0001). **C)** Quantification of centrosomal SPD-5 aspect ratio in *gfp::pcmd-1* (1.21±0.03, n=26 centrosomes) and *gfp::pcmd-1(ΔCC)* embryos (1.44±0.07, n=34 centrosomes). Mann-Whitney-U (**p<0.01). Data in **B)** and **C)** are represented in mean±SEM. Figure adapted from Stenzel et al. (2020).

3.2.3 The C-terminus of PCMD-1 is required for centrosomal localization

As GFP::PCMD-1(ΔCC) localized to centrosomes in most of the embryos, protein domains or regions other than the predicted coiled-coil domain might be responsible for the centrosomal targeting of PCMD-1.

To further map which part of the protein plays a role in centrosomal targeting, different truncated versions of PCMD-1 were investigated. While GFP::PCMD-1(N) comprises amino acid E2 until N117, containing the predicted coiled-coil domain and two IDRs, GFP::PCMD-1(C) spans the region from amino acid F118 until the stop codon, including the four predicted IDRs (**Figure 19A**). Single-copies of the truncated parts of the *pcmd-1*

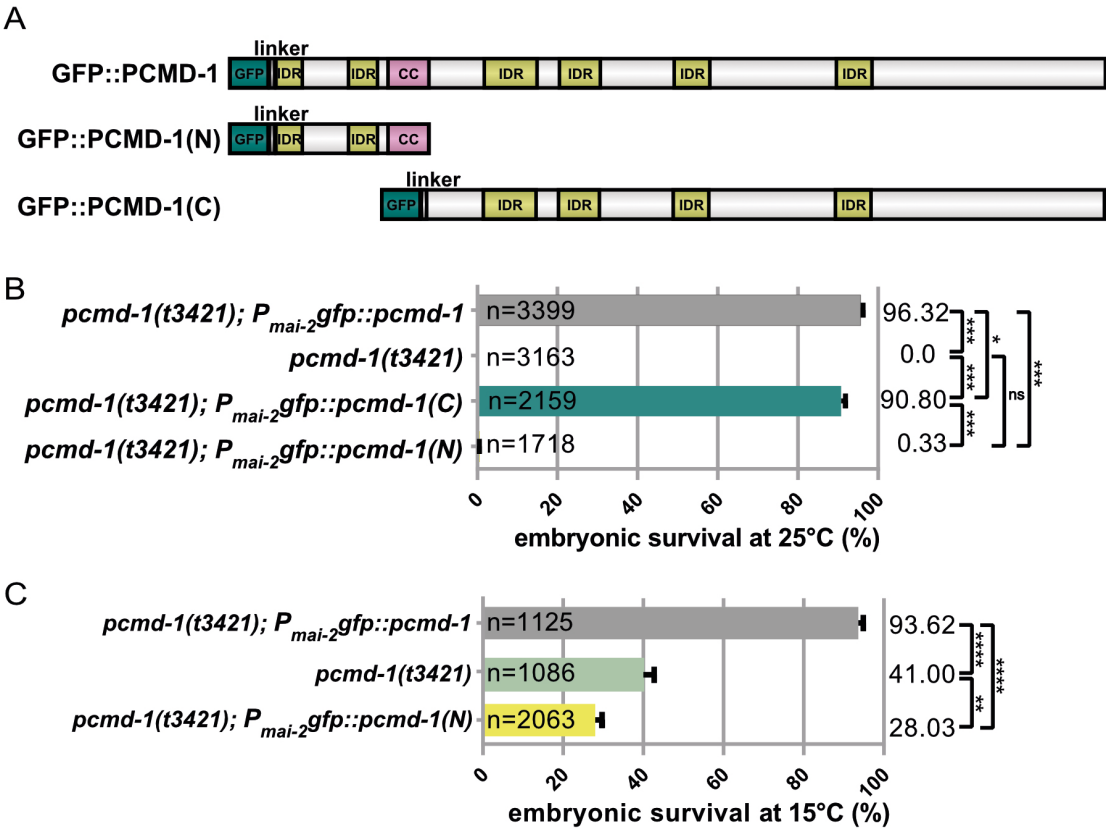

Figure 19. The C-terminus of PCMD-1 is required for embryonic viability. Schematic illustration of the domain structure of the different GFP tagged PCMD-1 constructs. The GFP::PCMD-1 full-length protein is shown on top, GFP::PCMD-1(N_2-117) spanning E2-N117 is shown in the middle, and GFP::PCMD-1(C_118-630) spanning F118-D630 is shown on the bottom. The predicted coiled-coil domain (CC) is highlighted in magenta and the IDRs are highlighted in yellow. Note that all domains except GFP are represented to the correct ratio; GFP is scaled down in a ratio of ~1:10. **B)** Embryonic survival assay performed at 25°C. The embryonic viability of *pcmd-1(t3421)* (0.00±0.00%, n=3163) was restored in *Pmai-2gfp::pcmd-1* (96.32±0.47%, n=3399) and *Pmai-2gfp::pcmd-1(C)* (90.80±1.09%, n=2159*)* embryos but not in *Pmai-2gfp::pcmd-1(N)* embryos (0.33±0.19%, n=1718) in the *pcmd-1(t3421)* background. Multiple comparison with Kruskal-Wallis test and post-hoc Dunn's test (Holm correction) (* p<0.05, *** p<0.001). **C)** Embryonic survival assay performed at 15°C. The embryonic partial viability of *pcmd-1(t3421)* embryos (40.99±2.68%, n=2063) was restored in *Pma-2gfp::pcmd-1* embryos (93.62±1.27%, n=1512), but not in *Pmai-2gfp::pcmd-1(N)* (28.03±1.72%, n=1086), which showed lower survival. Multiple Comparison with Kruskal Wallis test and post-hoc Dunn's test (Holm correction) (** p<0.01, **** p<0.0001). Data in **B)** and **C)** are represented as mean and SEM, n=total number of embryos. Data acquired together with J. Mehler and S. Üstüner. Figure adapted from Stenzel et al. (2020).

cDNA fused to *gfp* in the 5' end under *mai-2* regulatory elements in the *pcmd-1(t3421)* background were generated and analyzed regarding their function and localization.

In an embryonic survival assay performed at the restrictive temperature of 25°C (**Figure 19B**), the $P_{mai\text{-}2}$*gfp::pcmd-1* rescued the 100% *pcmd-1(t3421)* lethality with an embryonic survival rate of 96.32%. $P_{mai\text{-}2}$*gfp::pcmd-1(C)* could also rescue the embryonic lethality *pcmd-1(t3421)* phenotype with a survival rate of 90.80%, but the survival rate was significantly different to $P_{mai\text{-}2}$*gfp::pcmd-1* embryos. In contrast, the $P_{mai\text{-}2}$*gfp::pcmd-1(N)* embryos could not rescue the embryonic lethality, and only 0.33% of the embryos survived (**Figure 19B**). In an embryonic survival assay conducted at the permissive temperature of 15°C (**Figure 19C**), 41.00% of the *pcmd-1(t3421)* embryos could survive, similar as described previously (Erpf et al., 2019). The embryonic survival of 41.00% of the *pcmd-1(t3421)* embryos was significantly different from the embryonic survival rate of 93.62% in $P_{mai\text{-}2}$*gfp::pcmd-1* embryos (**Figure 19C**). Interestingly, the $P_{mai\text{-}2}$*gfp::pcmd-1(N)* embryos in *pcmd-1(t3421)* background showed a significantly lower survival rate of 28.03% compared to *pcmd-1(t3421)* embryos (**Figure 19C**). Thus, the expression of the truncated GFP::PCMD-1(N) construct even negatively impacts embryonic survival.

Next, the subcellular localization of the different constructs was monitored in one-cell embryos by live-cell imaging., GFP::PCMD-1(C) was detected at the centrosomes in all analyzed embryos in *pcmd-1(t3421)* background similar to the GFP::PCMD-1 full-length protein in *pcmd-1(t3421)* background (**Figure 20A**). In contrast, GFP::PCMD-1(N) was not detectable at centrosomes in any of the analyzed embryos in *pcmd-1(t3421)* background (**Figure 20A**) (Data and image T. Mikeladze-Dvali, Stenzel et al., 2020). Interestingly, the cytoplasmic signal is drastically increased in $P_{mai\text{-}2}$*gfp::pcmd-1(N)* embryos. Quantifications of the centrosomal fluorescence intensities of $P_{mai\text{-}2}$*gfp::pcmd-1* and $P_{mai\text{-}2}$*gfp::pcmd-1(C)* embryos in *pcmd-1(t3421)* background at the stage of PNEB confirmed that the mean centrosomal GFP::PCMD-1(C) intensity of 0.73 a.u. was significantly lower compared to the mean centrosomal GFP::PCMD-1 intensity of 1.00 a.u. (**Figure 20B**). The cytoplasmic fluorescence intensities were quantified to exclude that the mean centrosomal GFP::PCMD-1(C) intensity is lower due to lower expression levels. The mean cytoplasmic GFP::PCMD-1(C) intensity of 1.43 a.u. was even higher than the mean GFP::PCMD-1 cytoplasmic intensity of 1.0 a.u. However, the difference between the mean cytoplasmic GFP intensities is not significantly different.

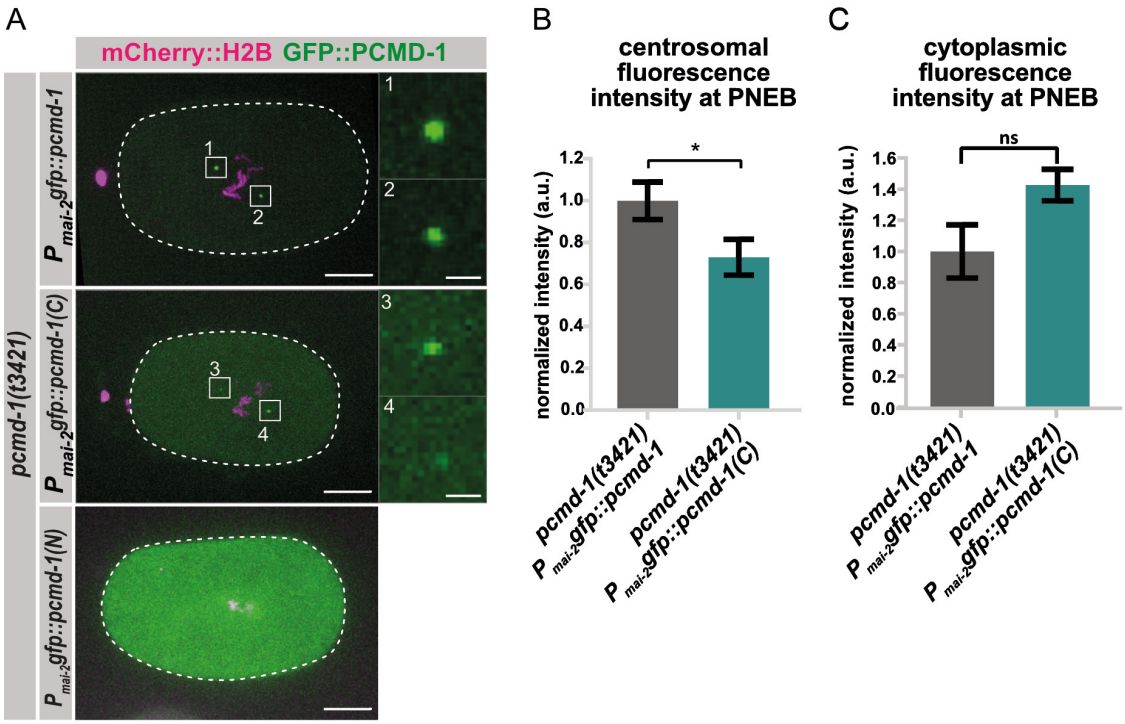

Figure 20. The C-terminus of PCMD-1 localizes to centrosomes but not the N-terminus of PCMD-1. A) Representative stills of time-lapse sequences at the time point of PNEB of *P*$_{mai-2}$*gfp::pcmd-1* (n=12), *P*$_{mai-2}$*gfp::pcmd-1(C)* (n=10), and *P*$_{mai-2}$*gfp::pcmd-1(N)* (n=7, image provided by T. Mikeladze-Dvali) one-cell embryos in *pcmd-1(t3421)* background with *P*$_{pie-1}$*mCherry::h2b* as a histone marker recorded with a spinning disc confocal microscope. PCMD-1 was detected at the centrosomes in *P*$_{mai-2}$*gfp::pcmd-1* and *P*$_{mai-2}$*gfp::pcmd-1(C)* embryos but not detected in *P*$_{mai-2}$*gfp::pcmd-1(N)* embryos. Images are displayed as merged z-projections. Insets show enlarged centrosomal areas labeled with corresponding numbers (1-4). Scale bars indicate 10 µm or 2 µm (insets). **B)** Quantification of centrosomal signal intensities in *pcmd-1(t3421); P*$_{mai-2}$*gfp::pcmd-1* (1.00±0.09 a.u., n=24 centrosomes) and *pcmd-1(t3421); P*$_{mai-2}$*gfp::pcmd-1(C)* (0.73±0.09 a.u., n=20 centrosomes) embryos at PNEB. Values were normalized to the mean intensity of GFP::PCMD-1. Mann-Whitney-U test (* $p<0.05$). Data are represented as mean±SEM. **C)** Quantification of cytoplasmic signal intensities in *P*$_{mai-2}$*gfp::pcmd-1* (1.00±0.17 a.u., n=12) and *P*$_{mai-2}$*gfp::pcmd-1(C)* (1.43±0.10 a.u., n=10) embryos at PNEB. Two-sample t-test (ns: not significant). Data in **B)** and **C)** are represented as mean±SEM. Figure adapted from Stenzel et al. (2020).

To further narrow down the region that targets PCMD-1 to the centrosome, my colleagues A. Schreiner and T. Mikeladze-Dvali subdivided the C-terminal part of PCMD-1 into two fragments and generated and analyzed worms expressing GFP::PCMD-1(C1_118-342) and GFP::PCMD-1(C2_342-630) in *pcmd-1(t3421)* background (**Figure 21A**). In an embryonic survival assay performed at 25°C, my colleague A. Schreiner found that both constructs did not rescue the embryonic lethality of *pcmd-1(t3421)* (Stenzel et al., 2020). When the subcellular localization was assayed, only GFP::PCMD-1(C2) was detected at the centrosome in all analyzed embryos, whereas GFP::PCMD-1(C1) was not visible at the centrosomes (**Figure 21B**, Data and images from T. Mikleldaze-Dvali, Stenzel et al., 2020).

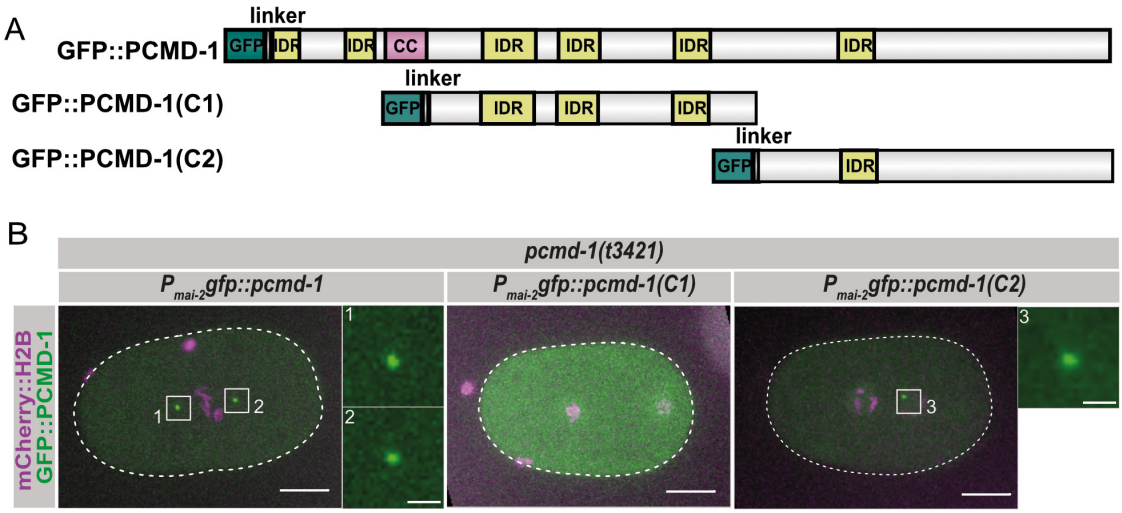

Figure 21. The C-terminal part (G343-D630) of PCMD-1 localizes to centrosomes, but not the middle part (F118-D342) of PCMD-1. A) Schematic illustration of the domain structure of the different GFP tagged PCMD-1 constructs. The GFP::PCMD-1 full-length protein is illustrated on top, GFP::PCMD-1(C1_118-342) spanning F118-D342 is illustrated in the middle, and GFP::PCMD-1(C2_343-630) spanning G343-D630 is illustrated on the bottom. The predicted coiled-coil domain (CC) is highlighted in magenta and the IDRs are highlighted in yellow. Note that all domains except GFP are represented to the correct ratio; GFP is scaled down in a ratio of ~1:10. **B)** Representative stills of time-lapse sequences of *P*$_{mai-2}$*gfp::pcmd-1* (n=9), *P*$_{mai-2}$*gfp::pcmd-1(C1)* (n=9), and *P*$_{mai-2}$*gfp::pcmd-1(C2)* (n=9) one-cell embryos in *pcmd-1(t3421)* background with *P*$_{pie-1}$*mCherry::h2b* as a histone marker at the time point of PNEB recorded with a spinning disc confocal microscope. PCMD-1 was detected at the centrosomes in *P*$_{mai-2}$*gfp::pcmd-1* and *P*$_{mai-2}$*gfp::pcmd-1(C2)* embryos but not detected in *P*$_{mai-2}$*gfp::pcmd-1(C1)* embryos. Images are displayed as merged z-projections. Insets show enlarged centrosomal areas labeled with corresponding numbers (1-3). Scale bars indicate 10 µm or 2 µm (insets). Images provided by T. Mikeladze-Dvali. Figure adapted from Stenzel et al. (2020).

Taken together, our data demonstrate that the N-terminal part of PCMD-1, including the coiled-coil domain, is not sufficient to anchor to the centrosome and cannot rescue the embryonic lethality of the *pcmd-1(t3421)* lethal phenotype. On the contrary, GFP::PCMD-1(N) negatively affects embryonic survival, and high cytoplasmic GFP intensities can be observed in those embryos. In contrast, the C-terminal part of PCMD-1, which lacks the coiled-coil domain and the first two predicted IDRs, rescues the lethality of the *pcmd-1(t3421)* mutant. Further, the results indicate that the C-terminal part of PCMD-1 is responsible for anchoring PCMD-1 to the centrosome.

3.2.4 The C-terminus of PCMD-1 without the coiled-coil domain cannot restore the organized PCM scaffold

Since the N-terminal part, including the coiled-coil domain, is missing in the C-terminal PCMD-1 construct, I assumed that the PCM scaffold would also be disorganized in *P*$_{mai-2}$*gfp::pcmd-1(C)* embryos in *pcmd-1(t3421)* background. One could speculate that the PCM is even more disturbed as the truncation is larger in the *P*$_{mai-2}$*gfp::pcmd-1(C)* embryos.

To test this hypothesis, I analyzed the shapes of the PCM. Therefore, immunofluorescence stainings of *P*$_{mai-2}$*gfp::pcmd-1* and *P*$_{mai-2}$*gfp::pcmd-1(C)* one-cell embryos in *pcmd-1(t3421)* background were performed against GFP and the PCM protein SPD-5. The DNA was visualized by Hoechst staining. In all analyzed embryos, SPD-5 could be detected at the centrosomes (**Figure 22A**). As expected, the SPD-5 signal in the GFP::PCMD-1(C) expressing embryos in *pcmd-1(t3421)* background appeared more disorganized, compared to the GFP::PCMD-1 full-length expressing embryos in *pcmd-1(t3421)* background (**Figure 22A**). The shape of the SPD-5 scaffolds was characterized by quantifying the centrosomal circularity and aspect ratio in one-cell embryos during mitosis. As explained in chapter **3.1.3**, a perfect circular centrosome would have a circularity and an aspect ratio of 1.00. The mean centrosomal circularity of 0.61 was significantly lower in *P*$_{mai-2}$*gfp::pcmd-1(C)* than the mean centrosomal circularity of 0.73 in *P*$_{mai-2}$*gfp::pcmd-1* embryos in *pcmd-1(t3421)* background (**Figure 22B**). Indeed, the quantified mean centrosomal aspect ratio of 1.34 in *pcmd-1(t3421); P*$_{mai-2}$*gfp::pcmd-1(C)* embryos was slightly increased in comparison to the quantified mean centrosomal aspect ratio of 1.26 in *pcmd-1(t3421); P*$_{mai}$*-gfp::pcmd-1* embryos, although a significance was not computable (**Figure 22C**). The hypothesis that the PCM is more disturbed due to the lack of the whole N-terminus cannot be confirmed.

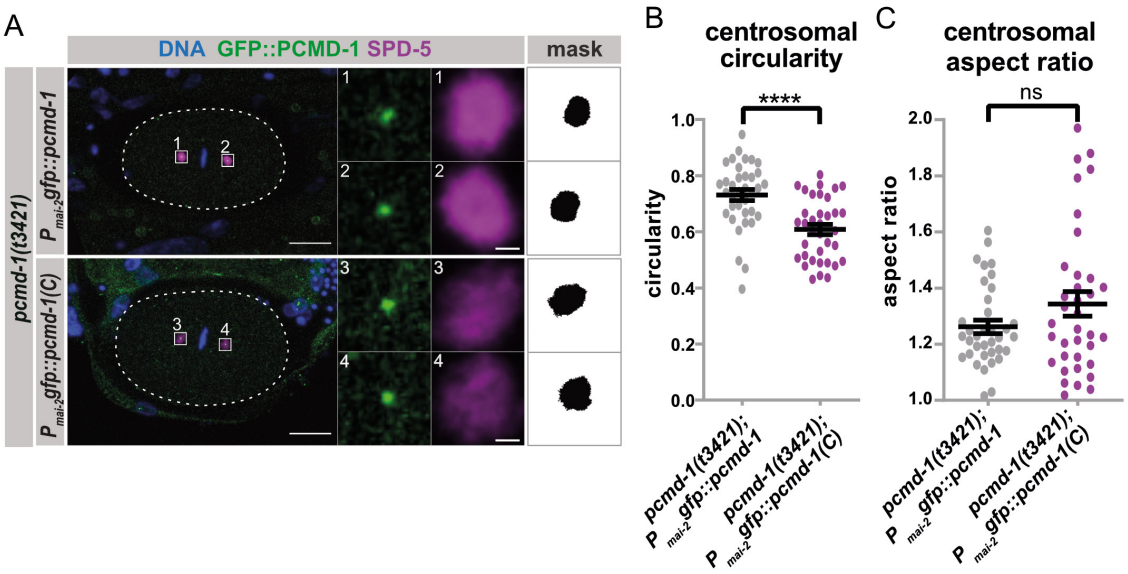

Figure 22. The C-terminus of PCMD-1 without the coiled-coil domain cannot restore the PCM scaffold organization. A) Representative z-projected fluorescent images of fixed *P*$_{mai-2}$*gfp::pcmd-1* (n=18) and *P*$_{mai-2}$*gfp::pcmd-1(C)* (n=18) in *pcmd-1(t3421)* background one-cell embryos during mitosis stained with antibodies against GFP and SPD-5. DNA was stained using Hoechst. Insets show enlarged centrosomal areas as single channels labeled with corresponding numbers, including the SPD-5 masks generated for the shape measurements. Scale bar indicate 10 µm and 1 µm (insets). **B)** Quantification of centrosomal SPD-5 circularity in *P*$_{mai-2}$*gfp::pcmd-1* (0.73±0.02, n=36 centrosomes) and *P*$_{mai-2}$*gfp::pcmd-1(C)* embryos (0.61±0.02, n=36 centrosomes). Unpaired two-sample t-test (**** p<0.0001). **C)** Quantification of centrosomal SPD-5 aspect ratio in *P*$_{mai-2}$*gfp::pcmd-1* (1.26±0.03, n=36) and *P*$_{mai-2}$*gfp::pcmd-1(C)* (1.34±0.04, n=36) embryos. Mann-Whitney-U test (ns: not significant). Data in **B)** and **C)** are represented in mean±SEM.

In summary, this finding demonstrates that the SPD-5 scaffold is less circular but not significantly deformed in embryos expressing the C-terminal part of PCMD-1 lacking the coiled-coil domain. Thus, The C-terminal part of PCMD-1 cannot restore the SPD-5 scaffold integrity in the *pcmd-1(t3421)* background, most probably because the coiled-coil domain is missing.

3.3 Genetic dependencies between PCMD-1 and centrosomal proteins

3.3.1 Genetic dependencies between PCMD-1 and SPD-5 or SPD-2

3.3.1.1 SPD-5 and SPD-2 expression is not downregulated in *pcmd-1(t3421)*

It has been shown that the recruitment of the PCM proteins SPD-5 and SPD-2 to the centrosome is compromised in *pcmd-1(t3421)* mutant embryos (Erpf et al., 2019). To investigate whether the PCM recruitment defects are due to the absence of the proteins on the cellular level or only the centrosomal levels are compromised in *pcmd-1(t3421)* embryos, protein levels of mixed-stage whole worm lysates were analyzed. Mixed-stage worm lysates were immunoblotted against the GFP::SPD-5 and SPD-2 in wild-type and *pcmd-1(t3421)* background. In addition, tubulin was probed as a loading control. In both wild-type and *pcmd-1(t3421)* worms, GFP::SPD-5 was present at similar levels (**Figure 23A**). Similarly, SPD-2 expression levels in *pcmd-1(t3421)* worms were at the wild-type levels (**Figure 23B**).

From these data, I conclude that the PCM recruitment defects in the absence of a functional PCMD-1 protein are not caused by the downregulation or degradation of SPD-5 or SPD-2.

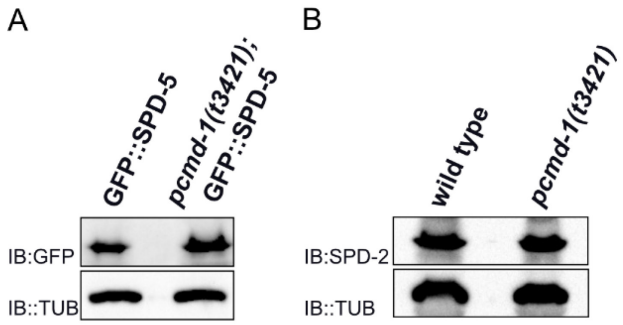

Figure 23. Expression levels of cellular SPD-5 and SPD-2 are not reduced in *pcmd-1(t3421)* mutants. A) Cellular GFP::SPD-5 in *pcmd-1(t3421)* background was expressed wild-type levels. Mixed-stage worm lysates were immunoblotted (IB) with an antibody against GFP and with an α-tubulin (TUB) antibody as a loading control. **B)** Cellular SPD-2 in *pcmd-1(t3421)* background was expressed at wild-type levels. Mixed-stage worm lysates were immunoblotted with antibodies against SPD-2 and an α-tubulin (TUB) antibody as a loading control. Figure adapted from Erpf et al. (2019).

3.3.1.2 Centrosomal localization of PCMD-1 is independent of SPD-5 and SPD-2

Previous data (Erpf et al., 2019) have shown that PCMD-1 is required to assemble the PCM core. To determine whether PCMD-1 localization to the centrosome conversely depends on the PCM proteins SPD-5 or SPD-2, endogenous GFP::PCMD-1 was monitored in *gfp::pcmd-1, spd-2(or293); gfp::pcmd-1* and *spd-5(or231); gfp::pcmd-1* embryos throughout the first and second cell cycle. Since *spd-2(or293)* and *spd-5(or231)* alleles are temperature-sensitive (Hamill et al., 2002; O'Rourke et al., 2011), the worms were grown at 25°C as described in chapter **2.2.1,** and the progeny was analyzed at the restrictive temperature of 25°C. As expected, GFP::PCMD-1 was detectable at the centrosomes in all analyzed *gfp::pcmd-1* control embryos during the first cell cycle. Centrosomes are not able to separate due to disrupted microtubule organization in *spd-5(or213)* and s*pd-2(or293)* mutant embryos (Hamill et al., 2002; Kemp et al., 2004; Pelletier et al., 2004). Nevertheless, in *spd-5(or13); gfp::pcmd-1* and *spd-2(or293); gfp::pcmd-1* mutant embryos, GFP::PCMD-1 was also visible, and two foci were distinguishable (**Figure 24**). Similarly, it has been described that downregulation of the PCM protein PLK-1 does not lead to loss of the centrosomal PCMD-1 localization (Erpf et al., 2019).

Based on these results, I propose that the PCM proteins SPD-5 and SPD-2 are not required for the centrosomal loading of PCMD-1.

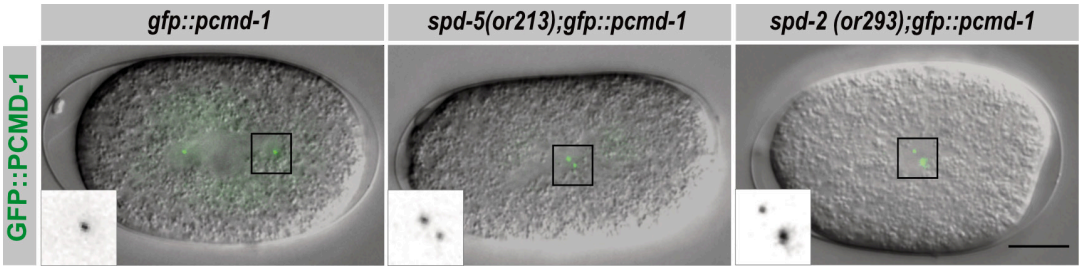

Figure 24. PCMD-1 localizes to the centrosome independent of SPD-5 and SPD-2. Representative stills of time-lapse sequences of one-cell embryos expressing GFP::PCMD-1 in *gfp::pcmd-1* (n=10), *spd-5(or213); gfp::pcmd-1* (n=11), and *spd-2(or293); gfp::pcmd-1* (n=10) recorded at 25°C with a 4D time-lapse microscope. Images are displayed as DIC merged with z-projected GFP channel. Insets show enlarged centrosomal areas of GFP inverted in black/white. Scale bar indicates 10 µm. Figure adapted from Erpf et al. (2019).

3.3.2 Genetic dependencies between PCMD-1, SAS-7, and SAS-4

SAS-7 localizes to the outermost of centrioles and is required to stabilize centrioles (Sugioka et al., 2017). Furthermore, it has been shown that SAS-7 regulates centriole duplication and PCM assembly by targeting SPD-2 to the centriole (Sugioka et al., 2017). Thus, a fraction of the *sas-7(or452ts)* mutant embryos form a monopolar spindle during the first cell division and cannot divide. This phenotype is similar to the observed *pcmd-1(t3421)* and *pcmd-1(syb975)* phenotype. The similarity of the mutant phenotypes

and the function of PCMD-1 and SAS-7 in PCM assembly prompted me to investigate whether SAS-7 and PCMD-1 are interdependent. More specifically, I aimed to determine whether one of the proteins regulates the recruitment of the other protein. Furthermore, since SAS-7 was shown to interact with the centriolar protein SAS-4 (Boxem et al., 2008), I wondered whether SAS-4 regulates the localization of the proteins.

3.3.2.1 PCMD-1 and SAS-7 colocalize at centrosomes dependent on SAS-4 and PCMD-1 localizes to MTs

First, the spatial relationship of PCMD-1 and SAS-7 was examined by generating in locus tagged GFP::PCMD-1 and RFP::SAS-7 expressing worms (*gfp::pcmd-1; rfp::sas-7)* and analyzing adult worms and embryos. GFP::PCMD-1 and RFP::SAS-7 colocalizing at centrosomes were monitored in embryos of all stages, for instance, in two-cell stage embryos (**Figure 25A**). Due to the small size of the centrosome in *C. elegans,* it was

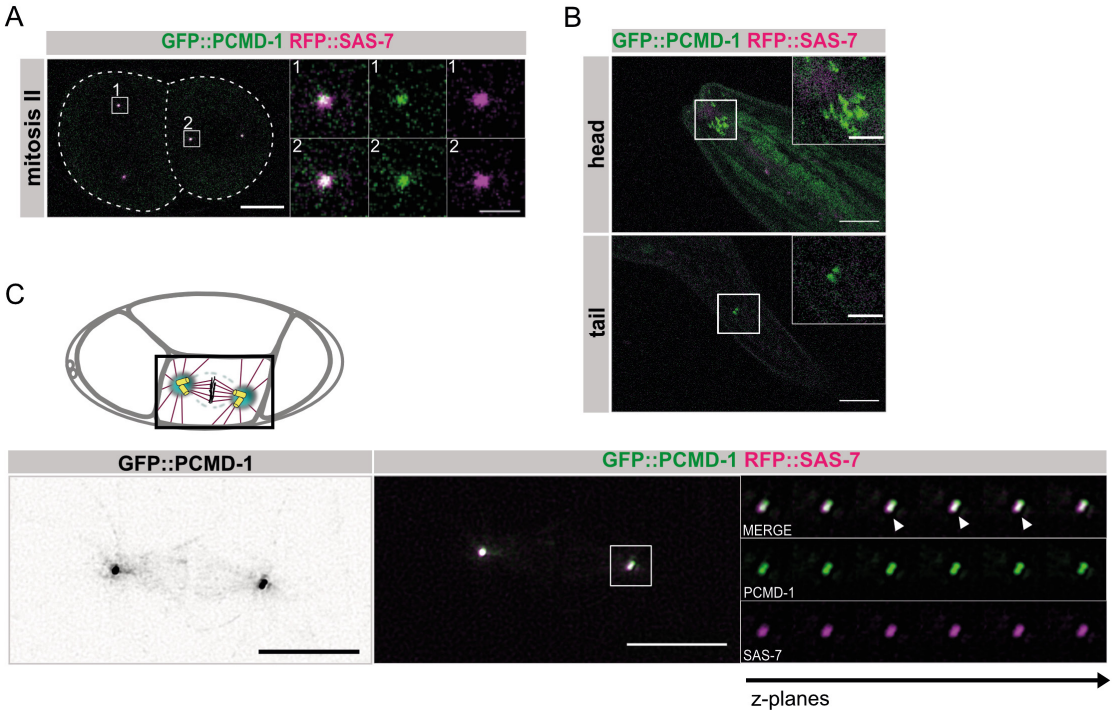

Figure 25. PCMD-1 and SAS-7 colocalize at centrosomes and PCMD-1 localizes to microtubules. A) Representative fluorescent image of a *gfp::pcmd-1; rfp::sas-7* two-cell stage embryo during mitosis (n=7) recorded with a confocal microscope. Endogenous GFP::PCMD-1 and RFP::SAS-7 signals largely overlapped at centrosomes. The image is displayed as merge. Insets show enlarged centrosomal areas as merge and single channels labeled with corresponding numbers (1-2). Scale bars indicate 10 µm and 2 µm (insets). **B)** Representative fluorescent images of cilia at sensory neurons (head and tail) of *gfp::pcmd 1; rfp::sas-7* worms (n=4). GFP::PCMD-1 was present at the cilia, while GFP::SAS-7 absent. Images are displayed as merged z-projections. Insets show enlarged area of cilia. Scale bars indicate 10 µm or 4 µm (insets). **C)** Representative z-projected image of mitotic centrosomes in a four-cell stage *gfp::pcmd-1; rfp::sas-7* embryo (n=6 centrosomes) recorded with a Elyra 7 SIM microscope (Zeiss, data and image by M. Gorelashvili and T. Mikeladze-Dvali). Note that GFP::PCMD-1 was visible at MTs (right site). GFP::PCMD-1 and RFP::SAS-7 colocalized at both centrioles. The image of the embryo is displayed as merge and the PCMD-1 channel in black/white. The panels on the right represent the z-planes spanning the centrioles displayed as merge and single channels. At one centriole more GFP::SAS-7 accumulated (arrowheads). Scalebar indicates 10 µm. Figure adapted from Stenzel et al. (2020).

technically impossible to resolve the two centrioles with standard confocal microscopy. However, super-resolution imaging with an Elyra 7 SIM microscope (Zeiss) revealed that GFP::PCMD-1 and RFP::SAS-7 localization mostly overlapped at both centrioles in early embryos undergoing mitosis (**Figure 25C**, data from M. Gorelashvili and T. Mikeladze-Dvali, Stenzel et al., 2020). Interestingly, we could observe that RFP::SAS-7 accumulated and colocalized more at one centriole than at the other centriole (**Figure 25C**, arrowheads). The function of SAS-7 in daughter centriole formation and maturation could explain its uneven distribution at the centrioles (Sugioka et al., 2017). Notably, GFP::PCMD-1 was also faintly detectable around centrioles and at MTs (**Figure 25C**). As PCMD-1 localizes to cilia, localization of GFP::PCMD-1 and RFP::SAS 7 was assayed at sensory cilia in adult *gfp::pcmd-1; rfp::sas-7* worms. However, in contrast to GFP::PCMD-1, which was visible at all analyzed sensory cilia in the heads and tails of the worms, RFP::SAS-7 was not detectable at cilia (**Figure 25B).**

SAS-4 is a centrosomal protein that localizes to both the centrioles and the PCM, and it is needed to assemble microtubules around the central tube (Dammermann et al., 2008; Delattre et al., 2006; Kirkham et al., 2003; Leidel and Gönczy, 2003). Furthermore, SAS-4 was shown to interact with SAS-7 in the Y2H system (Boxem et al., 2008). Therefore, I wondered whether SAS-4 is required for SAS-7 and PCMD-1 localization to the centrosome. Since one centriole pair in the one-cell embryo is derived from the sperm, each daughter cell contains one centriole. In the absence of functional SAS-4 induced by treatment with strong *sas-4(RNAi)*, the centriole proteins SAS-5 and SAS-6 are still recruited to the sites of nascent daughter centrioles (Dammermann et al., 2008, Delattre et al., 2004, Pelletier et al., 2006). However, centrioles cannot duplicate in the absence of functional SAS-4, and monopolar spindles are formed in the blastomeres of two-cell embryos (mitosis II), compared to bipolar spindles in wild-type embryos during mitosis II (**Figure 26A,** middle and top panel) (Kirkham et al., 2003; Leidel and Gönczy, 2003). In contrast, in some embryos treated with mild *sas-4(RNAi)*, structurally incomplete daughter centrioles can assemble (**Figure 26A**, bottom panel) (Kirkham et al., 2003).

When *gfp::pcmd-1; rfp::sas-7* embryos were treated with strong *sas-4*(*RNAi),* GFP::PCMD-1 and RFP::SAS-7 were only detectable at single foci (Data not shown, acquired by T. Mikeladze-Dvali, Stenzel et al., 2020). This observation indicates that SAS-7 and PCMD-1 are genetically dependent on SAS-4, but it needs to be considered that a daughter centriole is not assembled under strong *sas-4(RNAi)* conditions, and other factors regulating the recruitment of SAS-7 and PCMD-1 could also be missing. Therefore, I used the mild *sas-4(RNAi)* phenotype as a tool to investigate whether small amounts of SAS-4 are sufficient to recruit the proteins. In *gfp::pcmd-1; rfp::sas-7* embryos treated with *mock(RNAi)*, strong signals of both GFP::PCMD-1 and RFP::SAS-7 fusion proteins were detectable at both spindle poles in the anterior and the posterior cell in all analyzed embryos (**Figure 26B**). In contrast, under mild *sas-4(RNAi)* conditions, GFP::PCMD-1 and RFP::SAS-7 were either very weakly detected at one spindle pole and strongly at the

other spindle pole in 66.66% of the embryos (**Figure 26B**) or strongly visible at only one spindle pole in 33.33% of the embryos, similar to the strong *sas-4(RNAi)* phenotype.

Based on these observations, both PCMD-1 and SAS-7 localize to centrioles, and their localization largely overlaps. Thereby, SAS-7 is accumulating more at one centriole than at the other centriole. Both proteins are not recruited when centrioles are not duplicated in the absence of functional SAS-4. However, PCMD-1 and SAS-7 can be recruited to structurally incomplete daughter centrioles when little amounts of SAS-4 are present. Nevertheless, it was not feasible to distinguish which of the proteins is recruited first in this experiment. However, I can conclude from these data that SAS-4 acts upstream of SAS-7 and PCMD-1 in the centrosome assembly pathway.

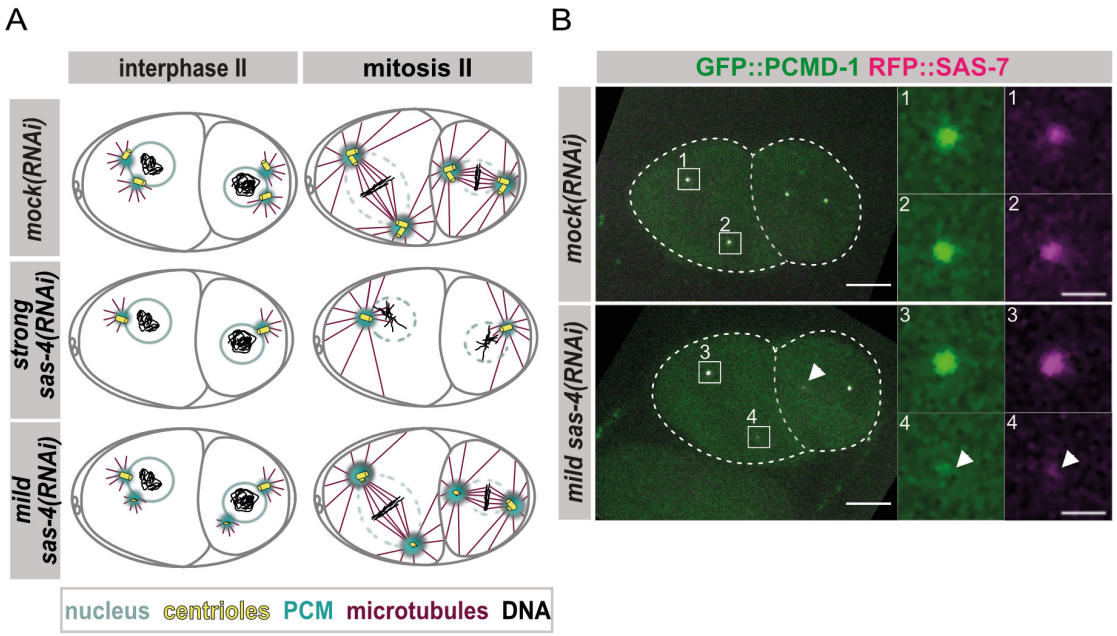

Figure 26. PCMD-1 and SAS-7 localization to centrosomes depend on SAS-4. A) Schematic of two-cell embryos in interphase II and mitosis II treated with *mock(RNAi)* or *sas-4(RNAi)* generated based on data from Kirkham et al., 2003 and Leidel and Gönczy, 2003. As one centriole pair is derived from the sperm in all scenarios, at least one centriole after centriole separation is present in each daughter cell in interphase II. When embryos are treated with *mock(RNAi)*, two centrioles are present in both daughter cells because centriole duplication can occur, and after another duplication, the mitosis II can proceed normally. When embryos are treated with strong *sas-4(RNAi)*, centriole duplication is impaired, and a monopolar spindle is formed during mitosis II in each daughter cell. When embryos are treated with mild *sas-4(RNAi)*, in some embryos structurally incomplete daughter centrioles can form, and the daughter cells can divide in mitosis II. **B)** Representative stills of time-lapse sequences of dividing *gfp::pcmd-1; rfp::sas-7* two-cell embryos expressing GFP::PCMD-1 and RFP::SAS-7 after treatment with *mock(RNAi)* (n=5) or mild *sas-4(RNAi)* (n=6). Strong signals of GFP::PCMD-1 and RFP::SAS-7 were visible at each spindle pole in both daughter cells after treatment with *mock(RNAi)*. In contrast, in 66.66% (n=4 of 6) of the embryos treated with mild *sas-4(RNAi)*, the GFP::PCMD-1 and RFP::SAS-7 signals were strong at one spindle pole and weak at the other pole in each daughter cell. In 33.36% (n=2 of 6) GFP::PCMD-1 and RFP::SAS-7 were detected at only one spindle pole. Images are displayed as merged z-projections. Insets show enlarged centrosomal areas as single channels labeled with corresponding numbers (1-4). Arrowhead points to weak spindle poles with weak signal. Scale bars indicate 10 µm or 2 µm (insets).

3.3.2.2 SAS-7 localization to centrioles is independent of PCMD-1

Since we observed that less SAS-7 than PCMD-1 is visible at one of the two centrioles (**Figure 25C**), I wondered whether PCMD-1 might act upstream of SAS-7 in the centrosome assembly pathway and be responsible for the recruitment of SAS-7.

To answer this question, GFP::SAS-7 was assayed in *gfp::sas-7* and *pcmd-1(t3421); gfp::sas-7* embryos by live-cell imaging. In all analyzed *gfp::sas-7* and *pcmd-1(t3421);gfp::sas-7* embryos, GFP::SAS-7 was detected at the centrioles (**Figure 27A**), and the embryos were normally dividing. In contrast, 60% of the *pcmd-1(t3421);gfp::sas-7* embryos were not dividing due to their mutant phenotype. Among those embryos, which failed the division, a monopolar spindle was formed in 50% of the analyzed embryos. The GFP::SAS-7 fluorescence signal appeared stronger in those embryos (**Figure 27A**, bottom and centrosomal area 5). Therefore, the sum of the centrosomal fluorescence intensities per embryo was used to calculate the mean centrosomal fluorescence intensities. The quantification of the centrosomal GFP::SAS-7

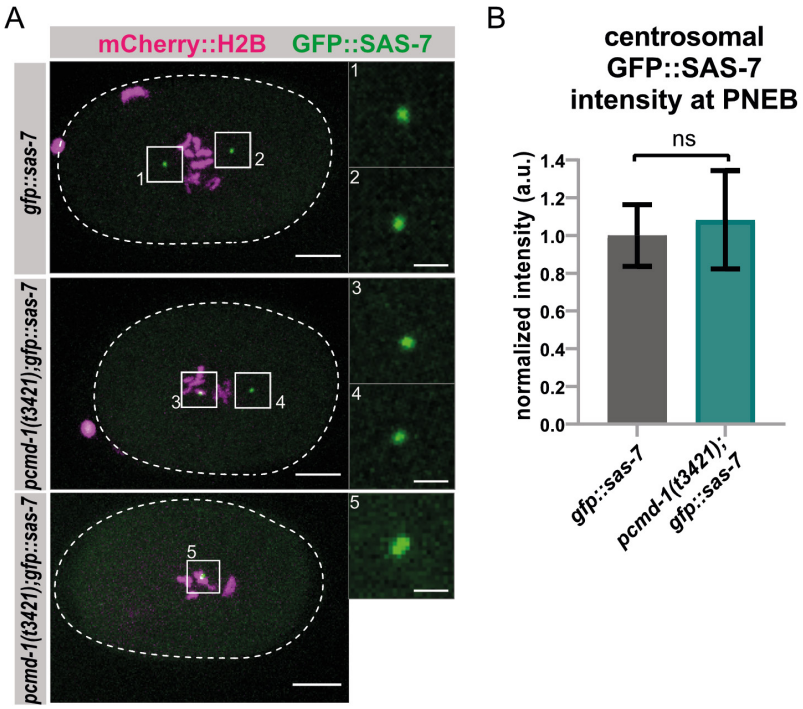

Figure 27. SAS-7 localizes to centrioles independent of PCMD-1. A) Representative stills of time-lapse sequences of *gfp::sas-7* (n=16) and *pcmd-1(t3421); gfp::sas-7* (n=10) one-cell embryos in *mCherry::h2b* background as a histone marker at the time point of PNEB recorded with a spinning disc confocal microscope. GFP::SAS-7 signal was detected in all *gfp::sas-7* and *pcmd-1(t3421); gfp::sas-7* one-cell embryos. Note that due to their mutant phenotype, 60.00% (n=6) of the *pcmd-1(t3421); gfp::sas-7* embryos failed to divide, and 50.00% of the non-dividing embryos (n=3) formed a monopolar spindle and centrosomes did not separate (bottom, centrosomal area 5). Images are displayed as merged z-projections. Insets show enlarged centrosomal areas labeled with corresponding numbers (1-5). Scale bars indicate 10 µm or 2 µm (insets). **B)** Quantification of centrosomal fluorescence intensities in *gfp::sas-7* (1.00±0.16 a.u., n=16) and *pcmd-1(t3421);gfp::sas-7* (1.09± 0.26 a.u.,n=10) embryos at PNEB. Values were normalized to the mean centrosomal intensity of GFP::SAS-7. Two-sample t-test (ns: not significant). Data are represented as mean±SEM. Figure adapted from Stenzel et al. (2020).

fluorescence intensities in early mitosis at the stage of PNEB revealed that the mean centrosomal GFP::SAS-7 intensity of 1.09 in *pcmd-1(t3421)* background was not significantly different from the mean centrosomal GFP::SAS-7 intensity of 1.00 a.u. in the wild-type background (**Figure 27B**).

Based on these observations, PCMD-1 is not required to anchor SAS-7 to the centriole, and consequently, SAS-7 localization to the centrosome is independent of PCMD-1 in the centrosome assembly pathway. Further, the results indicate that centriole duplication is not impaired in *pcmd-1(t3421)* mutant embryos, as the signal intensities of SAS-7 are not reduced at monopolar spindles.

3.3.2.3 Centrosomal localization of PCMD-1 depends on SAS-7

Since PCMD-1 was not regulating SAS-7 centrosomal localization, I aimed to investigate whether SAS-7 *vice versa* is involved in the anchoring of PCMD-1 to the centrioles,

Therefore, GFP::PCMD-1 was monitored in *sas-7(or452ts)* embryos by live-cell imaging. Since the *sas-7(or452ts)* allele is temperature-sensitive, worms were grown as described in chapter **2.2.1**, and the progeny was monitored at 25°C (Sugioka et al., 2017). As expected, all control *gfp::pcmd-1* embryos were normally dividing. Furthermore, GFP::PCMD-1 was visible at centrosomes throughout the first cell cycle with reduced signal intensities after mitosis (**Figure 28A**). In contrast, only 25.00% of the *gfp::pcmd-1; sas-7(or452ts)* embryos were dividing, and GFP::PCMD-1 was almost undetectable at the centrosome during the first cell cycle. The areas of the spindle poles were defined in DIC images. While a GFP::PCMD-1 signal with very low intensity was visible during interphase at PNMi, the signals became even weaker as the cell cycle progressed, and only at 5 out of 16 centrosomes, GFP::PCMD-1 was detectable during mitosis at PNEB (**Figure 28A**). Since detectable centrosomal GFP::PCMD-1 signal in *gfp::pcmd-1; sas-7(or452ts)* embryos was restricted to only a few pixels and the intensity was very low, it was not possible to measure the signal intensities with the method, which was consistently used in this work. However, measuring the GFP::PCMD-1 intensities using a different method revealed that, as expected, the centrosomal GFP::PCMD-1 intensities were significantly decreased at PNEB with almost no intensity in *gfp::pcmd-1; sas-7(or452ts)* embryos (performed by T. Mikeladze-Dvali, Data not shown). It has been shown that *sas-7(or452ts)* is a hypomorphic allele, and small amounts of GFP::SAS-7(*or452ts*) can localize to the centrosome (Sugioka et al., 2017). The remaining SAS-7 might be enough to recruit low amounts of PCMD-1 in early cell stages and higher amounts of PCMD-1 in later cell stages. To confirm the data in an alternative assay, an immunofluorescence staining against GFP and the centriole marker SAS-4 was performed in *gfp::pcmd-1* and *gfp::pcmd-1*; *sas-7(or452)* embryos. The DNA was visualized by Hoechst staining. In all analyzed *gfp::pcmd-1* control embryos,

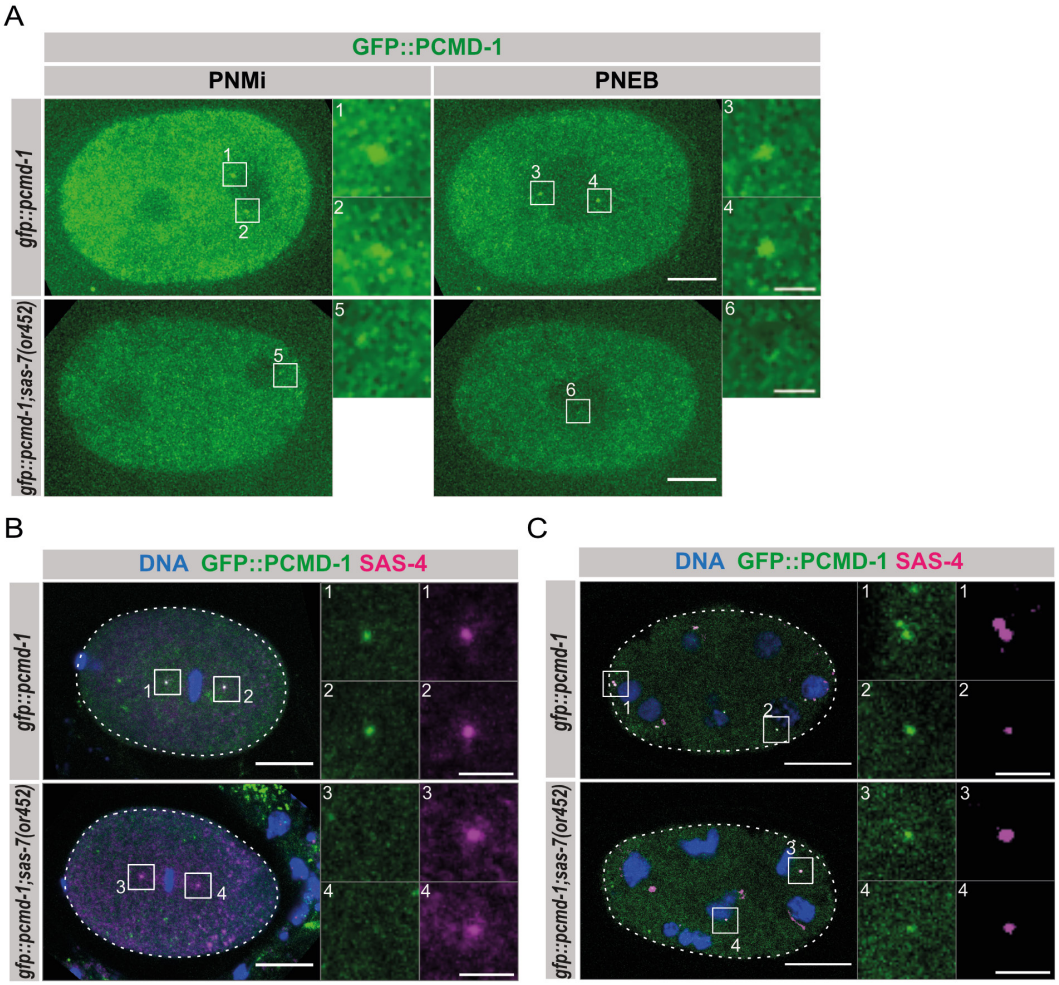

Figure 28. PCMD-1 localization to centrosomes depends on SAS-7 in early embryos. A) Representative stills of time-lapse sequences of *gfp::pcmd-1* (n=6) and *gfp::pcmd-1;sas-7(or452)* (n=8) one-cell embryos during PNMi and PNEB recorded with a spinning disc confocal microscope. All analyzed *gfp::pcmd-1* embryos were normally dividing and GFP::PCMD-1 localized to the centrosome. In contrast, only 25.00% (n=2) of *gfp::pcmd-1; sas-7(or452ts)* embryos were dividing, and GFP::PCMD-1 signal was visible at 10 of 16 sperm-derived centrosomes during PNMi, and at 5 of 16 centrosomes at PNEB. Images are displayed as z-projections. Insets show enlarged centrosomal areas labeled with corresponding numbers (1-6). Scale bars indicate 10 µm or 2 µm (insets). **B)** Representative z-projected fluorescent images of fixed *gfp::pcmd-1* (n=16) and *gfp::pcmd-1; sas-7(or452ts)* (n=6) one-cell embryo stained against GFP and SAS-4 as a centriole marker. DNA was visualized using Hoechst. GFP::PCMD-1 was colocalizing with SAS-4 foci in *gfp::pcmd-1* embryos but it was not colocalizing with SAS-4 foci in *gfp::pcmd-1; sas-7(or452ts)* embryos. Insets show enlarged centrosomal areas as single channels labeled with corresponding numbers (1-4). Scale bars indicate 10 µm or 2 µm (insets). **C)** Representative z-projected fluorescent images of fixed *gfp::pcmd-1* (n=3) and *gfp::pcmd-1; sas-7(or452ts)* (n=8) embryos (>6 nuclei) stained against GFP and SAS-4. DNA was visualized using Hoechst. GFP::PCMD-1 was colocalizing with SAS-4 foci in both *gfp::pcmd-1* and *gfp::pcmd-1; sas-7(or452ts)* embryos. Insets show enlarged centrosomal areas as single channels labeled with corresponding numbers (1-4). Scale bars indicate 10 µm or 2 µm (insets). Figure adapted from Stenzel et al. (2020).

GFP::PCMD-1 was colocalizing with SAS-4 at centrosomes (**Figure 28B, C**). In contrast, GFP::PCMD-1 was not detectable colocalizing with SAS-4 foci in any analyzed *gfp::pcmd-1*;*sas-7(or452)* one-cell embryos in this experiment (**Figure 28B**). As immunofluorescence stainings are less sensitive, the low levels of GFP::PCMD-1 might be

under the detection level. In later immunofluorescence stainings performed by T. Mikeladze-Dvali marginal amounts of PCMD-1 were detectable (Data not shown). Interestingly, in later cell-stage *gfp::pcmd-1*; *sas-7(or452)* embryos with more than six nuclei, GFP::PCMD-1 was colocalizing with centriolar SAS-4 foci similar as in *gfp::pcmd-1* control embryos (**Figure 28C**).

To summarize, I found that SAS-7 regulates PCMD-1 localization to the centrosome in early embryos. In later cell stage embryos, an alternative mechanism might regulate centrosomal recruitment of PCMD-1.

3.3.2.4 The PCM scaffold is disorganized in the absence of functional SAS-7

Previous data (Erpf et al., 2019) and data presented in chapter **3.1.3** have shown that the PCM scaffold recruitment to the centrosome and PCM integrity is compromised in the absence of functional PCMD-1. Furthermore, as described above, PCMD-1 localization was highly reduced or even lost in *sas-7(or452ts)* mutant embryos. Therefore, I reasoned that the PCM scaffold should also be missing or disorganized in *sas-7(or452ts)* embryos similar to *pcmd-1(t3421)* or *pcmd-1(syb975)* embryos.

To test this hypothesis, *gfp::pcmd-1* and *gfp::pcmd-1; sas-7(or452ts)* embryos were stained against SPD-5. In addition, the DNA was visualized by Hoechst staining. SPD-5 localization was assayed in *gfp::pcmd-1* and *gfp::pcmd-1; sas-7(or452ts)* one-cell embryos during mitosis (**Figure 29A**). As expected, in 100% of the *gfp::pcmd-1* embryos, centrosomal SPD-5 was visible. In contrast, centrosomal SPD-5 signal was present in 77.78% (n=7) and absent in 22.22% (n=2) of the *gfp::pcmd-1; sas-7(or452ts)* embryos. The variability of the SPD-5 absence or presence at the centrosome has already been described for the *pcmd-1(t3421)* and *pcmd-1(syb975)* mutant phenotypes. When SPD-5 centrosomal signal was present, similarly to the SPD-5 PCM shapes in *pcmd-1(t3421)* and p*cmd-1(syb975)* embryos, the detectable SPD-5 scaffold in *sas-7(or452ts)* embryos appeared disorganized (**Figure 29A**). The appearances of the PCM scaffold were characterized by quantifying the circularity and the aspect ratio of the SPD-5 shapes in *gfp::pcmd-1* and *gfp::pcmd-1*; *sas-7(or452ts)* one-cell embryos during mitosis ranging from PNM to early anaphase. As explained in chapter **3.1.3**, a perfect circle would have a circularity and an aspect ratio of 1.00. The mean centrosomal circularity of 0.44 in *gfp::pcmd-1*; *sas-7(or452ts)* embryos was significantly lower than the mean centrosomal circularity of 0.74 in *gfp::pcmd-1* embryos (**Figure 29B**). Furthermore, the mean centrosomal aspect ratio of 1.34 in *gfp::pcmd-1*; *sas-7(or452ts)* embryos was slightly increased compared to the quantified mean centrosomal aspect ratio of 1.26 in *gfp::pcmd-1* embryos, although this increase was not significant (**Figure 29C**). The small amounts of centrosomal GFP::PCMD-1, which were observed in some of the *sas-7(or452ts)* embryos in live-cell imaging (**Figure 28A**) but were not detectable in immunofluorescence

stainings (**Figure 28B**), might be enough to maintain the PCM shape, but not enough to maintain the PCM organization.

In summary, I propose that SAS-7 regulates PCMD-1 localization, and PCMD-1, in turn, regulates assembly of the PCM core and organization of the mitotic PCM. Therefore, the PCM is also absent or disorganized in the absence of SAS-7.

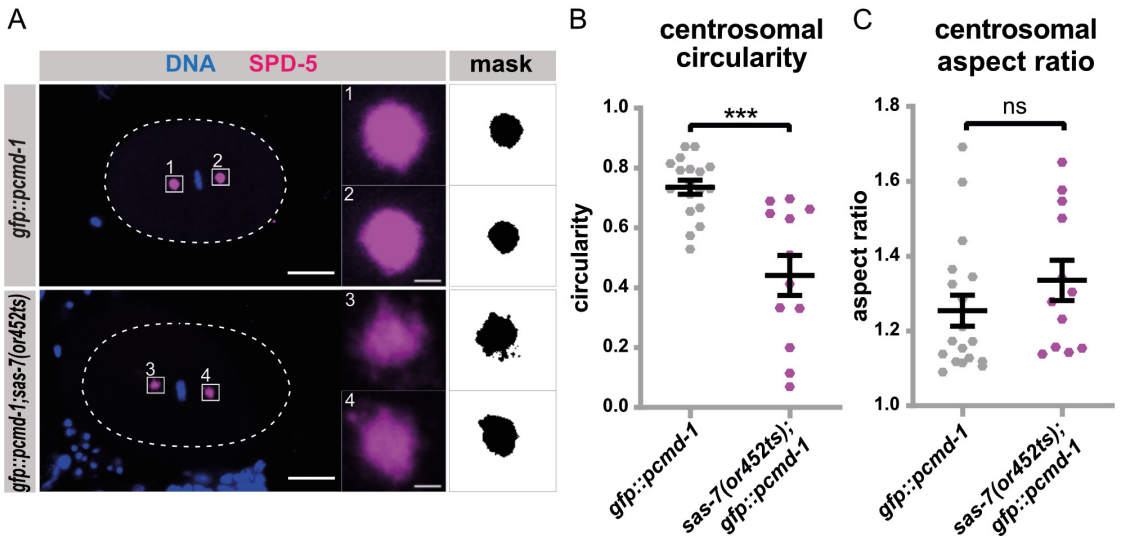

Figure 29. The PCM scaffold is disorganized in the absence of functional SAS-7. **A)** Representative z-projected fluorescence images of fixed *gfp:pcmd-1* (n=9) and *gfp::pcmd-1; sas-7(or452ts)* (n=9) one-cell embryos during mitosis recorded with a confocal microscope. The embryos were stained with an antibody against the PCM protein SPD-5. The DNA was stained using Hoechst. Insets show enlarged centrosomal areas labeled with corresponding numbers, including the SPD-5 masks, which were generated for the shape measurements. Scale bars indicate 10 µm or 1 µm (insets). **B)** Quantification of centrosomal SPD-5 circularity in *gfp::pcmd-1* (0.74±0.02, n=18 centrosomes) and *sas-7(or452ts); gfp::pcmd-1* (0.44±0.07, n=12 centrosomes) embryos. Welch two-sample t-test (*** p<0.001). **C)** Quantification of centrosomal SPD-5 aspect ratio in *gfp::pcmd-1* (1.26±0.04, n=18 centrosomes) and *sas-7(or452ts); gfp::pcmd-1* embryos (1.34±0.05, n=12 centrosomes). Mann-Whitney-U test (ns: not significant). Data in **B)** and **C)** are represented in mean±SEM.

3.4 Physical interactions between PCMD-1 and centrosomal proteins in a candidate-based yeast two-hybrid screen

Previously, it has been shown that PCMD-1 is required to recruit the PCM matrix proteins SPD-5, SPD-2, and PLK-1 to the centrosome (Erpf et al., 2019). As described in chapter **3.3.1.1**, cellular protein levels of SPD-5 and its interacting partner SPD-2 in *pcmd-1(t3421)* mutants are not degraded. This suggests that the lack of recruitment of these proteins might be due to compromised protein-protein interactions. Furthermore, I have shown evidence in chapter **3.3.2** that SAS-7 regulates PCMD-1 localization to centrosomes, and the localization of SAS-7 and PCMD-1 depends on functional SAS-4.

The strong genetic dependencies between PCMD-1 and other centrosomal proteins raised the possibility that PCMD-1 directly interacts with centriolar and PCM proteins.

To address whether PCMD-1 and SAS-7 directly interact with each other or with other centrosomal proteins, a candidate-based Y2H screen was conducted using the Grow'n'Glow GFP Yeast Two-Hybrid System (MoBiTec). This system is a LexA/B42-based version of the original Y2H system (Fields and Song, 1989). The Y2H system takes advantage of eukaryotic transcription activators, consisting of two modular physically separable domains, a transcriptional activation domain, and a DNA-binding domain. The transcriptional activator is reconstituted when the domains are in proximity. In the LexA/B42-based Y2H system, the bait protein is fused to the DNA-binding domain LexA, and the prey protein is fused to the transcriptional activation domain B42, respectively. Thus, when bait and prey directly bind to each other, the complex of both can bind to the LexA operator. When the complex binds to the LexA operator, transcription of the metabolic reporter LEU2 and the GFP reporter, expressed through an additional vector, is initiated. Therefore, growth on leucine-lacking medium and GFP expression are both used as positive readouts for interaction.

To investigate physical interactions, bait plasmids containing *pcmd-1* and *sas-7* cDNAs and prey plasmids containing cDNA of the following candidates *sas-4, sas-7, pcmd-1, plk-1, spd-5, spd-2, pcmd-1(ΔCC),* and *pcmd-1(C2)* were generated and expressed in yeast. First, it had to be excluded that the different bait proteins alone can activate the reporters. Here, GAL-4, which activates the LEU2 reporter, served as a positive control, and the empty bait plasmid as a negative control plasmid. For GFP autoactivation, the GFP reporter was coexpressed. Neither PCMD-1 nor SAS-7 was able to activate the reporters.

After generating and verifying the yeast strains by growth on selection media and amplifying the bait and prey DNA with subsequent sequencing, the strains were used for the Y2H interaction assay. While empty prey plasmids served as negative controls, the known interacting partners p53 and Large-T-Antigen (LTA) were used as positive controls showing both readouts after three days on leucine-lacking plates (**Figure 30A, 31A**). Hereafter, I classified proteins showing both readouts after three days as strong interactors and proteins showing one or both readouts after five days as weak interactors. Plates containing leucine were used as growth control plates (**Figure 30A, 31A**). To exclude false negatives, glucose agar plates lacking histidine, uracil, tryptophan, and leucine, where transcription should not be induced, were used as negative growth control plates.

As protein-protein interactions between SAS-7 and other centrosomal proteins have been shown previously (Boxem et al., 2008; Li et al., 2004; Sugioka et al., 2017), the SAS-7 bait was used as a positive control for centrosomal protein-protein interactions. Furthermore, it was utilized to examine whether it interacts with PCMD-1. A strong

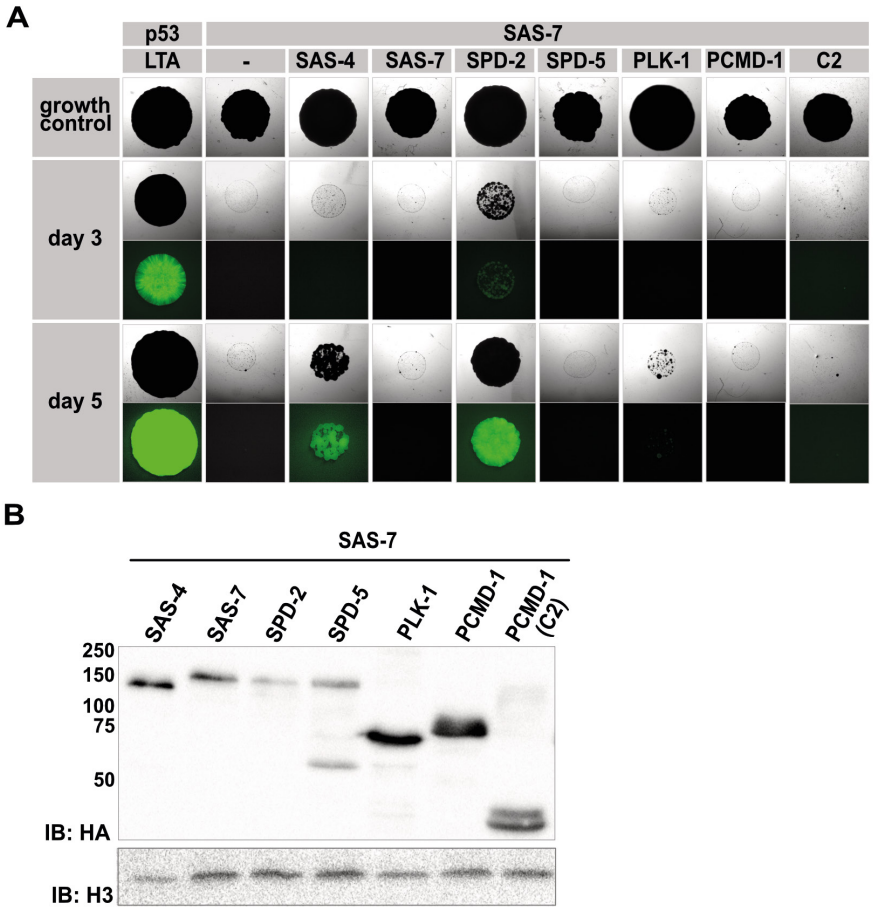

Figure 30. Yeast two-hybrid candidate-based screen for SAS-7 interactions. A) Representative brightfield and GFP images of spotted yeast strains coexpressing SAS-7 as a bait with different prey proteins. Positive control (p53+LTA), negative control (SAS-7+empty plasmid) and SAS-7 (bait) with the centrosomal proteins SAS-4, SAS-7, SPD-2, SPD-5, PLK-1, PCMD-1, and C2 (PCMD-1_C2(aa343-630)) as preys. The top panel shows growth controls, the middle panel shows yeast spots screened for growth on leucine-lacking medium and GFP fluorescence after three days, and the bottom panel shows yeast spots screened for growth on leucine-lacking medium and GFP fluorescence. Yeast strains were generated together with S. Üstüner. **B)** Western blot analysis of prey proteins expressed together with the SAS-7 bait in yeast. Yeast cell lysates were probed against the prey proteins, fused to the B42 activator and the HA epitope tag, with an antibody against the HA-tag. The histone H3 antibody was used to probe for histone H3 (15 kDa) as loading control. Bands of the fusion proteins were detected at the expected MW indicated in brackets: SAS-4 (104 kDa), SAS-7 (130 kDa), SPD-5 (146 kDa), PLK-1 (85 kDa), PCMD-1 (82 kDa), and PCMD-1(C2) (43 kDa). Note that the SPD-2 fusion protein (~145 kDa) was detected with a higher MW as its expected MW (103 kDa). The Western blot was performed together with E. Zuccoli. Figure **A)** adapted from Stenzel et al. (2020).

interaction between SAS-7 and SPD-2 was recapitulated by monitoring fluorescent colonies after three days (**Figure 30A**), and a weaker interaction between SAS-7 and SAS-4 by detecting fluorescent colonies after five days (**Figure 30A**). No growth, and in turn, no interaction in the Y2H system was observed for the protein combinations SAS-7 with SPD-5 and SAS-7 with SAS-7 (**Figure 30A**). Interestingly, weak growth of colonies expressing SAS-7 and PLK-1 was observed, although the GFP expression was below the detection level, and this interaction would need to be proven in another

way (**Figure 30A**). Moreover, yeast cells expressing SAS-7 as bait and PCMD-1 as prey did not grow, which leads to the conclusion that the proteins do not interact in this combination in yeast. It has been described in previous Y2H studies for *C. elegans* proteins that the expression of smaller cDNA fragments leads to a higher probability of identifying protein-protein interactions than full-length cDNA fragments (Boxem et al., 2008). Furthermore, data generated collectively by A. Schreiner, T. Mikeladze-Dvali, S. Üstüner, and myself have shown that a region in the C-terminal end of PCMD-1 is required for its localization to the centrosome (chapter **3.2.3**, Stenzel et al., 2020). Therefore, we wondered whether the fragment of the C-terminal region of PCMD-1 (PCMD-1(C2_343-630)) as prey could physically bind to the SAS-7 prey. However, no growth, hence no binding, was detectable between SAS-7 and PCMD-1(C2) in the Y2H system (**Figure 30A**). To exclude that negative results are due to weak or no expression of the prey proteins coexpressed with the SAS-7 bait protein, the prey proteins, which are fused to the B42 activator and the HA epitope tag, were probed with an anti-HA antibody against the HA-tag by Western blotting. In addition, Histone H3 was probed as a loading control. As expected, all prey proteins were expressed (**Figure 30B**).

When PCMD-1 was expressed as a bait protein and SAS-7 as a prey protein, there was also no growth, and in turn, no interaction in the Y2H detectable (**Figure 31A**). This suggests that full-length PCMD-1 and SAS-7 do not interact in yeast. However, a strong protein-protein interaction was observed for PCMD-1 with the centriole protein SAS-4 by monitoring fluorescent colonies after three days (**Figure 31A**). Growth and fluorescence after five days, and therefore weak interaction, was detected for PCMD-1 with SPD-5 and PLK-1 (**Figure 31A**). Furthermore, PCMD-1 did not show any growth when coexpressed with SPD-2 in this assay. A strong self-interaction for PCMD-1 was observed by detecting growth and fluorescence after three days (**Figure 31A**). Coiled-coil domains are known to be sites for protein-protein interactions and oligomerization (Lupas and Bassler, 2017; Truebestein and Leonard, 2016). The data presented in chapter **3.2.1** indicated that the coiled-coil domain in PCMD-1 plays a role in accumulating PCMD-1 at centrosomes *in vivo*. Therefore, it was assessed whether the coiled-coil domain in PCMD-1 might have oligomerization potential. To this end, it was tested whether a PCMD-1 prey protein lacking the coiled-coil domain (PCMD-1(ΔCC)) can physically interact with the PCMD-1 bait. Compared to the interaction between PCMD-1 and PCMD-1 and to the growth control, no growth was observed between PCMD-1 and PCMD-1(ΔCC) (**Figure 31A**). Western blot analysis of the different yeast strains with PCMD-1 as a bait protein, performed with an anti-HA antibody described above in **Figure 30B**, revealed that all prey proteins were expressed and negative results are not due to low or no expression (**Figure 31B**). Positive interactions were confirmed by reversing the bait and prey proteins by T. Mikeladze-Dvali.

Since PCMD-1 and PLK-1 were physically binding to each other, it is conceivable that PLK-1 binds to PCMD-1 via PLK phospho-binding sites. As explained in more detail in

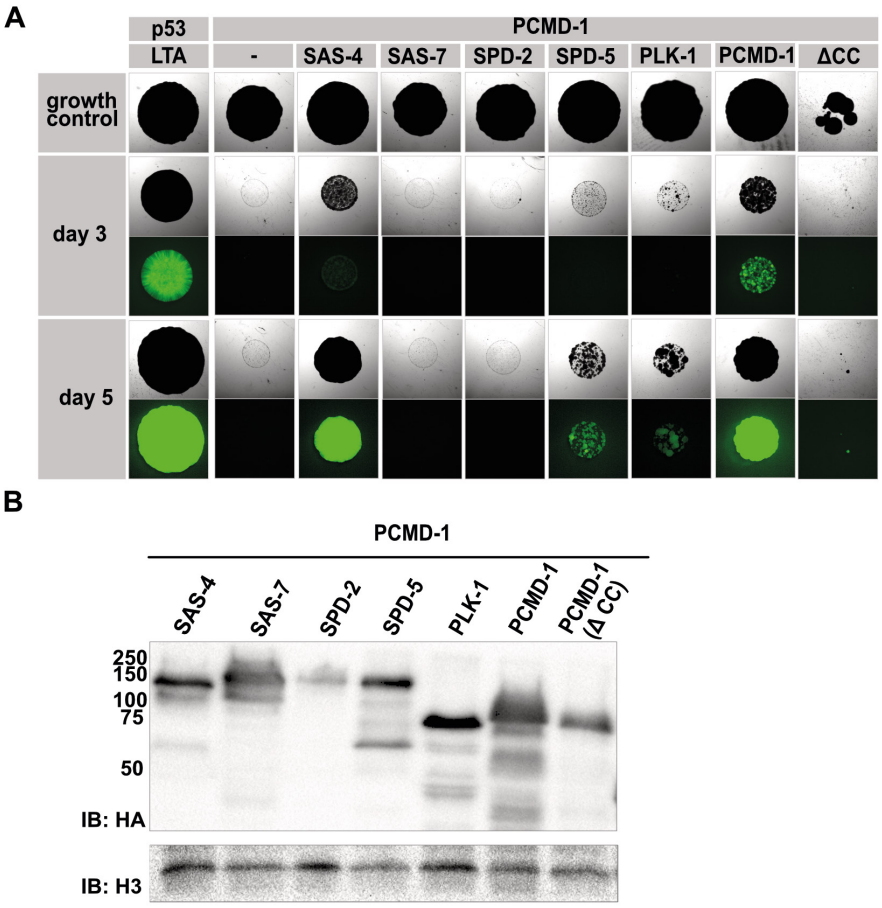

Figure 31. Yeast two-hybrid candidate-based screen for PCMD-1 interactions. A) Representative brightfield and GFP images of spotted yeast strains expressing PCMD-1 as a bait and different prey proteins. Positive control (p53+LTA), negative control (PCMD-1+empty plasmid) and PCMD-1 (bait) with the centrosomal proteins SAS-4, SAS-7, SPD-2, SPD-5, PLK-1, PCMD-1, and PCMD-1(ΔCC) as preys. The top panel shows growth controls, the middle panel shows yeast spots screened for growth on leucine-lacking medium and GFP fluorescence after three days, and the bottom panel shows yeast spots screened for growth on leucine-lacking medium and GFP fluorescence. **B)** Western blot analysis of prey proteins expressed together with the PCMD-1 bait in yeast. Yeast cell lysates were probed against the prey proteins, fused to the B42 activator and the HA epitope tag, with an antibody against the HA-tag. The histone H3 antibody was used to probe for histone H3 (15 kDa) as loading control. Bands of the fusion proteins were detected at the expected MW indicated in brackets: SAS-4 (104 kDa), SAS-7 (130 kDa), SPD-5 (146 kDa), PLK-1 (85 kDa), PCMD-1 (82 kDa), and PCMD-1(ΔCC) (78 kDa). Note that the SPD-2 fusion protein (~145 kDa) was detected with a higher MW as its expected MW (103 kDa) The Western blot was performed together with E. Zuccoli. Figure **A)** adapted from Stenzel et al. (2020).

chapter **3.6.1**, four PLK consensus phospho-binding sites were predicted using the prediction tool GPS-Polo 1.0 (Liu et al., 2012). To test whether the PCMD-1 interaction with PLK-1 would be abolished when the predicted PLK phospho-binding sites in PCMD-1 are phospho-resistant, a PCMD-1 bait with mutations encoding phospho-resistant alanine sites (PCMD-1(T228A, T298A, S56A, S359A)) was generated. However, the construct led to autoactivation in yeast. Also, mapping of PCMD-1 interaction sites using truncated PCMD-1 baits (PCMD-1_Nterm(aa2-117), PCMD-1_Cterm(aa118-630)) could not be examined further because their expression led to the activation of one or both reporters.

An overview of the Y2H results is displayed in **Table 16**. I confirmed protein-protein interactions between SAS-7 and SAS-4 or SPD-2, which were shown in previous Y2H screens, with our Y2H assay (Boxem et al., 2008; Li et al., 2004; Sugioka et al., 2017). While PLK-1 might be a potential interacting partner of SAS-7 with only weak interaction in the Y2H system, SAS-7, SPD-5, and the C-terminal region of PCMD-1 (C2) do not interact with SAS-7 in this system. Based on the observations, PCMD-1 and SAS-7 do not interact when expressed in yeast in both combinations as bait and prey, respectively. Protein-protein interactions identified between PCMD-1 and the centriole protein SAS-4 and the PCM proteins SPD-5 and PLK-1 suggest that PCMD-1 plays a role in bridging centrioles and PCM. The self-interaction of PCMD-1, which could not be shown, when PCMD-1 lacked the coiled-coil domain, further confirmed the hypothesis that PCMD-1 oligomerizes via the coiled-coil domain.

Table 16. Summary of the yeast two-hybrid results. Interactions are classified by the strengths of interaction. +: weak interaction, ++: strong interaction, NA: not available.

bait / prey	p53	PCMD-1	SAS-7
LTA	++	NA	NA
pJG45 (empty)	NA	-	-
SAS-4	NA	++	+
SAS-7	NA	-	-
PLK-1	NA	+	+
SPD-2	NA	-	+
SPD-5	NA	+	-
PCMD-1	NA	++	-
PCMD-1 (ΔCC)	NA	-	NA
PCMD-1(C2)	NA	NA	-

3.5 Translocation of PCMD-1 to the plasma membrane

The candidate-based Y2H screen showed that PCMD-1 interacts with both centriole and PCM proteins, as described in the previous chapter **3.4**. To determine whether PCMD-1 positioned at an ectopic location within the *C. elegans* embryo is sufficient to recruit both centriole and PCM proteins *in vivo*, a so-called translocation assay, collectively developed and optimized by our group, was performed. In this assay, PCMD-1 is targeted to the plasma membrane by generating a fusion protein consisting of the pleckstrin homology domain (PH) of human phospholipase C-δ1, which binds to the plasma membrane, mkate2 as a fluorescence marker, and PCMD-1 (Garcia et al., 1995; Haslam et al., 1993; Paterson et al., 1995). The fusion protein PH::mkate2::PCMD-1 was expressed under a heat-shock promoter. To test whether PCMD-1 positioned at an ectopic location is sufficient to tether different candidate centriole or PCM proteins to the plasma membrane, worm strains expressing GFP-tagged candidate proteins were crossed into the PH::mkate2::PCMD-1 expressing strain.

When multicellular *P_{hs}ph::mkate2::pcmd-1* embryos were heat-shocked for one hour at 30°C and recovered for two hours at 20°C, PH::mkate2::PCMD-1 was expressed and ectopically localized to the plasma membrane (**Figure 32**). There are two scenarios of how the GFP fusion proteins might behave. Either PCMD-1 positioned to an ectopic locus is sufficient to recruit the GFP fusion proteins, and the proteins colocalize with PH::mkate2::PCMD-1 at the plasma membrane, or PCMD-1 positioned to an ectopic locus is not sufficient to recruit the proteins, and GFP is not visible at the plasma membrane.

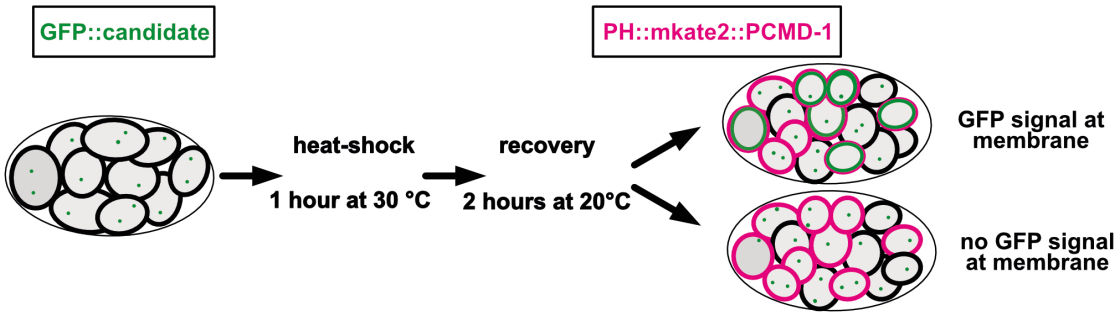

Figure 32. Schematic illustration of the translocation assay. Expression of PH::mKate2::PCMD-1 in multicellular embryos was induced by one hour heat-shock at 30°C. This was followed by two hours recovery at 20°C. PH::mKate2::PCMD-1 localized to the plasma membrane. If PH::mKate2::PCMD-1 recruits GFP-tagged candidate proteins, the proteins colocalize with PH::mKate2::PCMD-1 at the plasma membrane. If PH::mKate2::PCMD-1 cannot recruit the GFP-tagged candidate proteins, the proteins do not colocalize with PH::mKate2::PCMD-1 at the plasma membrane. Figure adapted from Stenzel et al. (2020).

3.5.1 PCMD-1 targets SPD-5 and PLK-1 to the plasma membrane

When embryos in the *pcmd-1(t3421)* background were imaged without heat-shock treatment, no PH::mkate2::PCMD-1 was detectable. All of the GFP-tagged candidate proteins, GFP::SPD-5 (**Figure 33Aa**), PLK-1::sGFP (**Figure 33Ab**), GFP::SAS-7 (**Figure 33Ac**), GFP::SAS-4 (**Figure 33Ad**), and GFP::PCMD-1 (**Figure 34Ae**), were visible at centrosomes but not at the plasma membrane. Both GFP::SPD-5 (**Figure 33Aa**) and PLK-1::sGFP (**Figure 33Ab**) were also present in the cytoplasm, and PLK-1::sGFP, as expected, at chromosomes.

After heat-shock treatment, in 95.24% of the GFP::SPD-5 expressing embryos in *pcmd-1(t3421)* background, GFP::SPD-5 colocalized with PH::mkate2::PCMD-1 at the plasma membrane beside its original subcellular localization to centrosomes and in the cytoplasm (**Figure 33Aa'**, **33B**). Similarly, in 41.38% of the PLK-1::sGFP expressing embryos in *pcmd-1(t3421)* background, PLK-1::sGFP colocalized with PH::mkate2::PCMD-1 at the plasma membrane beside its normal centrosomal, cytoplasmic, and chromosomal localization (**Figure 33Ab', 33B**). However, the centriole proteins GFP::SAS-4 (**Figure 33Ac'**, **33B**) and GFP::SAS-7 (**Figure 33Ad'**, **33B**), and GFP::PCMD-1 (**Figure 33Ae'**, **33B**), which is supposed to localize to both centrioles and

PCM, were not recruited to the cell membrane in any of the analyzed *pcmd-1(t3421)* embryos.

Based on these observations, I propose that positioning PH::mKate2::PCMD-1 to the plasma membrane is sufficient to target the PCM proteins SPD-5 and PLK-1. However, PCMD-1, SAS-4, and SAS-7 cannot be recruited to the plasma membrane by PH::mKate2::PCMD-1.

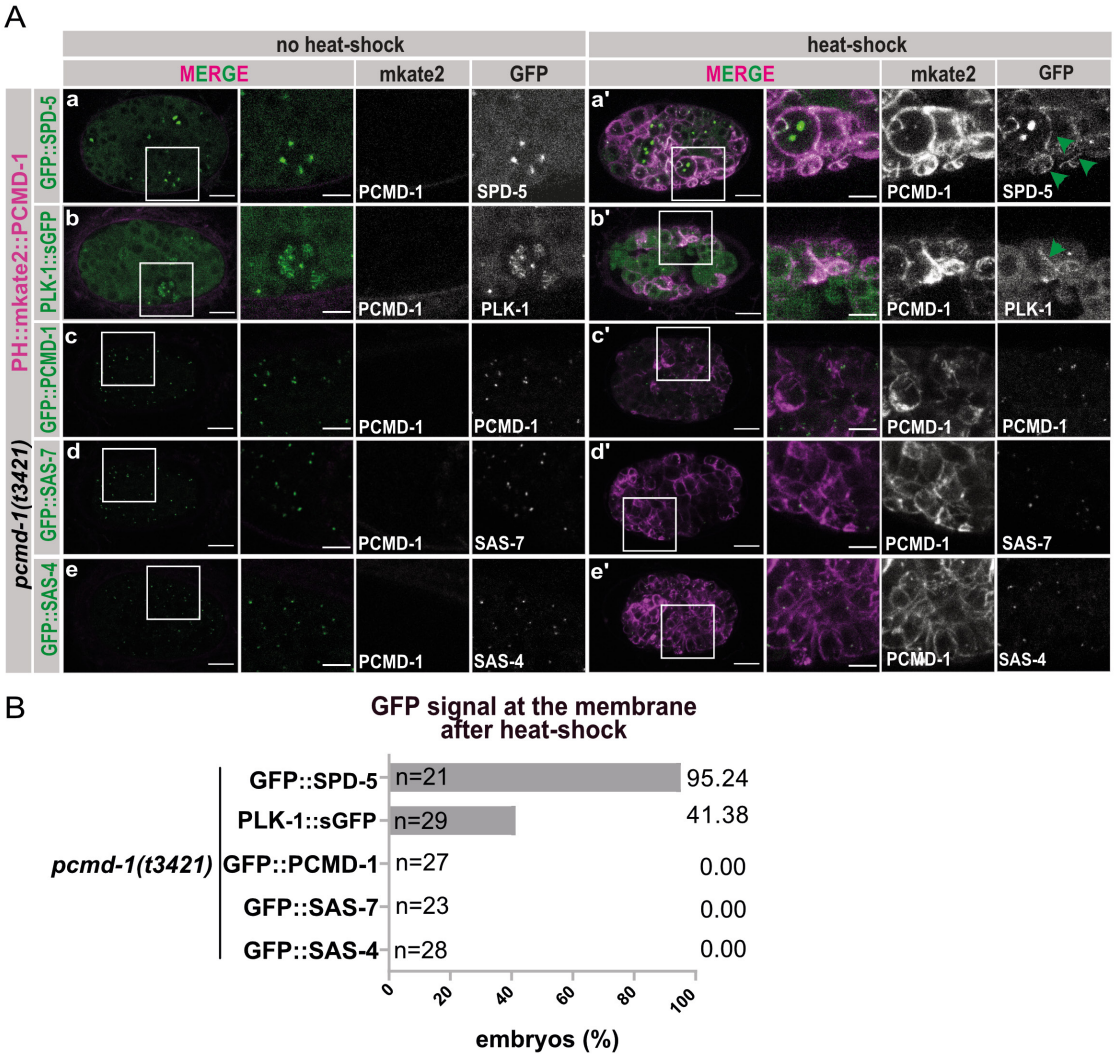

Figure 33. Translocation assay in *pcmd-1(t3421)* embryos. A) Representative z-projected images of multicellular embryos in *pcmd-1(t3421)* background without heat-shock treatment (a-e) and with heat-shock treatment (a'-e'). Without heat-shock, PH::mkate2::PCMD-1 was not expressed and a) GFP::SPD-5 (n=17), b) PLK-1::sGFP (n=21), c) GFP::PCMD-1 (n=25), d) GFP::SAS-7 (n=20), and e) GFP::SAS-4 (n=28) localized to centrosomes. After heat-shock treatment, PH::mkate2::PCMD-1 was expressed at the plasma membrane (a'-e'). While a') GFP::SPD-5 (n=21) and b') PLK-1::sGFP (n=29) colocalize with PH::mkate2::PCMD-1 at the plasma membrane, c') GFP::PCMD-1 (n=27), d') GFP::SAS-7 (n=27), and e') GFP::SAS-4 (n=28) did not localize to the membrane. Selected regions are enlarged and shown as merge and single channels. Green arrowheads point to colocalized GFP at the plasma membrane. Scale bars indicate 10 µm and 5 µm (insets). Data of c)-e) and c')-e') were generated by J. Mehler. **B)** Quantification of A); percentage of embryos (%) with GFP signal at the plasma membrane after heat-shock in *pcmd-1(t3421)* background; n=number of analyzed embryos. Figure adapted from Stenzel et al. (2020).

3.5.2 In the presence of endogenous PCMD-1 less SPD-5 and PLK-1 is targeted to the plasma membrane by the transgenic PCMD-1

To test whether the proteins would still be recruited to the membrane when endogenous PCMD-1 is present, the translocation assay was performed in a wild-type background.

As expected, without heat-shock treatment, PH::mkate2::PCMD-1 was not expressed in multicellular embryos, and GFP::SPD-5 and PLK-1::sGFP were detected at centrosomes, in the cytoplasm and PLK-1 additionally at chromosomes (**Figure 34Aa**). After heat-shock treatment, GFP::SPD-5 colocalized with PH::mkate2::PCMD-1 at the plasma membrane in addition to its normal centrosomal and cytoplasmic localization when endogenous PCMD-1 is present (**Figure 34Aa'**). However, the translocation efficiency of GFP::SPD-5 was reduced to 68.42% in the absence of endogenous PCMD-1 compared to the efficiency of 95.24% when endogenous PCMD-1 is not functional (**Figure 33B**, **34B**). Similarly, PLK-1::sGFP was still recruited to the plasma membrane and colocalized with PH::mkate2::PCMD-1 in the presence of endogenous PCMD-1, in addition to its usual localization to centrosomes, cytoplasm, and chromosomes (**Figure 34Ab'**). Indeed, the translocation efficiency of 26.32% was reduced when endogenous PCMD-1 was expressed compared to the efficiency of 41.38% when endogenous PCMD-1 is not functional (**Figure 33B**, **34B**).

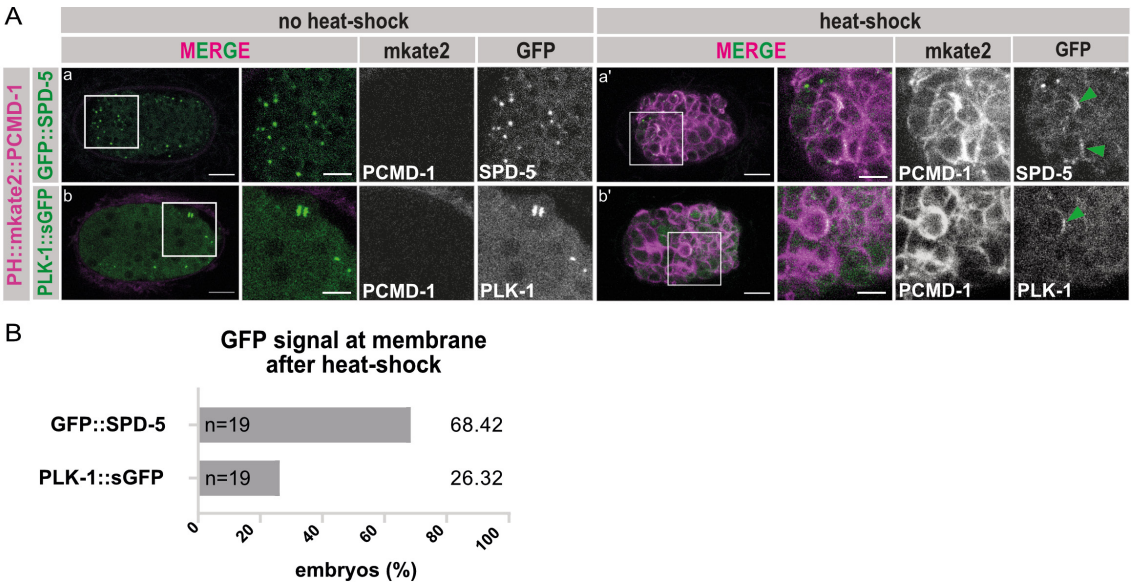

Figure 34. Translocation assay in wild-type embryos. A) Representative z-projected images of multicellular embryos in wild-type background without heat-shock treatment (a and b) and with heat-shock treatment (a' and b'). Without heat-shock, PH::mkate2::PCMD-1 was not expressed and a) GFP::SPD-5 (n=19) and b) PLK-1::sGFP (n=20) localized to centrosomes in the wild-type background. After heat-shock treatment, PH::mkate2::PCMD-1 was expressed at the plasma membrane (a' and b'), and a') GFP::SPD-5 (n=19) and b') PLK-1::sGFP (n=19) colocalize with PH:mkate2::PCMD-1 at the plasma membrane in the wild-type background. Selected regions are enlarged and shown as merge and single channels. Green arrowheads point to colocalized GFP at the plasma membrane. Scale bars are 10 µm and 5 µm (insets). **B)** Quantification of A); percentage of embryos (%) with GFP signal at the plasma membrane after heat-shock in wild-type background; n=number of analyzed embryos. Figure adapted from Stenzel et al. (2020).

Taken together, recruitment of SPD-5 and PLK-1 to the membrane through PH::mKate2::PCMD-1 is more powerful in the absence of the endogenous functional PCMD-1. Therefore, I propose that the membrane-bound PCMD-1 and the endogenous centrosomal PCMD-1 compete in the presence of the endogenous protein.

3.6 Phospho-regulation of PCMD-1

3.6.1 Phospho-resistant PLK binding sites in PCMD-1 lead to increased centrosomal PCMD-1 accumulation

Previously, it has been shown that PCMD-1 and SPD-5 promote PLK-1 accumulation at the centrosome in a SPD-2 dependent manner (Erpf et al., 2019). My findings presented in chapter **3.5** showed that PCMD-1 could even recruit PLK-1 to an ectopic locus in the cell. In contrast, PCMD-1 localization to the centrosome is independent of PLK-1, and GFP::PCMD-1 is still visible at centrosomes in embryos treated with *plk-1* RNAi (Erpf et al., 2019). However, in *C. elegans,* complete depletion of PLK-1 is not possible because of its early embryonic functions (Kim and Griffin, 2020). Evidence for direct protein-protein interaction between PCMD-1 and PLK-1 in the Y2H system was presented in chapter **3.4**. These findings posed the question of how PLK-1 binds to PCMD-1 and how PCMD-1 regulates PCMD-1. It is known that PLK-1 binds to phosphorylated serine/threonine sites of other substrates through its tandem Polo-box domains (Elia et al., 2003a; Elia et al., 2003b; Lee et al., 1998; Martino et al., 2017; Nishi et al., 2008).

To determine whether the PCMD-1 sequence contains potential consensus PLK phospho-binding sites, the sequence was analyzed using the prediction tool GPS-Polo 1.0 (Liu et al., 2012). It must be considered that this software is not PLK-1 specific and that other polo kinases exist in *C. elegans*. Nevertheless, data from five different eukaryotes, including *C. elegans,* were applied in this software, and for the performance evaluation of phospho-binding sites, a training data set of human PLK1 phospho-binding sites was used (Liu et al., 2012). In PCMD-1, four sites (S56, T228, T298, and S359) were predicted as potential serine/threonine PLK phospho-binding sites under a medium threshold, and only T228 with the typical serine-threonine-proline (S-T-P) recognition motif was predicted as a PLK phospho-binding site under a high threshold (**Figure 35A**).

Sequence conservation of PCMD-1 has been shown in other *Caenorhabditis* species (Erpf et al., 2019). To determine whether the consensus predicted PLK phospho-binding sites in PCMD-1 are conserved within nematodes, I performed a multiple sequence alignment (MUSCLE) in JalView Version 2 (Edgar, 2004). The consensus PLK phospho-binding site T298 was the only site conserved in all four analyzed *Caenorhabditis* sequences (**Figure 35B**). While the consensus PLK phospho-binding sites T228 and S359 were partially conserved, S56 was not conserved, but it seemed that all other species have a threonine site at this position instead (**Figure 35B**), which can also represent a phospho-

binding site. Note that in addition to the PLK phospho-binding sites, several PLK phosphorylation sites in PCMD-1 could be predicted using the GPS-Polo 1.0 software (Liu et al., 2012), which, however, are not examined in more detail in this work.

To investigate the role of the four predicted phospho-binding sites *in vivo*, the sites were substituted with phospho-resistant alanines. A worm strain with a single-copy insertion of the mutated *pcmd-1(S56A, T228A, T298A, S359A)* cDNA fused to *gfp* at the 5' end under *mai-2* regulatory elements was generated (**Figure 35A**). The *P*$_{mai-2}$*gfp::pcmd-1(S56A, T228A, T298A, S359A)* embryos, which are referred to as *P*$_{mai-2}$*gfp::pcmd-1(4A)*, were analyzed in the *pcmd-1(t3421)* background**.**

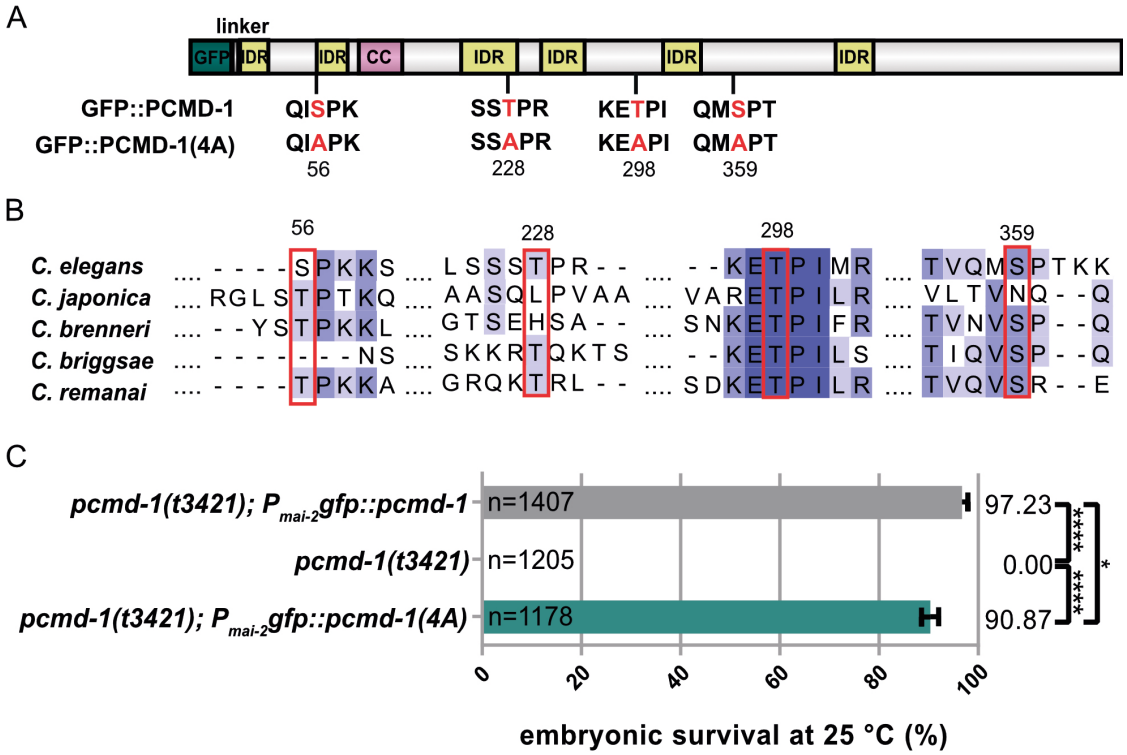

Figure 35. GFP::PCMD-1(4A) with phospho-resistant PLK binding sites only mildly affects embryonic viability. A) Schematic illustration of the domain structure of full-length GFP::PCMD-1(aa 2-630) with predicted serine/threonine (S/T) phospho-binding sites highlighted in red on top, and corresponding mutated sites in the GFP::PCMD-1 (S56, T228, T298, and S359), here referred to as GFP::PCMD-1(4A), highlighted in red on the bottom. The predicted coiled-coil domain (CC) is highlighted in magenta and the IDRs are highlighted in yellow. Note that all domains except GFP are represented to the correct ratio; GFP is scaled down in a ratio of ~1:10. **B)** Sequence alignment of PCMD-1 in *C. elegans* and its homologs in other *Caenorhabditis* species (*Caenorhabditis japonica, Caenorhabditis brenneri, Caenorhabditis briggsae*, and *Caenorhabditis remanei*)was performed using MUSCLE in Jalview Version 2. Conservation of amino acids is indicated by blue shading. Position of predicted PLK phospho-binding sites S56, T228, T298, S359 in *C. elegans* and the aligned the other *Caenorhabditis* species are highlighted with a red box. **C)** Embryonic survival assay performed at 25°C. The embryonic viability of *pcmd-1(t3421)* (0.00%±0.00, n=1205) was restored by *P*$_{mai-2}$*gfp::pcmd-1* (97.23±0.59%, n=1407) and *P*$_{mai-2}$*gfp::pcmd-1(4A)* (90.87±1.79%, n=1178). Multiple Comparison with Kruskal Wallis test and post-hoc Dunn's test (Holm correction) (* p<0.05, **** p<0.0001). Data are represented as mean and SEM, n=total number of embryos.

In an embryonic survival assay performed at the restrictive temperature of 25°C (**Figure 35C**), the *P_{mai-2}gfp::pcmd-1* rescued the lethality of the *pcmd-1(t3421)* embryos with an embryonic survival rate of 97.23%. Moreover, the lethality of *pcmd-1(t3421)* was also mainly rescued by *P_{mai-2}gfp::pcmd-1(4A),* but the embryonic survival rate is significantly reduced to 90.87% in comparison to *P_{mai-2}gfp::pcmd-1*.

Although it has been described that PCMD-1 is still able to localize to the centrosome in the absence of PLK-1 (Erpf et al., 2019), the question was raised whether the survival rates of GFP::PCMD-1(4A) expressing embryos are reduced because mutating the predicted PLK phospho-binding sites leads to deregulation of the localization or dynamics of the PCMD-1 protein. Therefore, GFP::PCMD-1 and GFP::PCMD-1(4A) were monitored over time in one-cell embryos in the *pcmd-1(t3421)* background by live-cell imaging. Both GFP::PCMD-1 and GFP::PCMD-1(4A) localized to centrosomes throughout the cell cycle in all analyzed embryos (**Figure 36A**). Interestingly, the centrosomal GFP::PCMD-1(4A) signal appeared much stronger without signal reduction at the end of mitosis (**Figure 36A**). To confirm this observation, GFP::PCMD-1 and GFP::PCMD-1(4A) signal intensities were quantified. The mean centrosomal fluorescence intensities at PNEB and cytokinesis onset were compared for GFP::PCMD-1 and GFP::PCMD-1(4A). As expected and already described in chapter **3.1.1**, the mean centrosomal GFP::PCMD-1 intensity significantly dropped from 1.00 a.u. at PNEB to 0.59 a.u. at cytokinesis onset (**Figure 36B**). In contrast, the mean centrosomal GFP::PCMD-1(4A) intensity of 1.00 at PNEB was not significantly different from the mean centrosomal intensity of 0.88 a.u. at cytokinesis onset (**Figure 36B**). For both time points, significantly different mean centrosomal fluorescence intensities for GFP::PCMD-1 and GFP::PCMD-1(4A) were revealed (**Figure 36C**). While the mean centrosomal GFP::PCMD-1(4A) intensity was 1.66 fold higher than the mean centrosomal GFP::PCMD-1 intensity at PNEB, the mean centrosomal GFP::PCMD-1(4A) intensity was even 2.31 fold higher than the mean centrosomal GFP::PCMD-1 intensity at cytokinesis onset.

As mentioned in chapter **3.4,** I attempted to examine the Y2H system whether the interaction between PCMD-1 and PLK-1 is abolished when the four predicted phospho-binding sites are substituted with phospho-resistant alanine. However, the PCMD-1 (S56A, T228A, T298A, S359A) bait construct could not be used further due to its autoactivation effect.

Based on my observations, inhibition of phosphorylation of at least one of the four predicted consensus binding sites leads to deregulation of the centrosomal PCMD-1 accumulation. Thus, at least one of the four sites seems to be phosphorylated in wild-type embryos, and the phosphorylation might be required for controlled centrosomal PCMD-1 accumulation or PCMD-1 removal. The slightly increased amounts of

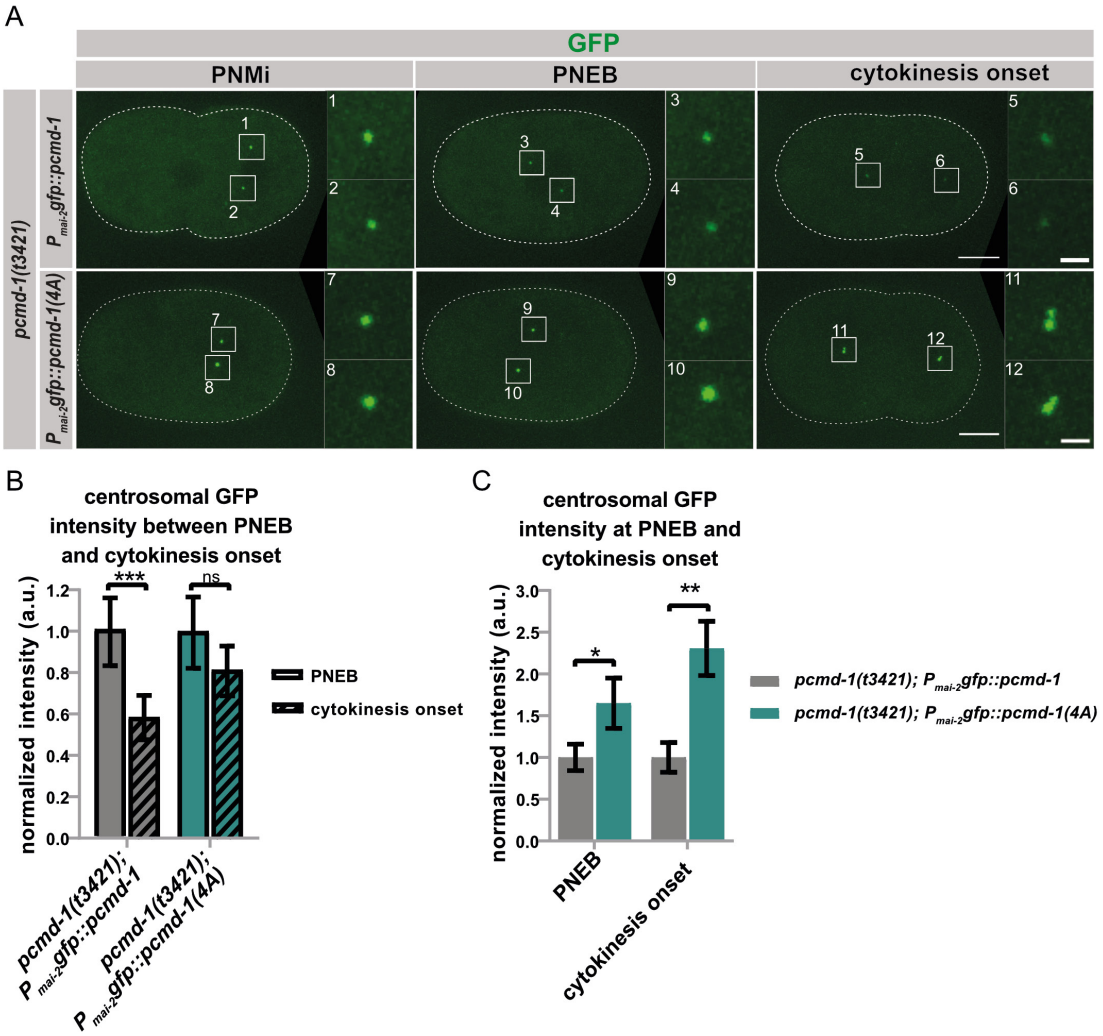

Figure 36. GFP::PCMD-1(4A) with phospho-resistant PLK binding sites shows increased centrosomal accumulation and maintenance. A) Representative stills of time-lapse sequences at PNMi, PNEB and cytokinesis onset of *P*$_{mai-2}$*gfp::pcmd-1* (n=5) and *P*$_{mai-2}$*gfp::pcmd-1(S56A, T228A, T298A, S359A)*, here referred to as *P*$_{mai-2}$*gfp::pcmd-1(4A)* (n=6), one-cell embryos in *pcmd-1(t3421)* background recorded with a spinning disc confocal microscope. GFP::PCMD-1 and GFP::PCMD-1(4A) were detected throughout the cell cycle in all analyzed embryos. Insets show enlarged centrosomal areas labeled with corresponding numbers (1-8). Scale bars indicate 10 µm or 2 µm (insets). **B)** Quantification of centrosomal signal intensities in *P*$_{mai\ 2}$*gfp::pcmd-1* between PNEB (1.00±0.16 a.u., n=10 centrosomes) and cytokinesis onset (0.59±0.10 a.u., n=10 centrosomes), and *P*$_{mai-2}$*gfp::pcmd-1(4A)* embryos between PNEB (1.0±0.16 a.u., n=12) and cytokinesis onset (0.81±0.11 a.u., n=12). Values were normalized to the mean intensities at PNEB. Paired two-sample t-test (*** p<0.001), paired Wilcoxon signed rank test (ns: not significant). **C)** Quantification of centrosomal signal intensities in *P*$_{mai-2}$*gfp::pcmd-1* (1.00±0.16 a.u., n=10 centrosomes) and *P*$_{mai-2}$*gfp::pcmd-1(4A)* embryos (1.66±0.27 a.u., n=12 centrosomes) at PNEB. Mann-Whitney-U test (* p<0.05). Quantification of centrosomal signal intensities in *P*$_{mai-2}$*gfp::pcmd-1* (1.00±0.18 a.u., n=10 centrosomes) and *P*$_{mai-2}$*gfp::pcmd-1(4A)* (2.31±0.33 a.u., n=12 centrosomes) embryos at cytokinesis onset. Welch two-sample t-test (** p<0,01). Values were normalized to the mean intensities of GFP::PCMD-1. Data in **B)**-**C)** are represented as mean±SEM. Note that quantifications of *P*$_{mai-2}$*gfp::pcmd-1* control embryos were pooled with control embryos in chapter 3.1.1/Figure 11 (same experimental setting).

GFP::PCMD-1(4A) might contribute to the decreased viability of *pcmd-1(t3421); P_{mai-2}gfp::pcmd-1(4A)* embryos. Notably, even if the PCMD-1 levels were drastically increased, a centriole separation defect at the end of mitosis was not observed in the *pcmd-1(t3421); P_{mai-2}gfp::pcmd-1(4A)* embryos (Data not shown).

Further, this indicates that PCMD-1 might be a substrate of other kinases and that the potential binding site might be superimposed with kinase sites. The prediction tool GPS 5.0 was applied to identify potential kinases, which might prime PLK-1 binding to PCMD-1 (Xue et al., 2008). With a medium threshold, the S56, T228, and S359 predicted consensus phospho-binding sites were superimposed with consensus substrate of cyclin-dependent kinases (CDK), mitogen-activated protein kinases (MAPK), glycogen synthase kinases (GSK), and dual-specificity tyrosine phosphorylation-regulated kinases (DYRK). However, the T298 site was only predicted to be potentially phosphorylated by MAPK. When a high threshold was applied, S56, S359 were predicted to be potential substrates of CDK and GSK, and T228 was only predicted to be a potential target of CDK.

3.6.2 Phospho-resistant predicted PLK binding sites in PCMD-1 do not affect the PCM scaffold organization and integrity

It was shown that PLK-1 binds to SPD-2 and phosphorylates SPD-5, which is essential for PCM expansion and maintenance (Cabral et al., 2019; Decker et al., 2011; Ohta et al., 2021). Since I have shown that PLK-1 also binds to PCMD-1 and seems to regulate PCMD-1 centrosomal accumulation, I wondered whether SPD-5 localization, expansion, or maintenance is impaired when the predicted PLK binding sites are mutated.

To answer this question, I performed immunofluorescence stainings of *P_{mai-2}gfp::pcmd-1* and *P_{mai-2}gfp::pcmd-1(4A)* one-cell embryos in *pcmd-1(t3421)* background against GFP and the PCM protein SPD-5. In addition, the DNA was visualized by Hoechst staining. In all analyzed embryos, GFP::PCMD-1 and SPD-5 could be detected at the centrosomes (**Figure 37A**). As in the live-cell recordings, GFP::PCMD-1(4A) accumulated more strongly at the centrosome than GFP::PCMD-1. However, the fluorescent signal and the scaffold organization of SPD-5 appeared similar in the GFP::PCMD-1 and GFP::PCMD-1(4A) expressing embryos (**Figure 37A**). The centrosomal circularity and aspect ratio were quantified in mitotic *P_{mai-2}gfp::pcmd-1* and *P_{mai-2}gfp::pcmd-1(4A)* one-cell embryos to examine whether there are subtle differences in the SPD-5 scaffold appearance. As explained in chapter **3.1.3**, a perfect circle would have a circularity and an aspect ratio of 1.00. The mean centrosomal circularity in *P_{mai-2}gfp::pcmd-1(4A)* embryos was 0.68 and, therefore, slightly decreased compared to the mean centrosomal circularity of 0.73 in *P_{mai-2}gfp::pcmd-1* embryos, but the difference was not significant (**Figure 37B**). The mean centrosomal aspect ratio of 1.21 in *P_{mai}-gfp::pcmd-1(4A)*

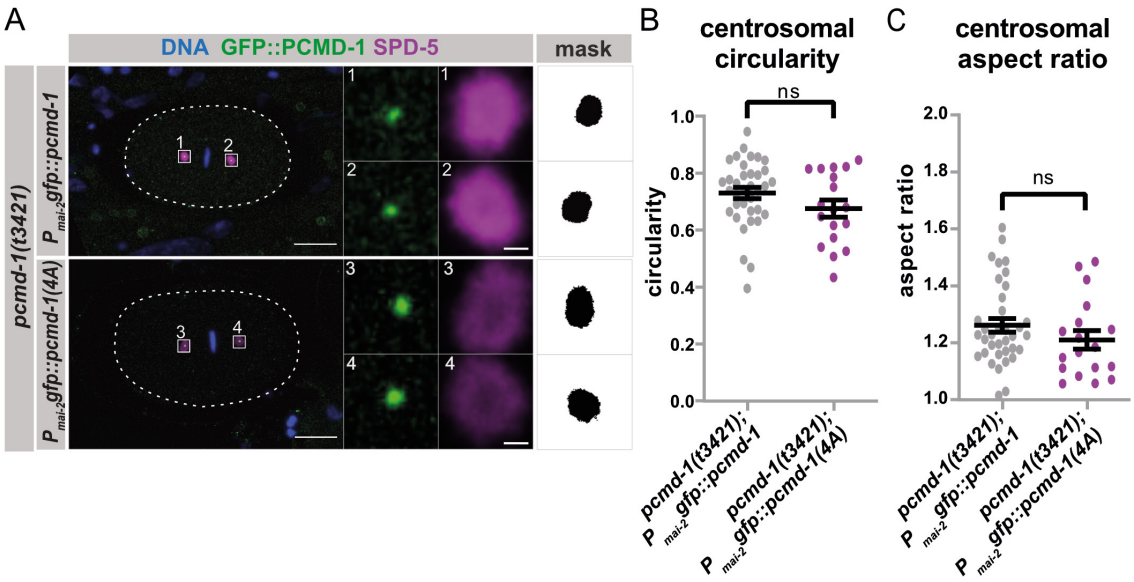

Figure 37. PCM scaffold organization is not impaired in phospho-resistant GFP::PCMD-1(4A). A) Representative z-projected fluorescent images of fixed *P*$_{mai-2}$*gfp::pcmd-1* (n=16) and *P*$_{mai-2}$*gfp::pcmd-1(S56A, T228A, T298A, S359A)*, here referred to as *P*$_{mai-2}$*gfp::pcmd-1(4A)* (n=9), one-cell embryos in *pcmd-1(t3421)* background during mitosis stained against GFP and SPD-5. The DNA was visualized using Hoechst. Insets show enlarged centrosomal areas labeled with corresponding numbers (1-4), and the centrosomal masks used for the shape measurements. Scale bars indicate 10 µm and 1 µm (insets). **B)** Quantification of centrosomal SPD-5 circularity in *pcmd-1(t3421); P*$_{mai-2}$*gfp::pcmd-1* (0.73±0.02, n=36 centrosomes) and *pcmd-1(t3421); P*$_{mai-2}$*gfp::pcmd-1(4A)* embryos (0.68±0.03, n=18 centrosomes). Two-sample t-test (ns: not significant). **C)** Quantification of centrosomal SPD-5 aspect ratio in *pcmd-1(t3421); P*$_{mai-2}$*gfp::pcmd-1* (1.26±0.02, n=36 centrosomes) and *pcmd-1(t3421); P*$_{mai-2}$*gfp::pcmd-1(4A)* embryos (1.21±0.03, n=18 centrosomes) embryos. Mann-Whitney-U test (ns: not significant). Data in **B)** and **C)** are represented as mean±SEM. *P*$_{mai-2}$*gfp::pcmd-1* control embryos that were quantified are the same as in chapter 3.2.4/Figure 22, as the data were acquired in the same experiment.

embryos was not significantly different from the mean centrosomal aspect ratio of 1.26 in *P*$_{mai}$*-gfp::pcmd-1* embryos (**Figure 37C**).

Taken together, the PCM scaffold is not deformed when the four predicted PLK binding sites in PCMD-1 are phospho-deficient. Thus, the findings indicate that PCMD-1 phosphorylation at the phospho-binding sites, and thus PLK-1 binding to PCMD-1, may not be required for the downstream recruitment and organization of the SPD-5 scaffold.

4 DISCUSSION

4.1 The centrosomal protein PCMD-1 recruits and organizes the PCM

4.1.1 Transgenic and endogenous PCMD-1 localize to centrioles, PCM, MTs, and cilia

Transgenic GFP::PCMD-1 was described to localize to centrosomes throughout development and cilia in adult worms (Erpf et al., 2019). By analyzing a transgenic PCMD-1 with a GFP-tag at the C-terminal end (PCMD-1::GFP) and the N-terminal end (GFP::PCMD-1) in *pcmd-1(t3421)* mutant background, I confirmed that the position of the GFP-tag does not influence the spatiotemporal PCMD-1 expression under the *mai-2* promoter. In addition, an endogenously GFP-tagged PCMD-1 expressing strain was generated to examine the endogenous expression of PCMD-1. Although I showed that endogenous PCMD-1 is expressed at lower levels than the transgenic PCMD-1 expressed under *mai-2* regulatory elements, I provide evidence that the subcellular localization of endogenous GFP::PCMD-1 resembles the localization pattern of the transgenic GFP::PCMD-1 localizing to centrosomes and cilia.

Structured illumination microscopy (SIM) of mitotic embryos revealed that the transgenic GFP::PCMD-1 under *mai-2* regulatory elements predominantly localizes to centrioles and weakly to the PCM (Erpf et al., 2019). Analyzing the endogenously GFP-tagged PCMD-1 localization in more detail, I found that it colocalized with the centriole protein SAS-7 and seemed spatially restricted to centrioles in confocal micrographs. A recent study used an independently generated GFP::PCMD-1 CRISPR/Cas9 strain and showed that PCMD-1 is localizing to centrioles and close to centrioles during mitosis (Magescas et al., 2021). Resolving the mitotic spindles of GFP::PCMD-1 embryos from our CRISPR/Cas9 strain using a Lattice SIM microscope enabled us to see that PCMD-1 is not only predominantly overlapping with centriolar SAS-7 but also very dimly localizing to the periphery of centrioles (M. Gorelashvili and T. Mikeladze-Dvali, Stenzel et al., 2020). Additionally, we observed a very dim GFP::PCMD-1 signal at microtubules. Interestingly, a very recent Y2H study showed that PCMD-1 interacts with transforming acid coiled-coil-containing protein 1 (TAC-1) (Nakajo et al., 2021), which regulates in a complex with zygote defective protein 9 (ZYG-9) MT growth and length during early embryogenesis in *C. elegans* (Bellanger and Gönczy, 2003; Le Bot et al., 2003; Srayko et al., 2005; Srayko et al., 2003). This suggests that PCMD-1 might bind to TAC-1 at MTs or even recruit TAC-1 to MTs, thus contributing to MT assembly.

During the first cell cycle, the centrosomal signal intensities of transgenic GFP::PCMD-1 decrease at the end of mitosis (Erpf, 2020). Similar dynamic changes were observed for the centrosomal protein PCNT that might be the potential functional homolog of PCMD-1 in humans (Lee and Rhee, 2012). I confirmed in this work that the decrease of the centrosomal PCMD-1 is comparable in embryos expressing N- or C-terminally GFP-tagged PCMD-1. Moreover, I showed that the centrosomal signal of transgenic GFP::PCMD-1(4A),

which contains phospho-resistant PLK binding sites, did not significantly decrease compared to transgenic GFP::PCMD-1. This suggests that the decreasing centrosomal signal of transgenic GFP::PCMD-1 levels are cell cycle-dependent and are not due to photobleaching. Similarly, endogenous GFP::PCMD-1 signal decreased towards the end of mitosis, indicating that PCMD-1 might have similar functions as the human PCNT and might be regulated by similar mechanisms as PCNT. This will be discussed in more detail in chapter **4.4.2**.

4.1.2 Validation of the function of PCMD-1 in PCM assembly and embryonic viability

It has been shown that PCMD-1 plays an important role in the assembly and organization of the PCM. PCM formation is severely compromised in *pcmd-1(t3421)* embryos (Erpf et al., 2019). The *pcmd-1(t3421)* mutant was described as a temperature-dependent allele. While *pcmd-1(t3421)* embryos are not viable at 25°C, a fraction of the embryos can survive at 15°C (Erpf et al., 2019). Since alternative start codons were identified in the *pcmd-1(t3421)* mutant allele after its point mutation (Erpf, 2020), it was speculated whether the variable phenotype is due to an alternatively transcribed truncated protein. RT-PCR on *pcmd-1(t3421)* worms cultured at permissive temperature resulted in a small amount of amplified cDNA (Erpf et al., 2019). This result indicates that small amounts of a truncated peptide are alternatively transcribed at 15°C, which might escape the elimination by mRNA nonsense-mediated decay.

Data presented in this work provided evidence that transgenic PCMD-1*(t3421)*::GFP, like GFP::PCMD-1*(t3421),* is not detectable at centrosomes and does not rescue the embryonic lethality of the *pcmd-1(t3421)* allele. Some of the PCMD-1*(t3421)*::GFP expressing embryos failed to divide. Furthermore, no bands were detectable for both PCMD-1*(t3421)*::GFP and GFP::PCMD-1*(t3421)* in Western blot analysis performed with worms cultured at the permissive temperature. Thus, the point mutation in the *pcmd-1(t3421)* allele causes a strong reduction of the protein. If small amounts of a truncated protein are transcribed downstream of the premature stop codon in the *pcmd-1(t3421)* mutant, these would be below the detection level of Western blots and confocal microscopy. Noteworthy, analysis of embryos expressing C-terminal parts of PCMD-1 (GFP::PCMD-1(C_218-630), GFP::PCMD-1(C2_343-630)) downstream of the first alternative start codon after the point mutation in *pcmd-1(t3421)* revealed that the C-terminus of PCMD-1 is sufficient to target the truncated protein to the centrosomes. So if PCMD-1*(t3421)* would be alternatively transcribed, it should be visible at the centrosomes.

To validate the *pcmd-1(t3421)* phenotype, another *pcmd-1(syb975)* allele, which deletes all predicted domains and leads to a frameshift, was generated (Erpf et al., 2019). Analyzing the *pcmd-1(syb975)* allele, I demonstrated that impaired PCM assembly,

shown in the *pcmd-1(t3421)* embryos, is resembled in *pcmd-1(syb975*) embryos. Immunofluorescence stainings revealed that the assembly of the PCM core and organization and integrity of the mitotic PCM scaffold were disturbed in *pcmd-1(syb975*) embryos but with some variability as observed in *pcmd-1(t3421)* embryos. However, the *pcmd-1(syb975)* allele was also shown to be temperature-dependent, and at the permissive temperature, a fraction of the embryo failed to divide as described for the *pcmd-1(t3421)* phenotype but with even lower survival rates (Erpf et al., 2019). The lower survival rate of the *pcmd-1(syb975)* embryos at the permissive temperature suggests that a larger deletion causes a more severe phenotype indicating that *pcmd-1(t3421)* might be a hypomorphic allele. Moreover, my data from RNAi experiments against *pcmd-1* and *gfp* in GFP::PCMD-1 expressing embryos confirmed that PCMD-1 is essential for embryonic viability at 25°C. The fact that *pcmd-1* was not discovered in earlier RNAi screens, which were performed at 20°C (Sönnichsen et al., 2005), could be due to both temperature-dependency of the PCMD-1 function or lower efficiency of the RNAi treatment at lower temperatures.

Some of the above-discussed findings, such as centrosomal anchoring of the C-terminus of PCMD-1 (GFP::PCMD-1(C2_343-630)), downstream of potential alternative start codons in the *pcmd-1(t3421)* and *pcmd-1(syb975)* alleles, suggest that *pcmd-1(t3421)* and *pcmd-1(syb975)* are null alleles. Nevertheless, lower survival rates of *pcmd-1(syb975*) embryos compared to *pcmd-1(t3421)* embryos and the cDNA product of RT-PCR on *pcmd-1(t3421)* worms indicate that *pcmd-1(t3421) and pcmd-1(syb975*) are hypomorphic alleles. Due to the contradictory findings, it is not possible to conclude that *pcmd-1(t3421) and pcmd-1(syb975*) are null alleles. Analyzing a complete deletion of *pcmd-1* would pinpoint this issue.

If *pcmd-1(t3421) and pcmd-1(syb975*) were null alleles, the temperature dependency of PCMD-1 could have different explanations. Biochemical reconstitution revealed that SPD-5 autocatalytically self-assembles *in vitro*, and the assembled SPD-5 recruits SPD-2 and PLK-1 (Woodruff et al., 2015). Since cell cycle progression is prolonged at lower temperatures (Begasse et al., 2015; Byerly et al., 1976), at 15°C, SPD-5 might have enough time to autocatalytically self-assemble *in vivo* in the *pcmd-1(t3421)* and *pcmd-1(syb975)* embryos. Alternatively, SPD-5 self-assembly itself is enhanced at lower temperatures. Since the *in vitro* experiments were performed at 23°C (Woodruff et al., 2015), it would be interesting to see whether the self-assembly rate changes at lower temperatures. Intriguingly, the assembled SPD-5 scaffolds observed *in vitro* do not resemble the spherical SPD-5 structures of wild-type embryos. Instead, the *in vitro* assemblies look like the disorganized SPD-5 structures in *pcmd-1(syb975)* mutant embryos analyzed in this work and *pcmd-1(t3421)* mutant embryos analyzed in previous work (Erpf et al., 2019). Furthermore, SPD-5 was shown to form the condensates by liquid-liquid phase separation, and it only can form the spherical condensates after induction with a crowding agent (Woodruff et al., 2017). Since it was described that some

proteins need an interacting protein to undergo LLPS (Wang et al., 2019), PCMD-1, which interacted with SPD-5 in my Y2H assay, may undergo phase separation and promote SPD-5 self-assembly. It would be interesting to see whether PCMD-1 could replace the crowding agent in the *in vitro* reconstitution experiments and whether the condensates would resemble the spherical centrosome structures observed *in vivo.*

4.2 PCMD-1 localization to the centrosome requires different domains

4.2.1 A region in the C-terminus targets PCMD-1 to the centrosome

The collective data generated by T. Mikeladze-Dvali, A. Schreiner, S. Üstüner, and me demonstrated that a region in the C-terminal part of PCMD-1 is required for centrosomal targeting. GFP-tagged PCMD-1 truncations missing the C-terminus of PCMD-1 (GFP::PCMD-1(N_2-117) and GFP::PCMD-1(C1_118-342)) did not localize to the centrosome and did not rescue the embryonic lethality of the *pcmd-1(t3421)* mutant at 25°C. In contrast, constructs including the C-terminal end of PCMD-1 (GFP::PCMD-1(C_118-630), GFP::PCMD-1(C2_343-630)) localized to the centrosomes. However, while GFP::PCMD-1(C_118-630) expressing embryos are viable, GFP::PCMD-1(C2_343-630) are not viable at 25°C. Previous investigations have shown that the *tm8972* allele, which deletes parts of the last exon and *pcmd-1* 3'UTR, is homozygous viable (National BioResource Project (NBRP), Erpf et al. 2019). As this deletion starts from aa L470, I speculate that the centrosomal targeting region is between aa G343 and L470. Dissecting the function of other regions of PCMD-1, especially the IDRs, would provide further insight.

A centrosomal targeting domain was mapped to the C-terminus of the putative functional homologs PCNT in humans and PLP in flies. Both proteins are targeted to the centrosomes through a pericentrin-AKAP450 centrosomal targeting (PACT) domain in their C-termini (Gillingham and Munro, 2000). Nevertheless, sequence conservation of the PACT domain was not observed in PCMD-1 (Erpf et al., 2019). The N-termini of both PCNT and PLP were described to extend to the periphery of the centrosome (Lawo et al., 2012; Mennella et al., 2012). *C. elegans* centrosomes and centrosomal proteins in *C. elegans* are relatively small compared to human and fly centrosomes and centrosomal proteins. Super-resolution imaging alone would not be sufficient to determine whether the C-terminus of PCMD-1 is anchored to centrioles and the N-terminus extends outwards as described for PCNT and PLP. Thus, super-resolution imaging of extremely enlarged centrosomes of PCMD-1::GFP expressing embryos stained with antibodies against the N-terminal end, possibly one of the antibodies generated in this work, and against GFP to label the C-terminal end could address this issue. Therefore, samples would need to be prepared by combining and adapting two recently published expansion techniques, centriole

expansion magnified analysis of the proteome (cMAP) and expansion of *C. elegans* (ExCel), for centrosomes in embryos (Sahabandu et al., 2019; Yu et al., 2020).

4.2.2 The coiled-coil domain promotes centrosomal PCMD-1 localization

Coiled-coil domains in centrosomal proteins exhibit different functions, such as mediating conformational changes, protein-protein interactions, and oligomerization (reviewed in Lupas and Bassler, 2017; Raff, 2019). The most prominent domain predicted in PCMD-1 is the coiled-coil domain (Erpf et al., 2019, Uniprot-KB O62071; UniProtConsortium, 2019).

Deleting the coiled-coil domain of PCMD-1 resulted in severely compromised PCMD-1 levels at the centrosome *in vivo*. Thus, the coiled-coil domain contributes to the accumulation of PCMD-1 at the centrosome. As explained above, C-terminal PCMD-1 constructs (GFP::PCMD-1(C_118-630), GFP::PCMD-1(C2_343-630)) lacking the coiled-coil domain are efficient to localize to the centrosome, and GFP::PCMD-1(N_2-117) including the coiled-coil domain cannot localize to the centrosome. Therefore, it is unlikely that the coiled-coil domain alone is a binding region for upstream regulators. The Y2H data of this work provided evidence for the physical binding of PCMD-1 with itself. This interaction was lost in the absence of the coiled-coil domain. Based on the *in vivo* and Y2H results, I hypothesize that PCMD-1 undergoes oligomerization mediated by its coiled-coil domain. However, PCMD-1 positioned at the plasma membrane could not recruit PCMD-1. The simplest explanation for this observation is that PCMD-1 recruitment might mainly depend on binding to another protein (see chapter **4.3.2**), and oligomerization might promote the recruitment locally at the centrosome. Hence, oligomerization alone does not facilitate translocation to the plasma membrane. Furthermore, it was shown that PCMD-1 is stably integrated at the centrosome, and its cytoplasmic exchange is very weak (Garbrecht et al., 2021).

It has been dissected that LLPS of the human PCNT is mediated through its coiled-coil domains and low-complexity enriched regions (Jiang et al., 2020). Therefore, it would be interesting to see whether the coiled-coil domain of PCMD-1, together with the low-complexity regions and the overlapping IDRs, could mediate the LLPS of PCMD-1.

Even though the centrosomal GFP::PCMD-1(ΔCC) signal is extremely reduced compared to the GFP::PCMD-1 signal, it is not surprising that the embryonic viability of the GFP::PCMD-1(ΔCC) expressing embryos is only mildly impaired. I showed that the PCM scaffold can still assemble in the absence of the coiled-coil domain in PCMD-1, albeit the PCM appears severely disorganized. It has been described earlier that embryos are viable even when the mitotic SPD-5 PCM is absent from the centrosome, and only the SPD-5 PCM core is remaining (Woodruff et al., 2015). How the coiled-coil domain might organize the PCM scaffold will be further discussed in chapter **4.3.1**.

4.3 PCMD-1 acts as a bridge between the centrioles and the PCM

Varadarajan and Rusan (2018) reviewed centrosomal bridge proteins of flies, humans, mice, and *C. elegans*. The authors define bridge proteins by two criteria: their radial distance to the centriole and data confirming a function in PCM assembly. CPAP/Sas4, CEP192/Spd2, Asl/Cep152, and PCNT/PLP were classified as bridge proteins in humans and flies. SAS-4 and SPD-2 were categorized as bridge proteins, and SAS-7 was also mentioned as a potential bridge protein. Data from this work and Erpf et al. (2019) describe that PCMD-1 localizes to centrioles and the PCM and is involved in PCM assembly. Furthermore, radial distances of centrosomal proteins in *C. elegans* have been reported previously (Magescas et al., 2019), and only recently PCMD-1 was shown to have a similar radial distance as SAS-4 but is smaller than the width of the PCM pool of SPD-2 (Magescas et al., 2021). Thus, the radial distance criterion suggests that PCMD-1 is a bridge protein. Furthermore, the role of PCMD-1 in PCM assembly, genetic dependencies, and protein-protein interactions identified in this work and Erpf et al. (2019) suggest that PCMD-1 is a bridge protein. In the following chapters, I will discuss how PCMD-1 interacts with centriole and PCM proteins and might act as a molecular bridge.

4.3.1 PCMD-1 interacts with PCM proteins

Data from this and previous work provided evidence that PCMD-1 is required to assemble the interphase PCM core and organize the mitotic PCM scaffold (Erpf et al., 2019). Additionally, marked-mating experiments revealed that PCMD-1 is initially recruited to the centrosomes at the end of meiosis II, and subsequently, SPD-5 is recruited (performed by T. Mikeladze-Dvali, Stenzel et al., 2020). Since my analysis of cellular protein levels revealed that PCM defects in the absence of functional PCMD-1 are not due to degradation of PCM proteins, it was concluded that protein-protein interactions must be compromised in the absence of functional PCMD-1. Indeed, Y2H results conducted in this work confirmed that PCMD-1 directly interacts with the downstream PCM scaffold protein SPD-5 and the PCM regulator PLK-1. Furthermore, the interactions between PCMD-1 and SPD-5 or PLK-1 were confirmed by another Y2H study conducted concurrently with our study (Nakajo et al., 2021). Moreover, I showed that ectopic positioning of PCMD-1 to the plasma membrane is sufficient to recruit SPD-5 and PLK-1. Thereby, the efficiency of transgenic PCMD-1 recruiting SPD-5 and PLK-1 to the plasma membrane was even higher in the absence of endogenous PCMD-1. This phenomenon might be explained by endogenous centrosomal PCMD-1 competing with the transgenic membrane-bound PCMD-1 in recruiting PLK-1 and SPD-5. It was observed that in the absence of endogenous SPD-5, transgenic phospho-resistant SPD-5 is tethered to the plasma membrane by PCMD-1 without being phosphorylated by PLK-1 (data from A. Schreiner in Stenzel et al., 2020). This observation is similar to a recent study of the recruitment of SPD-5 by PCMD-1 to the ciliary base of sensory neurons, where PLK-1 is

naturally absent (Garbrecht et al., 2021). Furthermore, PLK-1 was also recruited to the plasma membrane independently of SPD-5 (data from A. Schreiner in Stenzel et al., 2020). This observation shows that the proteins can be recruited by PCMD-1 independently of each other.

I observed that the coiled-coil domain of PCMD-1 plays a vital role in organizing the mitotic SPD-5 scaffold in one-cell embryos. Based on my findings, it is not surprising that the SPD-5 binding site was mapped to the N-terminal part of the PCMD-1 protein (amino acid 1-242), which includes the coiled-coil domain (Nakajo et al., 2021). Thus, the coiled-coil domain may mediate protein-protein interaction with SPD-5. In addition, PCMD-1 might stabilize the SPD-5 scaffold by oligomerization through its coiled-coil domain. Mapping interaction sites in Y2H studies with the *D. melanogaster* proteins Cnn (SPD-5 homolog) and PLP (putative functional PCMD-1 homolog) revealed that the proteins even interact at two distinct regions (Citron et al., 2018; Lerit et al., 2015). One interacting site in PLP overlaps with its first coiled-coil domain and the other with the PACT domain (UniProtKB: M9PI63 UniProtConsortium, 2019).

It would be of particular interest to further narrow down the binding site of SPD-5 in PCMD-1. To determine whether the coiled-coil domain of PCMD-1 is the binding site, a Y2H assay could be performed with a PCMD-1(ΔCC) bait and SPD-5 prey. Furthermore, it would be interesting to determine whether SPD-5 and PCMD-1 interact at two different sites, as shown for Cnn and PLP in *Drosophila* (Citron et al., 2018; Lerit et al., 2015). Therefore, a Y2H assay could be performed with a PCMD-1(C2) bait and SPD-5 prey.

PLK-1 binding sites are known to be phospho-regulated and will be discussed in chapter **4.4.1.**

4.3.2 PCMD-1 interacts with centriole proteins

Data of this and previous work uncovered that PCMD-1 is the most upstream PCM component in *C. elegans* (Erpf et al., 2019). Here I discuss how PCMD-1 itself is regulated and which proteins are responsible for PCMD-1 localization to the centrosome. A previous study has explained that SAS-7, the outermost centriole protein, is required for daughter centriole assembly and PCM assembly in *C. elegans* by regulating the bridge protein SPD-2 (Sugioka et al., 2017). Data presented in this work showed that the spatial localization of PCMD-1 and SAS-7 overlaps at centrosomes. Furthermore, *sas-4(RNAi)* experiments suggest that SAS-7 and PCMD-1 act downstream of SAS-4 in centrosome assembly. Both are not visible at centrosomes when SAS-4 is fully depleted and weakly visible at some centrosomes when SAS-4 is only partially depleted. I further dissected that SAS-7 centriolar localization is not dependent on PCMD-1, suggesting that PCMD-1, like SPD-2, acts downstream of SAS-7 in centrosome assembly. I demonstrated that SAS-7 regulates PCMD-1 localization to the centrosome in early embryos. Since the paddlewheel structures of *sas-7(or452)* mutant embryos are disturbed, these structures might be required for

PCMD-1 anchoring. However, in some *sas-7(or452)* mutant one-cell embryos analyzed by live-cell imaging, small amounts of PCMD-1 were still visible at centrosomes. This could reflect the nature of the hypomorphic *sas-7(or452)* allele. Marginal amounts of GFP::SAS-7(*or452ts*) were shown to localize to the centrosome (Sugioka et al., 2017), which might recruit the small amounts of PCMD-1. However, the analysis cannot exclude that the remaining PCMD-1 is tethered to the centrosome by another mechanism. Although it was demonstrated that SAS-7 regulates PCMD-1 localization to the centrosome, physical binding between PCMD-1 and SAS-7 with both proteins used as bait could not be demonstrated in the Y2H assay. Even with the smaller centrosomal targeting region of PCMD-1, an interaction was not provable. The Y2H assay harbors many limitations. For instance, interactions that require posttranslational modifications or another protein are not detected (Braun et al., 2009; Remmelzwaal and Boxem, 2019; Venkatesan et al., 2009). Therefore, one possibility is that the interaction between SAS-7 and PCMD-1 requires posttranslational modifications, such as phosphorylation, of one or both proteins. Another possibility is that the interaction between SAS-7 and PCMD-1 requires a third protein. Although SPD-2, which is regulated through SAS-7, could represent a potential linker (Sugioka et al., 2017), my *in vivo* experiments revealed that PCMD-1 localization is not dependent on SPD-2. Furthermore, I found that PCMD-1 does not interact with SPD-2 in the Y2H assay. Since SAS-4 was shown to interact with SAS-7 (Boxem et al., 2008) and PCMD-1, it would be an attractive candidate to mediate this interaction. However, data from this work concomitant with data from previous work show that SAS-4 is still present at centrosomes in *sas-7(or452)* mutant embryos, in which PCMD-1 is not detectable (Sugioka et al., 2017). This finding suggests that SAS-4 alone would not be able to anchor PCMD-1 at the centrosome. In *D. melanogaster*, Sas4 was shown to form cytoplasmic complexes with the PCM proteins Cnn, Asl, and Plp, the potential functional homolog of PCMD-1, and thereby tethers the proteins to centrioles (Gopalakrishnan et al., 2011). Bleaching experiments in *C. elegans* revealed that SAS-4 exchanges with the cytoplasm until it gets stably incorporated in the centrosome at prophase (Dammermann et al., 2008). Therefore, I speculated that the cytoplasmic SAS-4 might form a complex with PCMD-1 and tether PCMD-1 to centrosomes, where PCMD-1 is anchored to the centrioles by SAS-7. However, I showed in the translocation assay that PCMD-1 could not recruit SAS-4 or SAS-7 to the plasma membrane. This observation suggests that the interactions need to occur at the centrosome. If PCMD-1 forms a complex with the cytoplasmic SAS-4 pool, SAS-4 would most probably colocalize with PCMD-1 at the plasma membrane. In addition, my colleague A. Schreiner performed the translocation assay with SAS-4(ΔTCP), which only represents the SAS-4 PCM pool, but it could also not be recruited by PCMD-1. Therefore, I suggest that SAS-7 regulates recruitment of PCMD-1 locally at the centrosome, and SAS-4 might contribute to the recruitment at the centrosome. Interestingly, I observed that PCMD-1 is recruited to centrosomes in later stage *sas-7(or452)* mutant embryos. This observation could be

explained by the hypomorphic nature of the *sas-7(or452)* allele, in which marginal amounts of SAS-7 are still localizing to centrosomes. Another explanation would be an alternative mechanism of how PCMD-1 is recruited in later cell stage embryos.

Even if physical binding could not be shown, I propose that SAS-7 regulates PCMD-1 recruitment locally at the centrosome in early embryos. SAS-4 might be involved in the recruitment of PCMD-1. However, this needs further investigation. For future analysis, the interaction between SAS-7 and PCMD-1 could be tested by Co-immunoprecipitation to confirm the *in vivo* data. It would be interesting to see whether SAS-7 alone or SAS-7 with SAS-4 positioned at the plasma membrane are sufficient to recruit PCMD-1 to an ectopic locus.

Consistent with the decreased circularity and increased aspect ratio of the SPD-2 PCM pool in *sas-7(or452ts)* one-cell embryos (Sugioka et al., 2017), I showed that the SPD-5 scaffold also appeared disorganized with decreased circularity and slightly increased aspect ratios in *sas-7(or452ts)* one-cell embryos. The disorganization and deformation further argue that SAS-7 regulates the centrosomal localization of PCMD-1 in early-stage embryos, and in turn, PCMD-1 organizes the mitotic PCM scaffold.

We previously found that transgenic PCMD-1 localizes to cilia in *C. elegans* (Erpf et al., 2019), and the localization to cilia was also shown for endogenous PCMD-1 in this work. However, I could not detect SAS-7 at the cilia of sensory neurons in adult worms. Previous studies in *C. elegans* embryos found that the centrioles, including SAS-4, are degraded after migrating to the cell membrane during early ciliogenesis starting from the *C. elegans* 1.5-fold embryonic developmental stage (Li et al., 2017; Nechipurenko et al., 2017; Serwas et al., 2017). It would be interesting to see whether SAS-7 initially localizes to the centrioles before degradation and recruits PCMD-1 or whether another protein facilitates the initial localization of PCMD-1 to cilia. It was shown that SPD-5 maintains PCMD-1 in a feedback loop (Garbrecht et al., 2021). I speculate that SAS-7, if present in early ciliogenesis, and SAS-4 might play a role in the initial recruitment of PCMD-1 to cilia but are not retained at cilia because they do not play a role in maintaining PCMD-1. Alternatively, PCMD-1 recruitment to the cilia might underly a different mechanism than PCMD-1 recruitment to the centrosomes of early-stage embryos.

4.3.3 PCMD-1 interacts with both centriole and PCM proteins

This section summarizes the interactions between *C. elegans* bridge proteins and PCM core proteins by considering genetic localization dependencies and Y2H protein-protein interactions from this and earlier studies.

Based on my analysis, a picture of a pathway emerges (**Figure 38**), in which PCMD-1 and SPD-2 both function as molecular bridge proteins between centrioles and the PCM. I showed that the centriole protein SAS-7 regulates PCMD-1 localization, and SAS-7 and

PCMD-1 localization to the centrosome is dependent on the centriole protein SAS-4. For a long time, the conserved PCM core in *C. elegans* was described to consist of a limited number of proteins: SPD-5, SPD-2, and PLK-1 (Decker et al., 2011; Hamill et al., 2002; Kemp et al., 2004; Pelletier et al., 2004; Woodruff et al., 2015). However, PCMD-1 is a new important component required for the PCM core assembly like SPD-2. SAS-7 regulates the localization to the centrosome of both PCMD-1 and SPD-2 (Sugioka et al., 2017). Physical binding between SPD-2 and SAS-7 was demonstrated in this and previous Y2H studies (Boxem et al., 2008; Li et al., 2004; Sugioka et al., 2017). Besides its role in PCM recruitment, SPD-2 plays a role in daughter centriole assembly, and therefore SAS-4 is also dependent on SPD-2 (Pelletier et al., 2004). For PCMD-1 and SAS-7, physical binding could not be verified in the Y2H system. Instead, I could show physical binding between SAS-4 and PCMD-1 in yeast. Physical binding of SAS-7 with SAS-4 was shown in previous studies (Boxem et al., 2008). It is yet unclear whether SAS-4 mediates an interaction between SAS-7 and PCMD-1 or interacts in parallel, but SAS-4 alone is insufficient to recruit PCMD-1. The localization of PLK-1 and SPD-5 depends on SPD-2, confirmed by Y2H interactions (Boxem et al., 2008; Decker et al., 2011; Hamill et al., 2002; Kemp et al., 2004; Pelletier et al., 2004). While PCMD-1 localization to the centrosome does not depend on SPD-2, shown in this work, the recruitment of the SPD-2 PCM pool to the centrosome depends on PCMD-1 (Erpf et al., 2019). However, physical binding could not be proven. This suggests that PCMD-1 might indirectly regulate the localization of the SPD-2 PCM pool via SPD-5, known to be interdependent with SPD-2 (Wueseke et al., 2014). In fact, SPD-5 and PLK-1 interacted with PCMD-1 in my Y2H assay, and both are localization-dependent on PCMD-1 (Erpf et al., 2019). The assembled PCM core serves as a platform for PCM expansion upon mitotic entry. Interestingly, my data showed that PCMD-1 interacts with itself, similar to what is observed for the SPD-5 matrix protein (Boxem et al., 2008).

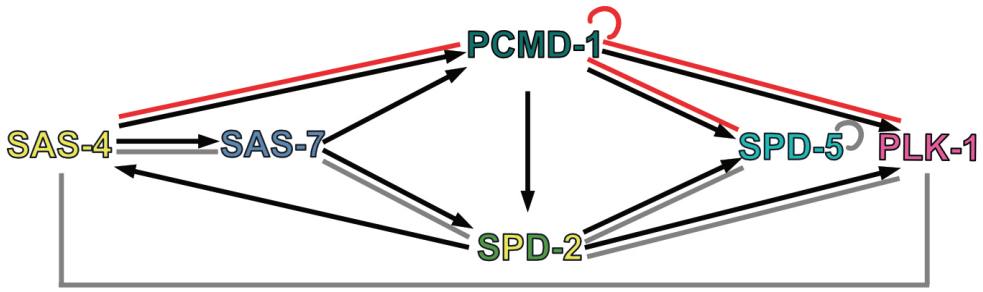

Figure 38. Proposed pathway of PCM core recruitment by bridge proteins. Black arrows represent localization dependencies found in this work and described in previous work (Decker et al., 2011; Erpf et al., 2019; Hamill et al., 2002; Kemp et al., 2004; Ohta et al., 2021; Pelletier et al., 2004; Sugioka et al., 2017). Red lines and half-circle describe interactions found in the Y2H system presented in this work, and grey lines and half-circles represent interactions found in earlier Y2H screens (Boxem et al., 2008; Li et al., 2004; Sugioka et al., 2017).

The protein-protein interactions and genetic localization dependencies demonstrated in this work immensely increase the understanding of the PCMD-1 and its relationship to other bridge proteins and PCM core proteins in *C. elegans*. However, the analysis here was only based on candidate proteins. A large-scale Y2H screen using a *C. elegans* cDNA library could identify even more interactors of PCMD-1. Reversing baits and preys in the Y2H system can lead to different results. Since the interaction between SAS-7 bait and PLK-1 prey was not reversed, I did not include this interaction in the model. Additionally, the novel translocation assay was applied to confirm genetic localization dependencies between PCMD-1 and PLK-1 or SPD-5 at an ectopic location in the cell. Retesting the interactions with an independent approach, such as coimmunoprecipitation, fluorescence resonance energy transfer (FRET), or surface plasmon resonance (Bioacore) (reviewed in Brückner et al., 2009), would additionally verify the interactions and further support the proposed model. The proposed model will serve as a foundation for future studies on understanding how the bridge proteins load the PCM core.

4.4 PCMD-1 regulation through phosphorylation

4.4.1 Phospho-regulation of PCMD-1 might control its centrosomal accumulation

PLK-1, which is the homolog of PLK1 in humans and Polo in flies, belongs to the family of polo-like kinases and is conserved in many systems (reviewed in Archambault and Glover, 2009; Zitouni et al., 2014). It is an essential regulator of several cellular processes. For instance, during cell division, PLK-1 is involved in centrosome maturation, spindle assembly, kinetochore-microtubule attachment, and cytokinesis (reviewed in Archambault and Glover, 2009; Lowery et al., 2005; Petronczki et al., 2008; Weerdt and Medema, 2006).

Physical binding of PLK-1 to PCMD-1 was proven in the Y2H assay in this work. It was also described that PCMD-1 promotes the centrosomal localization of PLK-1 (Erpf et al., 2019). In line with this, I demonstrated that ectopic positioning of PCMD-1 to the plasma membrane was sufficient to recruit PLK-1. PLK-1 binding is known to be facilitated through its Polo-box domain (PBD) in its C-terminus recognizing phospho-epitopes of other proteins (Elia et al., 2003a; Elia et al., 2003b). Therefore, I assume that PLK-1 binding to PCMD-1 is mediated through phosphorylation at consensus binding sites in PCMD-1. Analysis of embryos with phospho-resistant predicted PLK phospho-binding sites in PCMD-1 revealed that controlled PCMD-1 accumulation at the centrosome is phospho-regulated by at least one of these sites. The embryos showed increased centrosomal GFP::PCMD-1(4A) intensities. Further, the viability of these embryos was slightly reduced in the *pcmd-1(t3421)* background. The PLK phospho-binding site prediction was not specific for PLK-1, and it must be considered that the *C. elegans* genome encodes two

PLK-1 homologs, PLK-2 and PLK-3, which share substantial sequence similarity. PLK-2, for instance, also localizes to centrosomes but compared to PLK-1 to a lower extent (Nishi et al., 2008). Moreover, a recent study showed that PLK-2 interacts with PCMD-1 in the Y2H system (Nakajo et al., 2021). However, experiments with PLK triple mutants in *C. elegans* have shown a redundancy between the PLK homologs (Cabral et al., 2019). The observed phenotype of the GFP::PCMD-1(4A) expressing embryos, with four phospho-resistant predicted PLK bindings sites, is of particular interest and needs to be analyzed in-depth in the future. It would be interesting to investigate *in vivo* whether all four mutated sites contribute to the phenotype or whether single mutated sites also affect PCMD-1 regulation. Experiments using *gfp::pcmd-1* alleles with phospho-mimetic binding sites would complement the analysis. The phospho-mimetic PCMD-1 might be prematurely removed from the centrosome or not even loaded onto the centrosome. In the Y2H system, PCMD-1(S56A, T228A, T298A, S359A) could not be used as bait due to autoactivation. I hypothesize that the PBD of PLK-1 binds to one or more of the predicted PLK phospho-binding sites in PCMD-1. Therefore, PLK-1 binding through the PBD could also be studied in the Y2H system coexpressing PCMD-1 and PLK-1 lacking the PBD. Moreover, the PBD could be coexpressed with full-length PCMD-1 or PCMD-1 with mutated predicted binding sites as prey. Similar experiments were performed in earlier Y2H screens with *C. elegans* PLK binding proteins (Nishi et al., 2008; Tavernier et al., 2015). Alternatively, PLK-1 or PBD binding *in vitro* assays using purified PCMD-1 with multiple and single phospho-resistant and phospho-mimicking binding sites could be performed to map the interaction sites, as described for SPD-2 and PLK-1 binding (Decker et al., 2011).

The data presented in this work point towards PCMD-1 being a substrate for kinases. There are two different ways how PLK-1 can be primed to its substrates. Binding is either induced through phosphorylation by another kinase, termed non-self-priming, or through phosphorylation by itself, known as self-priming (reviewed in Lee et al., 2014; Lowery et al., 2005). Binding motifs were predicted to be most presumably recognized by proline-directed kinases CDK or MAPK, which are the only known PBD priming kinases (reviewed in Lowery et al., 2005). Therefore, I speculate that CDK-1 might be the priming kinase to phosphorylate PCMD-1 and mediate binding by PLK-1. CDK-1 is, besides PLK-1 and AIR-1, known as a primary PCM regulator (reviewed in Pintard and Archambault, 2018), and CDK-1 and CDK-2 were also suggested to be the priming kinases for PLK-1 binding sites in SPD-2 (Decker et al., 2011). Whether the priming kinase belongs to the CDK family requires further analysis. This could be tested by treating GFP::PCMD-1 expressing embryos with the CDK inhibitor flavopiridol at different time points, as described earlier for *C. elegans* embryos (Magescas et al., 2019; McCarthy Campbell et al., 2009; Yang and Feldman, 2015). Additionally, an *in vitro* kinase assay testing the dependency of the PLK-1/PCMD-1 interaction on CDK-1, as previously described for the CDK-1 dependent PLK-1/SPAT-1 interaction (Tavernier et al., 2015), could explain the binding mechanism. Immunoprecipitation of PCMD-1 with subsequent phosphorylation analysis by mass-

spectrometry could corroborate the *in vivo, in vitro,* and Y2H data and give further insight into the phospho-regulation of PCMD-1.

4.4.2 Potential functions of phosphorylated PCMD-1

Upon binding to PCMD-1, PLK-1 could distributively phosphorylate other targets. This was demonstrated for PLK-1 binding to SPD-2 and, in turn, phosphorylating SPD-5 (Ohta et al., 2021). The PLK-1 dependent phosphorylation of SPD-5 is further required for PCM expansion and maintenance (Cabral et al., 2019; Decker et al., 2011; Ohta et al., 2021).

My experiments, however, showed that phospho-resistant predicted PLK binding sites in PCMD-1 and thus potentially inhibited PLK-1 binding and phosphorylation, did not impair expansion, maintenance, or the appearance of the mitotic SPD-5 PCM scaffold. This observation indicates that distributive phosphorylation is unlikely, at least for SPD-5. Alternatively, PLK-1 could directly phosphorylate PCMD-1, a process termed processive phosphorylation (reviewed in Kumar et al., 2017; Park et al., 2010). This is very likely as several PLK phosphorylation sites were predicted in PCMD-1, and mutated PLK binding led to increased PCMD-1 levels. Inhibited PLK-1 binding would then, in turn, inhibit phosphorylation of PCMD-1 by PLK-1. Thus, the data in this thesis indicate that phosphorylation of predicted PLK binding sites in PCMD-1, and maybe processive phosphorylation by PLK-1, is not required to facilitate PCMD-1 accumulation at the centrosome but rather to control its dynamics or removal. How could PCMD-1 then be removed from the centrosome, and how could PLK-1 contribute to this process?

At the mitotic exit, PCM disassembles, and the centriole pair separates as a prerequisite of duplication for the next cell cycle. PCM disassembly in *C. elegans* is mainly processed through microtubule pulling forces and dephosphorylation of SPD-5 by the phosphatase PP2A and inhibition of CDK activity (Enos et al., 2018; Magescas et al., 2019). In contrast to PCM proteins, such as SPD-5, PCMD-1 is not ruptured into packets by pulling forces at centrosome disassembly (Magescas et al., 2021). Although PCM disassembly and thus centriole separation is mainly regulated by dephosphorylation and pulling forces, it is known that another crucial factor that contributes to centriole separation in humans is the proteolytic cleavage of the cohesin complex and the PCM protein PCNT by the cysteine protease separase (reviewed in Sluder, 2013). Interestingly, proteolytic cleavage of PCNT, the putative homolog of PCMD-1 in humans, requires prior phosphorylation of PCNT by PLK-1 (Kim et al., 2015; Lee and Rhee, 2012). The cleavage of PCNT leads to reduced PCNT levels at the end of mitosis and thus centriole disengagement (Lee and Rhee, 2012; Matsuo et al., 2012). In *C. elegans*, separase (SEP-1) activity and cleavage of cohesin through SEP-1 seem critical for centriole separation during meiosis and the first mitosis but not in later mitotic cell divisions (Cabral et al., 2013). Since the cohesin complex is not the only factor involved in centriole disengagement in humans, another protein could also be involved in centriole disengagement in *C. elegans*. Based on the data shown in

this work, PCMD-1 is likely a substrate of PLK-1. Additionally, I found a motif (EQAR) in the PCMD-1 sequence, which was identified as a consensus SEP-1 cleavage site in other *C. elegans* proteins (Monen et al., 2015). While endogenous GFP::PCMD-1 and transgenic GFP::PCMD-1 and PCMD-1::GFP centrosomal signals significantly dropped towards the end of mitosis, transgenic GFP::PCMD-1(4A) did not significantly decrease. Therefore, one could speculate that PCMD-1 might be proteolytically cleaved by separase in a PLK-1 dependent manner, as observed for the human PCNT (Kim et al., 2015). Furthermore, it was described that the C-terminus of PCNT, which is anchored to the centriole, is degraded immediately after the N-terminus of PCNT was cleaved (Kim et al., 2015; Matsuo et al., 2012), and only uncleaved PCNT is remaining at the centrosome (Matsuo et al., 2012). This would explain why I did not detect a significant difference between the C- and N-terminally GFP-tagged PCMD-1 intensities at the end of mitosis and that the remaining GFP::PCMD-1 signal might be uncleaved protein, as seen for PCNT. However, I did not observe centriole separation defects in GFP::PCMD-1(4A) expressing embryos, which contradicts the hypothesis that PLK-1 dependent PCMD-1 cleavage is necessary for centriole separation. Future analysis of a *gfp::pcmd-1* allele with a non-cleavable predicted SEP-1 cleavage motif, which has been generated in collaboration with my colleague E. Zuccoli, may address this issue. The analysis of this allele could unravel whether PCMD-1 is proteolytically cleaved by SEP-1 and whether the cleavage of PCMD-1 plays a role in centriole separation during meiotic or mitotic divisions.

4.5 Model: Functions of PCMD-1 in the centrosome cycle

This work focused on the *C. elegans* protein PCMD-1 and its role and regulation in centrosome assembly. Based on the data presented in my thesis, Stenzel et al. (2020), and Erpf et al. (2019), I propose a model in which PCMD-1 plays multiple essential roles throughout the centrosome cycle (**Figure 39**).

PCMD-1 localizes to centrioles in early *C. elegans* embryos and assembles a platform for PCM recruitment. Initially, PCMD-1 is recruited in late meiosis II before the centrioles separate, thus little PCMD-1 is present at the transition to mitosis. Its localization is regulated by the centriole protein SAS-7, which is required for paddlewheel formation. SAS-4, which physically binds to PCMD-1 and SAS-7 and which is required for their localization to the centrosome, potentially mediates the recruitment through SAS-7. However, the exact mechanism still needs to be elucidated. While a region in the C-terminus of PCMD-1 is sufficient to target PCMD-1 to the centrosome, the coiled-coil domain in the N-terminus promotes its centrosomal accumulation through self-interaction. PCMD-1 is bridging centrioles and the PCM by serving as a platform for the interphase PCM core. It independently recruits the PCM scaffold protein SPD-5 and the PCM regulator PLK-1 through protein-protein interactions. Meanwhile, the daughter centriole assembles. During centrosome maturation, when the PCM and the MT nucleation

activity expand dramatically (Woodruff et al., 2015; Wueseke et al., 2016), PCMD-1 functions as an organizer of the mitotic PCM. Thereby, its coiled-coil domain plays a distinct role in the organization of the PCM scaffold. However, it is unclear whether PCMD-1 directly organizes the mitotic PCM or the assembled PCM core serves as an organizing platform. PCMD-1 is also present at MTs indicating that it might play a role in regulating MT assembly during mitosis. Furthermore, PCMD-1 accumulation seems to be PLK-1 dependent. I speculate that PCMD-1 accumulation during maturation or the removal of PCMD-1 during PCM disassembly might be controlled by PLK-1. PCM disassembly licenses centriole separation and entering the next centrosome cycle (Magescas et al., 2019). Since PCMD-1 is not completely removed, some PCMD-1 is maintained when new PCMD-1 is recruited to assemble a new platform. The proposed roles of PCMD-1 in the centrosome cycle require careful and in-depth analysis in the future. Different mechanisms might be involved in later cell cycles.

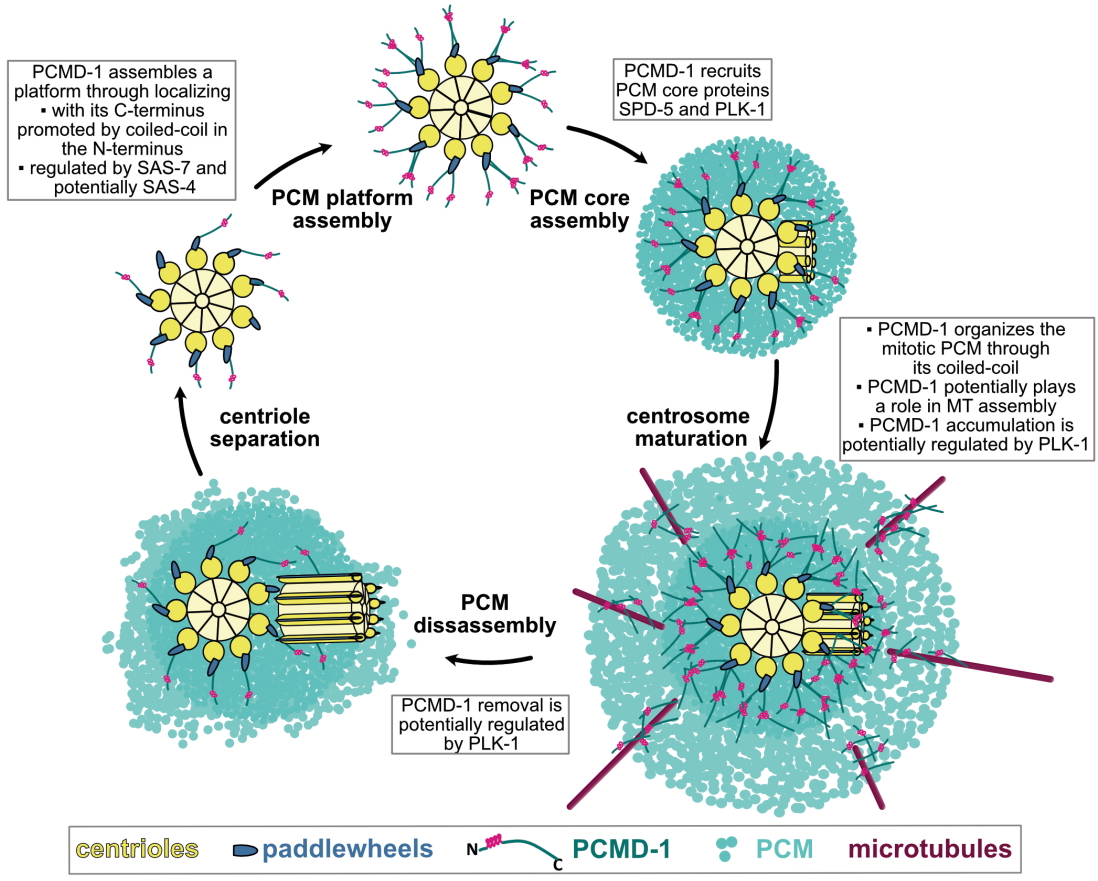

Figure 39. Potential functions of PCMD-1 in the centrosome cycle. PCMD-1 forms a platform for PCM assembly. It binds with its C-terminal end to centrioles, regulated by SAS-7 and mediated by SAS-4. The localization is promoted by the coiled-coil domain (magenta) of PCMD-1. During PCM core assembly, PCMD-1 recruits the PCM core proteins SPD-5 and PLK-1. Upon centrosome maturation, PCMD-1 organizes the mitotic PCM with its coiled-coil domain and localizes to MTs indicating a role in MT assembly. The centrosomal PCMD-1 accumulation during centrosome maturation and potentially removal during PCM disassembly at mitotic exit might be regulated by PLK-1. The PCM disassembly licenses centriole separation and another round of duplication. Parts of the schematic are modified based on Cabral et al. (2019), Magescas et al. (2019), Ohta et al. (2017), Stenzel et al. (2020), Sugioka et al. (2017).

4.6 Concluding remarks and future perspective

My work provides evidence that the functions of PCMD-1 in centrosome assembly resemble those of PCNT and PLP in humans and flies. It localizes to centrioles with its C-terminus, bridges the centrioles and the PCM by interacting with both centriole and PCM proteins, and serves as a platform for PCM assembly. Similarly, PCNT and PLP, categorized as bridge proteins (reviewed in Varadarajan and Rusan, 2018), localize to centrioles with their C-termini and span the PCM core with their N-termini extending outwards, and play a role in recruiting PCM proteins (Lawo et al., 2012; Mennella et al., 2012). Mutations in the human PCNT are linked to various severe diseases, such as cancer and primordial dwarfism (reviewed in Bober and Jackson, 2017; Delaval and Doxsey, 2010; Trulioff et al., 2017). Since the physiological role of PCNT in health and disease is not entirely understood, future studies on PCMD-1 in the model organism *C. elegans* might also contribute to a better understanding of the potential functional homolog PCNT and its association with diseases.

5 REFERENCES

Alberti, S., Gladfelter, A., and Mittag, T. (2019). Considerations and Challenges in Studying Liquid-Liquid Phase Separation and Biomolecular Condensates. Cell *176*, 419-434.

Alberti, S., Saha, S., Woodruff, J.B., Franzmann, T.M., Wang, J., and Hyman, A.A. (2018). A User's Guide for Phase Separation Assays with Purified Proteins. Journal of Molecular Biology *430*, 4806-4820.

Albertson, D.G. (1984). Formation of the first cleavage spindle in nematode embryos. Developmental Biology *101*, 61-72.

Albertson, D.G., and Thomson, J.N. (1993). Segregation of holocentric chromosomes at meiosis in the nematode *Caenorhabditis elegans*. Chromosome Research *1*, 15-26.

Archambault, V., and Glover, D.M. (2009). Polo-like kinases: conservation and divergence in their functions and regulation. Nature Reviews Molecular Cell Biology *10*, 265-275.

Arquint, C., Gabryjonczyk, A.M., Imseng, S., Böhm, R., Sauer, E., Hiller, S., Nigg, E.A., and Maier, T. (2015). STIL binding to Polo-box 3 of PLK4 regulates centriole duplication. eLife *4*.

Arquint, C., Gabryjonczyk, A.M., and Nigg, E.A. (2014). Centrosomes as signalling centres. Philosophical Transactions of the Royal Society B Biological Sciences *369*.

Azimzadeh, J., and Marshall, W.F. (2010). Building the centriole. Current Biology *20*, R816-825.

Banani, S.F., Lee, H.O., Hyman, A.A., and Rosen, M.K. (2017). Biomolecular condensates: organizers of cellular biochemistry. Nature Reviews Molecular Cell Biology *18*, 285-298.

Barbelanne, M., and Tsang, W.Y. (2014). Molecular and cellular basis of autosomal recessive primary microcephaly. BioMed Research International, 547986.

Barrera, J.A., Kao, L.R., Hammer, R.E., Seemann, J., Fuchs, J.L., and Megraw, T.L. (2010). CDK5RAP2 regulates centriole engagement and cohesion in mice. Developmental Cell *18*, 913-926.

Basto, R., Brunk, K., Vinadogrova, T., Peel, N., Franz, A., Khodjakov, A., and Raff, J.W. (2008). Centrosome amplification can initiate tumorigenesis in flies. Cell *133*, 1032-1042.

Basto, R., Lau, J., Vinogradova, T., Gardiol, A., Woods, C.G., Khodjakov, A., and Raff, J.W. (2006). Flies without Centrioles. Cell *125*, 1375-1386.

Begasse, M.L., Leaver, M., Vazquez, F., Grill, S.W., and Hyman, A.A. (2015). Temperature Dependence of Cell Division Timing Accounts for a Shift in the Thermal Limits of *C. elegans* and *C. briggsae*. Cell Reports *10*, 647-653.

Bellanger, J.M., and Gönczy, P. (2003). TAC-1 and ZYG-9 form a complex that promotes microtubule assembly in *C. elegans* embryos. Current Biology *13*, 1488-1498.

Berdnik, D., and Knoblich, J.A. (2002). *Drosophila* Aurora-A Is Required for Centrosome Maturation and Actin-Dependent Asymmetric Protein Localization during Mitosis. Current Biology *12*, 640-647.

Bettencourt-Dias, M., Hildebrandt, F., Pellman, D., Woods, G., and Godinho, S.A. (2011). Centrosomes and cilia in human disease. Trends in Genetics *27*, 307-315.

Bettencourt-Dias, M., Rodrigues-Martins, A., Carpenter, L., Riparbelli, M., Lehmann, L., Gatt, M.K., Carmo, N., Balloux, F., Callaini, G., and Glover, D.M. (2005). SAK/PLK4 is required for centriole duplication and flagella development. Current Biology *15*, 2199-2207.

Bober, M.B., and Jackson, A.P. (2017). Microcephalic Osteodysplastic Primordial Dwarfism, Type II: a Clinical Review. Curr Osteoporos Rep *15*, 61-69.

Bornens, M., and Gönczy, P. (2014). Centrosomes back in the limelight. Philosophical Transactions of the Royal Society London B Biological Sciences *369*.

Boudreau, V., Chen, R., Edwards, A., Sulaimain, M., and Maddox, P.S. (2019). PP2A-B55/SUR-6 collaborates with the nuclear lamina for centrosome separation during mitotic entry. Molecular Biology of the Cell *30*, 876-886.

Boveri, T. (1887). Über den Antheil des Spermatozoon an der Theilung des Eies. Sitzungsbericht der Gesellschaft für Morphologie und Physiologie in München *3*.

Boveri, T. (1888). Zellen-Studien 2: Die Befruchtung und Teilung des Eies von *Ascaris megalocephala* (Jena: G. Fischer).

Boveri, T. (1900). Zellen-Studien 4: Über die Natur der Centrosomen (Jena: G. Fischer).

Boveri, T. (1902). Über mehrpolige Mitosen als Mittel zur Analyse des Zelkerns. Verhandlungen der Physikalisch-Medizinischen Gesellschaft zu Würzburg, *35*, 67-90.

Boveri, T. (1914). Zur Frage der Entstehung maligner Tumoren (Jena: G. Fischer).

Boxem, M., Maliga, Z., Klitgord, N., Li, N., Lemmens, I., Mana, M., de Lichtervelde, L., Mul, J.D., van de Peut, D., Devos, M.*, et al.* (2008). A protein domain-based interactome network for *C. elegans* early embryogenesis. Cell *134*, 534-545.

Bradford, M.M. (1976). A rapid and sensitive method for the quantitation of microgram quantities of protein utilizing the principle of protein-dye binding. Analytical Biochemistry *72*, 248-254.

Braun, P., Tasan, M., Dreze, M., Barrios-Rodiles, M., Lemmens, I., Yu, H., Sahalie, J.M., Murray, R.R., Roncari, L., de Smet, A.S.*, et al.* (2009). An experimentally derived confidence score for binary protein-protein interactions. Nature Methods *6*, 91-97.

Brenner, S. (1974). The genetics of *Caenorhabditis elegans*. Genetics *77*, 71-94.

Brückner, A., Polge, C., Lentze, N., Auerbach, D., and Schlattner, U. (2009). Yeast two-hybrid, a powerful tool for systems biology. International Journal of Molecular Sciences *10*, 2763-2788.

Byerly, L., Cassada, R.C., and Russell, R.L. (1976). The life cycle of the nematode *Caenorhabditis elegans*: I. Wild-type growth and reproduction. Developmental Biology *51*, 23-33.

C. elegans Sequencing Consortium (1998). Genome sequence of the nematode *C. elegans*: a platform for investigating biology. Science *282*, 2012-2018.

Cabral, G., Laos, T., Dumont, J., and Dammermann, A. (2019). Differential Requirements for Centrioles in Mitotic Centrosome Growth and Maintenance. Developmental Cell *50*, 355-366.e356.

Cabral, G., Sans, S.S., Cowan, C.R., and Dammermann, A. (2013). Multiple mechanisms contribute to centriole separation in *C. elegans*. Current Biology *23*, 1380-1387.

Carvalho-Santos, Z., Azimzadeh, J., Pereira-Leal, J.B., and Bettencourt-Dias, M. (2011). Evolution: Tracing the origins of centrioles, cilia, and flagella. Journal of Cell Biology *194*, 165-175.

Castellanos, E., Dominguez, P., and Gonzalez, C. (2008). Centrosome dysfunction in *Drosophila* neural stem cells causes tumors that are not due to genome instability. Current Biology *18*, 1209-1214.

Cavanaugh, A.M., and Jaspersen, S.L. (2017). Big Lessons from Little Yeast: Budding and Fission Yeast Centrosome Structure, Duplication, and Function. Annual Review of Genetics *51*, 361-383.

Chang, C.W., Hsu, W.B., Tsai, J.J., Tang, C.J., and Tang, T.K. (2016). CEP295 interacts with microtubules and is required for centriole elongation. Journal of Cell Science *129*, 2501-2513.

Chavali, P.L., Pütz, M., and Gergely, F. (2014). Small organelle, big responsibility: the role of centrosomes in development and disease. Philosophical transactions of the Royal Society of London B Biological Sciences *369*.

Chitwood, B.G., and Chitwood, M.B. (1974). Introduction to nematology.

Citron, Y.R., Fagerstrom, C.J., Keszthelyi, B., Huang, B., Rusan, N.M., Kelly, M.J.S., and Agard, D.A. (2018). The centrosomin CM2 domain is a multi-functional binding domain with distinct cell cycle roles. PLoS ONE *13*, e0190530.

Cizmecioglu, O., Arnold, M., Bahtz, R., Settele, F., Ehret, L., Haselmann-Weiss, U., Antony, C., and Hoffmann, I. (2010). Cep152 acts as a scaffold for recruitment of Plk4 and CPAP to the centrosome. Journal of Cell Biology *191*, 731-739.

Clark-Maguire, S., and Mains, P.E. (1994). Localization of the *mei-1* gene product of *Caenorhabditis elegans*, a meiotic-specific spindle component. Journal of Cell Biology *126*, 199-209.

Conduit, P.T., Feng, Z., Richens, J.H., Baumbach, J., Wainman, A., Bakshi, S.D., Dobbelaere, J., Johnson, S., Lea, S.M., and Raff, J.W. (2014). The centrosome-specific phosphorylation of Cnn by Polo/Plk1 drives Cnn scaffold assembly and centrosome maturation. Developmental Cell *28*, 659-669.

Conduit, P.T., Wainman, A., and Raff, J.W. (2015). Centrosome function and assembly in animal cells. Nature Reviews Molecular Cell Biology *16*, 611-624.

Corsi, A.K., Wightman, B., and Chalfie, M. (2015). A Transparent Window into Biology: A Primer on *Caenorhabditis elegans*. Genetics *200*, 387-407.

Cottee, M.A., Muschalik, N., Wong, Y.L., Johnson, C.M., Johnson, S., Andreeva, A., Oegema, K., Lea, S.M., Raff, J.W., and van Breugel, M. (2013). Crystal structures of the CPAP/STIL complex reveal its role in centriole assembly and human microcephaly. eLife *2*, e01071.

Crick, F.H. (1952). Is α-keratin a coiled coil? Nature *170*, 882-883.

Crick, F.H. (1953). The Fourier transform of a coiled-coil. Acta Crystallographica *6*, 685-689.

Dammermann, A., Maddox, P.S., Desai, A., and Oegema, K. (2008). SAS-4 is recruited to a dynamic structure in newly forming centrioles that is stabilized by the gamma-tubulin-mediated addition of centriolar microtubules. Journal of Cell Biology *180*, 771-785.

Dammermann, A., Müller-Reichert, T., Pelletier, L., Habermann, B., Desai, A., and Oegema, K. (2004). Centriole assembly requires both centriolar and pericentriolar material proteins. Developmental Cell *7*, 815-829.

de Almeida, B.P., Vieira, A.F., Paredes, J., Bettencourt-Dias, M., and Barbosa-Morais, N.L. (2019). Pan-cancer association of a centrosome amplification gene expression signature with genomic alterations and clinical outcome. PLoS Computational Biology *15*, e1006832.

Decker, M., Jaensch, S., Pozniakovsky, A., Zinke, A., O'Connell, K.F., Zachariae, W., Myers, E., and Hyman, A.A. (2011). Limiting amounts of centrosome material set centrosome size in *C. elegans* embryos. Current Biology *21*, 1259-1267.

Delattre, M., Leidel, S., Wani, K. et al. (2004). Centriolar SAS-5 is required for centrosome duplication in *C. elegans*. Nature Cell Biology *6*, 656-664.

Delattre, M., Canard, C., and Gönczy, P. (2006). Sequential Protein Recruitment in *C. elegans* Centriole Formation. Current Biology *16*, 1844-1849.

Delaval, B., and Doxsey, S.J. (2010). Pericentrin in cellular function and disease. The Journal of Cell Biology *188*, 181-190.

Dickinson, D.J., and Goldstein, B. (2016). CRISPR-Based Methods for *Caenorhabditis elegans* Genome Engineering. Genetics *202*, 885-901.

Dix, C.I., and Raff, J.W. (2007). *Drosophila* Spd-2 recruits PCM to the sperm centriole, but is dispensable for centriole duplication. Current Biology *17*, 1759-1764.

Doxsey, S. (2001). Re-evaluating centrosome function. Nature Reviews Molecular Cell Biology *2*, 688-698.

Dumont, J., and Desai, A. (2012). Acentrosomal spindle assembly and chromosome segregation during oocyte meiosis. Trends in Cell Biology *22*, 241-249.

Dzhindzhev, N.S., Tzolovsky, G., Lipinszki, Z., Schneider, S., Lattao, R., Fu, J., Debski, J., Dadlez, M., and Glover, D.M. (2014). Plk4 phosphorylates Ana2 to trigger Sas6 recruitment and procentriole formation. Current Biology *24*, 2526-2532.

Dzhindzhev, N.S., Yu, Q.D., Weiskopf, K., Tzolovsky, G., Cunha-Ferreira, I., Riparbelli, M., Rodrigues-Martins, A., Bettencourt-Dias, M., Callaini, G., and Glover, D.M. (2010). Asterless is a scaffold for the onset of centriole assembly. Nature *467*, 714-718.

Edgar, L.G., and McGhee, J.D. (1988). DNA synthesis and the control of embryonic gene expression in *C. elegans*. Cell *53*, 589-599.

Edgar, R.C. (2004). MUSCLE: multiple sequence alignment with high accuracy and high throughput. Nucleic Acids Research *32*, 1792-1797.

Elia, A.E., Cantley, L.C., and Yaffe, M.B. (2003a). Proteomic screen finds pSer/pThr-binding domain localizing Plk1 to mitotic substrates. Science *299*, 1228-1231.

Elia, A.E., Rellos, P., Haire, L.F., Chao, J.W., Ivins, F.J., Hoepker, K., Mohammad, D., Cantley, L.C., Smerdon, S.J., and Yaffe, M.B. (2003b). The molecular basis for phosphodependent substrate targeting and regulation of Plks by the Polo-box domain. Cell *115*, 83-95.

Encalada, S.E., Willis, J., Lyczak, R., and Bowerman, B. (2005). A spindle checkpoint functions during mitosis in the early *Caenorhabditis elegans* embryo. Molecular Biology of the Cell *16*, 1056-1070.

Enos, S.J., Dressler, M., Gomes, B.F., Hyman, A.A., and Woodruff, J.B. (2018). Phosphatase PP2A and microtubule-mediated pulling forces disassemble centrosomes during mitotic exit. Biology Open *7*, bio029777.

Erpf, A.C. (2020). Functional Analysis of the centrosomal protein PCMD-1 and the establishment of a system for testing centrosome inheritance in *C. elegans* (Dissertation, Munich: Ludwig-Maximilians-Universität).

Erpf, A.C., Stenzel, L., Memar, N., Antoniolli, M., Osepashvili, M., Schnabel, R., Conradt, B., and Mikeladze-Dvali, T. (2019). PCMD-1 Organizes Centrosome Matrix Assembly in *C. elegans*. Current Biology *29*, 1324-1336.

Faheem, M., Naseer, M.I., Rasool, M., Chaudhary, A.G., Kumosani, T.A., Ilyas, A.M., Pushparaj, P., Ahmed, F., Algahtani, H.A., Al-Qahtani, M.H.*, et al.* (2015). Molecular genetics of human primary microcephaly: an overview. BMC Medical Genomics *8 Suppl 1*, S4.

Farina, F., Gaillard, J., Guérin, C., Couté, Y., Sillibourne, J., Blanchoin, L., and Théry, M. (2016). The centrosome is an actin-organizing centre. Nature Cell Biology *18*, 65-75.

Feng, Z., Caballe, A., Wainman, A., Johnson, S., Haensele, A.F.M., Cottee, M.A., Conduit, P.T., Lea, S.M., and Raff, J.W. (2017). Structural Basis for Mitotic Centrosome Assembly in Flies. Cell *169*, 1078-1089.e1013.

Fields, S., and Song, O. (1989). A novel genetic system to detect protein-protein interactions. Nature *340*, 245-246.

Fırat-Karalar, E.N., and Stearns, T. (2014). The centriole duplication cycle. Philos Trans R Soc Lond B Biol Sci *369*.

Fire, A., Xu, S., Montgomery, M.K., Kostas, S.A., Driver, S.E., and Mello, C.C. (1998). Potent and specific genetic interference by double-stranded RNA in *Caenorhabditis elegans*. Nature *391*, 806-811.

Flemming, W. (1875). Studien in der Entwicklungsgeschichte der Najaden. Sitzungsber. Math.-Naturwiss. Classe Kaiserl. Akad. Wiss. Wien *71*, 81-212.

Flibotte, S., Edgley, M.L., Chaudhry, I., Taylor, J., Neil, S.E., Rogula, A., Zapf, R., Hirst, M., Butterfield, Y., Jones, S.J.*, et al.* (2010). Whole-Genome Profiling of Mutagenesis in *Caenorhabditis elegans*. Genetics *185*, 431-441.

Fong, K.W., Choi, Y.K., Rattner, J.B., and Qi, R.Z. (2008). CDK5RAP2 is a pericentriolar protein that functions in centrosomal attachment of the gamma-tubulin ring complex. Molecular Biology of the Cell *19*, 115-125.

Fox, J., and Weisberg, S. (2019). An R companion to applied regression, Sage, Thousand Oaks CA, third edition.

Frøkjaer-Jensen, C., Davis, M.W., Hollopeter, G., Taylor, J., Harris, T.W., Nix, P., Lofgren, R., Prestgard-Duke, M., Bastiani, M., Moerman, D.G.*, et al.* (2010). Targeted gene deletions in *C. elegans* using transposon excision. Nature Methods *7*, 451-453.

Frøkjaer-Jensen, C., Davis, M.W., Hopkins, C.E., Newman, B.J., Thummel, J.M., Olesen, S.P., Grunnet, M., and Jorgensen, E.M. (2008). Single-copy insertion of transgenes in *Caenorhabditis elegans*. Nature Genetics *40*, 1375-1383.

Frøkjær-Jensen, C., Davis, M.W., Sarov, M., Taylor, J., Flibotte, S., LaBella, M., Pozniakovsky, A., Moerman, D.G., and Jorgensen, E.M. (2014). Random and targeted transgene insertion in *Caenorhabditis elegans* using a modified Mos1 transposon. Nature Methods *11*, 529-534.

Fry, A.M., Sampson, J., Shak, C., and Shackleton, S. (2017). Recent advances in pericentriolar material organization: ordered layers and scaffolding gels. F1000Research *6*, 1622.

Fu, J., and Glover, D.M. (2012). Structured illumination of the interface between centriole and peri-centriolar material. Open Biology *2*, 120104.

Fu, J., Lipinszki, Z., Rangone, H., Min, M., Mykura, C., Chao-Chu, J., Schneider, S., Dzhindzhev, N.S., Gottardo, M., Riparbelli, M.G.*, et al.* (2016). Conserved molecular interactions in centriole-to-centrosome conversion. Nature Cell Biology *18*, 87-99.

Gall, J. (1996). A pictorial history: Views of the Cell. (Bethesda).

Gall, J.G. (2004). Early studies on centrioles and centrosomes (Weinheim: Wiley-VCH Verlag).

Garbrecht, J., Laos, T., Holzer, E., Dillinger, M., and Dammermann, A. (2021). An Acentriolar Centrosome At The *C. elegans* Ciliary Base. Current Biology, S0960-9822(0921)00362-00366.

Garcia, P., Gupta, R., Shah, S., Morris, A.J., Rudge, S.A., Scarlata, S., Petrova, V., McLaughlin, S., and Rebecchi, M.J. (1995). The pleckstrin homology domain of phospholipase C-delta 1 binds with high affinity to phosphatidylinositol 4,5-bisphosphate in bilayer membranes. Biochemistry *34*, 16228-16234.

Giansanti, M.G., Bucciarelli, E., Bonaccorsi, S., and Gatti, M. (2008). *Drosophila* SPD-2 is an essential centriole component required for PCM recruitment and astral-microtubule nucleation. Current Biology *18*, 303-309.

Gillingham, A.K., and Munro, S. (2000). The PACT domain, a conserved centrosomal targeting motif in the coiled-coil proteins AKAP450 and pericentrin. EMBO Reports *1*, 524-529.

Godinho, S.A., Picone, R., Burute, M., Dagher, R., Su, Y., Leung, C.T., Polyak, K., Brugge, J.S., Théry, M., and Pellman, D. (2014). Oncogene-like induction of cellular invasion from centrosome amplification. Nature *510*, 167-171.

Goldstein, B., and Hird, S.N. (1996). Specification of the anteroposterior axis in *Caenorhabditis elegans*. Development *122*, 1467-1474.

Goldstein, B., Hird, S.N., and White, J.G. (1993). Cell polarity in early *C. elegans* development. Development *119*, 279-287.

Gomez-Ferreria, M.A., Rath, U., Buster, D.W., Chanda, S.K., Caldwell, J.S., Rines, D.R., and Sharp, D.J. (2007). Human Cep192 is required for mitotic centrosome and spindle assembly. Current Biology *17*, 1960-1966.

Gönczy, P. (2012). Towards a molecular architecture of centriole assembly. Nature Reviews Molecular Cell Biology *13*, 425-435.

Gopalakrishnan, J., Mennella, V., Blachon, S., Zhai, B., Smith, A.H., Megraw, T.L., Nicastro, D., Gygi, S.P., Agard, D.A., and Avidor-Reiss, T. (2011). Sas-4 provides a scaffold for cytoplasmic complexes and tethers them in a centrosome. Nature Communications *2*, 359.

Grill, S.W., Gönczy, P., Stelzer, E.H.K., and Hyman, A.A. (2001). Polarity controls forces governing asymmetric spindle positioning in the *Caenorhabditis elegans* embryo. Nature *409*, 630-633.

Habedanck, R., Stierhof, Y.D., Wilkinson, C.J., and Nigg, E.A. (2005). The Polo kinase Plk4 functions in centriole duplication. Nature Cell Biology *7*, 1140-1146.

Hamill, D.R., Severson, A.F., Carter, J.C., and Bowerman, B. (2002). Centrosome maturation and mitotic spindle assembly in *C. elegans* require SPD-5, a protein with multiple coiled-coil domains. Developmental Cell *3*, 673-684.

Hannak, E., Kirkham, M., Hyman, A.A., and Oegema, K. (2001). Aurora-A kinase is required for centrosome maturation in *Caenorhabditis elegans*. Journal of Cell Biology *155*, 1109-1116.

Haslam, R.J., Koide, H.B., and Hemmings, B.A. (1993). Pleckstrin domain homology. Nature *363*, 309-310.

Hatch, E.M., Kulukian, A., Holland, A.J., Cleveland, D.W., and Stearns, T. (2010). Cep152 interacts with Plk4 and is required for centriole duplication. Journal of Cell Biology *191*, 721-729.

Hernandez Alvarez, B., Bassler, J., and Lupas, A.N. (2019). Structural diversity of coiled coils in protein fibers of the bacterial cell envelope. International Journal of Medical Microbiology *309*, 351-358.

Hilbert, M., Erat, M.C., Hachet, V., Guichard, P., Blank, I.D., Flückiger, I., Slater, L., Lowe, E.D., Hatzopoulos, G.N., Steinmetz, M.O.*, et al.* (2013). *Caenorhabditis elegans* centriolar protein SAS-6 forms a spiral that is consistent with imparting a ninefold symmetry. PNAS *110*, 11373-11378.

Hill, D.P., Shakes, D.C., Ward, S., and Strome, S. (1989). A sperm-supplied product essential for initiation of normal embryogenesis in *Caenorhabditis elegans* is encoded by the paternal-effect embryonic-lethal gene, *spe-11*. Developmental Biology *136*, 154-166.

Hiraki, M., Nakazawa, Y., Kamiya, R., and Hirono, M. (2007). Bld10p constitutes the cartwheel-spoke tip and stabilizes the 9-fold symmetry of the centriole. Current Biology *17*, 1778-1783.

Hodgkin, J., and Doniach, T. (1997). Natural variation and copulatory plug formation in *Caenorhabditis elegans*. Genetics *146*, 149-164.

Hodgkin, J., Horvitz, H.R., and Brenner, S. (1979). Nondisjunction Mutants of the Nematode *Caenorhabditis Elegans*. Genetics *91*, 67-94.

Holway, A.H., Kim, S.H., La Volpe, A., and Michael, W.M. (2006). Checkpoint silencing during the DNA damage response in *Caenorhabditis elegans* embryos. Journal of Cell Biology *172*, 999-1008.

Hyman, A.A., Weber, C.A., and Jülicher, F. (2014). Liquid-Liquid Phase Separation in Biology. Annual Review of Cell and Developmental Biology *30*, 39-58.

Hyman, A.A., and White, J.G. (1987). Determination of cell division axes in the early embryogenesis of *Caenorhabditis elegans*. Journal of Cell Biology *105*, 2123-2135.

Ishikawa, H., Kubo, A., Tsukita, S., and Tsukita, S. (2005). Odf2-deficient mother centrioles lack distal/subdistal appendages and the ability to generate primary cilia. Nature Cell Biology *7*, 517-524.

Ishikawa, H., and Marshall, W.F. (2011). Ciliogenesis: building the cell's antenna. Nature Reviews Molecular Cell Biology *12*, 222-234.

Ito, D., Zitouni, S., Jana, S.C., Duarte, P., Surkont, J., Carvalho-Santos, Z., Pereira-Leal, J.B., Ferreira, M.G., and Bettencourt-Dias, M. (2019). Pericentrin-mediated SAS-6 recruitment promotes centriole assembly. eLife *8*.

Jaiswal, S., and Singh, P. (2021). Centrosome dysfunction in human diseases. Seminars in Cell & Developmental Biology.

Jiang, X., Tam Ho, D.B., Mahe, K., Mia, J., Sepulveda, G., Antkowiak, M., Yamada, S., and Jao, L.-E. (2020). Condensation of pericentrin proteins in human cells illuminates phase separation in centrosome assembly. bioRxiv, 2020.2005.2008.084749.

Joukov, V., Walter, J.C., and De Nicolo, A. (2014). The Cep192-organized aurora A-Plk1 cascade is essential for centrosome cycle and bipolar spindle assembly. Molecular Cell *55*, 578-591.

Kamath, R.S., and Ahringer, J. (2003). Genome-wide RNAi screening in *Caenorhabditis elegans*. Methods *30*, 313-321.

Kemp, C.A., Kopish, K.R., Zipperlen, P., Ahringer, J., and O'Connell, K.F. (2004). Centrosome maturation and duplication in *C. elegans* require the coiled-coil protein SPD-2. Developmental Cell *6*, 511-523.

Kilmartin, J.V. (2014). Lessons from yeast: the spindle pole body and the centrosome. Philosophical transactions of the Royal Society of London B Biological Sciences *369*.

Kim, A.J., and Griffin, E.E. (2020). PLK-1 Regulation of Asymmetric Cell Division in the Early *C. elegans* Embryo. Front Cell Dev Biol *8*, 632253.

Kim, J., Kim, J., and Rhee, K. (2019). PCNT is critical for the association and conversion of centrioles to centrosomes during mitosis. Journal of Cell Science *132*, jcs225789.

Kim, J., Lee, K., and Rhee, K. (2015). PLK1 regulation of PCNT cleavage ensures fidelity of centriole separation during mitotic exit. Nature Communications *6*, 10076.

Kim, T.S., Park, J.E., Shukla, A., Choi, S., Murugan, R.N., Lee, J.H., Ahn, M., Rhee, K., Bang, J.K., Kim, B.Y.*, et al.* (2013). Hierarchical recruitment of Plk4 and regulation of centriole biogenesis by two centrosomal scaffolds, Cep192 and Cep152. PNAS *110*, E4849-4857.

Kirkham, M., Müller-Reichert, T., Oegema, K., Grill, S., and Hyman, A.A. (2003). SAS-4 is a *C. elegans* centriolar protein that controls centrosome size. Cell *112*, 575-587.

Kitagawa, D., Vakonakis, I., Olieric, N., Hilbert, M., Keller, D., Olieric, V., Bortfeld, M., Erat, M.C., Flückiger, I., Gönczy, P.*, et al.* (2011). Structural basis of the 9-fold symmetry of centrioles. Cell *144*, 364-375.

Klingseisen, A., and Jackson, A.P. (2011). Mechanisms and pathways of growth failure in primordial dwarfism. Genes & Development *25*, 2011-2024.

Klinkert, K., Levernier, N., Gross, P., Gentili, C., von Tobel, L., Pierron, M., Busso, C., Herrman, S., Grill, S.W., Kruse, K.*, et al.* (2019). Aurora A depletion reveals centrosome-independent polarization mechanism in *Caenorhabditis elegans*. eLife *8*.

Kohlmaier, G., Loncarek, J., Meng, X., McEwen, B.F., Mogensen, M.M., Spektor, A., Dynlacht, B.D., Khodjakov, A., and Gönczy, P. (2009). Overly long centrioles and defective cell division upon excess of the SAS-4-related protein CPAP. Current Biology *19*, 1012-1018.

Kratz, A.S., Bärenz, F., Richter, K.T., and Hoffmann, I. (2015). Plk4-dependent phosphorylation of STIL is required for centriole duplication. Biology Open *4*, 370-377.

Kuhn, M., Hyman, A.A., and Beyer, A. (2014). Coiled-coil proteins facilitated the functional expansion of the centrosome. PLoS Computational Biology *10*, e1003657.

Kuijpers, M., and Hoogenraad, C.C. (2011). Centrosomes, microtubules and neuronal development. Molecular and Cellular Neuroscience *48*, 349-358.

Kumar, S., Sharma, G., Chakraborty, C., Sharma, A.R., and Kim, J. (2017). Regulatory functional territory of PLK-1 and their substrates beyond mitosis. Oncotarget *8*, 37942-37962.

Kutscher, L.M., and Shaham, S. (2014). Forward and reverse mutagenesis in *C. elegans*. WormBook, 1-26.

Labbé, J.-C., McCarthy, E.K., and Goldstein, B. (2004). The forces that position a mitotic spindle asymmetrically are tethered until after the time of spindle assembly. Journal of Cell Biology *167*, 245-256.

Landschulz, W.H., Johnson, P.F., and McKnight, S.L. (1988). The leucine zipper: a hypothetical structure common to a new class of DNA binding proteins. Science *240*, 1759-1764.

Lane, H.A., and Nigg, E.A. (1996). Antibody microinjection reveals an essential role for human polo-like kinase 1 (Plk1) in the functional maturation of mitotic centrosomes. Journal of Cell Biology *135*, 1701-1713.

Lawo, S., Hasegan, M., Gupta, G.D., and Pelletier, L. (2012). Subdiffraction imaging of centrosomes reveals higher-order organizational features of pericentriolar material. Nature Cell Biology *14*, 1148-1158.

Le Bot, N., Tsai, M.-C., Andrews, R.K., and Ahringer, J. (2003). TAC-1, a Regulator of Microtubule Length in the *C. elegans* Embryo. Current Biology *13*, 1499-1505.

Lee, K., and Rhee, K. (2011). PLK1 phosphorylation of pericentrin initiates centrosome maturation at the onset of mitosis. Journal of Cell Biology *195*, 1093-1101.

Lee, K., and Rhee, K. (2012). Separase-dependent cleavage of pericentrin B is necessary and sufficient for centriole disengagement during mitosis. Cell Cycle *11*, 2476-2485.

Lee, K.S., Grenfell, T.Z., Yarm, F.R., and Erikson, R.L. (1998). Mutation of the polo-box disrupts localization and mitotic functions of the mammalian polo kinase Plk. PNAS *95*, 9301-9306.

Lee, K.S., Park, J.E., Kang, Y.H., Kim, T.S., and Bang, J.K. (2014). Mechanisms underlying Plk1 polo-box domain-mediated biological processes and their physiological significance. Molecules and Cells *37*, 286-294.

Leidel, S., Delattre, M., Cerutti, L., Baumer, K., and Gönczy, P. (2005). SAS-6 defines a protein family required for centrosome duplication in *C. elegans* and in human cells. Nature Cell Biology *7*, 115-125.

Leidel, S., and Gönczy, P. (2003). SAS-4 is essential for centrosome duplication in C elegans and is recruited to daughter centrioles once per cell cycle. Developmental Cell *4*, 431-439.

Lerit, D.A., Jordan, H.A., Poulton, J.S., Fagerstrom, C.J., Galletta, B.J., Peifer, M., and Rusan, N.M. (2015). Interphase centrosome organization by the PLP-Cnn scaffold is required for centrosome function. Journal of Cell Biology *210*, 79-97.

Lettman, M.M., Wong, Y.L., Viscardi, V., Niessen, S., Chen, S.H., Shiau, A.K., Zhou, H., Desai, A., and Oegema, K. (2013). Direct binding of SAS-6 to ZYG-1 recruits SAS-6 to the mother centriole for cartwheel assembly. Developmental Cell *25*, 284-298.

Leung, B., Hermann, G.J., and Priess, J.R. (1999). Organogenesis of the *Caenorhabditis elegans* intestine. Developmental Biology *216*, 114-134.

Levine, M.S., Bakker, B., Boeckx, B., Moyett, J., Lu, J., Vitre, B., Spierings, D.C., Lansdorp, P.M., Cleveland, D.W., Lambrechts, D.*, et al.* (2017). Centrosome Amplification Is Sufficient to Promote Spontaneous Tumorigenesis in Mammals. Developmental Cell *40*, 313-322.e315.

Li, S., Armstrong, C.M., Bertin, N., Ge, H., Milstein, S., Boxem, M., Vidalain, P.O., Han, J.D., Chesneau, A., Hao, T.*, et al.* (2004). A map of the interactome network of the metazoan *C. elegans*. Science *303*, 540-543.

Li, W., Yi, P., Zhu, Z., Zhang, X., Li, W., and Ou, G. (2017). Centriole translocation and degeneration during ciliogenesis in *Caenorhabditis elegans* neurons. The EMBO Journal *36*, 2553-2566.

Lin, Y.C., Chang, C.W., Hsu, W.B., Tang, C.J., Lin, Y.N., Chou, E.J., Wu, C.T., and Tang, T.K. (2013). Human microcephaly protein CEP135 binds to hSAS-6 and CPAP, and is required for centriole assembly. The EMBO Journal *32*, 1141-1154.

Lingle, W.L., Barrett, S.L., Negron, V.C., D'Assoro, A.B., Boeneman, K., Liu, W., Whitehead, C.M., Reynolds, C., and Salisbury, J.L. (2002). Centrosome amplification drives chromosomal instability in breast tumor development. PNAS *99*, 1978-1983.

Lingle, W.L., Lutz, W.H., Ingle, J.N., Maihle, N.J., and Salisbury, J.L. (1998). Centrosome hypertrophy in human breast tumors: implications for genomic stability and cell polarity. PNAS *95*, 2950-2955.

Liu, Z., Ren, J., Cao, J., He, J., Yao, X., Jin, C., and Xue, Y. (2012). Systematic analysis of the Plk-mediated phosphoregulation in eukaryotes. Briefings in Bioinformatics *14*, 344-360.

Loncarek, J., Hergert, P., Magidson, V., and Khodjakov, A. (2008). Control of daughter centriole formation by the pericentriolar material. Nature Cell Biology *10*, 322-328.

Lowery, D.M., Lim, D., and Yaffe, M.B. (2005). Structure and function of Polo-like kinases. Oncogene *24*, 248-259.

Lucas, E.P., and Raff, J.W. (2007). Maintaining the proper connection between the centrioles and the pericentriolar matrix requires *Drosophila* centrosomin. Journal of Cell Biology *178*, 725-732.

Lüders, J., and Stearns, T. (2007). Microtubule-organizing centres: a re-evaluation. Nature Reviews Molecular Cell Biology *8*, 161-167.

Lupas, A. (1996a). Coiled coils: new structures and new functions. Trends in Biochemical Sciences *21*, 375-382.

Lupas, A. (1996b). Prediction and analysis of coiled-coil structures. Methods in Enzymology *266*, 513-525.

Lupas, A., Van Dyke, M., and Stock, J. (1991). Predicting coiled coils from protein sequences. Science *252*, 1162-1164.

Lupas, A.N., and Bassler, J. (2017). Coiled Coils - A Model System for the 21st Century. Trends in Biochemical Sciences *42*, 130-140.

Macůrek, L., Lindqvist, A., Lim, D., Lampson, M.A., Klompmaker, R., Freire, R., Clouin, C., Taylor, S.S., Yaffe, M.B., and Medema, R.H. (2008). Polo-like kinase-1 is activated by aurora A to promote checkpoint recovery. Nature *455*, 119-123.

Maeda, I., Kohara, Y., Yamamoto, M., and Sugimoto, A. (2001). Large-scale analysis of gene function in *Caenorhabditis elegans* by high-throughput RNAi. Current Biology *11*, 171-176.

Magescas, J., Eskinazi, S., Tran, M.V., and Feldman, J.L. (2021). Centriole-less pericentriolar material serves as a microtubule organizing center at the base of *C. elegans* sensory cilia. Current Biology.

Magescas, J., Zonka, J.C., and Feldman, J.L. (2019). A two-step mechanism for the inactivation of microtubule organizing center function at the centrosome. eLife *8*.

Martinez-Campos, M., Basto, R., Baker, J., Kernan, M., and Raff, J.W. (2004). The *Drosophila* pericentrin-like protein is essential for cilia/flagella function, but appears to be dispensable for mitosis. Journal of Cell Biology *165*, 673-683.

Martino, L., Morchoisne-Bolhy, S., Cheerambathur, D.K., Van Hove, L., Dumont, J., Joly, N., Desai, A., Doye, V., and Pintard, L. (2017). Channel Nucleoporins Recruit PLK-1 to Nuclear Pore Complexes to Direct Nuclear Envelope Breakdown in *C. elegans*. Developmental Cell *43*, 157-171.e157.

Masoud, K., Herzog, E., Chabouté, M.E., and Schmit, A.C. (2013). Microtubule nucleation and establishment of the mitotic spindle in vascular plant cells. The Plant Journal *75*, 245-257.

Matsuo, K., Ohsumi, K., Iwabuchi, M., Kawamata, T., Ono, Y., and Takahashi, M. (2012). Kendrin Is a Novel Substrate for Separase Involved in the Licensing of Centriole Duplication. Current Biology *22*, 915-921.

McCarthy Campbell, E.K., Werts, A.D., and Goldstein, B. (2009). A Cell Cycle Timer for Asymmetric Spindle Positioning. PLoS Biology *7*, e1000088.

McLamarrah, T.A., Buster, D.W., Galletta, B.J., Boese, C.J., Ryniawec, J.M., Hollingsworth, N.A., Byrnes, A.E., Brownlee, C.W., Slep, K.C., Rusan, N.M*., et al.* (2018). An ordered pattern of Ana2 phosphorylation by Plk4 is required for centriole assembly. Journal of Cell Biology *217*, 1217-1231.

Megraw, T.L., Li, K., Kao, L.R., and Kaufman, T.C. (1999). The centrosomin protein is required for centrosome assembly and function during cleavage in *Drosophila*. Development *126*, 2829-2839.

Mennella, V., Keszthelyi, B., McDonald, K.L., Chhun, B., Kan, F., Rogers, G.C., Huang, B., and Agard, D.A. (2012). Subdiffraction-resolution fluorescence microscopy reveals a domain of the centrosome critical for pericentriolar material organization. Nature Cell Biology *14*, 1159-1168.

Meraldi, P. (2016). Centrosomes in spindle organization and chromosome segregation: a mechanistic view. Chromosome Research *24*, 19-34.

Meunier, S., and Vernos, I. (2012). Microtubule assembly during mitosis – from distinct origins to distinct functions? Journal of Cell Science *125*, 2805-2814.

Meunier, S., and Vernos, I. (2016). Acentrosomal Microtubule Assembly in Mitosis: The Where, When, and How. Trends in Cell Biology *26*, 80-87.

Mikeladze-Dvali, T., von Tobel, L., Strnad, P., Knott, G., Leonhardt, H., Schermelleh, L., and Gönczy, P. (2012). Analysis of centriole elimination during *C. elegans* oogenesis. Development *139*, 1670-1679.

Mittasch, M., Tran, V.M., Rios, M.U., Fritsch, A.W., Enos, S.J., Ferreira Gomes, B., Bond, A., Kreysing, M., and Woodruff, J.B. (2020). Regulated changes in material properties underlie centrosome disassembly during mitotic exit. Journal of Cell Biology *219*.

Monen, J., Hattersley, N., Muroyama, A., Stevens, D., Oegema, K., and Desai, A. (2015). Separase Cleaves the N-Tail of the CENP-A Related Protein CPAR-1 at the Meiosis I Metaphase-Anaphase Transition in *C. elegans*. PLoS ONE *10*, e0125382.

Moritz, M., Braunfeld, M.B., Sedat, J.W., Alberts, B., and Agard, D.A. (1995). Microtubule nucleation by gamma-tubulin-containing rings in the centrosome. Nature *378*, 638-640.

Moritz, M., Zheng, Y., Alberts, B.M., and Oegema, K. (1998). Recruitment of the γ-Tubulin Ring Complex to *Drosophila* Salt-stripped Centrosome Scaffolds. Journal of Cell Biology *142*, 775-786.

Moyer, T.C., Clutario, K.M., Lambrus, B.G., Daggubati, V., and Holland, A.J. (2015). Binding of STIL to Plk4 activates kinase activity to promote centriole assembly. Journal of Cell Biology *209*, 863-878.

Moyer, T.C., and Holland, A.J. (2019). PLK4 promotes centriole duplication by phosphorylating STIL to link the procentriole cartwheel to the microtubule wall. eLife *8*.

Mullee, L.I., and Morrison, C.G. (2016). Centrosomes in the DNA damage response - the hub outside the centre. Chromosome Research *24*, 35-51.

Murphy, S.M., Preble, A.M., Patel, U.K., O'Connell, K.L., Dias, D.P., Moritz, M., Agard, D., Stults, J.T., and Stearns, T. (2001). GCP5 and GCP6: Two New Members of the Human γ-Tubulin Complex. Molecular Biology of the Cell *12*, 3340-3352.

Nakajo, M., Kano, H., Tsuyama, K., Haruta, N., and Sugimoto, A. (2021). Centrosome maturation requires phosphorylation-mediated sequential domain interactions of SPD-5. bioRxiv, 2021.2005.2020.444955.

Nechipurenko, I.V., Berciu, C., Sengupta, P., and Nicastro, D. (2017). Centriolar remodeling underlies basal body maturation during ciliogenesis in *Caenorhabditis elegans*. eLife *6*.

Nido, G.S., Mendez, R., Pascual-Garcia, A., Abia, D., and Bastolla, U. (2012). Protein disorder in the centrosome correlates with complexity in cell types number. Molecular BioSystems *8*, 353-367.

Nigg, E.A., and Holland, A.J. (2018). Once and only once: mechanisms of centriole duplication and their deregulation in disease. Nature Reviews Molecular Cell Biology *19*, 297-312.

Nigg, E.A., and Raff, J.W. (2009). Centrioles, Centrosomes, and Cilia in Health and Disease. Cell *139*, 663-678.

Nigon, V. (1949). Les modalites de la reproduction et le determinisme du sexe chez quelques nematodes libres. Annales de Sciences Naturelles *2*, 1-132.

Nishi, Y., Rogers, E., Robertson, S.M., and Lin, R. (2008). Polo kinases regulate *C. elegans* embryonic polarity via binding to DYRK2-primed MEX-5 and MEX-6. Development *135*, 687-697.

O'Connell, K.F., Caron, C., Kopish, K.R., Hurd, D.D., Kemphues, K.J., Li, Y., and White, J.G. (2001). The *C. elegans zyg-1* gene encodes a regulator of centrosome duplication with distinct maternal and paternal roles in the embryo. Cell *105*, 547-558.

O'Connell, K.F., Leys, C.M., and White, J.G. (1998). A genetic screen for temperature-sensitive cell-division mutants of *Caenorhabditis elegans*. Genetics *149*, 1303-1321.

O'Rourke, S.M., Carter, C., Carter, L., Christensen, S.N., Jones, M.P., Nash, B., Price, M.H., Turnbull, D.W., Garner, A.R., Hamill, D.R*., et al.* (2011). A survey of new temperature-sensitive, embryonic-lethal mutations in *C. elegans*: 24 alleles of thirteen genes. PLoS ONE *6*, e16644.

Oegema, K., Desai, A., Rybina, S., Kirkham, M., and Hyman, A.A. (2001). Functional analysis of kinetochore assembly in *Caenorhabditis elegans*. Journal of Cell Biology *153*, 1209-1226.

Oegema, K., and Hyman, A.A. (2006). Cell division. WormBook, 1-40.

Oegema, K., Wiese, C., Martin, O.C., Milligan, R.A., Iwamatsu, A., Mitchison, T.J., and Zheng, Y. (1999). Characterization of two related *Drosophila* gamma-tubulin complexes that differ in their ability to nucleate microtubules. Journal of Cell Biology *144*, 721-733.

Ogden, A., Rida, P.C., and Aneja, R. (2017). Prognostic value of CA20, a score based on centrosome amplification-associated genes, in breast tumors. Scientific Reports *7*, 262.

Ogle, D., Wheeler, P., and Dinno, A. (2019). FSA: Fisheries Stock Analysis.

Ohta, M., Ashikawa, T., Nozaki, Y., Kozuka-Hata, H., Goto, H., Inagaki, M., Oyama, M., and Kitagawa, D. (2014). Direct interaction of Plk4 with STIL ensures formation of a single procentriole per parental centriole. Nature Communications *5*, 5267.

Ohta, M., Desai, A., and Oegema, K. (2017). How centrioles acquire the ability to reproduce. eLife *6*.

Ohta, M., Zhao, Z., Wu, D., Wang, S., Harrison, J.L., Gómez-Cavazos, J.S., Desai, A., and Oegema, K.F. (2021). Polo-like kinase 1 independently controls microtubule-nucleating capacity and size of the centrosome. Journal of Cell Biology *220*.

Pagan, J.K., Marzio, A., Jones, M.J., Saraf, A., Jallepalli, P.V., Florens, L., Washburn, M.P., and Pagano, M. (2015). Degradation of Cep68 and PCNT cleavage mediate Cep215 removal from the PCM to allow centriole separation, disengagement and licensing. Nature Cell Biology *17*, 31-43.

Park, J.E., Soung, N.K., Johmura, Y., Kang, Y.H., Liao, C., Lee, K.H., Park, C.H., Nicklaus, M.C., and Lee, K.S. (2010). Polo-box domain: a versatile mediator of polo-like kinase function. Cellular and Molecular Life Sciences *67*, 1957-1970.

Paterson, H.F., Savopoulos, J.W., Perisic, O., Cheung, R., Ellis, M.V., Williams, R.L., and Katan, M. (1995). Phospholipase C delta 1 requires a pleckstrin homology domain for interaction with the plasma membrane. Biochemical Journal *312 (Pt 3)*, 661-666.

Pauling, L., and Corey, R.B. (1953). Compound helical configurations of polypeptide chains: structure of proteins of the α-keratin type. Nature *171*, 59-61.

Pelletier, L., O'Toole, E., Schwager, A., Hyman, A.A., and Müller-Reichert, T. (2006). Centriole assembly in *Caenorhabditis elegans*. Nature *444*, 619-623.

Pelletier, L., Ozlu, N., Hannak, E., Cowan, C., Habermann, B., Ruer, M., Müller-Reichert, T., and Hyman, A.A. (2004). The *Caenorhabditis elegans* centrosomal protein SPD-2 is required for both pericentriolar material recruitment and centriole duplication. Current Biology *14*, 863-873.

Petronczki, M., Lénárt, P., and Peters, J.-M. (2008). Polo on the Rise–from Mitotic Entry to Cytokinesis with Plk1. Developmental Cell *14*, 646-659.

Piano, F., Schetter†, A.J., Mangone, M., Stein, L., and Kemphues, K.J. (2000). RNAi analysis of genes expressed in the ovary of *Caenorhabditis elegans*. Current Biology *10*, 1619-1622.

Pihan, G.A., Purohit, A., Wallace, J., Knecht, H., Woda, B., Quesenberry, P., and Doxsey, S.J. (1998). Centrosome defects and genetic instability in malignant tumors. Cancer Research *58*, 3974-3985.

Pintard, L., and Archambault, V. (2018). A unified view of spatio-temporal control of mitotic entry: Polo kinase as the key. Open Biology *8*.

Pintard, L., and Bowerman, B. (2019). Mitotic Cell Division in *Caenorhabditis elegans*. Genetics *211*, 35-73.

Prosser, S.L., and Pelletier, L. (2017). Mitotic spindle assembly in animal cells: a fine balancing act. Nature Reviews Molecular Cell Biology *18*, 187-201.

Pruss, R.M., Mirsky, R., Raff, M.C., Thorpe, R., Dowding, A.J., and Anderton, B.H. (1981). All classes of intermediate filaments share a common antigenic determinant defined by a monoclonal antibody. Cell *27*, 419-428.

Qiao, R., Cabral, G., Lettman, M.M., Dammermann, A., and Dong, G. (2012). SAS-6 coiled-coil structure and interaction with SAS-5 suggest a regulatory mechanism in *C. elegans* centriole assembly. The EMBO Journal *31*, 4334-4347.

R Core Team (2019). R: A language and environment for statistical computing. R Foundation for Statistical Computing, Vienna, Austria.

Raff, J.W. (2019). Phase Separation and the Centrosome: A Fait Accompli? Trends in Cell Biology *29*, 612-622.

Remmelzwaal, S., and Boxem, M. (2019). Protein interactome mapping in *Caenorhabditis elegans*. Current Opinion in Systems Biology *13*, 1-9.

Ren, J., Wen, L., Gao, X., Jin, C., Xue, Y., and Yao, X. (2009). DOG 1.0: illustrator of protein domain structures. Cell Res *19*, 271-273.

Rieder, C.L., Faruki, S., and Khodjakov, A. (2001). The centrosome in vertebrates: more than a microtubule-organizing center. Trends in Cell Biology *11*, 413-419.

Robert, V., and Bessereau, J.-L. (2007). Targeted engineering of the *Caenorhabditis elegans* genome following Mos1-triggered chromosomal breaks. The EMBO Journal *26*, 170-183.

Rogala, K.B., Dynes, N.J., Hatzopoulos, G.N., Yan, J., Pong, S.K., Robinson, C.V., Deane, C.M., Gönczy, P., and Vakonakis, I. (2015). The *Caenorhabditis elegans* protein SAS-5 forms large oligomeric assemblies critical for centriole formation. eLife *4*, e07410.

Sabat-Pośpiech, D., Fabian-Kolpanowicz, K., Prior, I.A., Coulson, J.M., and Fielding, A.B. (2019). Targeting centrosome amplification, an Achilles' heel of cancer. Biochemical Society Transactions *47*, 1209-1222.

Sahabandu, N., Kong, D., Magidson, V., Nanjundappa, R., Sullenberger, C., Mahjoub, M.R., and Loncarek, J. (2019). Expansion microscopy for the analysis of centrioles and cilia. Journal of Microscopy *276*, 145-159.

Salisbury, J.L. (2003). Centrosomes: Coiled-Coils Organize the Cell Center. Current Biology *13*, R88-R90.

Saurya, S., Roque, H., Novak, Z.A., Wainman, A., Aydogan, M.G., Volanakis, A., Sieber, B., Pinto, D.M., and Raff, J.W. (2016). *Drosophila* Ana1 is required for centrosome assembly and centriole elongation. Journal of Cell Science *129*, 2514-2525.

Scheer, U. (2014). Historical roots of centrosome research: discovery of Boveri's microscope slides in Würzburg. Philosophical transactions of the Royal Society of London B Biological Sciences *369*.

Schindelin, J., Arganda-Carreras, I., Frise, E., Kaynig, V., Longair, M., Pietzsch, T., Preibisch, S., Rueden, C., Saalfeld, S., Schmid, B.*, et al.* (2012). Fiji: an open-source platform for biological-image analysis. Nature Methods *9*, 676-682.

Schmidt, T.I., Kleylein-Sohn, J., Westendorf, J., Le Clech, M., Lavoie, S.B., Stierhof, Y.D., and Nigg, E.A. (2009). Control of centriole length by CPAP and CP110. Curr Biol *19*, 1005-1011.

Schnackenberg, B.J., Khodjakov, A., Rieder, C.L., and Palazzo, R.E. (1998). The disassembly and reassembly of functional centrosomes *in vitro*. Proceedings of the National Academy of Sciences *95*, 9295-9300.

Schvarzstein, M., Pattabiraman, D., Bembenek, J.N., and Villeneuve, A.M. (2013). Meiotic HORMA domain proteins prevent untimely centriole disengagement during *Caenorhabditis elegans* spermatocyte meiosis. Proc Natl Acad Sci U S A *110*, E898-907.

Seki, A., Coppinger, J.A., Jang, C.-Y., Yates, J.R., and Fang, G. (2008). Bora and the Kinase Aurora A Cooperatively Activate the Kinase Plk1 and Control Mitotic Entry. Science *320*, 1655-1658.

Serwas, D., Su, T.Y., Roessler, M., Wang, S., and Dammermann, A. (2017). Centrioles initiate cilia assembly but are dispensable for maturation and maintenance in *C. elegans*. Journal of Cell Biology *216*, 1659-1671.

Sharma, A., Aher, A., Dynes, N.J., Frey, D., Katrukha, E.A., Jaussi, R., Grigoriev, I., Croisier, M., Kammerer, R.A., Akhmanova, A.*, et al.* (2016). Centriolar CPAP/SAS-4 Imparts Slow Processive Microtubule Growth. Developmental Cell *37*, 362-376.

Shaye, D.D., and Greenwald, I. (2011). OrthoList: A Compendium of *C. elegans* Genes with Human Orthologs. PLoS ONE *6*, e20085.

Shin, Y., and Brangwynne, C.P. (2017). Liquid phase condensation in cell physiology and disease. Science *357*, eaaf4382.

Sin, O., Michels, H., and Nollen, E.A.A. (2014). Genetic screens in *Caenorhabditis elegans* models for neurodegenerative diseases. Biochimica et Biophysica Acta - Molecular Basis of Disease *1842*, 1951-1959.

Sluder, G. (2013). Centriole Engagement: It's Not Just Cohesin Any More. Current Biology *23*, R659-R660.

Sonnen, K.F., Schermelleh, L., Leonhardt, H., and Nigg, E.A. (2012). 3D-structured illumination microscopy provides novel insight into architecture of human centrosomes. Biology Open *1*, 965-976.

Sönnichsen, B., Koski, L.B., Walsh, A., Marschall, P., Neumann, B., Brehm, M., Alleaume, A.M., Artelt, J., Bettencourt, P., Cassin, E.*, et al.* (2005). Full-genome RNAi profiling of early embryogenesis in *Caenorhabditis elegans*. Nature *434*, 462-469.

Srayko, M., Kaya, A., Stamford, J., and Hyman, A.A. (2005). Identification and Characterization of Factors Required for Microtubule Growth and Nucleation in the Early *C. elegans* Embryo. Developmental Cell *9*, 223-236.

Srayko, M., Quintin, S., Schwager, A., and Hyman, A.A. (2003). *Caenorhabditis elegans* TAC-1 and ZYG-9 form a complex that is essential for long astral and spindle microtubules. Current Biology *13*, 1506-1511.

Stenzel, L., Mehler, J., Schreiner, A., Üstüner, S., Zuccoli, E., Zanin, E., and Mikeladze-Dvali, T. (2020). PCMD-1 bridges the centrioles and the PCM scaffold in *C. elegans*. bioRxiv, doi: 10.1101/2020.11.09.375865.

Sugioka, K., Hamill, D.R., Lowry, J.B., McNeely, M.E., Enrick, M., Richter, A.C., Kiebler, L.E., Priess, J.R., and Bowerman, B. (2017). Centriolar SAS-7 acts upstream of SPD-2 to regulate centriole assembly and pericentriolar material formation. eLife *6*.

Sulston, J.E., and Horvitz, H.R. (1977). Post-embryonic cell lineages of the nematode *Caenorhabditis elegans*. Developmental Biology *56*, 110-156.

Sulston, J.E., Schierenberg, E., White, J.G., and Thomson, J.N. (1983). The embryonic cell lineage of the nematode *Caenorhabditis elegans*. Developmental Biology *100*, 64-119.

Tabara, H., Grishok, A., and Mello, C.C. (1998). RNAi in *C. elegans*: soaking in the genome sequence. Science *282*, 430-431.

Tang, C.J., Fu, R.H., Wu, K.S., Hsu, W.B., and Tang, T.K. (2009). CPAP is a cell-cycle regulated protein that controls centriole length. Nature Cell Biology *11*, 825-831.

Tavernier, N., Noatynska, A., Panbianco, C., Martino, L., Van Hove, L., Schwager, F., Léger, T., Gotta, M., and Pintard, L. (2015). Cdk1 phosphorylates SPAT-1/Bora to trigger PLK-1 activation and drive mitotic entry in *C. elegans* embryos. Journal of Cell Biology *208*, 661-669.

Teixidó-Travesa, N., Roig, J., and Lüders, J. (2012). The where, when and how of microtubule nucleation – one ring to rule them all. Journal of Cell Science *125*, 4445.

Thornton, G.K., and Woods, C.G. (2009). Primary microcephaly: do all roads lead to Rome? Trends in Genetics *25*, 501-510.

Timmons, L., Court, D.L., and Fire, A. (2001). Ingestion of bacterially expressed dsRNAs can produce specific and potent genetic interference in *Caenorhabditis elegans*. Gene *263*, 103-112.

Tinevez, J.Y., Perry, N., Schindelin, J., Hoopes, G.M., Reynolds, G.D., Laplantine, E., Bednarek, S.Y., Shorte, S.L., and Eliceiri, K.W. (2017). TrackMate: An open and extensible platform for single-particle tracking. Methods *115*, 80-90.

Tolić, I.M. (2018). Mitotic spindle: kinetochore fibers hold on tight to interpolar bundles. European Biophysics Journal *47*, 191-203.

Truebestein, L., and Leonard, T.A. (2016). Coiled-coils: The long and short of it. BioEssays *38*, 903-916.

Trulioff, A., Ermakov, A., and Malashichev, Y. (2017). Primary Cilia as a Possible Link between Left-Right Asymmetry and Neurodevelopmental Diseases. Genes (Basel) *8*.

Tsuchiya, Y., Yoshiba, S., Gupta, A., Watanabe, K., and Kitagawa, D. (2016). Cep295 is a conserved scaffold protein required for generation of a bona fide mother centriole. Nature Communications *7*, 12567.

UniProtConsortium (2019). UniProt: a worldwide hub of protein knowledge. Nucleic Acids Research *47*, D506-d515.

Uzbekov, R., and Alieva, I. (2018). Who are you, subdistal appendages of centriole? Open Biology *8*.

van Beneden, E. (1876). Recherches sur les Dicyémides, survivant actuels d´un embranchement des Mésozoaires. Bull Acad Royale Belgique 2éme sér *41:1160-1205*, 35-97.

van Beneden, E. (1883). Recherches sur la maturation de l´oeuf, la fécondation et la division cellulaire.

van Beneden, E., and Neyt, A. (1887). Nouvelles recherches sur la fécondation et la division mitosique chez l'Ascaride mégalocéphale. Bull Acad Royale Belgique 3éme sér *14*, 215-295.

Varadarajan, R., and Rusan, N.M. (2018). Bridging centrioles and PCM in proper space and time. Essays in Biochemistry *62*, 793-801.

Venkatesan, K., Rual, J.F., Vazquez, A., Stelzl, U., Lemmens, I., Hirozane-Kishikawa, T., Hao, T., Zenkner, M., Xin, X., Goh, K.I.*, et al.* (2009). An empirical framework for binary interactome mapping. Nature Methods *6*, 83-90.

Walczak, C.E., and Heald, R. (2008). Mechanisms of Mitotic Spindle Assembly and Function. International Review of Cytology *265*, 111-158.

Wang, Z., Zhang, G., and Zhang, H. (2019). Protocol for analyzing protein liquid–liquid phase separation. Biophysics Reports *5*, 1-9.

Ward, S., and Carrel, J.S. (1979). Fertilization and sperm competition in the nematode *Caenorhabditis elegans*. Developmental Biology *73*, 304-321.

Watanabe, S., Meitinger, F., Shiau, A.K., Oegema, K., and Desai, A. (2020). Centriole-independent mitotic spindle assembly relies on the PCNT-CDK5RAP2 pericentriolar matrix. Journal of Cell Biology *219*.

Waterhouse, A.M., Procter, J.B., Martin, D.M.A., Clamp, M., and Barton, G.J. (2009). Jalview Version 2—a multiple sequence alignment editor and analysis workbench. Bioinformatics *25*, 1189-1191.

Weerdt, B.C.M.v.d., and Medema, R.H. (2006). Polo-Like Kinases: A Team in Control of the Division. Cell Cycle *5*, 853-864.

Winey, M., and O'Toole, E. (2014). Centriole structure. Philosophical transactions of the Royal Society of London B Biological Sciences *369*, 20130457.

Woodruff, J.B. (2021). The material state of centrosomes: lattice, liquid, or gel? Current Opinion in Structural Biology *66*, 139-147.

Woodruff, J.B., Ferreira Gomes, B., Widlund, P.O., Mahamid, J., Honigmann, A., and Hyman, A.A. (2017). The Centrosome Is a Selective Condensate that Nucleates Microtubules by Concentrating Tubulin. Cell *169*, 1066-1077 e1010.

Woodruff, J.B., Wueseke, O., and Hyman, A.A. (2014). Pericentriolar material structure and dynamics. Philosophical transactions of the Royal Society of London B Biological Sciences *369*.

Woodruff, J.B., Wueseke, O., Viscardi, V., Mahamid, J., Ochoa, S.D., Bunkenborg, J., Widlund, P.O., Pozniakovsky, A., Zanin, E., Bahmanyar, S.*, et al.* (2015). Regulated assembly of a supramolecular centrosome scaffold *in vitro*. Science *348*, 808-812.

Wu, J., and Akhmanova, A. (2017). Microtubule-Organizing Centers. Annual Review of Cell & Developmental Biology *33*, 51-75.

Wueseke, O., Bunkenborg, J., Hein, M.Y., Zinke, A., Viscardi, V., Woodruff, J.B., Oegema, K., Mann, M., Andersen, J.S., and Hyman, A.A. (2014). The *Caenorhabditis elegans* pericentriolar material components SPD-2 and SPD-5 are monomeric in the cytoplasm before incorporation into the PCM matrix. Molecular Biology of the Cell *25*, 2984-2992.

Wueseke, O., Zwicker, D., Schwager, A., Wong, Y.L., Oegema, K., Julicher, F., Hyman, A.A., and Woodruff, J.B. (2016). Polo-like kinase phosphorylation determines *Caenorhabditis elegans* centrosome size and density by biasing SPD-5 toward an assembly-competent conformation. Biology Open *5*, 1431-1440.

Xue, Y., Ren, J., Gao, X., Jin, C., Wen, L., and Yao, X. (2008). GPS 2.0, a tool to predict kinase-specific phosphorylation sites in hierarchy. Molecular & Cellular Proteomics *7*, 1598-1608.

Yang, H.Y., McNally, K., and McNally, F.J. (2003). MEI-1/katanin is required for translocation of the meiosis I spindle to the oocyte cortex in *C. elegans*. Developmental Biology *260*, 245-259.

Yang, R., and Feldman, Jessica L. (2015). SPD-2/CEP192 and CDK Are Limiting for Microtubule-Organizing Center Function at the Centrosome. Current Biology *25*, 1924-1931.

Yu, C.-C., Barry, N.C., Wassie, A.T., Sinha, A., Bhattacharya, A., Asano, S., Zhang, C., Chen, F., Hobert, O., Goodman, M.B.*, et al.* (2020). Expansion microscopy of *C. elegans*. eLife *9*, e46249.

Zheng, X., Ramani, A., Soni, K., Gottardo, M., Zheng, S., Ming Gooi, L., Li, W., Feng, S., Mariappan, A., Wason, A.*, et al.* (2016). Molecular basis for CPAP-tubulin interaction in controlling centriolar and ciliary length. Nature Communications *7*, 11874.

Zheng, Y., Wong, M.L., Alberts, B., and Mitchison, T. (1995). Nucleation of microtubule assembly by a gamma-tubulin-containing ring complex. Nature *378*, 578-583.

Zhu, F., Lawo, S., Bird, A., Pinchev, D., Ralph, A., Richter, C., Müller-Reichert, T., Kittler, R., Hyman, A.A., and Pelletier, L. (2008). The mammalian SPD-2 ortholog Cep192 regulates centrosome biogenesis. Current Biology *18*, 136-141.

Zipperlen, P., Fraser, A.G., Kamath, R.S., Martinez-Campos, M., and Ahringer, J. (2001). Roles for 147 embryonic lethal genes on *C.elegans* chromosome I identified by RNA interference and video microscopy. The EMBO Journal *20*, 3984-3992.

Zitouni, S., Nabais, C., Jana, S.C., Guerrero, A., and Bettencourt-Dias, M. (2014). Polo-like kinases: structural variations lead to multiple functions. Nature Reviews Molecular Cell Biology *15*, 433-452.

Zwicker, D., Decker, M., Jaensch, S., Hyman, A.A., and Jülicher, F. (2014). Centrosomes are autocatalytic droplets of pericentriolar material organized by centrioles. PNAS *111*, E2636-E2645.

APPENDIX

Acknowledgments

This work was only made possible because of many people's incredible support, to whom I express my deepest gratitude.

I would like to thank Dr. Tamara Mikeladze-Dvali for giving me the opportunity to work in her research group. Thank you for introducing me to the fascinating world of centrosomes, for the opportunity to work on such an exciting project, and for your trust in my work.

I want to express my gratitude to my principal supervisor, Prof. Barbara Conradt, for allowing me to conduct my thesis in the Department of Cell and Developmental Biology, for the professional advice, support, and for evaluating my thesis.

I am grateful to Prof. Michael Boshart, Prof. Magdalena Götz, Dr. Stephané Rolland, and Dr. Mikeladze-Dvali for their helpful advice and support as my Thesis Advisory Committee members. I also want to thank my examination board members Prof. Michael Boshart, Prof. Wolfgang Enard, Prof. Heinrich Jung, Prof. Angelika Böttger, and Prof. Herwig Stibor for reading and evaluating this thesis.

I would like to thank CIPSM and the Graduate School of Life Science Munich (LSM) for their financial support. I am immensely grateful for the education outside the laboratory offered by the LSM Graduate School. I wish to thank the LSM coordinators Nadine Hamze and Francisca Rosa Mende for their guidance.

I want to thank all my colleagues in the Cell and Developmental Biology Department, who made the laboratory a great place to work. It was a pleasure to work with you. Especially, I am deeply grateful to get to know my wonderful colleague, Anna. Even though our time together in the Mikeladze-Dvali group was short, you continued to support me all the time, even after you left our group. Most of all, I would like to thank you for your helpful feedback on this work. Moreover, I would like to thank Dr. Nadine Memar for her valuable advice. Thanks to my talented students Judith, Nupur, Sim, and Elisa. It was a great experience to supervise you and work with you.

Thanks to all Ph.D. students for the fun times we shared inside and outside the lab. I will never forget the cheerful 'PhDinners' and visits to the Oktoberfest and Starkbierfest. I want to thank Jenny, Anna, Laura, Adi, Elisabeth, Sandra, and Fritzi, for our daily coffee breaks and the great conversations. Special thanks go to my office mate Marion, for getting through the highs and lows during the last few years.

A warm thank you belongs to all of my friends for their support during the last few years. Special thanks go to Larissa and Kristina, who have spent exactly nine years with me at the Biocenter. Now that our career paths will part, I already miss our coffee breaks and countless personal and scientific conversations! However, I am sure that our great friendships will last!

I wish to thank my wonderful family from the bottom of my heart. Mama, Papa und Julia, ich bin stolz euch als Familie zu haben! Danke für eure kontinuierliche Unterstützung, euer offenes Ohr und euren Glauben in mich. An dieser Stelle möchte ich auch meiner Großeltern gedenken, die leider die Fertigstellung meiner Doktorarbeit nicht mehr miterleben durften, aber immer an mich geglaubt haben. Ich vermisse euch!

Last but not least, I want to express my heartfelt gratitude to my husband, Alec. Thanks for your love, patience, and endless support, whether this means picking me up from the Biocenter in the late evenings or listening to science stuff you did not even understand. Thank you for your incredible humor, which you always kept when I lost mine!